Distribution and characterization of marine iron-rich particles

by
Bjorn Phillip von der Heyden

Dissertation presented for the degree of *Doctor of Earth Sciences in the Faculty of Science at Stellenbosch University*

Supervisor: Prof. Alakendra N. Roychoudhury
Co-supervisor: Prof. Satish C.B. Myneni

December 2013

DECLARATION

By submitting this thesis electronically, I declare that the entirety of the work contained therein is my own, original work, that I am the sole author thereof (save to the extent explicitly otherwise stated), that reproduction and publication thereof by Stellenbosch University will not infringe any third party rights and that I have not previously in its entirety or in part submitted it for obtaining any qualification.

Signed:
Bjorn von der Heyden
Date: 25 November 2013

ABSTRACT

This thesis investigates questions surrounding the role that iron-rich colloids (nominally sized between 0.02 µm and 0.2 µm) and particulates (>0.2-0.45 µm) play in the context of the greater iron biogeochemical cycle. To this end, this study complements a review of reported size-fractionated iron (Fe) measurements with chemical and mineralogical data derived from synchrotron-based x-ray measurements. From an extensive literature review, the global surface ocean colloidal iron (cFe) pool is found to be highly dynamic, frequently exhibiting seasonal trends and nutrient-like behaviour. Spatial variability in surface ocean colloidal iron concentration is primarily a function of total iron supply, although the concentration and strength of iron-binding ligands, and inorganic thermodynamic constraints are additional influential factors. The size-fractionated study of colloidal Fe has rendered considerable evidence pointing towards direct or indirect biological utilization of this cFe pool; however, a more complete understanding of cFe-biological interaction necessarily requires better knowledge of cFe chemistry and mineralogy.

To address these issues, this thesis documents the development of a novel x-ray microscopy and spectroscopy technique for determining the Fe speciation of individual Fe-rich particles under environmental conditions. Variations in the peak splitting in iron L_3-edge XANES (X-ray Absorption Near-Edge Structure) spectra reflect changes in the local coordination environment surrounding the metal centre. Specifically, the energy splitting (ΔeV) and intensity ratio of the split peaks at the L_3-edge vary as a function of the Fe valence state, the number and chemistry of coordinating ligands and polyhedral distortion effects; and combinations of the two parameters are found to be characteristic of individual Fe minerals.

To understand Fe speciation, the ΔeV versus intensity ratio plot was successfully applied to a variety of environmental Fe particles (greater than 20 nm diameter) collected from two ocean basins; the Southern Ocean and the south western Pacific Ocean. Speciation differences in Fe particles collected from the Southern Ocean show distinct compositional trends between the coasts of South Africa and Antarctica, with different Fe pools associated with the different oceanographic frontal zones. Despite the oxygenated nature of the seawater sampled, the presence of significant particle-hosted Fe(II) was observed in both the Southern Ocean at high latitudes, and at sampling sites proximal to the Kermadec Ridge in the Pacific Ocean. Ferrous iron particles at the latter study area were shown to be strongly associated with carbon functional groups, notably alcohol and carboxamine moieties. These findings, relating to particle chemical differences and associations

with organic matter, have significant implications for our understanding of particle behaviour, their surface interactions and the role that they play in primary productivity and global elemental cycles.

Keywords: *Iron, Fe, colloids, speciation, L-edge, XANES, Southern Ocean*

OPSOMMING

Hierdie tesis ondersoek kwessies met betrekking tot die rol wat ysterryke kolloïede (van nominale groottes tussen 0.02 µm en 0.2 µm) en partikels (>0.2-0.45 µm) in die konteks van die groter ysterbiogeochemiese siklus speel. Vir hierdie doel bou die studie voort op ’n oorsig van aangemelde grootte-gefraksioneerde yster- (Fe-)metings met behulp van chemiese en mineralogiese data wat uit sinchrotrongebaseerde x-straalmetings verkry is. Na aanleiding van ’n uitvoerige literatuurstudie, blyk die globale poel kolloïdale yster (cFe) op die see-oppervlak hoogs dinamies te wees en toon dit dikwels seisoenale tendense en voedingstofagtige gedrag. Ruimtelike veranderlikheid in die cFe-konsentrasie op die see-oppervlak is hoofsaaklik ’n funksie van totale ystervoorsiening, hoewel die konsentrasie en sterkte van ysterbindende ligande sowel as anorganiese termodinamiese beperkings ook ’n invloed kan hê. Die grootte-gefraksioneerde studie van kolloïdale Fe het beduidende bewyse opgelewer wat op die direkte of indirekte biologiese benutting van hierdie cFe-poel dui. Tog verg ’n vollediger begrip van cFe- biologiese interaksie noodwendig meer kennis van die chemie en mineralogie van cFe.

Om hierdie kwessies te ondersoek, dokumenteer hierdie tesis die ontwikkeling van ’n innoverende X-straalmikroskopie- en X-straalspektroskopietegniek om die Fe-soortvorming van individuele Fe-ryke partikels in omgewingsomstandighede te bepaal. Variasies in die pieksplitsing van yster-L_3 rand-XANES- (“X-ray absorption near-edge structure”-)spektra weerspieël veranderlikheid in die lokale koördinasie-omgewing rondom die metaalkern. In die besonder wissel die energiesplitsing (ΔeV) en intensiteitsverhouding van die splitsingspieke by die L_3-rand na gelang van die Fe-valensietoestand, die getal en chemie van koördinasie-ligande, en poliëdriese distorsie-effekte, en kombinasies van die twee parameters blyk kenmerkend van individuele Fe-minerale te wees.

Om Fe-soortvorming te verstaan, is die stipping van ΔeV versus intensiteitsverhouding suksesvol toegepas op ’n verskeidenheid Fe-omgewingspartikels (groter as 20 nm in deursnee) wat uit twee oseaankomme – die Suidelike Yssee en die suidwestelike Stille Oseaan – bekom is. Soortverskille in Fe-partikels wat uit die Suidelike Yssee bekom is, toon kenmerkende samestellingspatrone tussen die kus van Suid-Afrika en Antarktika, en verskillende Fe-poele word met die verskillende oseanografiese frontsones verbind. Ondanks die suurstofhoudende aard van die seewatermonsters, is beduidende Fe(II) in partikels opgemerk in die Suidelike Yssee by hoë breedteliggings sowel as op studieterreine naby die Kermadec-rif in die Stille Oseaan. Ysterhoudende partikels van laasgenoemde studieterrein het ’n sterk verband met koolstof- funksionele groepe, veral alkohol en

karboksamien, getoon. Hierdie bevindinge met betrekking tot die chemiese verskille tussen partikels en die verband met organiese materie het beduidende implikasies vir ons begrip van partikelgedrag, die oppervlak-interaksies van partikels, en die rol wat dit in primêre produktiwiteit en globale elementsiklusse speel.

Trefwoorde: *yster, Fe, kolloïede, soortvorming, L-rand, XANES, Suidelike Yssee*

ACKNOWLEDGEMENTS

This thesis could not have been made possible, and indeed would not have come to fruition, without the guidance, support and enthusiasm of my two supervisors, Prof Alakendra Roychoudhury and Prof Satish Myneni. To Roy; I owe you the most immense gratitude for, over the last five years, your supervision has been the single biggest influence on my development as a scientist. Thank you for guiding my ability to think critically and write concisely, and thank you for the innumerable opportunities that have benefitted both this work as well as my personal growth. I have appreciated your approach to supervision; the open-door policy meant I was never hesitant to seek your advice when needed, and although you promote a diligent work ethic, I always felt that I was allowed sufficient freedom in terms of decision-making, time-management and creativity. Coupled with the various responsibilities that you entrusted me with, this freedom has given me significant confidence in my abilities as a young scientist- something that was lacking before I benefitted from your supervision. To Satish; I am eternally grateful for all of the opportunities that you provided me during my year at Princeton, as well as for your continued support throughout the duration of this project. I have benefitted greatly from my daily interactions with you during this time, in which I fostered and, to a degree, adopted your passion, enthusiasm and inquisitiveness for science. Thank you for equipping me with a unique x-ray skill-set which has set me apart from other young South African scientists, and thank you for instilling in me the importance of combining attention to detail with good 'flow' when writing up academic work. Thus, to be my supervisors, thank you for the time and effort that you have invested in me. I look up to you both with the utmost respect and admiration and look forward to nurturing continued relationships into the future.

Aside from my supervisors, there are several other academics with whom I have enjoyed beneficial discussion relating to science, my thesis and general life. Thank you to John Compton for providing various samples, useful discussion and an initial hypothesis from which this project has stemmed. I would like to acknowledge George Philander for making my year-long visit to Princeton University possible and for encouraging a holistic, open-minded and community-spirited approach to science. Thank you also to Sophie von der Heyden, Cathy Clark, Warren Joubert, Alessandro Tagliabue, Angelique Laurie and Bruce Anderson for the various gems of advice and insights that you have passed on and that have helped me to make a success of my academic career. My appreciation extends beyond the scope of pure academics to those of you involved in the technical and administrative aspects behind a smooth and successful project. I think particularly of Tannie Loxie Conradie, George Olivier and the administrative staff at Princeton University. I would also like to

thank all of those who have been involved in my education prior to post-graduate level study, including undergraduate lecturers and primary- and high school teachers. It is my firm belief that the only way in which South Africa can move forward as a country, is if every youngster has the privilege of experiencing access to the same high quality of education that I experienced, right from a grass-roots level.

This thesis would also not have been possible without the temporary release from an undergraduate bursary obligation. Thank you to Hennie van der Berg from Exxaro, firstly for the support during undergraduate study and secondly for your foresight and flexibility that allowed me to further my education.

Much of my work has relied on the collection of high-quality and contamination-free ocean water samples during various oceanographic cruises. Foremost in this respect, I would like to thank Thato Mtshali and Raimund Rentel for the effort that they have put into collecting samples on my behalf. I have also thoroughly enjoyed working the long hours as part of the 'Iron Team' alongside you both. Thanks must be extended to the crew of the SA Agulhas as well as to the scientific staff, especially the chief scientists and Fe chemists, involved in SANAE 49, 50 and 51 oceanographic cruises. My appreciation must also be extended to the crew and scientists on board the RS Discovery during GEOTRACES D357 cruise into the Cape Basin, it was during this cruise that I was taught the importance of, and procedures involved in trace-metal clean sampling protocols.

Accurate and successful data analyses would not have been possible without the patient assistance of Tolek Tyliszczak, the responsible scientist at beam-line 11.0.2 whose tireless efforts, at often ungodly hours, have saved my skin on numerous occasions. Thank you also to the rest of the Myneni lab-group, especially Matt Frith, who have helped out and shared time with me during the long hours at the Advanced Light Source. Furthermore, the work would not have been possible without significant financial backing from various funding bodies, including the National Research Foundation, South Africa; Stellenbosch University; the National Science Fund, USA; the U.S. Department of Energy; and the Princeton in Africa program.

I have been unbelievably blessed in that my project has encompassed both of my major passions; geology and the ocean. I would like to make special mention of all my friends, both from within the various geological departments as well as from my circles involved in surfing and the beach lifestyle. The experiences and memories that I have shared with you all, both those that revolved purely around nurturing a love for the ocean, as well as those that dealt more with trying to

understand the mineralogical aspects of the Earth system, will be cherished forever. Finally, I would like to thank explicitly my family, particularly my immediate family (Mom, Pap, Faf, Karli and Uncle Stu) for all of the love, support, encouragement and faith that you have invested in me over these first twenty seven years of my life. Thank you especially to Mom and Pap for all of the opportunities that you have made available to me through financial, educational and emotional support, and for providing me with a stable home environment in which my energies could be focussed on happiness and care-free personal growth.

This thesis is dedicated to both my surviving gran, Ulla von der Heyden (Oma) as well as to my late grand-parents; Dorelle and Desmond Horn (Granny and Gramps) and Gisella von der Heyden (Omi).

"A child needs a grandparent, anybody's grandparent, to grow a little more securely into an unfamiliar world." – Charles and Ann Morse

"To forget one's ancestors is to be a brook without a source, a tree without a root." – Chinese Proverb

TABLE OF CONTENTS

LIST OF FIGURES

Page

Chapter 4: Chemically and geographically distinct solid-phase iron pools in the Southern Ocean

Chapter 5: Ubiquitous presence of Fe(II) in aquatic colloids and its association with organic carbon

LIST OF TABLES

CHAPTER 1

Introduction

1. GENERAL IRON BIOGEOCHEMISTRY

The landmark iron (Fe) hypothesis of John Martin and co-authors in the late 1980's saw the advent of the "Iron Age" in marine biogeochemistry (Martin et al., 1988; Martin, 1992; Martin et al., 1994). It concerns the role that Fe plays in controlling primary productivity and sustaining phytoplankton growth, particularly in, but not limited to, the high nutrient low chlorophyll (HNLC) regions of the world's oceans. A host of iron seeding experiments conducted during the subsequent two decades confirmed this hypothesis, whereby Fe additions to remote marine surface waters were shown to initiate and stimulate phytoplankton blooms and thus primary productivity (de Baar et al., 2005; Boyd et al., 2007). Iron is essential for marine photosynthetic organisms because Fe, particularly in the form of heme groups or iron-sulphur proteins, is an essential functional component in photosynthesis, respiration, nitrogen assimilation and DNA replication reactions (Michel and Pistorius, 2004). Yet Fe limitation commonly exists, in both coastal waters and the open ocean, when macro-nutrient concentrations are in excess and Fe concentrations are significantly smaller than the stoichiometric cellular Fe requirements associated with the growth of ambient phytoplankton populations (Ho et al., 2003). In these regions (up to half the of the world ocean (Moore et al., 2001)) Fe limitation plays a defining role in controlling marine primary productivity, thereby impacting on biologically-mediated ocean-atmosphere carbon dioxide (CO_2) exchange (Boyd and Ellwood, 2010).

Since the advent of trace-metal clean techniques, the study of marine Fe has progressed significantly and expanded to incorporate all aspects of biogeochemical cycling (see Turner and Hunter, 2001; Breitbarth et al., 2010 for syntheses of international Fe workshops). Major themes that have received wide attention in the literature include biological and physico-chemical cycling of Fe, Fe source and sink budgets and modelling, Fe-ligand interactions, and global Fe distributions and size fractionation.

1.1. Physical, chemical and biological cycling of Fe

Fe is a redox active transition metal occurring in the natural environment in two oxidation states, as ferrous iron (Fe(II)) and as ferric iron (Fe(III)). Because of the oxygenated nature of seawater, Fe(III) is thermodynamically favoured throughout the marine water column, except in reducing environments. Only a very small fraction (<0.1 pM, Rue and Bruland, 1995) of this Fe(III) is present in its truly dissolved aqueous form (Fe') and most is either strongly bound within the structure of sparingly-soluble Fe oxyhydroxides or coordinated to binding sites associated with the excess of organic Fe-binding ligands present in seawater (Gledhill and van den Berg, 1994; Rue and Bruland, 1995). These ligands include both strong-binding siderophore complexes, produced by bacterial species as part of an Fe-acquisition mechanism (Sunda, 2001;

Kraemer, 2004); as well as weaker binding ligand classes. Although the exact speciation of the 'ligand soup' (incorporating a range of organic species produced during cell lysis and organic degradation or as cellular exudates) remains enigmatic, a significant proportion is available for phytoplankton uptake (e.g. saccharides (Hassler et al., 2011)).

Despite its relative prevalence, Fe(III) first needs to be reduced before it can be taken up by marine eukaryotes (Shaked et al., 2005). This reduction process is facilitated predominantly by phytoplankton membrane enzymes (Shaked et al., 2005), although microbial reduction (Weber et al., 2006), photo-reduction (Miller et al., 1995; Barbeau, 2006) and superoxide and H_2O_2 attack (Voelker and Sedlak, 1995; Gonzalez-Davila, 2006) may also play a significant role in determining the magnitude of the available Fe(II) pool.

Iron cycling in marine systems is not limited merely to inter-conversions between its two valence states. Processes governing the distribution of iron into different size classes and forms (i.e. inter-conversions between lithogenic, biogenic and detrital particulate Fe pools (Tortelle, 1999; Frew et al., 2006)) are also highly important biogeochemical considerations. These processes include dissolution, aggregation, biological utilization, photochemistry and recycling through grazing, respiration and re-mineralization activities (Boyd and Ellwood, 2010, and references therein). The influences of these processes specifically to the colloidal Fe pool represent a central theme to this thesis (see Chapter 2).

1.2. Fe sources, sinks and modelling

A large volume of marine Fe studies are devoted to the elucidation and quantification of Fe source terms to marine waters, particularly to HNLC regions such as the climatologically-important Southern Ocean. Although most works focus on the role of a single specific Fe source term, it is generally accepted that productivity in the open ocean is affected by the combined effects of multiple Fe sources. Some of the major Fe source terms include wet and dry atmospheric dust deposition (Jickells et al., 2005; Cassar et al., 2007), fluvial, glacial and groundwater sources (Poulton and Raiswell, 2002; Raiswell et al., 2006), sediment re-suspension from continental and island shelves (Elrod et al., 2004; Lam et al., 2006; Compton et al., 2009; Chever et al., 2010), iceberg and pack-ice melting (Smith et al., 2007; Lannuzel et al., 2008; Aguilar-Islas et al., 2008), hydrothermal inputs (Tagliabue et al., 2010) and upwelling and mixing of deeper Fe-replete water masses (de Baar et al., 1995). Some of these sources are depicted, along with related biological utilization and cycling, in figure 1.

The deep ocean sea-floor represents the terminal sink for marine Fe, and any sinking losses from the euphotic zone can decrease the size of the Fe reservoir available for primary productivity. The sinking flux of Fe from the euhotic zone and through the water column is typically dominated by iron in the particulate form. Sinking rates range between 0.05-18 m (Ridame and Guieu, 2002) to over 100 m per day (Fischer and Karakas, 2009), depending on the size, density and hydrodynamic considerations of the respective particles.

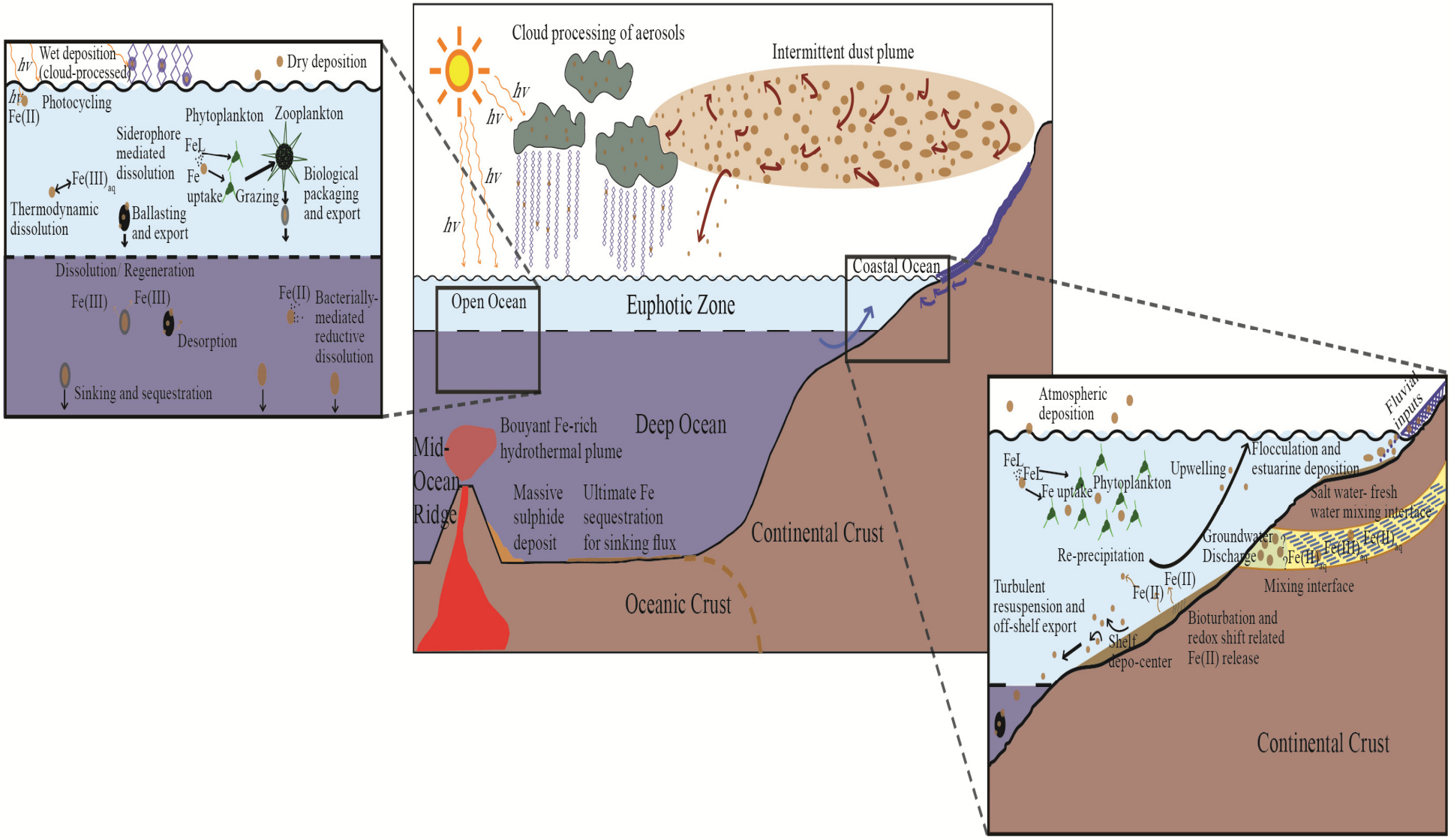

Figure 1: *A selection of the major transport routes of Fe into particularly the euphotic zone of the coastal and open ocean. Inset boxes highlight some of the complexities introduced into the marine Fe cycle by biological processing and by the range of processes acting in shelf settings.*

Losses are promoted by packaging of Fe in the form of faecal pellets and by aggregation reactions that increase particles size and thus sinking rates (Wells and Goldberg, 1993; Kepkay, 1994). A proportion of the sinking Fe flux is regenerated by inorganic dissolution and by bacterial remineralization, particularly at greater depths; where temperature and bacterial count factors render these processes more effective (Liu and Millero, 2002; Boyd and Trull, 2007). The balance between these aggregation and regeneration terms is partially responsible for controlling colloidal Fe concentration down the water column (Wells, 1998).

An enhanced understanding of these source and sink fluxes is highly relevant to developing budgets and associated biogeochemical models of marine Fe (Archer and Johnson, 2002; Parekh et al., 2004). These models have been used to evaluate different Fe source terms (Moore and Braucher, 2008; Tagliabue et al., 2010) and, as our understanding of Fe biogeochemistry progresses and as models improve, their predictions relating to the effects of global change on Fe speciation and associated productivity, are expected to increase in accuracy (Tagliabue and Volker, 2011).

1.3. Fe-ligand interactions

Early voltammetry studies have indicated that the majority of marine dissolved iron (dFe; <0.2/0.4 µm) is complexed to organic ligands (Gledhill and van den Berg, 1994; Rue and Bruland, 1995). These ligands thus play a substantive role in governing the behaviour and size-fractionation of Fe in the marine biogeochemical system (Cullen et al., 2006; Boye et al., 2010; Thuroczy et al., 2011a, b). Organic ligands buffer dissolved Fe concentration to levels above their thermodynamic solubility (Wu et al., 2001; Liu and Millero, 2002) and further have the capacity to influence Fe stability, solubility and bioavailability (Wu and Luther, 1995; Hutchins et al., 1999). Although much progress has been made relating to Fe-ligand interactions, the field is still very much in its infancy with only limited studies focussing on the chemistry and behaviour of individual ligand classes and functional groups (e.g. Mawji et al., 2008).

1.4. Global Fe distributions and size fractionation

The advent of trace-metal clean sampling techniques has enabled the collection of over 13 000 dissolved iron (dFe) measurements, spanning all the world's major ocean basins (Tagliabue et al., 2012). A large proportion of these measurements focuses on the Fe concentrations in HNLC regions, particularly the Southern Ocean and the equatorial and sub-Arctic Pacific Ocean basins, where Fe is known to be a limiting nutrient (Sunda, 2001). Dissolved Fe profiles frequently display shapes that are characteristic of the major nutrients (silicate, phosphate and nitrate) owing to utilization by photosynthetic biology in the upper water column (Johnson et al., 1997). However, because dFe concentrations are also affected by variable inputs and scavenging and remineralisation processes, their depth profiles are typically referred to as hybrid-type profiles. Compilations of dissolved Fe measurements have allowed for comment on the inter- and intra-basin variability of dFe concentration with depth (Boyd and Ellwood, 2011), development and evaluation of biogeochemical models,

and determination of the importance of different Fe source terms to the ocean (Moore and Braucher, 2008; Tagliabue et al., 2012).

Although most studies have focussed on reporting dFe (<0.2/0.4 µm (cut-offs chosen to exclude biologically-hosted intra-cellular Fe)) and total dissolvable Fe (TDFe; unfiltered) concentrations, modern ultra-filtration techniques have allowed for additional determination of the soluble Fe pool (sFe; <0.02 µm/ <1000 kDa). Using these operational definitions, the colloidal Fe pool (cFe) could be calculated as [dFe]-[sFe]; and this size fraction has since been shown to be an important and dynamic component of the marine Fe inventory (Wu et al., 2001; Bergquist et al., 2007).

2. COLLOIDAL IRON: TECHNIQUES AND RESEARCH OBJECTIVES

Historically, marine Fe chemistry has focused largely on the distribution of size- fractionated and operationally-defined Fe pools. Although proven invaluable to scientific understanding of marine biogeochemistry, this approach is associated with inherent limitations concerning the lack of precise physico-chemical speciation data that can be derived. This PhD thesis attempts to contribute to the state of knowledge surrounding the colloidal iron pool, both by reviewing a global compilation of cFe measurements and by employing an x-ray technique to probe the chemistry and mineralogy of marine Fe particles (20 nm-1 µm in diameter).

The small size of marine Fe particles, down to the nano-scale, coupled with the fact that they are present in extremely low (*p*M- µM) concentrations in surface seawater (e.g. Bowie et al., 2003), means that bulk geochemical techniques are rendered relatively ineffectual for marine Fe particle analysis. Advances in synchrotron x-ray technology have resulted in vastly improved energy and spatial resolutions; and this research incorporates the analysis of 20 nm diameter particles at a spectral resolution of 0.2 eV. Iron L-edge spectromicroscopy at the Molecular Environmental Beamline 11.0.2 (Lawrence Berkeley National Laboratory, CA, USA) (Bluhm et al., 2006) was the chosen technique as it provides detailed information, from spectral fine structure, of particles in their pristine state and at ambient temperature and pressure.

Sampling focused primarily on the remote Southern Ocean, where macronutrient excesses due to Fe limitation are greatest, and where deep water formation processes represent an important sink for air-sea exchanged atmospheric CO_2 (Caldeira and Duffy, 2000). Samples were collected during three oceanographic cruises and encompass all of the frontal zones found along two transects between Cape Town, SANAE (Antarctica) and the South Sandwich Island chain. These samples were complemented by depth resolved ocean water samples from the south western Pacific Ocean, where an abundance of ferrous-rich phases enabled further investigation into the factors that contribute towards stabilizing Fe in its thermodynamically-unfavourable reduced form. Given the sampling sites, the analysis techniques employed and the focus on colloidal Fe; the primary aims of this research are as follows:

- To compile a global dataset of reported soluble Fe (and thus colloidal Fe) measurements for use in subsequent analyses that investigate trends in the distribution and values of euphotic zone cFe concentrations.

- To evaluate measured Fe L-edge data in terms of theoretical concerns, thereby developing a tool for environmental Fe particle analysis.

- To investigate the spatial differences in Fe particle chemistry and link them to particle source regions, in situ processing and transformations; and to provide insight into their relationship with the ambient marine biota.

- To understand chemical relationships between iron and carbon species associated in Fe-rich particles in order to shed light on the factors that aid in preventing oxidation of ferrous particles.

3. MAJOR THEMES AND THESIS STRUCTURE

This thesis consists of six chapters written in the format of stand-alone scientific papers. Each section deals with a separate aspect pertaining to the study of environmental Fe particle chemistry; including their speciation, distribution, solubility and stability.

Chapter 2 is written as an additional background chapter stressing the importance of operationaly-defined colloidal Fe in biogeochemical cycling. Particular emphasis is placed on the euphotic zone of the open ocean where Fe is commonly a limiting nutrient to photosynthetic eukaryotes and prokaryotes. Interaction between these biota and colloidal Fe thus has implication for the global carbon cycle (Boyd and Ellwood, 2011). In spite of the importance of this implication, surprisingly little is known about the distribution and speciation of colloidal Fe species. Using published data, this chapter reviews scientific knowledge on these vital aspects and makes a strong case for the inclusion of particle-by-particle analyses when attempting to fully understand Fe biogeochemistry. The chapter has been prepared for submission to *Marine Chemistry* in 2013.

The study of environmental Fe particles in the colloidal size range (~0.02 µm - >0.2 µm) is complicated by their small size, the need to maintain their pristine sample integrity and, in the case of open ocean samples, their presence in only extremely low concentration. Chapter 3 details the development of a soft x-ray synchrotron radiation technique that allows for particle speciation studies, using both spectroscopy and microscopy, despite all of these complications. The double peaks of the Fe L_3-edge spectra are quantified according to their peak splitting parameter (ΔeV) and their peak intensity ratios (IR). Variations in these two parameters, between different standard Fe oxide and oxyhydroxide phases, are explained in terms of molecular level chemistry. This chapter will be submitted to *Geochemica and Cosmochemica Acta* in 2013.

Application of the technique outlined in Chapter 3 is portrayed in Chapter 4, which focuses on the speciation of Fe-rich particles in the South Atlantic and Southern Oceans. Fe particle speciation data are presented for two transects in the Southern Ocean between Cape Town, SANAE and South Georgia Island. Fe colloids were classified into five distinctive categories based on their predominant valence state and mineralogy. Along the transects studied, remarkable particle heterogeneity was observed and particular attention drawn to the predominant distributions of ferrous Fe and ferric Fe and their relation to averaged primary productivity. These results have been published in *Science* in 2012 (von der Heyden et al., 2012).

Results from the analysis of Southern Ocean colloids showed a high concentration of ferrous Fe colloids in the high latitudes. This observation was confirmed by preliminary results from colloids collected above the Kermadec Ridge in the south western Pacific Ocean. As ferrous Fe is not expected to be thermodynamically stable in oxic surface waters; Chapter 5 investigates the associations with organic matter which may aid in maintaining this form of Fe in seawater. A manuscript documenting the results from this investigation has been prepared for submission to *Environmental Science and Technology* in 2013.

The concluding chapter (Chapter 6) presents a brief synopsis of the thesis, providing a summary of the findings outlined in the preceding chapters. Furthermore, possible avenues for future research and outstanding gaps in knowledge regarding marine Fe particle chemistry are identified.

At the end of each chapter, a complete list of the relevant references is included, formatted to the style prescribed by the journal to which the chapter has been or will be submitted. One appendix is included at the end of the document, containing the complete dataset of sFe and cFe measurement related to Chapter 2.

4. DEFINITIONS AND ABBREVIATIONS

This thesis (except Chapter 2) does not explicitly subscribe to the nomenclature dictated by the current oceanographic paradigm, in which Fe is operationally-defined as particulate/colloidal/dissolved/soluble according to the ultra-filtration size cut-offs employed. In this work, the terms ‘colloid’ and ‘particle’ are used interchangeably to describe the small-sized (20 nm to greater than 2 µm diameter) solid-phase bound Fe phases suspended in the marine water column. This 20 nm size restriction relates purely to the detection limit associated with the resolution of the x-ray microscopy technique used.

In Chapter 2, however, discussion relating to colloidal iron (cFe) and iron colloids makes reference to the operational size definitions employed in the literature. Total dissolvable iron (TDFe), used interchangeably with the term total iron (TFe), is the the total iron measured in unfiltered samples that have been stored for six months at a pH of 1.8 or 2. Dissolved iron (dFe) concentration measurements refer to the concentration of Fe present in seawater that hs been filtered through 0.45 µm, 0.4 µm or 0.2 µm pore-size fiters. Similarly the soluble iron (sFe) concentration is the total Fe concentration that can pass through 0.02 µm, 200 kDa or 1000

kDa filters. Colloidal iron (cFe) and particulate iron (PFe) measurements are calculated empirically as [dFe]-[sFe] and [TDFe]-[dFe] respectively, where square brackets indicate measured concentrations. Size fractions can be differentiated using either the pore size of the membrane filter used (in microns (µm)) or by molecular weight cut-offs (in kilodaltons (kDa)), if hollow fibre filtration was used.

The L-edge is a quantum chemistry term that refers to electronic transitions from the 2p orbitals to higher energy states. The difference in energy between the L_2 and the L_3 edge, which both contain the same information, arises because the same electronic transitions are made but with electrons of opposite spin. This study focuses on the L_3 edge which has sharper features and is thus easier to quantify.

Abbreviations of all terms are given in the respective chapter in which they are found, following the first usage of the term. Abbreviations that are typically used in this thesis include: Fe (iron), Fe_{Oh} (iron in octahedral coordination), Fe_{Td} (iron in tetrahedral coordination), FeOOH (iron oxyhydroxide), Al (aluminum), C (carbon), HNLC (High Nutrient Low Chlorophyll region), SANAE (South African National Antarctic Expedition (place name)), XAS (X-ray Absorption Spectroscopy), XANES (X-ray Absorption Near-Edge Structure), STXM (Scanning Transmission X-ray Microscopy), eV (electron volts), ΔeV (difference in energy in electron volt units), IR (Intensity Ratio), $nmol.L^{-1}$ or nM (nano-molar concentration), nm (nanometers), µm (micrometers), kDa (kilodaltons).

REFERENCES

Aguilar-Islas, A.M., Rember, R.D., Mordy, C.W., Wu, J., 2008. Sea ice-derived dissolved iron and its potential influence on the spring algal bloom in the Bering Sea. Geophysical Research Letters 35, L24601.

Archer, D.E., Johnson, K.S., 2002. A model of the iron cycle in the ocean. Global Biogeochemical Cycles 14, 269-279.

Barbeau, K., 2006. Photochemistry of organic iron(III) complexing ligands in oceanic systems, Photochemistry and Photobiology., 82(6).

Bergquist, B.A., Wu, J., Boyle, E.A., 2007. Variability in oceanic dissolved iron is dominated by the colloidal fraction. Geochimica et Cosmochimica Acta 71, 2960-2974.

Bluhm, H., Andersson, K., Araki, T., Benzerara, K., Brown, G.E., Dynes, J.J., Ghosal, S., Gilles, M.K., Hansen, H.-Ch., Hemminger, J.C., Hitchcock, A.P., Ketteler, G., Kilcoyne, A.L.D., Kneedler, E., Lawrence, J.R., Leppard, G.G., Majzlam, J., Mun, B.S., Myneni, S.C.B., Nilsson, A., Ogasawara, H., Ogletree, H.F., Pecher, K., Salmeron, M., Shuh, D.K., Tonner, B., Tyliszczak, T., Warwick, T., Yoon, T.H., 2006. Soft X-ray microscopy and spectroscopy at the molecular environmental science beamline at the Advanced Light Source. Journal of Electron Spectroscopy and Related Phenomena 150, 86-104.

Bowie, A. R., Achterberg, E.P., Blain, S., Boye, M., Croot, P.L., de Baar, H.J.W., Laan, P., Sarthou, G., Worsfold, P.J., 2003. Shipboard analytical intercomparison of dissolved iron in surface waters along a north–south transect of the Atlantic Ocean. Marine Chemistry 84(1), 19-34.

Boyd, P.W., Ellwood, M.J., 2010. The biogeochemical cycle of iron in the ocean. Nature Geoscience 3, 675-682.

Boyd, P.W., Trull, T.W., 2007. Understanding the export of biogenic particles in oceanic waters: Is there consensus? Progress in Oceanography 72(4), 276-312.

Boyd, P.W., Jickells, T., Law, C.S., Blain, S., Boyle, E.A., Buesseler, K.O., Coale, K.H., Cullen, J.J., de Baar, H.J.W., Follows, M., Harvey, M., Lancelot, C., Levasseur, M., Owens, N.P.J., Pollard, H., Rivkin, R.B., Sarmiento, J., Schoemann, V., Smetacek, V., Takeda, S., Tsuda, A., Turner, S., Watson, A.J., 2007. Mesoscale iron enrichment experiments 1993-2005: Synthesis and future directions. Science 315, 612-617.

Boye, M., Nishioka, J., Croot, P., Laan, P., Timmermans, K.R., Strass, V.H., Takeda, S., and de Baar, H.J.W., 2010. Significant portion of dissolved organic Fe complexes in fact is colloids. Marine Chemistry 122, 20-27.

Breitbarth, E., Achterberg, E.P., Ardelan, M.V., Baker, A.R., Bucciarelli, E., Chever, F., Croot, P.L., Duggen, S., Gledhill, M., Hasselöv, M., Hassler, C., Hoffmann, L.J., Hunter, K.A., Hutchins, D.A., Ingri, J., Jickells, T., Lohan, M.C., Nielsdóttir, M.C., Sarthou, G., Schoemann, V., Trapp, J.M., Turner, D.R., Ye, Y., 2010. Iron biogeochemistry across marine systems- progress from the past decade. Biogeosciences 7, 1075-1097.

Caldeira, K., Duffy, P.B., 2000. The role of the Southern Ocean in uptake and storage of anthropogenic carbon dioxide. Science 287, 620-622.

Cassar, N., Bender, M.L., Barnett, B.A., Fan, S., Moxim, W.J., Levy, H., Tilbrook, B., 2007. The Southern Ocean biological response to aeolian iron deposition. Science 317, 1067-1070.

Chever, F., Sarthou, G., Bucciarelli, E., Blain, S., Bowie, A.R., 2010. An iron budget during the natural iron fertilisation experiment KEOPS (Kerguelen Islands, Southern Ocean). Biogeosciences 7, 455-468.

Compton, J., Herbert, C., Schneider, R., 2009. Organic-rich mud on the western margin of southern Africa: Nutrient source to the Southern Ocean? Global Biogeochemical Cycles 23(4), GB4030.

Cullen J.T., Bergquist B.A., Moffett J.W., 2006. Thermodynamic characterization of the partitioning of iron between soluble and colloidal species in the Atlantic Ocean. Marine Chemistry 98, 295-303.

de Baar, H.J.W., de Jong, J.T.M., Bakker, D.C.E., Löscher, B.M., Veth, C., Bathmann, U., Smetacek, V., 1995. Importance of iron for plankton blooms and carbon dioxide drawdown in the Southern Ocean. Nature 373, 412–415.

de Baar, H.J.W., Boyd, P.W., Coale, K.H., Landry, M.R., Tsuda, A., Assmy, P., Bakker, D.C.E., Bozec, Y., Barber, R.T., Brzezinski, M.A., Buesseler, K.O., Boyé, M., Croot, P.L., Gervais, F., Gorbunov, M.Y., Harrison, P.J., Hiscock, W.T., Laan, P., Lancelot, C., Law, C.S., Levasseur, M., Marchetti, A., Millero, F.J., Nishioka, J., Nojiri, Y., van Oijen, T., Riebesell, U., Rijkenberg, M.J.A., Saito, H., Takeda, S., Timmermans, K.R., Celdhuis, M.J.W., Waite, A.M., Wong, C.-S., 2005. Synthesis of iron fertilization experiments: From the Iron Age in the Age of Enlightenment. Journal of Geophysical Research: Oceans (1978–2012) 110(C9).

Elrod, V.A., Berelson, W.M., Coale, K.H., Johnson, K.S., 2004. The flux of iron from continental shelf sediments: a missing source for global budgets. Geophysical Research Letters 31, L12307.

Fischer, G., Karakaş, G., 2009. Sinking rates and ballast composition of particles in the Atlantic Ocean: implications for the organic carbon fluxes to the deep ocean. Biogeosciences 6(1), 85-102.

Frew, R. D., Hutchins, D. A., Nodder, S., Sanudo-Wilhelmy, S., Tovar-Sanchez, A., Leblanc, K., Hare, C. E., Boyd, P. W., 2006. Particulate iron dynamics during FeCycle in subantarctic waters southeast of New Zealand, Global Biogeochemical Cycles 20(1).

Gledhill, M., van den Berg, C.M.G., 1994. Determination of complexation of iron(III) with natural organic complexing ligands in seawater using cathodic stripping voltammetry. Marine Chemistry 47, 41-54.

Gonzalez-Davila, M., Santana-Casiano, J.M., Millero, F.J., 2006. Competition between O_2 and H_2O_2 in the oxidation of Fe(II) in natural waters, Journal of Solution Chemistry 35(1), 95-111.

Hassler, C.S., Schoemann, V., Nichols, C.M., Butler, E.C.V., Boyd, P.W., 2011. Saccharides enhance iron bioavailability to Southern Ocean phytoplankton. Proceedings of the National Academy of Sciences 108(3), 1076-1081.

Ho, T.Y., Quigg, A., Finkel, Z.V., Milligan, A.J., Wyman, K., Falkowski, P.G., Morel, F.M.M., 2003. The elemental composition of some marine phytoplankton. Journal of Phycology 39, 1145-1159.

Hutchins, D.A., Witter, A.E., Butler, A., Luther III, G.W., 1999. Competition among marine phytoplankton for different chelated iron species. Nature 400, 858-861.

Jickells, T. D., An, Z.S., Andersen, K.K., Baker, A.R., Bergametti, G., Brooks, N., Cao, J.J., Boyd, P.W., Duce, R.A., Hunter, K.A., Kawahata, H., Kubilay, N., laRoche, J., Liss, P.S., Mahowald, N., Prospero, J.M., Ridgwell, A.J., Tegen, I., Torres, R., 2005. Global iron connections between desert dust, ocean biogeochemistry, and climate. Science 308, 67-71.

Johnson, K.S., Gordon, R.M., Coale, K.H., 1997. What controls dissolved Iron concentration in the World Ocean? Marine Chemistry 57, 137–161.

Kepkay, P.E., 1994. Particle aggregation and the biological reactivity of colloids. Marine Ecology Progress Series 109 (2–3), 293-304.

Kraemer, S.M., 2004. Iron oxide dissolution and solubility in the presence of siderophores. Aquatic Sciences 66, 3-18.

Lannuzel, D., Schoemann, V., de Jong, J., Chou, L., Delille, B., Becquevort, S., Tison, J.L., 2008. Iron study during a time series in the western Weddell pack ice. Marine Chemistry 108(1), 85-95.

Lam, P.J., Bishop, J.K., Henning, C.C., Marcus, M.A., Waychunas, G.A., Fung, I.Y., 2006. Wintertime phytoplankton bloom in the subarctic Pacific supported by continental margin iron. Global Biogeochemical Cycles 20(1).

Liu, X.W., Millero, F.J. 2002. The solubility of iron in seawater. Marine Chemistry 77, 43-54.

Martin, J.H., Fitzwater, S.E., 1988. Iron deficiency limits phytoplankton growth in the northeast Pacific subarctic. Nature 331, 341-343.

Martin, J.H., 1992. Iron as a limiting factor in oceanic productivity. Primary Productivity and Biogeochemical Cycles in the Sea, 123-137.

Martin, J. H., Coale, K.H., Johnson, K.S., Fitzwater, S.E., Gordon, R.M., Tanner, S.J., Hunter, C.N., Elrod, V.A., Nowicki, J.L., Coley, T.L., Barber, R.T., Lindley, S., Watson, A.J., van Scoy, K., Law, C.S., Liddicoat, M.I., Ling, R., Stanton, T., Stockel, J., Collins, C., Anderson, A., Bidigare, R., Ondrusek, M., Latasa, M., Millero, F.J., Lee, K., Yao, W., Zhang, J.Z., Friederich, G., Sakamoto, C., Chavez, F., Buck, K., Kolber, Z., Greene, R., Falkowski, P., Chisholm, W., Hoge, F., Swift, R, Yungel, J., Turner, S., Nightingale, P., Hatton, A., Liss, P., Tindale, N.W., 1994. Testing the iron hypothesis in ecosystems of the equatorial Pacific Ocean. Nature 371, 123-129.

Mawji, E., Gledhill, M., Milton, J.A., Tarran, G.A., Ussher, S., Thompson, A., Wolff, G.A., Worsfold, P.J., Achterberg, E.P., 2008. Hydroxamate siderophores: occurrence and importance in the Atlantic Ocean. Environmental Science & Technology 42(23), 8675-8680.

Michel, K.-M., Pistorius, E.K., 2004. Adaptation of the photosynthetic electron transport chain in cyanobacteria to iron deficiency: The function of IdiA and IsiA. Physiologia Plantarum 120, 36-50.

Miller, W.L., King, D.W., Lin, J., Kester, D.R.,1995. Photochemical redox cycling of iron in coastal seawater. Marine Chemistry 50, 63-77.

Moore, J.K., Doney, S.C., Glover, D.M., Fung, I.Y., 2001. Iron cycling and nutrient-limitation patterns in surface waters of the World Ocean. Deep-Sea Research 49, 463-507.

Moore, J. K., Braucher, O., 2008. Sedimentary and mineral dust sources of dissolved iron to the world ocean, Biogeosciences 5, 631-656.

Parekh, P., Follows, M.J., Boyle, E., 2004. Modeling the global ocean iron cycle. Global Biogeochemical Cycles 18, GB1002.

Poulton, S.W., Raiswell, R., 2002. The low temperature geochemical cycle of iron: from continental fluxes to marine sediment deposition. American Journal of Science 302, 774-805.

Raiswell, R., Tranter, M., Benning, L.G., Siegert, M., De'arth, R., Huybrechts, P., Payne, T., 2006. Contributions from glacially derived sediment to the global iron (oxyhydr)oxide cycle: Implications for iron delivery to oceans. Geochimica et Cosmochimica Acta 70, 2765-2780.

Ridame, C., Guieu, C., 2002. Saharan input of phosphorus to the oligotrophic water of the open western Mediterranean. Limnology and Oceanography 47(3), 856-869.

Rue, E.L., Bruland, K.W., 1995. Complexation of iron(III) by natural organic ligands in the central north Pacific as determined by a new competitive ligand equilibration/absorptive cathodic stripping voltammetric method. Marine Chemistry 50, 117-138.

Shaked, Y., Kustka, A.B., Morel, F.M.M., 2005. A general kinetic model for iron acquisition by eukaryotic phytoplankton. Limnology and Oceanography 50, 872-882.

Smith, K.L., Robison, B.H., Helly, J.J., Kaufmann, R.S., Ruhl, H.A., Shaw, T.J., Twining, B.S., Vernet, M., 2007. Free-drifting icebergs: Hot spots of chemical and biological enrichment in the Weddell Sea. Science 317, 478-482.

Sunda, W.G., 2001. Bioavailability and bioaccumulation of iron in the sea. IUPAC Series on Analytical and Physical Chemistry of Environmental Systems 7, 41-84.

Tagliabue, A., Bopp, L., Dutay, J.-C., Bowie, A.R., Chever, F., Jean-Baptiste, P., Bucciarelli, E., Lannuzel, D., Remenyi, T., Sarthou, G., Aumont, O., Gehlen, M., Jeandel, C., 2010. Hydrothermal contribution to the dissolved iron inventory. Nature Geoscience 3(4), 252-256.

Tagliabue, A., Volker, C., 2011. Towards accounting for dissolved iron speciation in global ocean models. Biogeosciences Discussions 8, 2775-2810.

Tagliabue, A., Mtshali, T., Aumont, O., Bowie, A.R., Klunder, M.B., Roychoudhury, A.N, Swart, S., 2012. A global compilation of dissolved iron measurments: focus on distributions and processes in the Southern Ocean. Biogeosciences 9, 2333-2349.

Thuróczy, C.-E., Gerringa, L.J.A., Klunder, M.B., Laan, P., de Baar, H.J.W., 2011. Observations of consistent trends in the organic complexation of dissolved iron in the Atlantc Sector of the Southern Ocean. Deep-Sea Research II 58, 2695-2706.

Thuróczy, C.-E.; Gerringa, L.J.A.; Klunder, M.; Laan, P., Le Guitton; de Baar, H.J.W., 2011. Distinct trends in the speciation of iron between the shallow shelf and the deep basins of the Arctic Ocean. Journal of Geophysical Research 116, C10009.

Tortelle, P.D., Maldonado, M.T., Granger, J., Price, N.M., 1999. Marine bacteria and biogeochemical cycling of iron in oceans. FEMS Microbiology Ecology 29, 1-11.

Turner, D.R., Hunter, K.A., 2001. The Biogeochemistry of Iron in Seawater, IUPAC Series on Analytical and Physical Chemistry of Environmental Systems, JohnWiley and Sons Ltd.,West Sussex, England, 396 pp.

Voelker, B.M., Sedlak D.L., 1995. Iron reduction by photoproduced superoxide in seawater. Marine Chemistry 50, 93-102.

Von der Heyden, B.P., Roychoudhury, A.N., Mtshali, T.N., Tyliszczak, T., Myneni, S.C.B., 2012. Chemically and geographically distinct solid-phase iron pools in the Southern Ocean. Science 338, 1199-1201.

Weber, K.A., Achenbach, L.A., Coates, J.D., 2006. Microorganisms pumping iron: anaerobic microbial iron oxidation and reduction. Nature Reviews Microbiology 4(10), 752-764.

Wells, M.L., Goldberg, E.D., 1993. Colloid aggregation in seawater. Marine Chemistry 41, 353-358.

Wells, M.L., 1998. Marine colloids: A neglected dimension. Nature 391, 530-531.

Wu, J.F., Luther III, G.W., 1995. Complexation of Fe(III) by natural organic ligands in the Northwest Atlantic Ocean by competitive ligand equilibration method and a kinetic approach. Marine Chemistry 50, 159-178.

Wu, J., Boyle, E.A., Sunda, W., Wen, L., 2001. Soluble and colloidal iron in the oligotrophic North Atlantic and North Pacific. Science 293, 847-849.

CHAPTER 2

Colloidal iron in the surface open ocean

A presentation of the prepared research paper

This research manuscript has been prepared for submission to the journal *Marine Chemistry*. I am the lead author on the work and Prof. Alakendra Roychoudhury is co-author.

This manuscript reviews the status of knowledge in the field of size-fractionated marine colloidal iron measurements and behaviour. It presents a global compilation of soluble (sFe) and dissolved (dFe) iron measurements from which corresponding colloidal iron (cFe) values could be empirically derived. The cFe dataset is evaluated for spatial and seasonal trends. Controls on cFe concentration, and limitations associated with size-fractionated Fe study are further discussed.

Data compilation, through extensive literature review, was performed by me, although the obliging contribution by a host of the cited authors and the British Oceanographic Data Centre must also be acknowledged. I was also responsible for the written work and the creation of all of the diagrams. Prof. Alakendra Roychoudhury conceptualized the idea of a review paper and contributed towards the writing in the capacity of a typical second author. Dr. Alessandro Tagliabue must also be acknowledged for useful discussion that aided in giving the manuscript initial direction.

Colloidal iron in the surface open ocean

B.P. von der Heyden[a], A.N. Roychoudhury[a,*]

a. Department of Earth Sciences, Stellenbosch University, Private Bag X1, Matieland, 7602, South Africa

ABSTRACT

The results of early work suggest that different size fractions of iron have differing biogeochemical behaviour [Science 293 (2001) 847]. Since then, various studies have utilized Fe size-fractionated data to investigate aspects of Fe cycling and interactions with biology. Here we present and review a compilation of over 750 soluble and corresponding dissolved Fe concentration measurements from which operationally-defined colloidal Fe (cFe) data can be extracted. We find that the distribution of surface ocean cFe is controlled predominantly by the magnitude of Fe source terms and the concentration of Fe-binding ligands, with thermodynamic considerations playing a secondary role. Indirect evidence suggests that a significant proportion of this cFe pool is involved in supporting and sustaining biological growth. However, the issue of Fe colloid bioavailability can only be resolved once the phytoplankton Fe uptake mechanisms have been related to the functional group chemistry of organic Fe colloids and the surface chemistry of inorganic Fe colloids. Future work should endeavour to investigate these molecular level considerations more fully by complementing size-fractionated data with data attained by directly probing colloid chemistry.

1. INTRODUCTION

Despite the ubiquity of iron in terrestrial systems, its exceedingly low solubility has resulted in its status as a trace metal in the open ocean, where Fe concentrations typically range between pico-molar levels and 2-3 nmol.L^{-1}. Iron is also an essential nutrient for marine biological growth and functioning (Boyd and Ellwood, 2010) and these low open ocean Fe concentrations can control and limit optimal primary productivity and thus, biologically-mediated air-sea CO_2 exchange. For these reasons and in order to more fully understand the ocean system, marine biogeochemists have included Fe concentration measurements into their suite of analytical tools.

Recent advances in trace-metal clean sampling techniques (Cutter and Bruland, 2012) coupled with the enhanced detection limits of modern Fe analytical methods (Bowie et al., 2003) have enabled focused studies into the distribution, profiling and size fractionation of Fe along a multitude of transects throughout the world's ocean basins (see Tagliabue et al., 2012 for a recent compilation of over 13 000 measurements). These studies typically distinguish between "particulate" (PFe) and "dissolved" (dFe) size fractions, using either a 0.2 µm or 0.4 µm filter pore size as the nominal size cut-off. Particulate Fe includes the largest size

fraction of lithogenic Fe which is typically associated with ballasting processes and rapid sinking to depth (Croot et al., 2004), although there is indication of a more dynamic PFe cycle in the upper water column, involving efficient conversions to the biogenic PFe pool (Frew et al., 2006). Biogenic PFe can be intracellular or extracellular and can be converted to smaller size classes and made available by recycling processes such as cell lysis and grazing (Strzepek et al., 2005; Sarthou et al., 2008). Dissolved Fe profiles commonly exhibit a nutrient-like profile with biological uptake and scavenging in the upper water column and remineralisation at depth (Johnson et al., 1997). Values for dFe in the surface (upper 200 m) waters of the open ocean generally range between 0.02 to 1 nmol.L^{-1} (avg: 0.49 ± 0.57 nmol.L^{-1} (Tagliabue et al., 2012)) and can reach concentrations that are up to two orders of magnitude greater in coastal surface waters (Bruland and Rue, 2002). Excesses in the reported dFe concentrations, relative to the thermodynamic stability of Fe oxyhydroxides (0.08 nmol.L^{-1}; Wu et al., 2001), are commonly attributed to the enhanced solubility of Fe in the presence of organic ligands (Kuma et al., 1996; Liu and Millero, 2002). However, an alternative or perhaps complementary explanation invokes the presence of a substantial contribution of colloidal-bound Fe to the operationally-defined dFe pool (Nishioka et al., 2001; Bergquist et al., 2007).

With the advent of ultra-filtration techniques, researchers are now able to determine the concentration of "soluble" iron (sFe); constituting the smallest size fraction of Fe passing through a 0.02 µm, 200 kDa or 1000 kDa filter (Wu et al., 2001; Nishioka et al., 2001; Thuróczy et al., 2010). Because the smaller pore sizes give a better approximation of the truly dissolved inorganic Fe (Fe') concentration and because sFe depth profiles also commonly exhibit nutrient profiles (Wu et al., 2001), reported sFe values are generally deemed a better proxy for measuring the size of the bioavailable Fe pool (Boye et al., 2010). Just as importantly, sFe measurements allow for the empirical determination of the "colloidal" Fe pool (cFe), given as the difference between the concentrations of dFe and sFe. Although marine colloids have long been identified as the dominant class of particles in the ocean (Wells, 1998), it was the seminal work by Wu *et al.* (2001) that first used ultrafiltration techniques to demonstrate a decoupling between cFe and sFe behaviour and cycling. Colloidal Fe has been shown to play an important role in controlling dFe variability (Bergquist et al., 2007), and cFe utilization by phytoplankton has been revealed through direct experimentation (Chen et al., 2003, Nodwell and Price, 2001) and suggested from a host of indirect evidence derived from size-fractionated oceanographic data (Hurst and Bruland, 2007; Chever et al., 2010; Ussher et al., 2010; Thuróczy et al., 2011).

To our knowledge, there has not as yet been a global compilation of sFe, and thus cFe measurements, which can be used to broaden our understanding of these important Fe pools in the context of the world ocean. Here we review the current understanding of the cFe pool and evaluate its importance and significance in the context of the marine biogeochemical system. We present an up-to-date compilation of over 750 sFe and cFe measurements, which is made available to the scientific community and will augment the current global dFe database (Tagliabue et al., 2012). Our analyses focus on the upper 200 meters of the water column, representing the euphotic zone where light penetration can facilitate the growth of photosynthetic organisms.

We further assess the factors that control cFe concentration values in the open ocean euphotic zone and attempt to understand the behaviour of this important and dynamic pool in terms of seasonal and inter-basin variations. Finally, a part of this review is devoted to evaluating the limitations and merits of operationally-defined size-fractionated Fe study, given that utilization and inter-conversion between different Fe pools will be more strongly controlled by chemical constraints, especially organic- and ligand-metal interactions and, for inorganic colloids, surface chemistry and mineralogy.

2. METHODS

We have assimilated a database of 818 sFe measurements (Fig. 1a; Appendix A) collected from 26 size-fractionated ocean studies, including one database collected by Simon Ussher and made available by the British Oceanographic Data Center (BODC). In these studies, the sFe ultra-filtration pore-size cut-offs ranged between 1 nm and 1000 kDa (Table 1). The depth and concentration values for each data point were either collected from published tables or, in cases where only profiles were presented, accessed through direct communication with the relevant and obliging corresponding author. In the rare instances where the corresponding author could not be accessed (two data sets), the published figures were digitized using the graphics program GIMP2 and values were thus determined manually. The error introduced through this manual derivation of the concentration values is deemed to be negligible relative to standard deviations reported in other datasets. All sFe measurements were collected along with, where presented, the corresponding dFe, total Fe, salinity and temperature datasets (Table 1).

At each sample site, cFe concentrations are calculated by subtracting the Fe concentration measured in the sFe fraction (all Fe passing through a 0.02 µm, 200 kDa or 1000 kDa filter) from the concentration in the dFe size fraction (Fe that passes through a 0.2, 0.4 or 0.45 µm filter). Because of a general paucity in stated standard deviations associated with reported measurements, our work does not attempt to quantify or track error propagation through the various analyses. However, in reviewing the precision of reported size-fractionated Fe measurements, error propogation was used when expanding the discussion to include the precision of cFe measurements. Other artefacts associated with this simple difference method for calculating the cFe pool have been noted in Wells (2003) and are further discussed in subsequent sections of this manuscript.

Because of the biologically-mediated link between Fe availability and the carbon cycle, our analyses focus on the euphotic zone of the water column, where light penetration has the potential to drive photosynthetic productivity. Because transmittance data were not provided with each dataset, the depth limit of the euphotic zone was deemed to have a base at 200 meters. This assumption does thus not differentiate out sampling sites that are characterized by lower light depth-penetration; such as sites at high latitudes that receive a lower incidence light, or sites with high particle loading and thus higher light attenuation due to absorption and scattering. The averaged Fe concentration was considered to be constant between the depths of 0 and 200

meters, irrespective of the depth of the mixed layer, sampling depth biases or structure of the Fe concentration profile in the upper 200m. Biological activity is often strongly seasonal (Thomalla et al., 2011) and for the purposes of this study, the year is divided into quarters accordingly: Dec, Jan, Feb (austral summer/boreal winter); Mar, Apr, May (austral autumn/boreal spring); June, July, Aug (austral winter/boreal summer) and Sept, Oct, Nov (austral spring/boreal autumn).

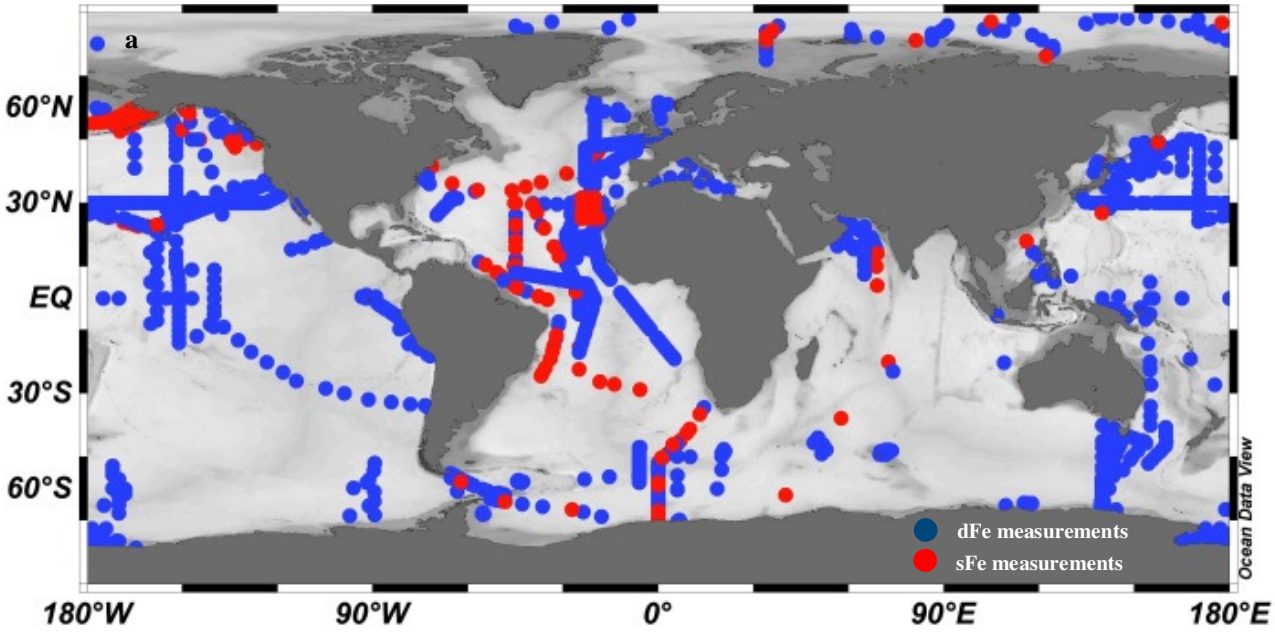

Figure 1a: *Global distribution of sampling sites for marine dFe (blue) and sFe (red) concentration measurements. Data for dFe are from Tagliabue et al. (2012) and data for sFe are reported in Appendix A.*

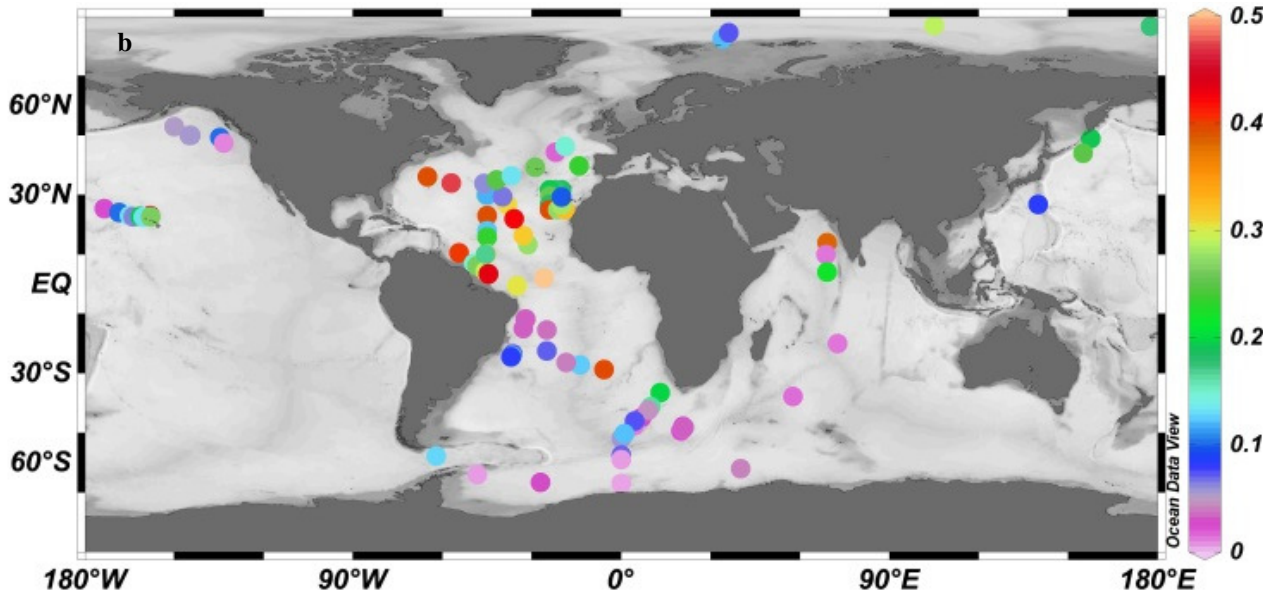

1b: *Distribution and depth-averaged cFe values for the open ocean euphotic zone sampling sites focussed on in this study. Colour scale bar gives concentration values measured in nmol.L^{-1}.*

The majority of our analyses are limited to the euphotic zone of the most remote regions of the oceans ('open ocean' sites; Fig. 1b). Fresh Fe supply terms to open ocean sites, whether from circulation dynamics or terrestrial sources, are least likely to skew the observed trends reported in our analyses. Additional data from shelf settings and semi-enclosed water masses (i.e. marginal seas and gulf settings) have however been included in the presented dataset (Appendix A) and are used for comparative purposes to highlight the low cFe concentration values associated with the open ocean (Fig. 2). 'Open ocean' sites are distinguished from 'shelf' sites (which are plausibly influenced by shelf sources and dynamics) by using a bathymetric bottom depth assigned at 2000 m. 'Coastal' sites were further distinguished as being on the shelf but with the additional stipulation by respective authors that they were sampled within a bay. In figure 3, the open ocean data are further compared across the six of the world's major ocean basins. The Southern Ocean is defined as the water mass located south of the sub-Antarctic Front and the Arctic Ocean is found north of 70°N. The Pacific, Atlantic and Indian Oceans are divided up using the southern-most tips of South America, Africa and Australia and the equator is used to sub-divide basins into northern and southern sections.

Finally, inorganic controls (including pH, salinity and temperature) can also have a pronounced influence on Fe size-partitioning and behaviour (Liu and Millero, 2001, Kuma et al., 1996). The dataset presented in Appendix A has been expanded to include 164 salinity data points (32.5- 37.5) and to 143 temperature data points (-1.9°C- 29.1°C) for comparison to the compiled size-fractionated Fe data. Where both the corresponding salinity and temperature values were reported, cFe and sFe data were compared to the theoretical solubility of Fe, as calculated by the equations of Liu and Millero (2002).

3. RESULTS

The entire compilation of literature sFe values is listed in Appendix A at the end of this thesis. The table includes 756 cFe concentration values from sampling sites ranging from estuarine and coastal settings to the remotest parts of the open ocean. There are an additional fifteen sFe datapoints for which there are no dFe measurements, and for which no cFe values could thus be derived. A further 46 datapoints reported in the literature were necessarily removed from our compilation, either because they had been flagged by the original author or because reported dFe measurements were smaller than the reported sFe measurements, rendering an inaccurate (negative) cFe value.

The dataset is comprised of 51 coastal bay cFe values, 78 cFe values regarded as shelf values (bottom depth <2000 m), 91 values from marginal seas (South China Sea (Wen et al., 2006), Bering Sea (Hurst et al., 2010; Hurst and Bruland, 2007)) and 534 values taken from the open ocean, of which roughly half are located in the upper 200m (Fig. 2). Although not the focus of the study, an additional two estuarine data points have been incorporated into this data set because they were reported within one of the relevant coastal studies (Kuma et al., 1998). The highest cFe values are found at coastal and estuarine sites (0-19 $nmol.L^{-1}$), decrease in shelf settings (avg. 0.91 $nmol.L^{-1}$) and are lowest at open ocean sites, where concentration values range

Table 1: Complementary datasets presented along with sFe/cFe data, and size cut-offs employed in various, pertinent published studies.

Study	Ocean Basins	sFe size fraction	dFe size fraction	TFe[1]	Temp	Salinity	pH	Bio[2]	O_2	NO_2/ NO_3	SO_4	PO_4	Ligand sizes	Other
Baeyens et al, 2011	N. Pacific S. Ocean	1nm 10nm		X										Co, Cu, Cd, Ni, Pb
Bergquist et al, 2007	N.+S. Atlantic	0.02µm	0.4µm			X		X	X		X			
Boye et al, 2010	S. Ocean	200kDa	0.2µm		X	X		X		X	X		X	
Boyle et al, 2005	N. Pacific	0.02µm	0.4µm	X	X	X			X					
Chever et al, 2010	S. Atlantic S. Ocean	0.02µm	0.2µm	X	X	X								
Cullen et al, 2006	N.+S. Atlantic	0.02µm	0.4µm										X	
Fitzsimmons and Boyle, 2012	N. Pacific	0.02µm	0.2µm 0.4µm											
Hurst et al, 2010	Bering Sea	0.03µm	0.2µm	X	X	X		X		X	X	X		Al, Mn
Hurst and Bruland, 2007	Bering Sea	0.03µm	0.2µm	X		X		X						
Hurst and Bruland, 2008	N. Pacific	200kDa	0.2µm	X	X	X		X		X	X	X		Al, Zn, Cu, Pb, Cd, Mn
Kuma et al, 1998	N. Pacific	0.025µm	0.45µm		X	X		X		X	X	X		
Kuma et al, 2000	N. Pacific	0.025µm	0.22µm	X	X	X		X		X	X	X		
Nishioka and Takeda, 2000	N. Pacific	200kDa	0.2µm	X										
Nishioka et al, 2001	N. Pacific	200kDa 0.03µm	0.2µm 0.45µm	X	X	X			X	X	X	X		
Nishioka et al, 2003	N. Pacific	200kDa	0.2µm	X										
Nishioka et al, 2013	Indian S. Ocean	1000kDa	0.2µm		X	X			X	X		X		
Thuroczy et al, 2010	N. Atlantic	1000kDa	0.2µm	X	X	X		X					X	
Thuroczy et al, 2011	Arctic	1000kDa	0.2µm	X	X	X		X	X				X	
Thuroczy thesis	S. Atlantic S. Ocean	1000kDa	0.2µm	X	X	X		X		X	X	X	X	
Ussher et al, 2010	N. Atlantic	0.02µm	0.2µm		X	X		X		X		X		
Ussher AMT16[3]	N.+S. Atlantic	0.02µm	0.2µm	X	X	X								
Wen et al, 2006	S. China Sea	1kDa	0.4µm		X	X		X	X	X	X	X		Cu, Cd, Ni, NH_3
Wells, 2000	N. Atlantic	1kDa 8kDa	0.2µm	X		X	X			X	X	X		Mn, Cu, Ni, Zn
Wu et al, 2001	N. Atlantic N. Pacific	0.02µm	0.4µm										X	
Wu et al, 2009	N. Pacific	0.025µm	0.4µm	X		X		X		X	X			

[1]TFe: range of methodologies employed to measure total (dissolvable) Fe; [2]Biology data includes fluorescence and chl-a data; [3]BODC dataset

between 0 and 0.81 nmol.L^{-1} in surface waters and between 0 and 1.13 nmol.L^{-1} at depths greater than 200 m. This trend in increasing cFe concentration with depth is not observed for shelf samples, where high concentrations in the surface waters (<200 m) are likely caused by shelf born and terrestrial fluxes- particularly at sites with shallow bathymetry.

The dataset was collected from a total of 25 different studies, each employing different choices in pore-sizes, analysis methodologies and supporting data (Table 1). Despite the intimate link between Fe chemistry, biological growth and major nutrient drawdown, only 52% of these studies have included biological data, chlorophyll-a values or fluorescence; and between 35-50% of the studies report corresponding nutrient data for silicate, nitrate and nitrite and phosphate concentrations.

Analyses in this study have been limited to measurements reported for the open ocean, with the focus primarily on the euphotic zone (N=258). Figure 3 depicts the distribution of the different operationally-defined size fractions of Fe among the various ocean basins. The particulate Fe fraction (PFe) is defined as the concentration of total (or total-dissolvable) Fe less the reported concentration of dFe, as measured by filtration through 0.2 µm or 0.4 µm filters. The PFe measurements reported in this figure are limited to those that correspond to our sFe and cFe measurements (Appendix A), and thus do not represent a global compilation of all available PFe measurements. In total, 94 PFe values are used in the analyses with an additional eight having been excluded because their values were negative, or because they were significant outliers (two points). Because PFe study is largely beyond the scope of this work, no attempt is made to distinguish between biogenic and lithogenic particulate Fe (Frew et al., 2006). In increasing order, the calculated average concentration for cFe in the euphotic zone of the various ocean basins is; Southern Ocean (0.04 nmol.L^{-1}, N= 36), South Atlantic (0.10 nmol.L^{-1}, N= 20), Indian Ocean (0.13 nmol.L^{-1}, N= 16), North Pacific (0.13 nmol.L^{-1}, N= 69), Arctic Ocean (0.16 nmol.L^{-1}, N= 9) and North Atlantic (0.24 nmol.L^{-1}, N=106). Ocean basins with the largest TFe

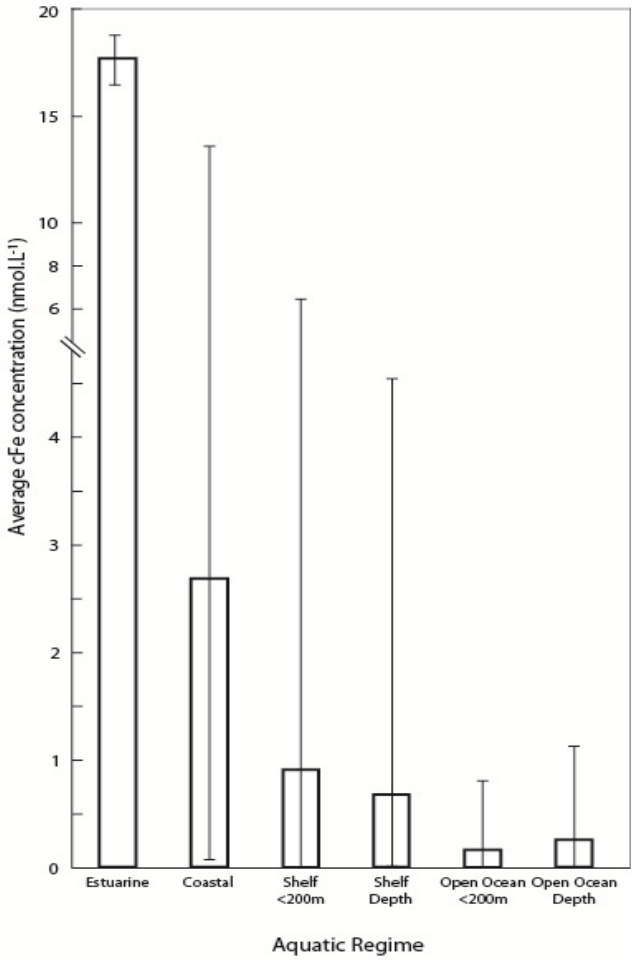

Figure 2: *Average cFe concentration values according to the aquatic regime from which they were sampled (boxes). Bars give the minimum and maximum reported concentration value per sampling regime. Note the break in the scale of the y-axis.*

concentration typically have the largest sFe and cFe concentrations and a linear correlation is observed between cFe and TFe concentrations reported in our dataset (r^2 = 0.541, N = 94; Fig. 4).

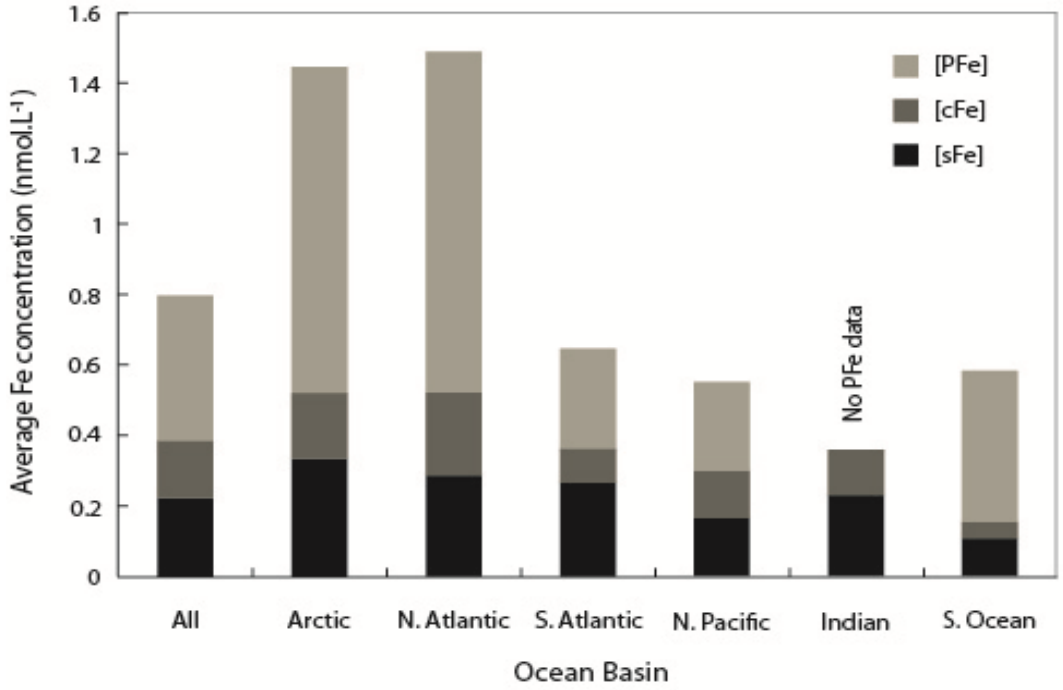

Figure 3: *Open ocean size-fractionated Fe data for the surface (upper 200m) waters generated from the subset of data which included total Fe (TFe) measurements (N=94). The height of each bar gives the average concentration per ocean basin and the cFe data are generated by subtracting reported soluble Fe (sFe) measurements dissolved Fe (dFe) measurements. Similarly, the particulate Fe (PFe) data are calculated by subtracting reported dFe measurements from reported TFe values.*

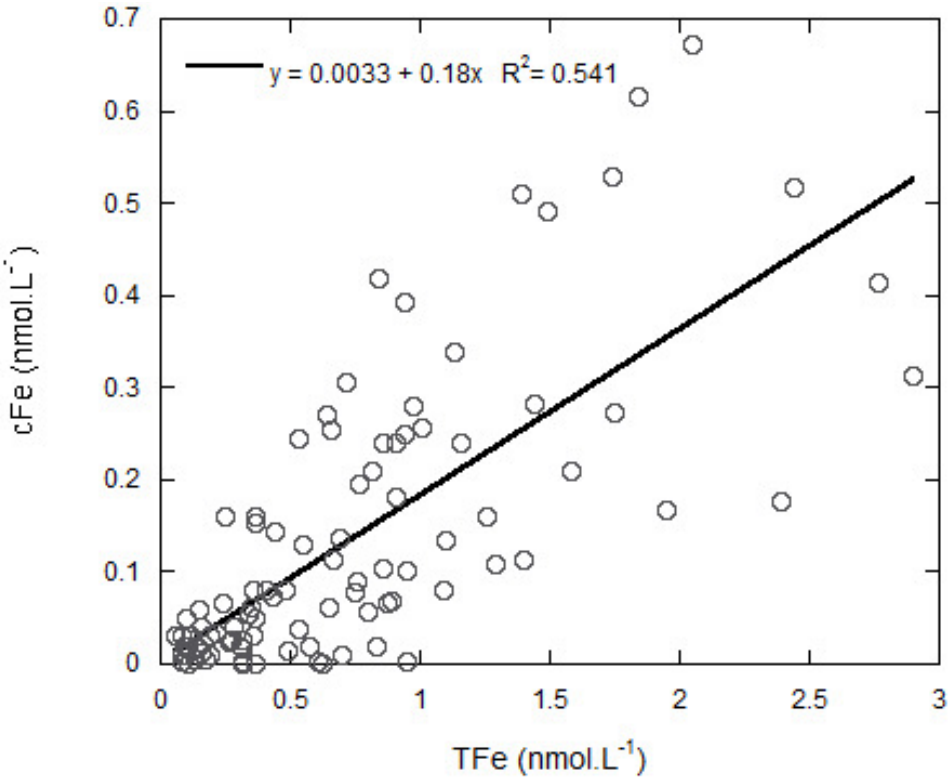

Figure 4: *Linear correlation between measured total Fe values (TFe) and calculated cFe values for all open ocean surface water sampling sites.*

4. DISCUSSION

4.1. Measurements of sFe and cFe concentration

Even under optimum sampling and analysis conditions, there are significant difficulties associated with generating accurate and precise size-fractionated Fe measurements. The empirical generation of cFe data requires sample collection from two size categories. The larger dFe size fraction is typically collected using cartridge filters (e.g. Acropak (PALL Co.)) and the smaller sFe measurements require a subsequent ultrafiltration procedure, using molecular size (membrane filters), molecular weight (hollow fibre filters) or molecular diffusion rate (field flow fractionation) cut-offs. This two-step process increases the handling, and thus potential for sampling-related error; and each ultrafiltration methodology is hampered by its own set of potential sampling artefacts. Multiple usages of the same filter, particularly the initial-step dFe Acropak filters, provide the potential for solubilisation of retained particulates- especially if the waters in subsequent filtrations are under-saturated with respect to Fe (Boye et al., 2010). Furthermore, the initial filtration step has the potential to cause disequilibrium in seawater by removal of the dFe fraction, which could induce repartitioning between the various size fractions (Thuróczy et al., 2011; Chin et al., 1998). Colloid disaggregation (Thuróczy et al., 2011), the unintended loss of undersized material (Howell et al., 2006) and preferential particle adsorption to filters (Boye et al., 2010) have also been suggested as a potential experimental artefacts during filtration and ultrafiltration processes.

Sample handling and storage introduce additional point sources for contamination and experimental artefacts. Particularly, adsorption of >50% of dFe to bottle walls has been shown to occur over a 70 hour period, but no clear trend was evident for cFe adsorption (Fitzsimmons and Boyle, 2012). Previous studies; however, have reported much smaller adsorption of labile Fe concentrations (<1% (Nishioka and Takeda, 2000)). Prolonged sample storage between subsequent filtrations can change the thermodynamic conditions experienced by the seawater sample. The volume of headspace in sample bottles allows for CO_2 outgassing causing shifts in pH and thus in the Fe solubility (Fitzsimmons and Boyle, 2012). These authors also found that warming the sample to room temperature resulted in increase in the cFe concentration, possibly caused by changes in the thermodynamic equilibrium (Liu and Millero, 2002), temperature-dependent aggregation reactions (Fitzsimmons and Boyle, 2012) or macrogel re-equilibration (Chin et al., 1998).

Finally, sampling biases can also be introduced during the measurement phase of data collection. Low concentrations (pM-nM) of Fe can be measured using voltammetric methods, chemiluminescence methods or Inductively Coupled Plasma Mass Spectrometry (ICP-MS) (Bowie et al., 2003, 2007). Electrochemical voltammetric methods provide the most direct study of Fe concentration as they do not require an initial pre-concentration step (Wen et al., 2006 and refs therein). These methods are however hampered by issues associated with lability, ligand heterogeneity, irreversible metal binding, adsorption of organics to the electrodes, and the size of the detection window (Mota and Correia Dos Santos, 1995). The other methods,

requiring a pre-concentration step, are susceptible to under-representation of Fe concentration if Fe is bound too strongly to ligands, thus limiting complete recovery by the resin column (Obata et al., 1997; Nishioka and Takeda, 2000; Fardy et al., 1992; Bowie et al., 2003). The degree of sample acidification can also impact on final Fe concentration measurements (Lohan et al., 2006; Johnson et al., 2007; Takata et al., 2009; Fujita et al., 2010), as can the presence of Fe(II), if hydrogen peroxide is not added to the sample prior to pre-concentration (Lohan et al., 2005; Nishioka et al., 2013).

The exceedingly low concentrations of Fe, characteristic of oceanic waters, make measurements especially sensitive to contamination. Given the ubiquity of potential contamination sources associated with shipboard measurements, it is particularly crucial to ensure that trace metal-clean conditions and handling protocols are rigorously observed at all times (Cutter et al., 2010). Yet, in spite of the awareness of this contamination issue within the marine Fe scientific community, a surprisingly high number (N= 46) of sFe measurements are reported either alongside dFe measurements that have been flagged, or as having greater concentration than their corresponding dFe measurements. These inaccuracies are spread over 9 of the 25 studies considered in Table 1 and constitute 10.5% of the total open ocean euphotic zone measurements reported in the literature. Further compounding these inaccuracies, is the level of precision associated with samples for which there are multiple measurements and for which standard deviation values have been reported. For example; for open ocean euphotic zone values reported with standard deviations, the average sFe value is 0.23 ±0.03 nmol.L^{-1}. An sFe imprecision factor can thus be calculated as the (sFe stdev)/[sFe] x 100 to give a 10.3% degree of imprecision. The imprecision associated with the corresponding dFe measurements is 7.1% and, because cFe data are derived empirically, error propagations result in an averaged imprecision factor of 77.4% for all cFe measurements for which standard deviation data have been reported (N= 160).

Inter-comparison between different size-fractionated Fe studies is further complicated by the use of different filtration methodologies and size cut-offs. Most notable is the use of molecular weight cut-offs (in kDa) as a proxy for the physical size of Fe particles. In reality, there is no simple or direct relationship between these two parameters, because macromolecules of the same molecular weight can exist in a variety of sizes, shapes and chemical compositions. The common understanding among scientists working with these kinds of filters, is that 200 kDa filters can be compared to a 0.03 µm size cut-off (Boye et al., 2010; Hurst et al., 2010) and the retentate after 1000 kDa filtration is comparable to a >0.1 µm size fraction (Thuróczy pers. comm.). When comparing cFe values generated from different data sets in which differing nominal size cut-offs have been employed, it is thus also critical to consider the influence that the difference in filter pore sizes has on the calculated empirical cFe concentration. Pore size differences do not appear to have an obvious effect on the measured cFe concentrations reported by different authors (Fig. S1), although some high cFe values have been recorded when 0.4 µm pore size cut-offs were used for dFe measurements (Wu et al., 2001; Cullen et al., 2006). Similarly, there is no significant correlation between the average measured cFe concentration and the average pore-size difference when evaluating and comparing cFe data between different ocean basins (Fig. S2). Figure 5 plots the average pore size used against averaged cFe measurements from different depths

and from different aquatic regimes. Additional cFe data (averaged over the entire surface ocean dataset, irrespective of author or ocean basin) are plotted against different standard pore-size differences (cross symbols). Although there is a slight positive trend observed in both the depth samples (r^2=0.39) and the surface samples (r^2= 0.08), the distribution of data points along the vertical axis indicate that the effects of sampling depth and sampling regime are much more important for controlling cFe concentrations than the effects of pore size differences.

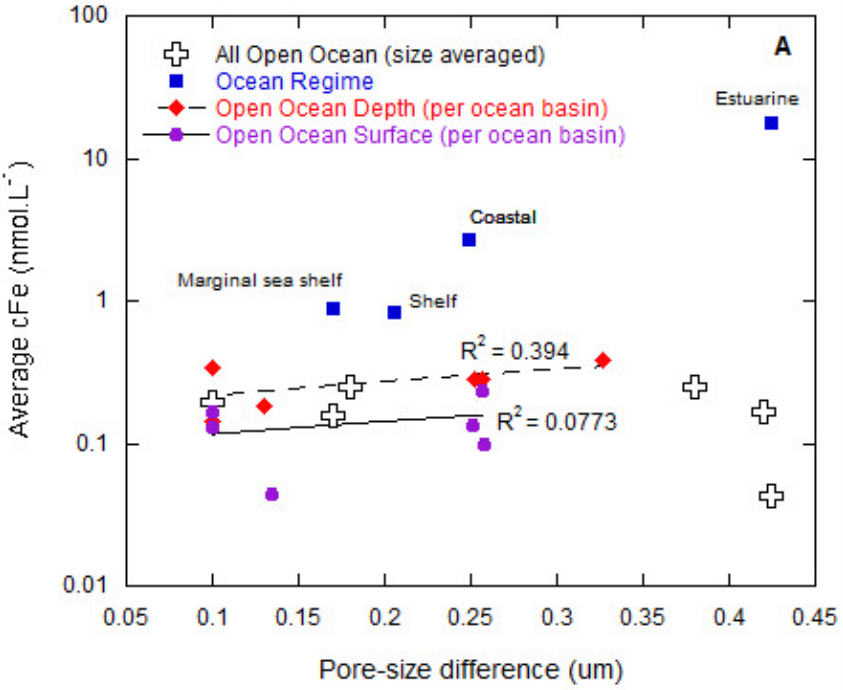

Figure 5: *Analyses of the effects of pore-size difference on calculated cFe values. The sampling regime and sampling depth are found to have larger impact on averaged cFe values than the impacts caused by artefacts associated with pore-size difference. Note the log scale on the y-axis.*

4.2. Controls on cFe concentration and partitioning

4.2.1. Geographical distribution and controls

Colloidal iron measurements are not evenly distributed throughout the global ocean. They are typically concentrated in regions where there is a high density of dFe measurements, and there is a noticeable paucity in data measurements in both the South Pacific and Indian Oceans (Fig. 1a). The spatial distribution and cFe concentration data depicted in Fig. 1b highlight the importance of various Fe sources in influencing surface water cFe concentrations. For example, Saharan dust is known to be a major flux of aerosol-derived Fe in the North Atlantic Ocean (Duce and Tindale, 1991; Jickells et al., 2005) and aerosol Fe is has been shown to preferentially release into the cFe pool (Aguilar-Islas et al., 2010). High cFe values are also found in the Arabian Sea and proximal to the South American continental margin, where shelf and fluvial (Indus River

and Amazon River, respectively) fluxes are expected to be high. Through a range of physical processes including lateral advection (Lam et al., 2008; Compton et al., 2009) and eddy transport (Johnson et al., 2005), continental margins (typically characterized by marine waters with high cFe concentrations (Fig. 2)) can play an important role in governing open ocean cFe values. Further evidence supporting the role in Fe supply terms in controlling cFe concentration is found in the high positive correlation factor (r^2 value = 0.54) between complementary cFe and TFe values; indicative that regions that receive high total iron inputs are typically characterized by high cFe concentrations (Fig. 4).

4.2.2. Solubility of iron and cFe

In an open marine system, it is only in the deep ocean that a state of quasi equilibrium between soluble and colloidal Fe forms can be approached (Ussher et al., 2010). Despite solubility being a term reserved for equilibrium conditions, we expect factors that control Fe inorganic solubility (temperature, salinity, pH, organic ligand concentration) to have some influence on the stability of the cFe pool. In spite of the strong impact of pH on Fe chemistry, only one size-fractionated Fe study has reported corresponding pH data (Wells 2000, Table 1). With current anthropogenic influence on ocean acidity, the predicted pH decrease is expected to increase Fe(III) solubility by 40% (Millero et al., 2009).

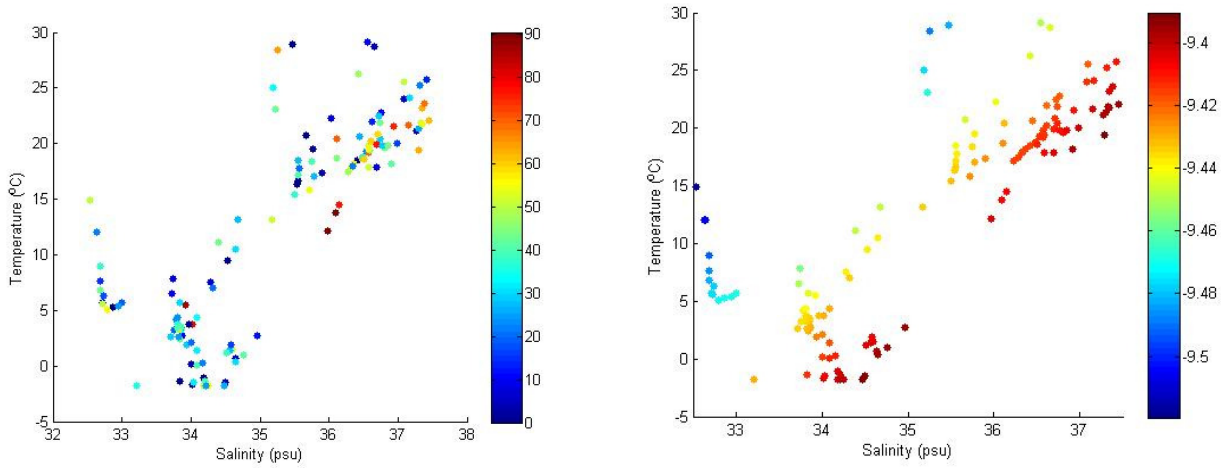

Figure 6a: *The percentage of the dFe pool comprised of cFe concentration (%cFe) plotted on the colour axis against sample-specific salinity and temperature data.* ***6b:*** *Theoretical Fe solubility (colour axis in log[Fe(III)] values) calculated using equations of Liu and Milllero (2002) and the temperature and salinity relevant to each sample point in Fig. 6a.*

Temperature and salinity have previously been used to compare size fractionated Fe data to water-mass properties and degree of fresh water mixing (Bergquist et al., 2007; Wu and Boyle, 2002; Wu et al. 2009), however these factors are also known to control Fe solubility (Liu and Millero, 2002). In surface oceans neither temperature nor salinity on its own showed any strong correlation with cFe (r^2 values= 0.044 and 0.078 respectively) or to sFe concentrations (r^2 values= 0.072 and 0.157 respectively). However, combined together the effects of temperature and salinity appear to have some influence on the partitioning of dissolved Fe into cFe and sFe (Fig. 6). The highest %cFe values are observed for surface waters

characterized with warmer temperatures and high salinity (Fig. 6a). In colder waters, the %cFe decreases as expected, due to an increase in Fe solubility (Fig. 6b; Liu and Millero, 2002). At higher solubility, we can expect that more Fe will dissolve and partition into the sFe pool, thereby lowering the measured %cFe values. However, results from Liu and Millero (2002) suggest that for marine waters 0.4-0.5 nM of unknown Fe ligand concentration, as salinity increases above ~24.5, we should expect increased Fe solubility and thus lower %cFe values. This expected result is not reflected in our data, where we find high %cFe values at increased salinity (Fig. 6a). The thermodynamic relationships between Fe solubility, temperature, salinity and variable ligand composition and concentration may thus need to be re-addressed.

4.2.3. Organic ligand binding

The presence of organic iron-binding chelates has been invoked to explain the apparent increase in seawater Fe solubility (0.2-0.6 nmol.L^{-1}; Millero et al., 1998; Kuma et al., 1996; Liu and Millero, 2002) relative to its inorganic solubility (0.08 nmol.L^{-1}; Wu et al., 2001) measured in UV-irradiated seawater. In the surface open ocean, most sFe (73.3%) and dFe (83.3%) measurements are oversaturated with respect to this inorganic solubility value. Excess iron is typically hosted by soluble and colloidal organic Fe-binding ligands (Wu et al., 2001, Cullen et al., 2006; Boye et al., 2010; Thuróczy et al., 2011), although a significant fraction may be stable as discrete Fe-rich inorganic colloids and nano-particulates (von der Heyden et al., 2012). In both the soluble and dissolved size-fractions, organic chelates have the capacity to buffer Fe concentrations above this solubility limit to levels dictated by the ligand concentrations and their respective Fe-binding affinities (Wu and Luther, 1995). In this way, the presence and concentration of organic ligands can have a pronounced control on the size of the cFe pool.

Organic Fe-binding ligands exist in a variety of forms characterized by differences in size, stability and functional group chemistry. Because of a general paucity in data relating to the complete characterization of marine organic ligands, there are still many unknowns surrounding their interactions with Fe. Major Fe-binding organic groups that have been identified in marine settings include siderophores (produced by bacteria as an Fe acquisition strategy (Kraemer 2004)) and saccharides (Hassler et al., 2011; Benner 2011) and humic substances (Laglera and van den Berg, 2009), both of which can occur in colloidal forms. Voltammetric methods have successfully been applied to the study of ligand behaviour and characterization, with early work distinguishing between strong (L1) and weak (L2) Fe-binding ligand classes (Rue and Bruland, 1995). This has been extended by later work incorporating ligand size fractionation (Cullen et al., 2006; Boye et al. 2010) and saturation state (Thuróczy et al. 2010, 2011) into the scope of their analyses. The results attained by these different studies indicate that organic ligand concentration and reactivity likely exert a strong control on the distribution and concentration of dissolved and soluble Fe.

There are additional factors, which lie largely beyond the scope of this work, that affect Fe partitioning between the various size fractions in surface waters. For example, photochemistry is known to cause changes

to Fe-ligand speciation (Barbeau, 2006; Barbeau et al., 2001; Fan, 2008) and Fe colloids are known to be photo-active (Wells and Mayer, 1991); however, experiments conducted under light and dark conditions did not find any photo-induced differences to measured Fe size-fractionated concentrations (Nishioka and Takeda, 2000). The influences of photosynthetic biology on Fe chemistry are also confined to the surface ocean waters, but interactions are complex and require further study and review.

4.3. Global cFe utilization

In many parts of the global ocean, Fe bioavailability is a critical factor controlling primary productivity (Boyd and Ellwood, 2011). Because cFe makes up a substantial proportion of the surface water Fe inventory in all ocean basins (Fig. 3), it is critical to evaluate the availability of this quantitatively important Fe pool. Although an early laboratory study showed that not all inorganic Fe colloids are available for direct utilization by phytoplankton (Rich and Morel, 1990), the emerging consensus, based on both direct and indirect evidence, is that at least some fraction of the natural cFe pool aids in sustaining growth (e.g. Chen and Wang, 2001; Chen et al., 2003; Chever et al., 2010; Hurst and Bruland, 2007). Phagotrophy or the ingestion of abiotic Fe particles (Barbeau et al., 1996) has been shown to be an important means of Fe acquisition for several marine species including some mixotrophic flagellates (Nodwell and Price, 2001), metazoans, protozoans and phagotrophic algae (Maranger et al., 1998). Colloid hosted Fe has also been found to be available to non-phagotrophic phytoplankton species (Chen and Wang, 2001; Chen et al., 2003). Aside from phagotrophy, Fe uptake mechanisms from colloidal Fe have not yet been clearly elucidated, although reduction at the cell surface (Maldonado and Price, 2001) and rapid exchange with a sFe intermediary (Wells, 2003; Morel et al., 2008) have been suggested. Aging (Chen and Wang, 2001) and photo-reactivity (Wells and Mayer, 1991; Barbeau, 2001; Fan, 2008) can however, have a mechanistic influence on the cFe bioavailability

Colloidal Fe utilization is also supported by a host of indirect evidence derived from size-fractionated oceanographic Fe data, although interpretations may be complicated by our inability to differentiate between biological utilization and sinking/scavenging removal terms. Most commonly, surface depletion of cFe is used to invoke biological utilization (Benner, 2011; Chever et al., 2010; Hurst and Bruland, 2007); although previous studies have also shown that cFe is utilized preferentially (Nishioka and Takeda, 2000), and that Fe concentrations in the <1 kDa fraction never fell below critical levels during bloom events (Gelting et al., 2010). Colloidal Fe relationships with nitrite (Ussher et al., 2010) and fluorescence (Thuróczy et al., 2011) maxima have also been considered as indirect evidence for cFe- biology interactions. Figure 7a summarizes the proportion of open ocean sampling sites that exhibit nutrient-like profiles for their sFe and cFe concentration measurements. From qualitative analysis of 45 cFe depth profiles, 64% displayed nutrient-like profiles characterized by significant surface depletion (Fig. 7b). Most of these corresponded to sites where sFe profiles also displayed nutrient behaviour although at four of the sites, only the cFe profiles were nutrient-like. Additionally, at five of the sites neither size fraction exhibited nutrient behaviour (Fig. 7a, c). In agreement with previous work (Johnson et al., 1997), the majority (79%) of dFe profiles show nutrient-

like behaviour and these included some profiles where cFe profiles were not nutrient-like. At these sites, however, variability in the dFe profile was skewed by the majority of Fe concentration occurring in the smaller sFe size fraction.

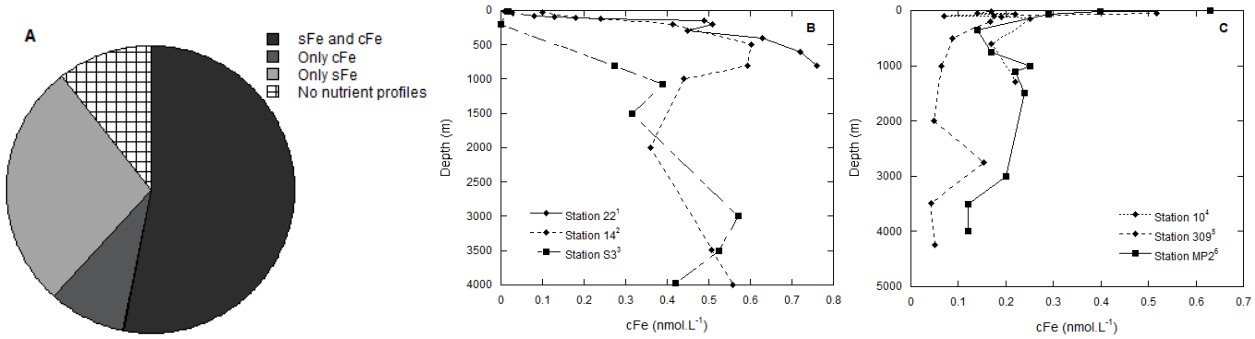

Figure 7a: *Pie chart showing the apportioning of cFe and sFe profiles that display nutrient-like characteristics.* ***7b:*** *Selected cFe profiles that show characteristic nutrient behavior ([1]Nishioka et al. (2009), [2]Thuroczy et al. (2010), [3]Chever et al. (2010)).* ***7c:*** *Selected example profiles that do not show nutrient behavior ([4]Ussher et al. (2010), [5]Thuroczy et al. (2011), [6]Wu et al. (2001)).*

Assuming that biology is responsible for this observed drawdown of cFe in surface waters, we can expect surface cFe measurements to reflect the strong seasonality often associated with phytoplankton growth (Thomalla et al., 2011). Figure 8 plots the global seasonal euphotic zone cFe and sFe concentrations averaged over the upper 200 m and across both hemispheres. Pore-size differences may have an effect on the averaged values reported for seasonal cFe data (Fig. S3); however, because pore-size differences are typically a secondary effect on cFe values (Fig. S1, Fig. S2, Fig. 5), we believe that the observed trends are caused by seasonal differences in physical processes and biological utilization.

Between summer and autumn sFe concentrations remain relatively constant whereas cFe concentrations increase. In winter time, there is a sharp increase in both size fractions, likely associated with either deep wintertime mixing, or because biological utilization rates have slowed down sufficiently for scavenging and organic complexation to become the dominant controls on size fractionation. With the onset and persistence of spring bloom conditions, the concentrations of Fe in both fractions decrease markedly, with sFe displaying a more drastic drop to concentrations levels that are smaller than the ambient cFe concentrations. This may represent a preferential utilization of sFe over cFe, or this may be due to the presence of sparingly soluble colloidal phases with slow dissolution kinetics (e.g. aged FeOOH's (Kuma and Matsunaga, 1995; Yoshida et al., 2006)). The latter argument is supported by global surface data where 40 measurements report sFe concentrations smaller than the inorganic solubility of Fe (0.08 nmol.L^{-1} (Wu et al., 2001)). Despite under-saturation of Fe at these sites, 26 ±22% of dissolved Fe remains hosted in the colloidal size fraction, indicating that these persistent colloids have either very slow dissolution kinetics or that the Fe is incorporated into colloidal phases with higher solubility constants than the solubility constant for FeOOH.

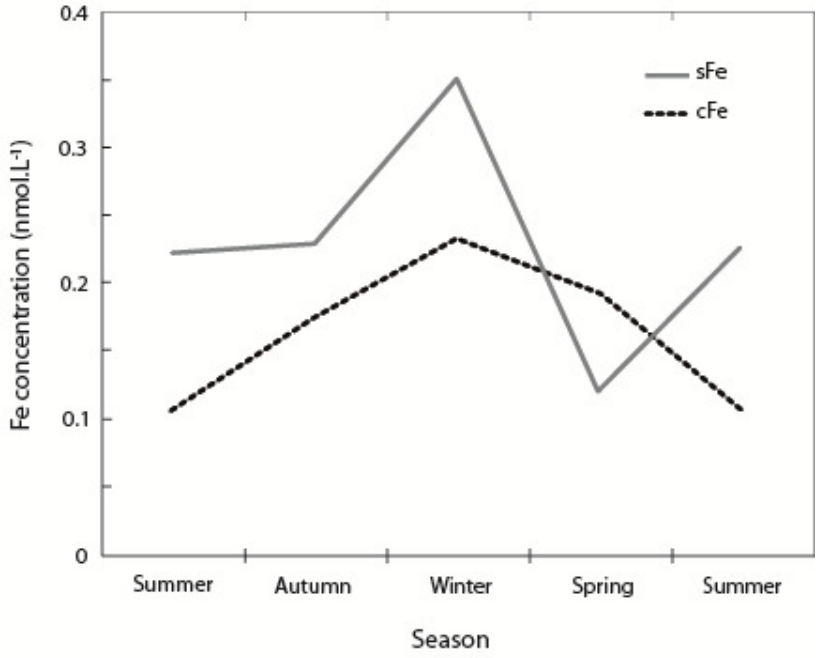

Figure 8: *Seasonally averaged trends (combined for both hemispheres) in sFe and cFe data in the upper 200 m of the water column.*

During summer months, cFe concentrations continue to decline, whereas sFe concentrations rebound to levels greater than 0.2 nmol.L^{-1}. The continued decline in the cFe concentration may represent the sustained dissolution (perhaps promoted by biological reductants and siderophores (Bligh and Waite, 2010)) of more recalcitrant colloidal phases. In this way, the cFe pool can thus act as a repository of Fe which can restock the depleted sFe pool through dissolution mechanisms. If this hypothesis is true, it would argue for a seawater solubility limit for the sFe size fraction of around 0.2 nmol.L^{-1}; in good agreement with values reported by Kuma et al., 1992 (0.28 nmol.L^{-1}) and Millero, 1998 (0.2 nmol.L^{-1}).

4.4. Chemical speciation of Fe-rich colloids

Ultrafiltration studies have found wide-application at a variety of marine sampling sites (Fig 1a) and resulting interpretations have yielded useful insights into the processes governing the cycling of Fe between different size classes. Although the study of marine Fe chemistry is focused largely on understanding the impacts of this important trace nutrient on biological growth, only limited comment regarding this relationship can and has been made by considering Fe size fractionation. The major limitation inherent in size-fractionated datasets is that measurements are differentiated according to size cut-offs, with each size pool encompassing a range of different Fe chemical forms and species (Fig. 9). The behaviour of these different species is dictated more strongly by their individual chemical and mineralogical properties than by their size distribution. Because size is a physical property, size-fractionated data have the most applicability to interpretations relating to diffusion rates (impacts on bioavailability), residence times (can impact on extent of dissolution), sinking rates and surface area and bio-accessibility. To more fully understand the

behaviour of Fe in the biogeochemical system, size-fractionated Fe data should be complemented with data that investigate the chemistry of Fe in more detail.

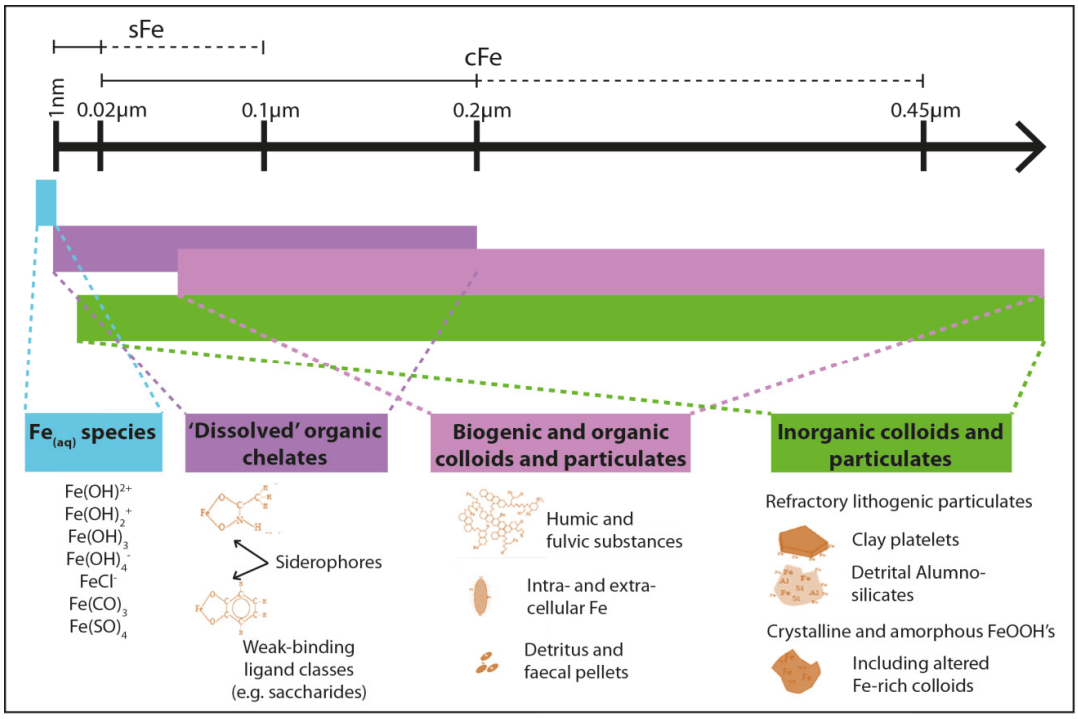

Figure 9: *Size scale comparing the operational size-classes to the range of chemical forms potentially present within each fraction. The fact that each chemical form is expected to behave differently in the biogeochemical system is the major limitation associated with size-fractionated Fe study.*

Sequential column methods (Lewis and Landing, 1991; Ozturk and Biezel, 2003) provide operational definitions of the Fe pools based on chemical separations and have previously been used to complement size separations (Wen et al., 2006). Wet chemical extraction with oxine has been suggested as a proxy for determining the labile or bioavailable fraction in seawater particulates (Wells et al., 1991). The labile or bioavailable fraction however, is perhaps better estimated using a recently developed Diffusive Gradients in Thin-film (DGT) technique (Baeyens et al., 2011) which enables the separation of labile Fe species that are smaller than the pore sizes in algal cell walls. The mineralogy and chemistry of discrete Fe-rich particles have also recently been investigated using a direct x-ray probe at a particle-by-particle resolution (von der Heyden et al., 2012). Techniques such as these, which analyse Fe species on a chemical basis, should find increased applicability in future studies and will be a useful complement to traditional size-fractionated data. Combining size data (sinking rates) with surface chemistry data (affinity for aggregation through surface interaction) should shed light on whether the colloidal Fe pool is more important as a sink (colloid pump) or as a potential reserve source of available Fe for biology. For enhanced biogeochemical relevance, Fe speciation studies should focus on the mineralogy and surface chemistry of inorganic colloids; and the characterization, concentration (density), saturation and binding affinity of Fe-binding sites in organic colloids. Combined with a better understanding of phytoplankton Fe acquisition mechanisms, these molecular level considerations should allow us to better estimate the pool of bioavailable and labile (weakly

chelated to organic functional groups) Fe. We would also then be better positioned to comment on the importance of the inorganic colloidal pool and the strongly-chelated organic Fe pool as repositories of Fe which can subsequently become available via dissolution and dissociation processes, especially when marine waters become under-saturated with respect to bioavailable Fe.

5. CONCLUSIONS AND FUTURE WORK

Despite differences in size cut-offs employed in various Fe size-fractionation studies and caveats associated with ultrafiltration methodologies, evaluation of over 500 depth and surface measurements from the open ocean have rendered viable and interesting insights into the distribution and behavior of the colloidal Fe pool. Colloidal Fe distribution in the global surface ocean is controlled primarily by the proximity and magnitude of Fe source fluxes and the concentration and size distribution of organic Fe binding ligands. Site-specific thermodynamic considerations play a secondary role in governing cFe distribution, by influencing the partitioning of iron between colloidal and soluble Fe size pools. Analysis of the seasonal variations of averaged euphotic zone cFe data coupled with analysis of open ocean cFe depth profiles give significant indication that a fraction of the cFe pool is involved in sustaining biological growth. This finding emphasizes the importance of continued study of the characterization, distribution and behaviour of colloid-hosted Fe.

Future work should strive towards a more chemically-relevant approach to marine Fe speciation studies, by employing techniques that directly probe chemical and mineralogical properties. These studies should proceed in addition to, and not in place of, classical size-fractionated Fe studies. Standardized sample collection protocols, the use of standard size cut-offs for the sFe and dFe pools, and routine inter-calibration efforts will greatly benefit future inter-comparison exercises. Obvious suggestions for a standardized sFe cut-off include the 0.02 µm pore-size (to fit in with established datasets) or the smallest possible cross-flow filtration cut-off (e.g. 1 kDa), which will give the nearest possible representation of the concentration of inorganic truly dissolved Fe'.

With the collection of chemically-precise data pertaining to colloidal Fe, scientific attention will be able to focus on molecular level considerations that impact on its behaviour in the marine biogeochemical system. These molecular-scale considerations include the effects of photochemistry (Sherman, 2005) and interaction with Fe-binding ligands (e.g. siderophores (Hocking et al., 2010)) on colloid stability and dissolution. Furthermore, investigations should endeavour to determine whether colloid-hosted Fe is directly accessible to phytoplankton, or if there is necessity for prior exchange to the sFe pool (Wells et al., 2003; Morel et al., 2008). Although all of these factors will aid in our understanding of what makes Fe colloids bioavailable, complete understanding of the colloidal Fe-biology relationship will only be attained once focused future study has elucidated the precise phytoplankton Fe uptake mechanisms.

ACKNOWLEDGEMENTS

This research is supported by grants from NRF, South Africa (Blue Skies Program) and Stellenbosch University VR(R) fund. The authors would like to thank all of the scientists that contributed raw data related to their published work as well as the BODC for supplying Fe size-fractionated data, salinity and temperature data from cruise AMT16. This work benefitted from discussions with Dr Alessandro Tagliabue. All Fe data used in this study can be obtained from the authors.

REFERENCES

Aguilar-Islas, A.M., Wu, J., Rember, R., Johansen, A.M., Shank, L.M., 2010. Dissolution of aerosol-derived iron in seawater: Leach solution chemistry, aerosol type, and colloidal iron fraction. Marine Chemistry 120(1), 25-33.

Baeyens, W., Bowie, A.R., Buesseler, K., Elskens, M., Gao, Y., Lamborg, C., Leermakers, M., Remenyi, T., Zhang, H., 2011. Size-fractionated labile trace elements in the Northwest Pacific and Southern Oceans. Marine Chemistry 126(1), 108-113.

Barbeau, K., Moffett, J., Caron, D., Croot, O., Erdner, D., 1996. Role of protozoan grazing in relieving iron limitation of phytoplanlton. Nature 380, 61-64.

Barbeau, K., Rue, E., Bruland, K., Butler, A., 2001. Photochemical cycling of iron in the surface ocean mediated by microbial iron(III)-binding ligands. Nature 413, 409-413.

Barbeau, K., 2006. Photochemistry of organic iron(III) complexing ligands in oceanic systems. Photochemistry and Photobiology 82, 1505-1516.

Bergquist, B.A., Wu, J., Boyle, E.A., 2007. Variability in oceanic dissolved iron is dominated by the colloidal fraction. Geochimica et Cosmochimica Acta 71, 2960-2974.

Benner, R. Loose ligands and available iron in the ocean. Proceedings of the National Academy of Sciences 108(3), 893-894.

Bligh, M.W., Waite, T.D., 2010. Formation, aggregation and reactivity of amorphous ferric oxyhydroxides on dissociation of Fe (III)–organic complexes in dilute aqueous suspensions. Geochimica et Cosmochimica Acta 74(20), 5746-5762.

Boyd, P.W., Ellwood, M.J., 2010. The biogeochemical cycle of iron in the ocean. Nature Geoscience 3, 675-682.

Boye, M., Nishioka, J., Croot, P., Laan, P., Timmermans, K.R., Strass, V.H., Takeda, S., de Baar, H.J.W., 2010. Significant portion of dissolved organic Fe complexes in fact is colloids. Marine Chemistry 122, 20-27.

Boyle, E.A., Bergquist, B.A., Kayser, R.A., Mahowald, N., 2005. Iron, manganese, and lead at Hawaii Ocean Time-series station ALOHA: Temporal variability and an intermediate water hydrothermal plume. Geochimica et Cosmochimica Acta 69(4), 933-952.

Bowie, A. R., Achterberg, E.P., Blain, S., Boye, M., Croot, P.L., de Baar, H.J.W., Laan, P., Sarthou, G., Worsfold, P.J., 2003. Shipboard analytical intercomparison of dissolved iron in surface waters along a north–south transect of the Atlantic Ocean. Marine Chemistry 84(1), 19-34.

Bowie, A.R., Ussher, S.J., Landing, W.M., Worsfold, P.J., 2007. Intercomparison between FI-CL and ICP-MS for the determination of dissolved iron in Atlantic seawater. Environmental Chemistry 4(1), 1-4.

Bruland, K.W., Rue, E.L., 2001. Iron: analytical methods for the determination of concentrations and speciation. The Biogeochemistry of Iron in Seawater, 255-289.

Chen, M., Wang, W.X., 2001. Bioavailability of natural colloidal Fe to marine plankton: influence of colloidal size and aging. Limnology and Oceanography 46, 1956-1967.

Chen, M., Dei, R.C.H., Wang, W., Guo, L., 2003. Marine diatom uptake of iron bound with natural colloids of different origins. Marine Chemistry 81, 177-189.

Chever, F., Bucciarelli, E., Sarthou, G., Speich, S., Arhan, M., Penven, P., Tagliabue, A., 2010. Physical speciation of iron in the Atlantic sector of the Southern Ocean along a transect from the subtropical domain to the Weddell Sea Gyre. Journal of Geophysical Research: Oceans (1978-2012), 115(C10).

Chin, W.C., Orellana, M.V., Verdugo, P., 1998. Spontaneous assembly of marine dissolved organic matter into polymer gels. Nature, 391(6667), 568-572.

Compton, J., Herbert, C., Schneider, R., 2009. Organic-rich mud on the western margin of southern Africa: Nutrient source to the Southern Ocean? Global Biogeochemical Cycles 23(4), GB4030.

Croot, P.L., Streu, P., Baker, A.R., 2004. Short residence time for iron in surface seawater impacted by atmospheric dry deposition from Saharan dust events. Geophysical Research Letters 31(23).

Cullen J.T., Bergquist B.A., Moffett J.W., 2006. Thermodynamic characterization of the partitioning of iron between soluble and colloidal species in the Atlantic Ocean. Marine Chemistry 98, 295-303.

Cutter, G., Andersson, P., Codispoti, L., Croot, P., Francois, R., Lohan, M., Obata, H., van der Loeff, M.R., 2010. Sampling and sample-handling protocol for GEOTRACES cruises. 39-51.

Cutter, G.A., Bruland, K.W., 2012. Rapid and noncontaminating sampling system for trace elements in global ocean surveys. Limnology and Oceanography: Methods 10, 425-436.

Duce, R.A., Tindale, N.W., 1991. Atmospheric transport of iron and its deposition in the ocean. Limnology and Oceanography 36, 1715-1726.

Fan, S.-M., 2008. Photochemical and biochemical controls on reactive oxygen and iron speciation in the pelagic surface ocean. Marine Chemistry 109, 152-164.

Fardy, J.J., 1992. Preconcentration of trace elements by ion exchangers. Preconcentration Techniques for Trace Elements, 181-210.

Fitzsimmons, J.N., Boyle, E.A., 2012. An intercalibration between the GEOTRACES GO-FLO and the MITES/Vanes sampling systems for dissolved iron concentration analyses (and a closer look at adsorption effects). Limnology and Oceanography: Methods 10, 437-450.

Frew, R. D., Hutchins, D. A., Nodder, S., Sanudo-Wilhelmy, S., Tovar-Sanchez, A., Leblanc, K., Hare, C. E., Boyd, P. W., 2006. Particulate iron dynamics during FeCycle in subantarctic waters southeast of New Zealand, Global Biogeochemical Cycles 20(1).

Fujita, S., Kuma, K., Ishikawa, S., Nishimura, S., Nakayama, Y., Ushizaka, S., Isoda, Y., Otosaka, S., Aramaki, T., 2010. Iron distributions in the Japan Basin and Yamato Basin (Japan Sea). Journal of Geophysical Research: Oceans (1978-2012) 115(C12).

Gelting, J., Breitbarth, E., Stolpe, B., Hassellöv, M., Ingri, J., 2010. Fractionation of iron species and iron isotopes in the Baltic Sea euphotic zone, Biogeosciences 7, 2489-2508.

Hassler, C.S., Schoemann, V., Nichols, C.M., Butler, E.C.V., Boyd, P.W., 2011. Saccharides enhance iron bioavailability to Southern Ocean phytoplankton. Proceedings of the National Academy of Sciences 108(3), 1076-1081.

Hocking, R.K., De Beer George, S., Raymond, K.N., Hodgson, K.O., Hedman, B., Solomon, E.I., 2010. Fe L-edge X-ray absorption spectroscopy determination of differential orbital covalency of siderophore model compounds: electronic structure contributions to high stability constants. Journal of the American Chemical Society 132(11), 4006-4015.

Howell, K. A., Achterberg, E. P., Tappin, A. D., Worsfold, P. J.: Colloidal metals in the Tamar Estuary and their influence on metal fractionation by membrane filtration, Environmental Chemistry 3, 199-207.

Hurst, M.P., Bruland, K.W., 2007. An investigation into the exchange of iron and zinc between soluble, colloidal, and particulate size-fractions in shelf waters using low-abundance isotopes as tracers in shipboard incubation experiments. Marine Chemistry 103, 211-226.

Hurst, M.P., Bruland, K.W., 2008. The effects of the San Francisco Bay plume on trace metal and nutrient distributions in the Gulf of the Farallones. Geochimica et Cosmochimica Acta 72(2), 395-411.

Hurst, M.P., Aguilar-Islas, A.M., Bruland, K.W., 2010. Iron in the southeastern Bering Sea: Elevated leachable particulate Fe in shelf bottom waters as an important source for surface waters. Continental Shelf Research 30, 467-480.

Jickells, T.D., An, Z.S., Andersen, K.K., Baker, A.R., Bergametti, G., Brooks, N., Cao, J.J., Boyd, P.W., Duce, R.A., Hunter, K.A., Kawahata, H., Kubilay, N., laRoche, J., Liss, P.S., Mahowald, N., Prospero, J.M., Ridgwell, A.J., Tegen, I., Torres, R., 2005. Global iron connections between desert dust, ocean biogeochemistry, and climate. Science 308, 67-71.

Johnson, K. S., Gordon, R. M., Coale, K. H., 1997. What controls dissolved Iron concentration in the World Ocean? Marine Chemistry 57, 137-161.

Johnson, W.K., Miller, L.A., Sutherland, N.E., Wong, C.S., 2005. Iron transport by mesoscale Haida eddies in the Gulf of Alaska. Deep-Sea Research II 52, 933-953.

Johnson, K.S., Elrod, V., Fitzwater, S., Plant, J., Boyle, E., Bergquist, B., Bruland, K., Aguilar-Islas, A., Buck, K., Lohan, M., Smith, G.J., Sohst, B., Coale, K., Gordon, M., Tanner, S., Measures, C., Moffett, J., Barbeau, K., King, A., Bowie, A., Chase, Z., Cullen, J., Laan, P., Landing, W., Mendez, J., Milne, A., Obata, H., Doi, T., Ossiander, L., Sarthou, G., Sedwick, P., van den Berg, S., Laglera-Baquer, L., Wu, J., Cai, Y., 2007. Developing standards for dissolved iron in seawater. Eos, Transactions American Geophysical Union 88, 131-132.

Kraemer, S.M., 2004. Iron oxide dissolution and solubility in the presence of siderophores. Aquatic Sciences 66, 3-18.

Kuma, K., Nakabayashi, S., Suzuki, Y., Matsunaga, K., 1992. Dissolution rate and solubility of colloidal hydrous ferric oxide in seawater. Marine Chemistry 38, 133-143.

Kuma, K., Matsunaga, F.L., 1995. Availability of colloidal ferric oxides to coastal marine phytoplankton. Marine Biology 122, l-11.

Kuma, K., Nishioka, J., Matsunaga, K., 1996. Controls on iron(III) hydroxide solubility in seawater: the influence of pH and natural organic chelators. Limnology and Oceanography 41, 396-407.

Kuma, K., Katsumoto, A., Nishioka, J., Matsunaga, K., 1998. Size-fractionated iron concentrations and Fe(III) hydroxide solubilities in the various coastal waters. Estuarine Coastal Shelf Science 47, 275-283.

Kuma, K., Katsumoto, A., Shiga, N., Sawabe, T., Matsunaga, K., 2000. Variation of size-fractionated Fe concentrations and Fe (III) hydroxide solubilities during a spring phytoplankton bloom in Funka Bay (Japan). Marine Chemistry 71(1), 111-123.

Laglera, L.M., van den Berg, C.M.G., 2009. Evidence for geochemical control of iron by humic substances in seawater. Limnology and Oceanography 54, 610-619.

Lam, P.J., Bishop, J.K., Henning, C.C., Marcus, M.A., Waychunas, G.A., Fung, I.Y., 2006. Wintertime phytoplankton bloom in the subarctic Pacific supported by continental margin iron. Global Biogeochemical Cycles 20(1).

Lewis, B.L., Landing, W.M., 1991. The biogeochemistry of manganese and iron in the Black Sea. Deep-Sea Research 38, 773-803.

Liu, X.W., Millero, F.J., 2002. The solubility of iron in seawater. Marine Chemistry 77, 43-54.

Lohan, M.C., Aguilar-Islas, A.M., Franks, R.P., Bruland, K.W., 2005. Determination of iron and copper in seawater at pH 1.7 with a new commercially available chelating resin, NTA Superflow. Analytica Chimica Acta 530, 121-129.

Lohan, M.C., Aguilar-Islas, A.M., Bruland, K.W., 2006. Direct determination of iron in acidified (pH 1. 7) seawater samples by flow injection analysis with catalytic spectrophotometric detection: Application and intercomparison. Limnology and Oceanography: Methods 4, 164-171.

Maldonado, M.T., Price, N.M., 2001. Reduction and transport of organically bound iron by Thalassiosira oceanica (Bacillariophyceae). Journal of Phycology 37, 298-310.

Maranger, R., Bird, D.F., Price, N.M., 1998. Iron acquisition by photosynthetic marine phytoplankton from ingested bacteria. Nature 396, 248-251.

Millero, F.J., 1998. Solubility of Fe(III) in seawater. Earth and Planetary Science Letters 154, 323-330.

Millero, F.J., Woosley, R., DiTrolio, B., Waters, J., 2009. Effect of ocean acidification on the speciation of metals in natural waters. Oceanography 22(4), 72-85.

Morel, F.M.M., Kustka, A.B., Shaked, Y., 2008. The role of unchelated Fe in the iron nutrition of phytoplankton. Limnology and Oceanography 53(1), 400-404.

Mota, A.M., Correia Dos Santos, M.M., 1995. Trace metal speciation of labile chemical species in natural waters: electrochemical methods. In: Tessier, A., Turner, D.R. (Eds.), Metal Speciation and Bioavailability in Aquatic Systems. John Wiley & Sons, pp. 205-257.

Nishioka, J., Takeda, S., 2000. Change in the concentrations of iron in different size fractions during growth of the oceanic diatom Chaetoceros sp.: Importance of small colloidal iron. Marine Biology 137(2), 231-238.

Nishioka, J., Takeda, S., Wong, C.S., Johnson, W.K., 2001. Size-fractionated iron concentrations in the northeast Pacific Ocean: distribution of soluble and small colloidal iron. Marine Chemistry 74, 157-179.

Nishioka, J., Takeda, S., Kudo, I., Tsumune, D., Yoshimura, T., Kuma, K., Tsuda, A., 2003. Size-fractionated iron distributions and iron limitation processes in the subarctic NW Pacific. Geophysical Research Letters, 30(14), 1730.

Nishioka, J., Takeda, S., de Baar, H.J., Croot, P.L., Boye, M., Laan, P., Timmermans, K.R., 2005. Changes in the concentration of iron in different size fractions during an iron enrichment experiment in the open Southern Ocean. Marine Chemistry, 95(1), 51-63.

Nishioka, J., Obata, H., Tsumune, D., 2013. Evidence of an extensive spread of hydrothermal iron in the Indian Ocean. Earth and Planetary Science Letters 361, 26-33.

Nodwell L.M., Price N.B., 2001. Direct use of inorganic colloidal iron by marine mixotrophic phytoplankton. Limnology and Oceanography 46, 765-777.

Obata, H., Karatani, H., Matsui, M., Nakayama, E., 1997. Fundamental studies for chemical speciation of iron in seawater with an improved analytical method. Marine Chemistry 56, 97-106.

Ozturk, M., Bizsel, N., 2003. Iron speciation and biogeochemistry in different nearshore waters. Marine Chemistry 83, 145-156.

Rich, H.W., Morel, F.M.M., 1990. Availability of well-defined iron colloids to the marine diatom Thalassiosira weissflogii. Limnology and Oceanography 35, 652-662.

Rue, E. L., Bruland, K. W., 1995. Complexation of iron(III) by natural organic ligands in the Central North Pacific as determined by a new competitive ligand equilibration/adsorptive cathodic stripping voltammetric method. Marine Chemistry 50, 117–138.

Sarthou, G., Vincent, D., Christaki, U., Obernosterer, I., Timmermans, K.R., Brussaard, C.P.D., 2008. The fate of biogenic iron during a phytoplankton bloom induced by natural fertilisation: Impact of copepod grazing. Deep Sea Research Part II: Topical Studies in Oceanography 55(5), 734-751.

Sherman, D.M., 2005. Electronic structures of iron (III) and manganese (IV)(hydr) oxide minerals: Thermodynamics of photochemical reductive dissolution in aquatic environments. Geochimica et Cosmochimica Acta 69(13), 3249-3255.

Strzepek, R.F., Maldonado, M.T., Higgins, J.L., Hall, J., Safi, K., Wilhelm, S.W., Boyd, P.W., 2005. Spinning the "Ferrous Wheel": The importance of the microbial community in an iron budget during the FeCycle experiment. Global Biogeochemical Cycles 19(4).

Tagliabue, A., Mtshali, T., Aumont, O., Bowie, A.R., Klunder, M.B., Roychoudhury, A.N., Swart, S., 2012. A global compilation of dissolved iron measurments: focus on distributions and processes in the Southern Ocean. Biogeosciences 9, 2333-2349.

Takata, H., Kuma, K., Saitoh, Y., Chikira, M., Saitoh, S.I., Isoda, Y., Takagi, S., Sakaoka, K., 2006. Comparing the vertical distribution of iron in the eastern and western North Pacific Ocean. Geophysical Research Letters, 33(2).

Thomalla, S.J., Fauchereau, N., Swart, S., Monteiro, P.M.S., 2011. Regional scale characteristics of the seasonal cycle of chlorophyll in the Southern Ocean. Biogeosciences 8(10), 2849-2866.

Thuróczy, C.-E., Gerringa, L.J.A., Klunder, M.B., Middag, R., Laan,P., Timmermans, K.R., de Baar, H.J.W., 2010. Speciation of Fe in the Eastern North Atlantic Ocean. Deep-Sea Research I 57(11), 1444-1453.

Thuróczy, C.-E., Gerringa, L.J.A., Klunder, M., Laan, P., Le Guitton, M., de Baar, H.J.W., 2011. Distinct trends in the speciation of iron between the shallow shelf and the deep basins of the Arctic Ocean. Journal of Geophysical Research 116, C10009.

Thuróczy, C.-E. Physical and chemical speciation of iron in the polar oceans. Thesis. University of Groningen. 2011, http://irs.ub.rug.nl/ppn/338020667

Ussher, S.J., Achterberg, E.P., Sarthou, G., Laan, P., de Baar, H.J.W., Worsfold, P.J., 2010. Distribution of size fractionated dissolved iron in the Canary Basin. Marine Environmental Research 70(1), 46-55.

Von der Heyden, B.P., Roychoudhury, A.N., Mtshali, T.N., Tyliszczak, T., Myneni, S.C.B., 2012. Chemically and geographically distinct solid-phase iron pools in the Southern Ocean. Science 338, 1199-1201.

Wells, M.L., Mayer, L.M., 1991. The photoconversion of colloidal iron oxyhydroxides in seawater. Deep Sea Research Part A. Oceanographic Research Papers 38(11), 1379-1395.

Wells, M.L., Mayer, L.M., Guillard, R.R.L., 1991. A chemical method for estimating the availability of iron to phytoplankton in seawater. Marine Chemistry 33, 23-40.

Wells, Mark L., 1998. Marine colloids: A neglected dimension. Nature 391, 530-531.

Wells, M.L., Smith, G.J., Bruland, K.W., 2000. The distribution of colloidal and particulate bioactive metals in Narragansett Bay, RI. Marine Chemistry 71, 143-163.

Wells, M.L., 2003. The level of iron enrichment required to initiate diatom blooms in HNLC waters. Marine Chemistry 82, 101-114.

Wen, L.-S.; Jiann, K.-T.; Santschi, P. H., 2006. Physicochemical speciation of bioactive trace metals (Cd, Cu, Fe, Ni) in the oligotrophic South China Sea. Marine Chemistry 101, 104-129.

Wu, J.F., Luther III, G.W., 1995. Complexation of Fe(III) by natural organic ligands in the Northwest Atlantic Ocean by competitive ligand equilibration method and a kinetic approach. Marine Chemistry 50, 159-178.

Wu, J., Boyle, E.A., Sunda, W., Wen, L., 2001. Soluble and colloidal iron in the oligotrophic North Atlantic and North Pacific. Science 293, 847-849.

Wu, J., Boyle, E.A., 2002. Iron in the Sargasso Sea: implications for the processes controlling dissolved Fe distribution in the ocean. Global Biogeochemical Cycles 16, 1086-1094.

Wu, J., Aguilar-Islas, A., Rember, R., Weingartner, T., Danielson, S., Whitledge, T., 2009. Size-fractionated iron distribution on the northern Gulf of Alaska. Geophysical Research Letters 36, L11606.

Yoshida, M., Kuma, K., Iwade, S., Isoda, Y., Takata, H., Yamada, M., 2006. Effect of aging time on the availability of freshly precipitated ferric hydroxide to coastal marine diatoms. Marine Biology 149 (2), 379-392.

SUPPLEMENTARY FIGURES

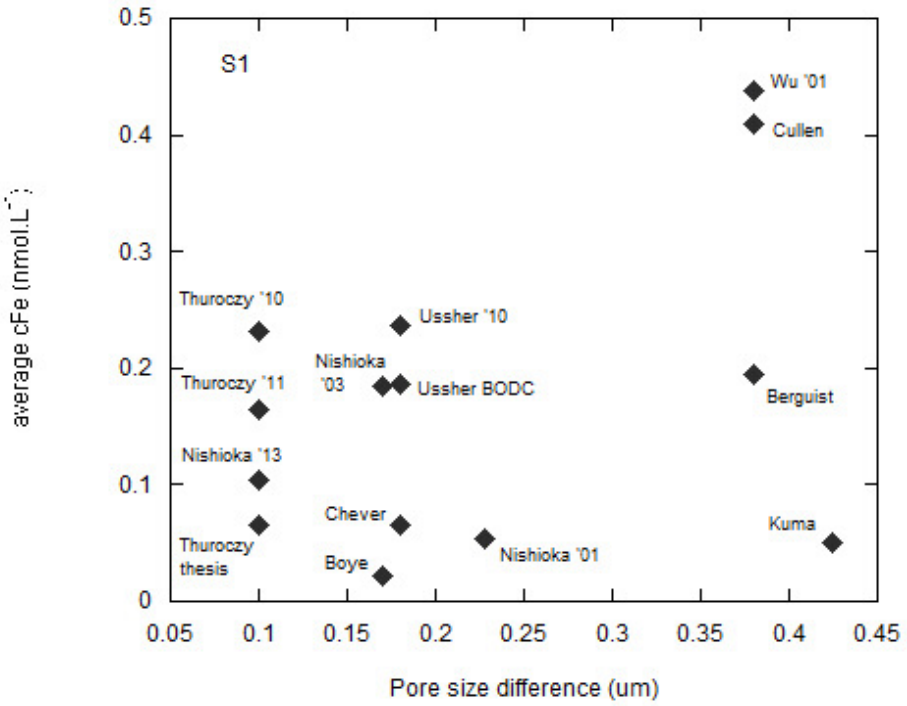

Figure S1: *Average cFe measured per author compared to the difference in pore sizes (i.e. dFe filter pore size less sFe filter pore size) used in each respective study. Aside from the Wu et al. (2001) and Cullen et al. (2006) datapoints, there is no significant relationship between the reported average cFe concentrations abd the filter pore sizes employed.*

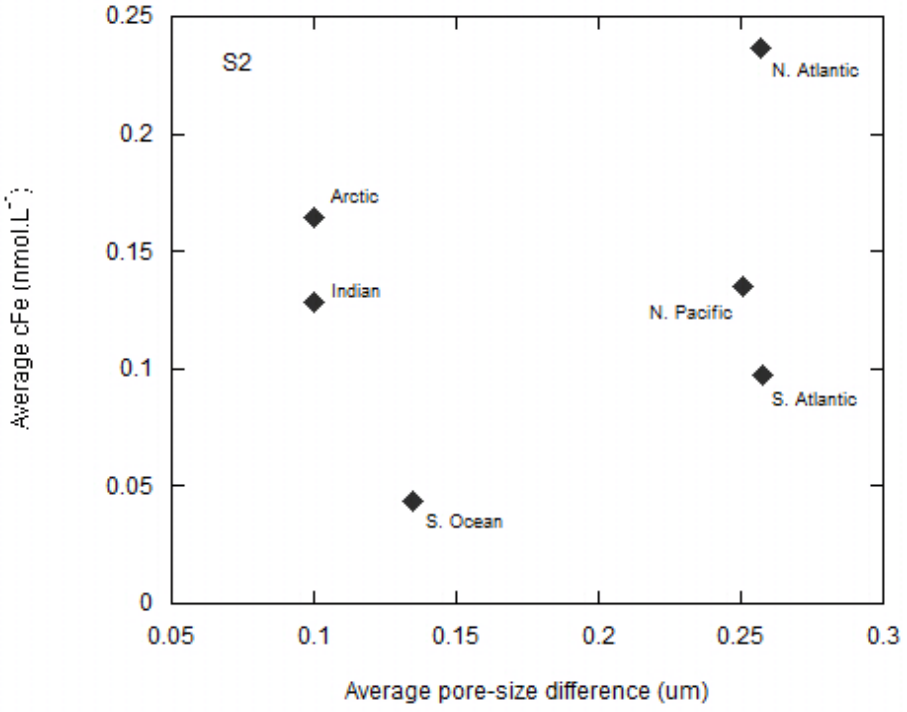

Figure S2: *Average pore-size difference (see S1) versus the average reported cFe concentration per ocean basin. There is no significant effect of pore size on cFe measurements.*

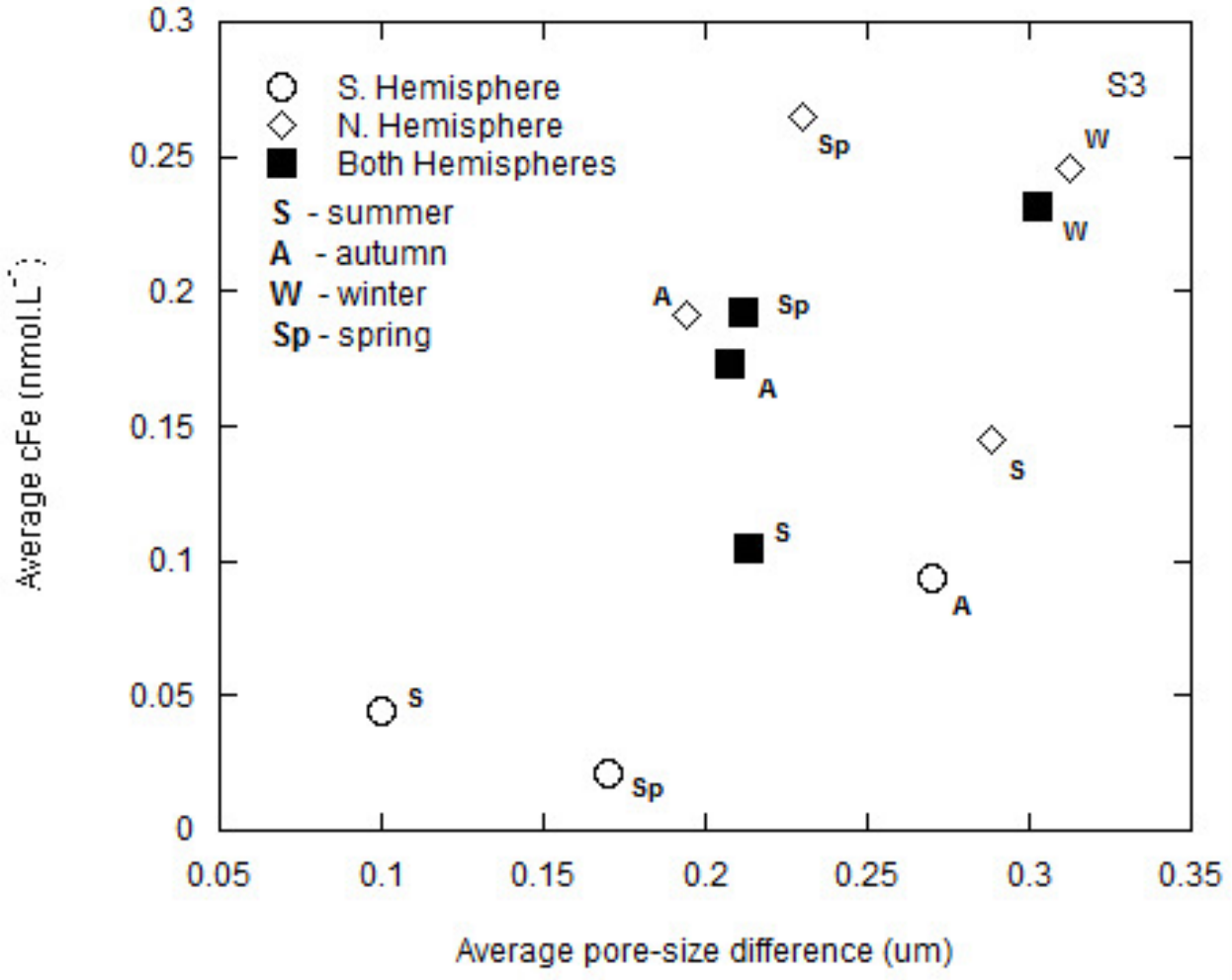

Figure S3: *Average pore-size difference (see S1) versus the average reported cFe concentration per season and according to hemisphere. Although there is an apparent correlation over the entire dataset, the correlation does not hold true if the hemispheric data are considered separately. Furthermore, because no correlations were observed in our other analyses (Figs. S1, S2 and Fig. 5 (main text)), we believe that this apparent correlation is coincidental and that the seasonal signal is more important in controlling average cFe concentrations.*

CHAPTER 3

L_3-edge spectroscopic determination of Fe Coordination Environment in Fe oxides and oxyhydroxides

A presentation of the prepared research paper

This manuscript is prepared for submission to the research journal *Geochimica et Cosmochimica Acta*. I am the first author and Prof Satish Myneni, Prof Alakendra Roychoudhury and Dr Tolek Tyliszczak are the co-authors.

Because of its sensitivity to the local coordination environment surrounding Fe metal centres, the Fe L-edge is a useful probe for understanding particle speciation. Standard Fe-rich minerals are characterized by Fe in distinct coordination environments, as dictated by their respective mineralogies. This manuscript details the development of an L-edge X-ray Absorption Fine Structure (XANES) spectroscopic technique for characterizing the speciation of Fe oxide and Fe oxyhydroxide phases. Variations in spectral parameters (ΔeV and intensity ratio), linked to splitting in the L_3-edge peak, are used to differentiate between different Fe minerals and are explained in terms of molecular level considerations. The theoretical findings discussed in this manuscript can be applied to Fe systems beyond the simple Fe-O-H system and our ΔeV versus intensity ratio plot is thus a useful tool for examining Fe speciation in natural systems.

I was responsible for the writing of this manuscript as well as for the creation of all of the figures. I synthesised one of the standards (maghemite) and all other standards were synthesised in the Myneni Lab at Princeton University. XANES data collection was shared equally by me and Prof Satish Myneni, and all subsequent data analyses were conducted by me under the supervision of Prof Myneni. Dr Tolek Tyliszczak is the beamline scientist at beamline 11.0.2 (Advanced Light Source, CA, USA) and he provided the magnetite standard spectrum and helped out immeasurably with the experimental set-up and during data collection. Prof Alakendra Roychoudhury played a supervisory role in this project and was responsible for securing parts of the funding.

L_3-edge spectroscopic determination of Fe Coordination Environment in Fe oxides and oxyhydroxides

B.P. von der Heyden[a], S.C.B. Myneni[b,*], A.N. Roychoudhury[a], T. Tyliszczak[c]

a. Department of Earth Sciences, Stellenbosch University, Private Bag X1, Matieland, 7602, South Africa

b. Department of Geosciences, Princeton University, Princeton, NJ 08544, USA.

c. Advanced Light Source, Lawrence Berkeley National Laboratory, University of California, Berkeley, CA 94720, USA.

ABSTRACT

The Fe $L_{2,3}$-edge spectrum is sensitive to the local coordination environment around the Fe metal centre, making it a useful probe for understanding Fe speciation. Here we utilize Fe L_3-edge x-ray absorption spectroscopy (XAS) to explore and understand local coordination differences between various Fe oxide and oxyhydroxide standards. We parameterize the Fe L_3-edge spectrum according to the difference in energy (ΔeV value), and the intensity ratio of its constituent split peaks. Theoretically, the ΔeV value is related to the crystal field splitting whereas the intensity ratio value is affected by orbital composition. These two parameters are found to vary as a function Fe valence state and coordination number, chemical differences in the coordinating ligands, and the degree of distortion in the Fe polyhedra. These influences on the spectral parameters can easily explain the distribution of Fe oxide and oxyhydroxide phases on a ΔeV value versus intensity ratio plot. The two-parameter plot is thus presented as a phase-specific identification tool for use in Fe speciation studies.

1. INTRODUCTION

Iron $L_{2,3}$ edge x-ray absorption spectroscopy (XAS) provides important electronic information about the local atomic structure around the Fe centre, and this technique has thus been utilized in a considerable number of scientific studies; ranging from biogeochemistry (Wang et al., 1995; Calvert et al., 2005; Benzerara et al., 2007; Chan et al., 2009; Miot et al., 2009) and mineralogy (van Aken et al., 1998; Miyajima et al., 2004), to materials chemistry (Labatut et al., 1998; Grandjean et al., 1999; Mikhlin et al., 2005; Augustsson et al., 2005; Chen et al., 2007; Shirakawa et al., 2007). Much of this work, especially in hydrated systems, is possible because of the advancements in soft x-ray instrumentation (Cramer et al., 1992; Padmore and Warwick, 1994) and because of the volumes of early work devoted to developing a fundamental understanding of L-edge spectral features (van der Laan and Kirkman, 1992; Cressey et al., 1993;

Crocombette et al., 1995; de Groot, 2005). The Fe L-edge represents the probability and occurrence of dipole-allowed electronic transitions from 2p ground states to 3d-like molecular orbitals, and variations in the resultant spectra are interpreted as a function of valence state, site occupation, symmetry, spin state and degree of distortion (van der Laan and Kirkman, 1992; Schofield et al., 1995; de Groot, 2005; Miedema and de Groot, 2013). In addition to providing complementary information, the Fe L-edge is often preferred to Fe K-edge analyses because of better resolution of fine structure, higher absorption cross section, and lower intrinsic life-time broadening (de Groot, 2005).

The 2s and 2p electronic transitions of Fe can be probed by either XAS techniques using a synchrotron light source, or by Electron Energy-Loss Spectroscopy (EELS) using a transmission electron microscope (TEM). A comprehensive evaluation of these two techniques suggests that XAS is superior over EELS particularly when environmentally relevant hydrated samples are considered (e.g. Dynes et al., 2006; Bluhm et al., 2006). The fore-most reason for this is that XAS allows for the molecular level investigation of samples in their pristine state, without the need for sample drying, which can alter the chemical state of the elements of interest and can induce shrinkage, aggregation and water loss from the chemically-important hydration shells.

Application of the Fe $L_{2,3}$ edge for speciation and mineralogical studies, especially in samples of mineralogical and environmental significance, have thus far largely been limited to valence state quantification (Cressey et al., 1993; van Aken and Liebscher, 2002; Miyajima et al., 2004; Calvert et al., 2005; Cavé et al., 2006; Dynes et al., 2006). Fe oxidation state is undoubtedly a fundamental parameter governing Fe behaviour in biogeochemical and material science systems. However, given that the Fe L-edge probes local electronic structure (van der Laan and Kirkman, 1992; Cressey et al., 1993); the resultant spectrum is also sensitive to variations in coordination and ligands. Although a recent study has made use of this sensitivity to investigate ferrihydrite structure (Peak and Regier, 2012), to our knowledge, there has not as yet been a systematic and meticulous experimental study investigating the changes in XAS spectral features in response to varying Fe speciation. Miedema and de Groot (2013) present a comprehensive review of L-edge literature; however their focus is primarily on fundamental and theoretical L-edge interpretations. A number of studies have used the Fe L-edge as a speciation probe for investigating environmental Fe. Chan et al. (2004) uses Fe L-edge x-ray photoelectron emission spectromicroscopy to infer that mineralised bio-filaments consist of amorphous Fe oxyhydroxide. Bio-mineralization has also been investigated by Miot et al. (2009), who use the Fe L-edge to measure rates and extent of Fe oxidation by bacteria. The Fe L-edge has also been used to conclude that observed Fe(II) in hydrothermal systems is not present as finely dispersed Fe(II) minerals, but rather that the Fe(II) is stabilized by complexation with particulate organic matter (Toner et al., 2009). Here we combine an experimental approach with theoretical interpretation to produce a tool that will be useful for phase-specific identification in future environmental studies.

To this end, we utilize the differences in both L_3-edge peak splitting (ΔeV), and their peak intensity ratios (Fig. 1a) to explore the changes in Fe coordination environment. The L_3-edge peak-splitting can largely be attributed to the ligand field splitting of Fe d-orbitals into t_{2g} and e_g subsets, which can be further re-enforced by the formation of molecular orbitals that are split more intensely (Todd et al., 2003a; de Groot, 2005). The ΔeV value is thus strongly linked to the energy positions of these molecular orbitals, whereas the intensity ratio value is more greatly affected by the respective orbital compositions- with selection rules governing the likelihood of electronic transition occurrences. By interpreting high-resolution XANES (X-ray Absorption Near-edge Structure) spectra, this study investigates the factors that influence the ΔeV and intensity ratio values of the Fe L_3-edge for the polymorphs of the Fe oxide and oxyhydroxide system. These phases, which play an integral role in biogeochemical systems (von der Heyden, 2012) and contaminant transport processes (Hochella et al., 2005), are often small and difficult to differentiate using traditional methods. Considering that modern L-edge x-ray spectromicroscopic techniques have spatial resolution of down to 12 nm, we present a phase identification tool for application to experimental systems as well as to environmental fields, including colloid chemistry (Lead and Wilkinson, 2006; Wiggington et al., 2007) and aerosol speciation (Krueger et al., 2004; Majestic et al., 2007, Takahama et al., 2008).

2. EXPERIMENTAL

Synthesis of standards: Fe oxide and Fe (oxy-) hydroxide standards (goethite (α-FeOOH), akaganeite (β-FeOOH), lepidocrocite (γ-FeOOH), hematite (α-Fe_2O_3), maghemite (γ-Fe_2O_3), magnetite (Fe_3O_4) and amorphous iron oxyhydroxide) were prepared following the methods outlined in Schwertmann and Cornell (2000). The purities of the prepared standards were confirmed by X-ray diffraction (Rigaku XRD) and infrared spectroscopy (Bruker IFS 66v/s).

Data collection: The scanning transmission x-ray microscopy (STXM) experimentation was conducted at the Molecular Environmental Sciences (MES) beamline 11.0.2 at the Advanced Light Source, Lawrence Berkeley National Laboratory, USA (see Bluhm et al., 2006). A few µL of the suspended particulate standard was placed on a 100 nm thick Si_3N_4 sample window and allowed to air-dry for three to five minutes before being placed in the end-station for x-ray analysis. All x-ray scans were conducted in a 1 atm He environment and at ambient temperature. The end-station specifications; a 17 nm zone plate, a 1200 l/mm grating and 25 µm exit slits ensured theoretical spatial and spectral resolutions of 12 nm and 0.2 eV respectively. Energy calibration was achieved by setting the peak for neon 1s→3p transitions to 867.3 eV.

Particles were located using transmission mode x-ray microscopy at the Fe L-edge (705-701 eV). Once located, chemical analysis focussed on the smallest sized particles (20 nm to 400 nm) as transmission mode XANES data collection is best suited to thin particles, through which x-rays can pass without excessive absorption artifacts. Spectral stacks, representing image sequences taken at incremental energy levels between 695 eV and 730 eV, were collected of between 60 and 90 particles from each sample. Energy step-

sizes between successive images were 0.5 eV for the regions below and above the L_3 edge and 0.2 eV at the L_3 edge region (705 eV–715 eV). Spectral stacks were corrected using Zimba code in the software Axis2000 (Hitchcock, 2008) by implementing Sobel edge-enhancement and ensuring that the stacks were accurately aligned. Thereafter, particle-free areas of the map were chosen as the I_o representing a back-ground denominator and individual particles could be identified and analysed for averaged XANES spectra. For spectral interpretation, the software program WinXAS (Ressler, 1998) was used to ensure further background normalization to a polynomial fit, and peak positions and heights were located using the 'Search Min-Max' function. Spectral information for additional Fe-rich phases was compiled from published literature. Peak height and energy data were obtained either by contacting the corresponding author directly or by digitizing the published figures.

Additional comparisons were made between our spectral dataset and various physical parameters of the respective Fe-oxide and –oxyhydroxide coordination polyhedra. Structural details for the different Fe phases were obtained from the published crystal structure data (akaganeite (Post and Buchwald, 1991), ferrihydrite (Michel et al., 2007), goethite (Gualtieri et al., 1999), hematite (Blake et al., 1966), lepidocrocite (Wyckoff, 1963), maghemite (Shmakov et al., 1995), and magnetite (Fleet, 1986)). The investigations into their coordination environments were conducted using the crystallographic programs IVTON (Balic-Zunic and Vickovic, 1996) and XSeed (Atwood and Barbour, 2003).

3. RESULTS AND DISCUSSION

3.1 Theoretical influences of Fe L-edge spectral parameters

Although the L_3- and L_2-edges contain the same chemical information, the L_3-edge (representing the dipole-allowed $2p_{3/2}$ electronic transitions to the valence orbitals) shows sharper and better resolved spectral features than the corresponding L_2 edge (Fig. 1a). The splitting in the L_3 edge peak is largely due to the crystal field interaction; however, the spectral shape of the L_3 edge can also be influenced by inter-electronic repulsions, spin-orbit coupling, electrostatic multiplet effects, orbital covalency and core-hole effects (de Groot et al., 1990; Hocking et al., 2010; Miedema and de Groot, 2013). The split peaks of the L_3 edge can be parameterized by their peak intensity ratio value and a ΔeV value, representing the energy difference between the two peak positions (Fig. 1). Here we investigate and rank the physical and chemical factors that influence the ΔeV and intensity ratio values, thus determining the effects of mineralogical speciation on L_3-edge spectral features.

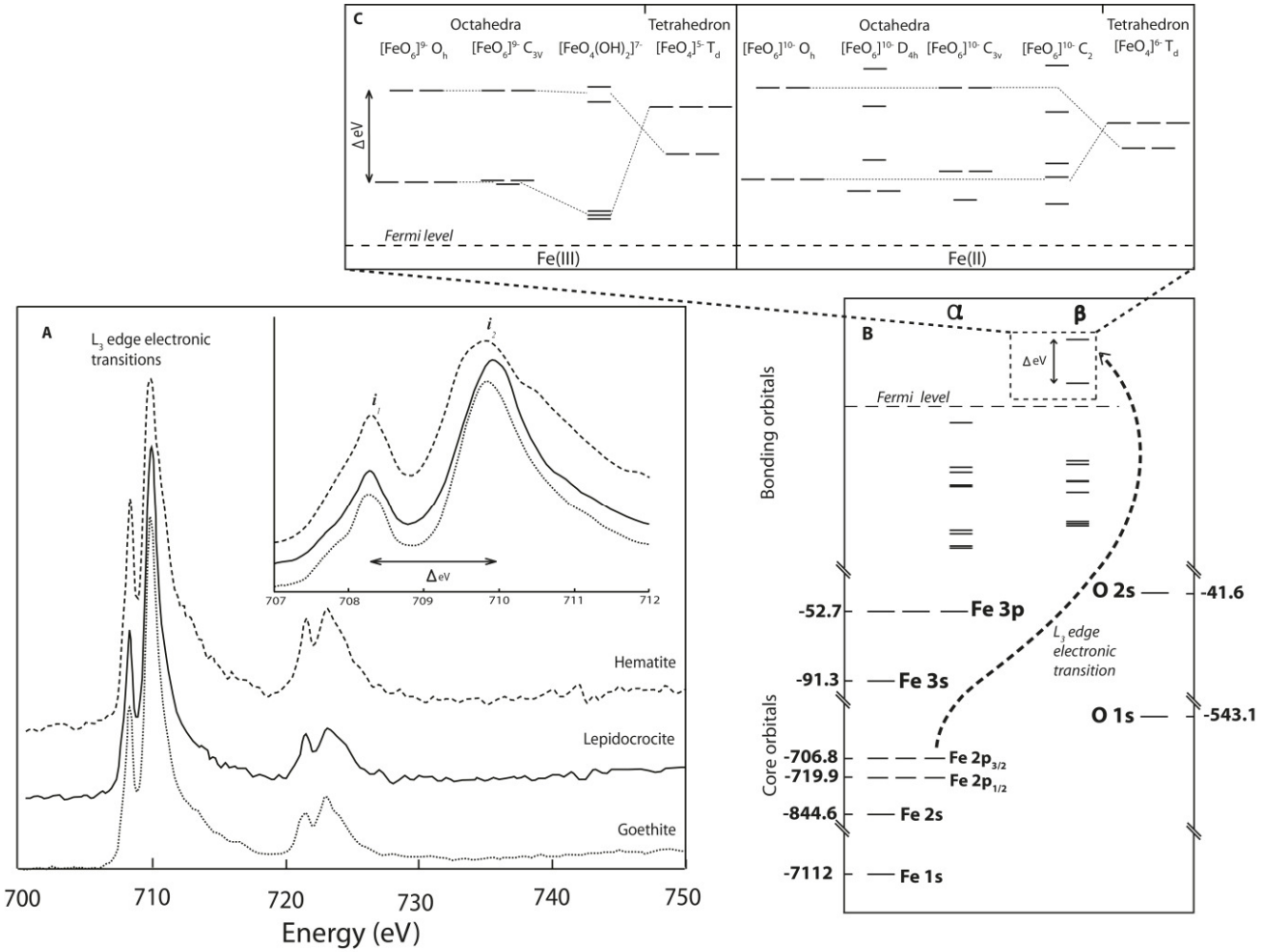

Fig. 1a: *XANES $L_{2,3}$-edge spectra of selected iron oxides and iron oxyhydroxides showing spectral shapes typical of ferric iron centers. Vertically exaggerated inset of the L_3 edge split peaks shows variations in intensity ratio (i_1/i_2) between hematite (--) and the oxyhydroxide phases; and variation in the ΔeV value between the polymorphs goethite (¨) and lepidocrocite (⁻). **1b:** Molecular orbital diagram highlighting the Fe $2p_{3/2}$ electronic transitions to the t_{2g} and e_g valence orbital subsets. The energy difference between these subsets gives rise to the observed spectral splitting ΔeV (Fig. 1a). **1c:** Variations in local coordination environment around the Fe centre can induce additional degeneracy in the valence orbitals and shifts in their relative energy positions (reflected in ΔeV). Modeled energy level data are from Sherman, 1985a (FeO_6^{9-} O_h; FeO_6^{9-} C_{3v} (trigonal distortion) and FeO_4^{5-} T_d); Sherman, 1985b ($FeO_4(OH)_2^{7-}$); Tossell et al., 1974 (FeO_6^{10-}); Vaughan et al., 1974 (FeO_4^{6-}) and Burns, 1970 (Fe(II) octahedra with D_{4h} (elongated along tetrad axis); C_{3V} (compressed along tetrad axis) and C_2 (monoclinic) symmetries).*

3.1.1 ΔeV

Fe orbital interaction with a ligand field removes Fe 3d orbital degeneracy and induces peak splitting in the corresponding L-edge spectrum. Because of their strong impact on the ligand field splitting parameter, Fe valence state and Fe coordination number represent first order impacts on the ΔeV value. Fe(II) phases show a larger degree of variability in their ΔeV value (1.1 eV- 2.8 eV (Fig. 2a)), with Fe(II) silicates showing particularly high values (2.2 eV- 2.8 eV). The Fe(III) system is relatively more constrained comprising of ΔeV values ranging between 1.3 eV- 2.0 eV. Fe coordination environment impacts directly on ligand field splitting ($\Delta_t = {}^4/_9\Delta_o$) (Fig 1c) and detailed analyses show that $Fe(III)_{Td}$ phases have lower ΔeV values (average:

1.42) compared to $Fe(III)_{Oh}$ phases (average ΔeV: 1.57). To further test the relationship between ΔeV and the ligand splitting parameter, Table 1 shows a comparison between STXM ΔeV measurements and conventional UV-vis measurements of valence electron transitions in Fe oxide and oxyhydroxide phases. With the exception of the maghemite data point, there exists good agreement (r^2 = 0.67) between the optical (Hocking et al., 2010) and STXM data and the observed average offset of about 0.3 eV between these two data sets is attributed to the absence of core-hole effects in the optically-measured values. Oxygen K-edge values can also be used to infer ΔeV values in the Fe oxide system (Table 1). Again, a discrepancy in measured values is observed when comparing STXM data to the O K-edge data and this has been attributed to the greater orbital relaxations associated with Fe 2p transitions to the t_{2g} and e_g orbitals (Fig 1b), relative to similar O 1s transitions (de Groot et al., 1989; Todd et al., 2003b). Comparisons with the O K-edge are limited to the pure oxide phases, because the presence of hydroxyl oxygen results in additional spectral structure.

Table 1: Comparison between various methods for determining d-orbital splitting

Species	ΔeV (STXM)	Optical 10Dq	Oxygen K-edge
Goethite	1.541[1]	1.902[2]	-[a]
Lepidocrocite	1.653[1]	1.980[2]	-[a]
Hematite	1.525[1]	1.738[2]	1.406[3]
Maghemite	1.427[1]	1.913[2]	0.909[4]

[1]Our data, [2]Sherman and Waite (1985), [3]Sherman (2005), [4]Gilbert et al. (2010). [a]Presence of both oxo- and hydroxyl ligands prevents direct determination of orbital splitting from the oxygen K-edge. Dataset limited to the Fe-oxide and oxyhydroxide system because of the scope of this study and because 10Dq values for Fe-silicate species are difficult to estimate due to low symmetry and trace impurities (Burns, 1970). Data for maghemite (γ-Fe_2O_3) may be complicated by the presence of Fe in both octahedral (O_h) and tetrahedral (T_d) sites.

Ligand effects, which can influence the extent of ligand field splitting, play a second order role in impacting spectral ΔeV values. Specifically, the spectrochemical series can be used as a semi-quantitative measure in determining relative ligand field splitting with strong field ligands such as SO_4^{2-} (ΔeV = 1.58-1.65 (Shirakawa et al., 2007; Peak et al., 2012) displaying the high ΔeV whereas weak field ligands such as NO_3^- (ΔeV = 1.41 (Peak et al., 2012)) have lower values. To exclude ligand-specific effects, additional comparisons were made using only the spectral parameters of the polymorphs of the Fe oxide and oxyhydroxide system (only ligands: O^{2-} and OH^-) (Fig 2b). Because Fe L-edge spectroscopy probes only the local coordination environment (van der Laan and Kirkman, 1992); additional differences in the measured ΔeV values in this system must be related to variations in the coordination polyhedra. Mineralogical aspects of the different phases dictate the geometry, and number and type (face-, edge- or point-sharing) of linkages of local Fe coordination polyhedra (Fig. 3) and these third order effects results in ΔeV shifts of around 0.12 eV (Fig 2b).

Figure 4 summarizes the relationship between spectral parameters and a number of properties of coordination polyhedra. Angle variance and quadratic elongation relate to the variations in ligand bond angle and length respectively (Robinson et al., 1971), whereas volume distortion percentage is measured relative to the volume of an ideal polyhedron (Makovicky and Balic-Zunic, 1998; Balic-Zunic, 2007). The ΔeV spectral

parameter displays a strong and positive correlation with increasing bond-angle variation and shows a strong negative correlation with variability in ligand bond length. Comparison between the polyhedral volume distortion and the ΔeV value yields a strong positive correlation. The number and types of polyhedral linkages also influence the local bonding environment within the Fe coordination polyhedron. The ΔeV value shows only moderate and negative correlation to the total number of polyhedral linkages with the prevalence of edge-sharing linkages over corner-sharing linkages favouring higher ΔeV values. Finally, additional distortion effects can occur for example, with the presence of trace impurities. These distortion effects can exert profound influence the geometry and point group symmetry of coordination polyhedra, with the ability to remove degeneracy of molecular orbitals (Fig. 1c; Sherman, 1985a). Such multiplet effects can lead to spectral peak broadening and shifts in the ΔeV value, depending on the composition of the orbitals resulting from distorted symmetry.

3.1.2 Intensity Ratio

The intensity ratio of the constituent split peaks of the Fe L_3 edge spectrum have traditionally been used in valence state quantification studies (Cressey et al., 1993; van Aken and Liebscher, 2002; Miyajima et al., 2004; Calvert et al., 2005; Cavé et al., 2006; Dynes et al., 2006). Accordingly, Fe oxidation state and the corresponding number of vacancies in the valence orbitals exert the strongest control on Fe L_3 edge intensity ratio (Fig. 2a). An intensity ratio of ~1 can be used to clearly differentiate between ferric Fe species and ferrous species, the former having an intensity ratio around 0.51 (±0.18) whereas the latter averages around 2.00 (±1.50). Mixed valence species reported in published literature have an average intensity ratio that is closer to 1 (0.69±0.31). Additional first order influences on the number of orbital vacancies, and thus the L_3-edge intensity ratio, include the coordination number (O_h versus T_d) and the spin state (high spin versus low spin) of the Fe species.

Second order influences on the intensity ratio value are attributed to ligand effects on the chemical character of available singly-occupied and unoccupied molecular orbitals. In accordance with the Laporte selection rule (Burns, 1970), it is particularly the amount of Fe d-character (or conversely, the amount of ligand p-character) in these valence orbitals that determines the likelihood of dipole-allowed 2p→3d electronic transitions. In their work on differential orbital covalency in Fe chelators, the L-edge splitting data of Hocking et al. (2010) shows good correlation with both the bond length (affected by bond covalency/ionicity) and the % d-character (inversely proportional to bond covalency) in valence orbitals (Table 2). Bond covalency is closely tied to π-bonding interaction which occurs exclusively between ligand p-orbitals and the Fe 3d t_{2g} subset of orbitals. If the low and high energy peaks in the Fe L_3 edge spectrum are tentatively assigned t_{2g} and e_g character respectively, then changes in the overall bond covalency, a ligand-specific effect, will impact on the observed spectral intensity ratio. Ligand effects influence the intensity ratio by up to a value of 0.2 when ligands are similar (e.g. O^{2-} vs OH^-, Fig. 2b), and this influence can exceed

0.4 when ligands are vastly different (S^{2-}: 0.816 (Bornite (Miklin et al., 2005)) versus NO^{3-}: 0.387 (Peak and Regier, 2012)).

Table 2: Intensity ratio correlation to bond length and orbital character in organic Fe chelates

Species	Intensity Ratio	Average bond length	Average % d-character in valence orbitals
$[Fe(ox)_3]^{3-}$	0.490	2.008	84
$[Fe(pha)_3]$	0.428	2.013	68
$[Fe(cat)_3]^{3-}$	0.3868	2.017	65
	Correlation R^2 value:	0.997 (-)	0.934 (+)

*** All data after Hocking et al. (2010)*

Polyhedral distortion also affects the orbital composition by inducing multiplet structure in which the ligand p-character is further split among orbitals at different energy levels. Considering the Robinson et al. (1971) measure distortion, the intensity ratio values for species from the Fe –oxide and –oxyhydroxide do not correlate with variations in bond angle and show only relatively weak positive correlation with the changes in bond length (Fig. 4a). The correlation between intensity ratio value and the volume distortion percentage is negative (r^2 = 0.5878, Fig. 4c), indicating that high ratios are favoured when the degree of polyhedral distortion is low. The intensity ratio shows better correlation with the number and type of polyhedral linkages experienced between adjacent Fe coordination polyhedra: large intensity ratios are strongly favoured as the number of polyhedral linkages increases, particularly when the proportion of corner-sharing linkages increases preferentially (Fig. 4a).

3.2 Application of L_3-edge XAS to Fe-oxide and -oxyhydroxide speciation

The sensitivity of the Fe $L_{2,3}$-edge to local coordination (i.e. variations in ligand arrangement and type) renders it an ideal probe to investigate Fe mineralogy. Figure 2b plots the spectral parameters (ΔeV and intensity ratio) of environmentally relevant Fe oxide and –oxyhydroxide mineral phases: amorphous Fe oxide, goethite (α-FeOOH), akaganeite (β-FeOOH), lepidocrocite (γ-FeOOH), hematite (α-Fe_2O_3), maghemite (γ-Fe_2O_3) and magnetite (Fe_3O_4). The plot is limited to the Fe-O and Fe-OH system to limit any additional ligand-specific effects (e.g. electronegativity, ionic size and charge, and specific bonding interaction) to the value of the spectral parameters. Each solid square represents the average ΔeV and intensity ratio value for each phase, taken from analyses of between 60-90 particles, and the error bars reflect their respective standard deviations. Particles ranged in size between 20 and 400nm and only particles with an L_3 edge high energy peak intensity of between 0.17 and 0.83 were used for the plot. This matched the intensity range observed in natural samples (von der Heyden et al., in prep) and limits x-ray saturation effects from thicker particles and noise interference from thinner samples with weak spectra. Despite constraining this range, some saturation was still observed and resulted in broader horizontal error bars associated with the intensity ratio averages (Fig 2b).

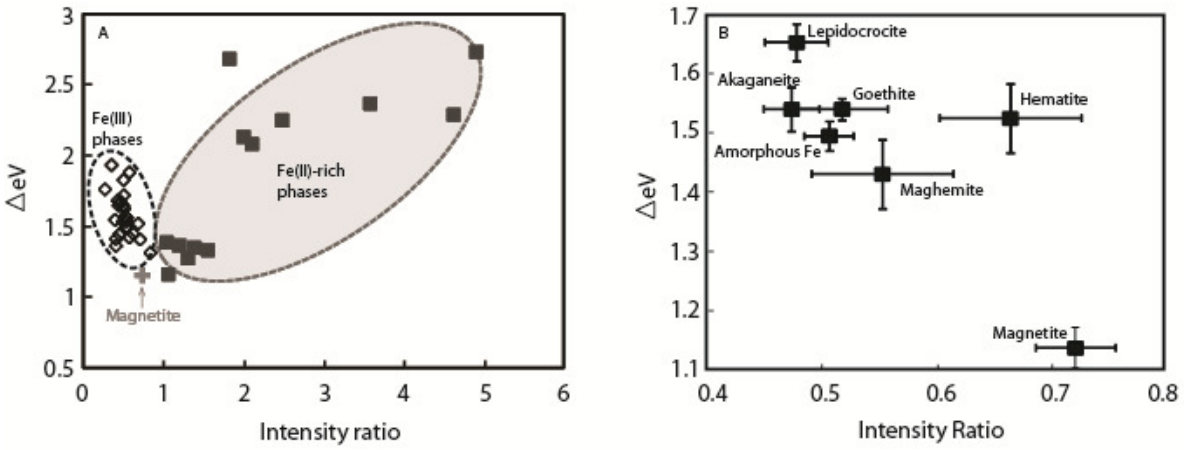

Fig. 2a: *ΔeV versus intensity ratio plot of spectral parameters of various published Fe phases. An intensity ratio of ~1 can be used to distinguish between Fe(II)-rich and Fe(III)-rich phases (adapted from von der Heyden et al., 2012 SM).* ***2b:*** *ΔeV versus intensity ratio plot for the Fe oxide and Fe oxyhydroxide system, showing how characteristic spectral features can be used to differentiate between phases with differing structure and chemistry.*

The most noticeable controls on the phase distribution in the plot are the first order and second order effects of coordination number and ligand type respectively. Mineral phases characterized by the presence of tetrahedral iron (magnetite (Fig. 3j), maghemite (Fig. 3m), and possibly ferrihydrite (Fig. 3g; Michel et al., 2007)) typically have the lowest values for ΔeV. This is in agreement with the generalized chemical trend for ligand field splitting in which $\Delta_t = {}^4/_9\Delta_o$ (e.g. Burns, 1970) (Fig. 1c). Although the number of different types of ligands has been limited in this dataset, the presence of hydroxyl ligands causes marked shifts in the molecular orbital structure of Fe polyhedra (Fig. 1c; $FeO_4(OH)_2^{7-}$ octahedron). This is reflected in the ΔeV versus intensity ratio plot where the polymorphs of the Fe-oxyhydroxide system have a larger average ΔeV value than the Fe-oxides, although this average may be skewed by other structural factors (e.g. valence state and coordination environment). The presence of the hydroxyl ligands in the FeOOH mineral structure also results in lower intensity ratio values (<0.55), relative to pure oxide phases (intensity ratio greater than 0.55). The lower intensity ratio values in Fe oxyhydroxide phases indicate that bonding to hydroxyl groups results in modifications to the valence orbital compositions, making transitions to the high energy orbitals relatively more favourable.

By virtue of their polymorphism, the Fe oxyhydroxides have equivalent chemical stoichiometry and are closely grouped on the ΔeV versus intensity ratio diagram. Third order distortion effects need to be invoked to explain the small differences in their distribution on the plot. Goethite (αFeOOH) has a tunnel structure (Cornell and Schwertmann, 2003) characterized by one type of Fe octahedron showing only moderate percentage volume distortion (Fig. 3a). Distortion in the goethite octahedron is caused by differences in the coordinating ligand (hydroxyl oxygen bond distances >2 Å, oxygen groups bond distances <2 Å) and by variations in the type of linkages to adjacent Fe octahedral (e.g. the longest bonds are between the Fe centre and hydroxyl ligands which are shared by two adjacent edge-sharing octahedral).

Akaganeite is structurally similar to its polymorph goethite as they both have equal number and types of polyhedral linkages between adjacent octahedra. It is thus not surprising that their fields in the ΔeV versus intensity ratio plot are very close and partially overlap. There is insignificant difference in the degree of splitting in the valence orbital structure (both ΔeV values ~ 1.54) and their plotted fields are thus only offset by a difference in intensity ratio of ~0.05. Although the spectral interpretation of akaganeite may be slightly complicated by the presence of chloride ions and two structurally different Fe sites, the relationships in figure 4 should still be explored when explaining the observed shift in intensity ratio. The relationship between goethite intensity ratio (0.52) and akaganeite intensity ratio (0.47) does not conform to the trends in the either the angle variance or the quadratic elongation distortion parameters, both of which are only weak to moderate trends. The higher averaged volume distortion in the akageneite octahedra relative to the goethite octahedron is in good agreement with the strong negative correlation between intensity ratio and percentage volume distortion (Fig. 4c). The effect of volume distortion may be larger than alluded to by the average value reported for the akaganeite structure, as the resolved values for each centre show that the akaganeite Fe1 octahedron has the highest degree of volume distortion for any of the Fe oxide or -oxyhydroxide polyhedra (Fig. 3c).

Lepidocrocite differs from its polymorphs in that it has a layered structure and each Fe octahedron consists of only two hydroxyl groups. Mineral stoichiometry is achieved by the linkage arrangement between adjacent polyhedral, as each hydroxyl group is only shared by one edge-sharing octahedron whereas each oxygen ligand is shared by two adjacent Fe octahedra. This low proportion of corner-sharing linkage interactions is one reason that lepidocrocite has a higher ΔeV value than its polymorphs (Figs. 3, 4). The increased ΔeV value relative to its polymorphs is in agreement with previous studies that have shown lepidocrocite to have a higher degree of crystal field splitting (Sherman and Waite, 1985). The degree of polyhedral distortion likely compounds the effects of the low percentage of corner sharing polyhedra and can further be used to explain the observed high ΔeV value. This is true for all three distortion parameters as lepidocrocite has a high angle variance (+ correlation to ΔeV), the lowest quadratic elongation value (-correlation to ΔeV) and the highest volume distortion percentage (+ correlation to ΔeV). The average lepidocrocite intensity ratio value (0.48) is very similar to that of akaganeite and its dissimilarity to the goethite value can only be attributed to the differences in volume distortion percentage and the percentage of corner sharing polyhedra.

The Fe oxide side of the plot (intensity ratio > 0.55) consists of the polymorphs of the Fe_2O_3 system and the mixed-valence phase magnetite. The magnetite point is plotted from data collected from only one spectrum and the associated error bars are estimated from the average of the standard deviations found in the other six data points. The magnetite spectral shape and position of this field on the plot matches well with other published data (Kendelewicz et al., 2000; Regan et al., 2001; de Smit et al., 2009). Magnetite has a low ΔeV value that can largely be attributed to the presence of tetrahedral Fe(II)- which has a particularly low degree of crystal field splitting (Fig. 1c). The low volume distortion in the polyhedra can further lower the observed

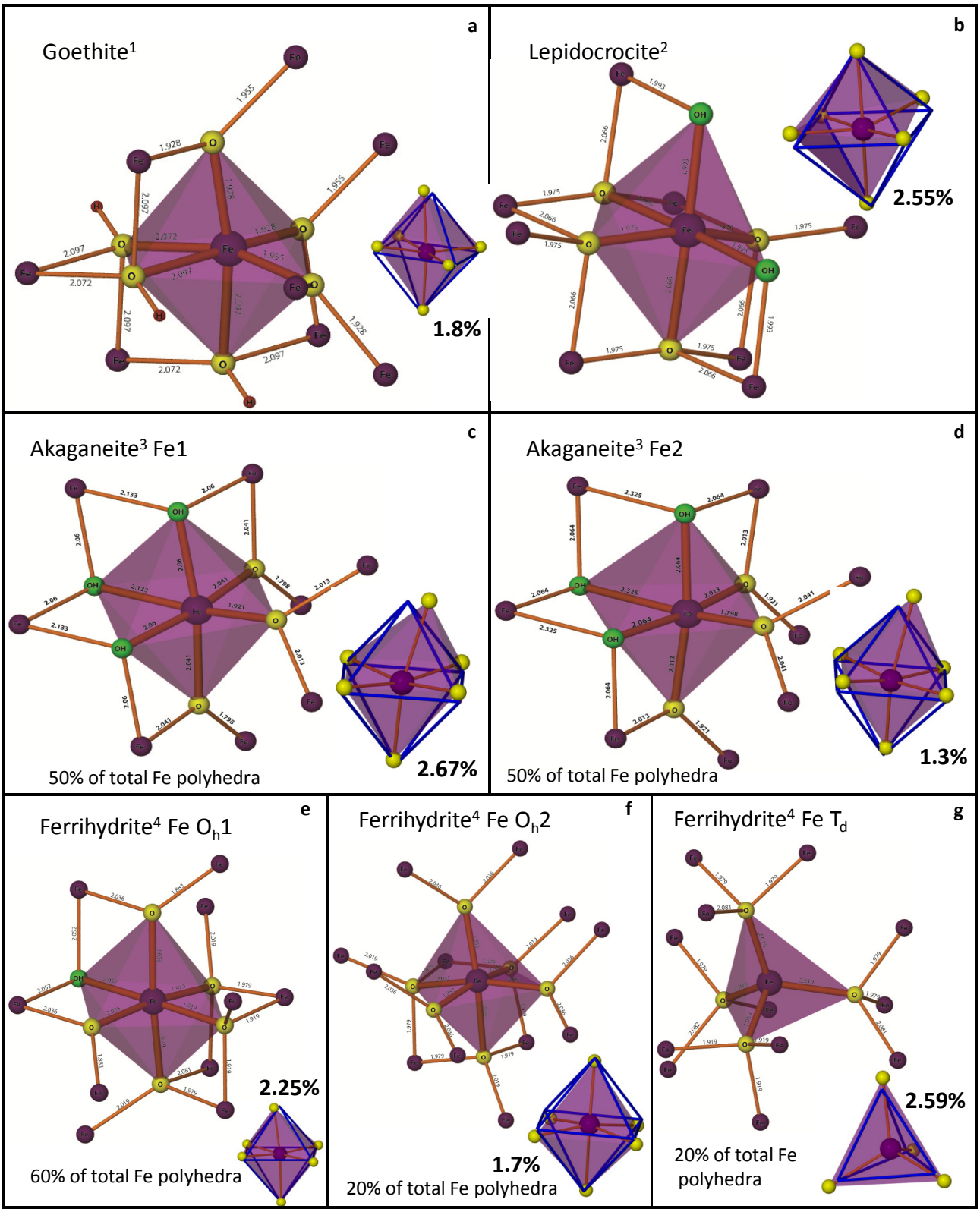

Fig. 3: *Iron polyhedra with local coordination for the Fe oxide and oxy-hydroxide mineral phases analyzed in this study. Polyhedral distortions are the result of chemical and mineralogical (i.e. number and type of polyhedral linkages) properties of the respective phases. Inset octahedra are relative to a perfect octahedron and give an idea of the bond angle distortions and volume distortion (% volume distortion measure indicated in bold). All bond lengths are in Angstrom units (Å) and all images were generated using XSeed (Atwood and Barbour, 2003) and crystallographic data from published references: [1]Gualtieri et al, 1999; [2]Wyckoff, 1963; [3]Post and Buchwald, 1991; [4]Michel et al, 2007; [5]Blake et al, 1966; [6]Fleet, 1986; [7]Shmakov et al, 1995.*

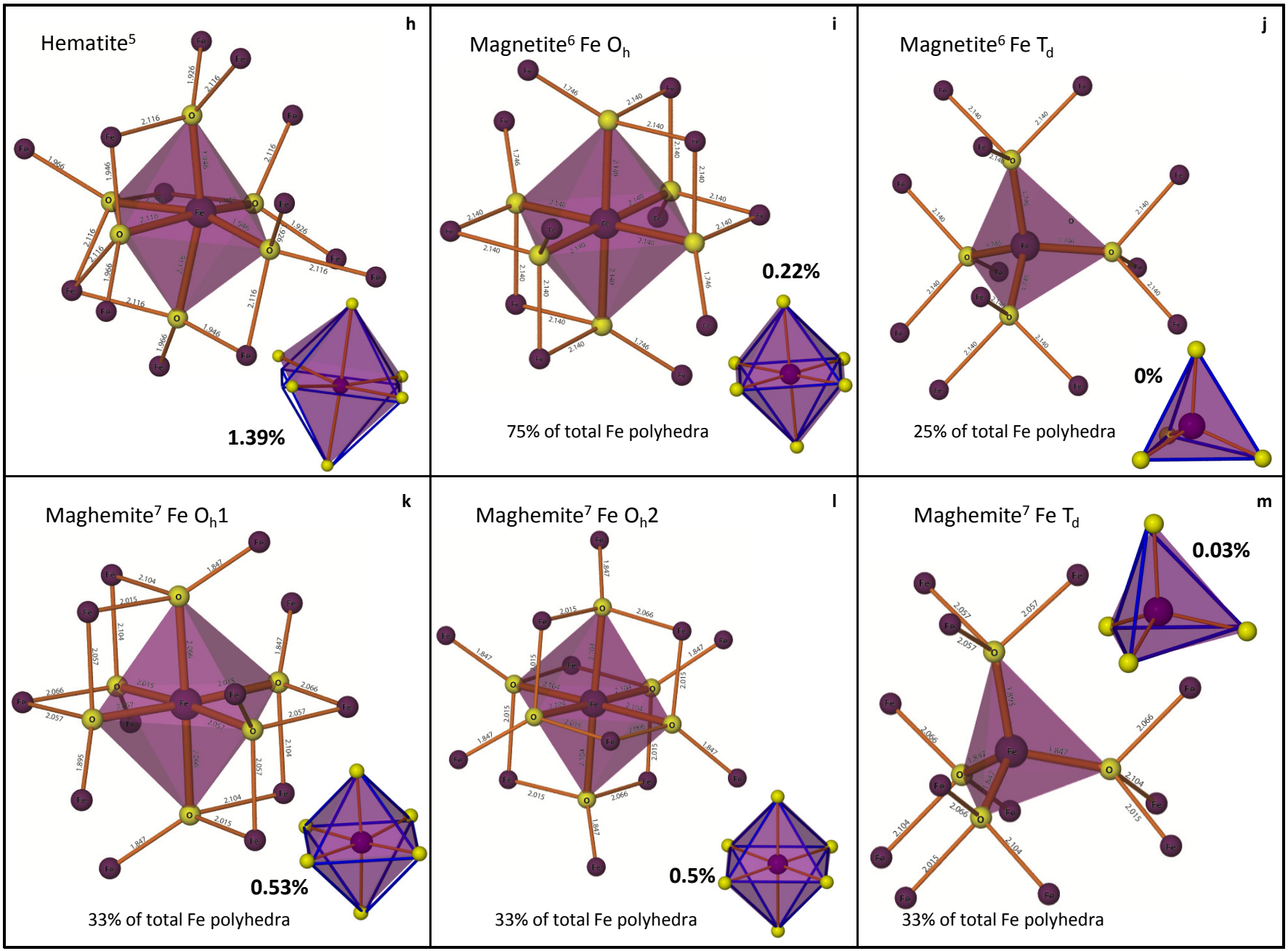

ΔeV value, as can the large percentage of corner-sharing linkages (Fig. 3i, j). Magnetite has the highest intensity ratio due to structural Fe(II), the absence of hydroxyl ligands, a high number adjacent polyhedra and a large proportion of the polyhedral linkages connecting via corner-shared oxygen atoms.

Maghemite and hematite are both polymorphs of Fe_2O_3 with the former having a cubic crystal structure and the latter belonging to the trigonal crystal system. Spectral interpretation of the maghemite data points may be complicated by the presence of three different types of Fe sites (Fig. 3k-m), which can lead to additional multiplicity in the number and energies of the transitions to valence orbitals. Despite being structural similar to magnetite, the maghemite point plots away from the magnetite point on the ΔeV versus intensity ratio plot (Fig. 2b). This discrepancy is predominantly due to differences ΔeV value. Although both phases have low ΔeV values due to the presence of tetrahedral Fe, the magnetite ΔeV value (1.13) is lower than the maghemite ΔeV value (1.43). This can be explained by maghemite having a higher proportion of its Fe in tetrahedral coordination.

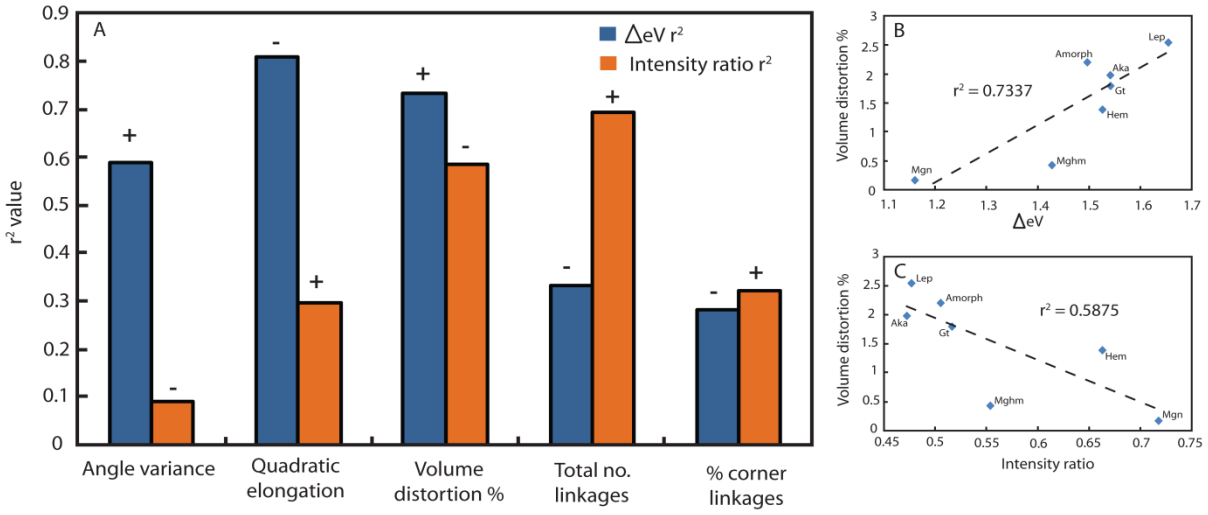

Fig. 4a: *Goodness of fit plot obtained from r^2 values derived from comparisons between spectral parameters and various structural and distortion parameters. Plus and minus symbols refer to positive and negative correlations respectively and it is noted that there is typically an inverse relationship between the effects on ΔeV and intensity ratio.* ***4b:*** *Volume distortion versus ΔeV and,* ***4c:*** *volume distortion versus intensity ratio plots for polyhedra from the Fe oxide and oxyhydroxide system. Trend lines reflect the degree of correlation between the respective parameters.*

Relative to the oxyhydroxide phases, hematite also has a slightly lower ΔeV value and, although this may be a ligand effect due to the absence of hydroxyl groups, the total number of linkages and the percentage corner linkages could also be playing a role. Additional support for the positioning of hematite above maghemite on the ΔeV scale is given by hematite's higher angle variance, lower quadratic elongation and higher percentage volume distortion. Aside from the absence of hydroxyl groups, the major factors increasing the intensity ratio of the oxide phases relative to the oxyhydroxides, is the higher total number of polyhedral linkages associated with each Fe polyhedron and the enhanced proportion of these being corner-sharing linkages.

Amorphous iron-oxide, or ferrihydrite, plots with a ΔeV value of 0.51 ±0.02 and an intensity ratio value of 1.50 ±0.02. The position of this field on the ΔeV versus intensity ratio plot may render some insights into the controversy that currently ensues over the structure of ferrihydrite (Jambor and Dutrizac, 1998; Janney et al., 2001; Michel et al., 2007; Peak and Regier, 2012; Manceau, 2012). Amorphous Fe has an intensity ratio that is less than 0.55, suggesting that a proportion of the ligands present in the local coordination environment are in fact hydroxyl groups. The amorphous Fe field plots closest to goethite suggesting a degree of structural similarity between the two phases, particularly that amorphous Fe is likely to have a more contained structure relative to the layered lepidocrocite. Because of its greater intensity ratio, amorphous Fe is likely to have a lower degree of average percentage volume distortion to lepidocrocite and akaganeite. Despite the assumed presence of hydroxyl ligands, the ΔeV value for amorphous Fe plots in the lower range of ΔeV values; values which are more strongly associated with the Fe oxide phases. This suggests that other structural properties are responsible for the decreased ΔeV value. Plausible structural explanations for the lowered ΔeV value include the presence of tetrahedral Fe, a lower proportion of hydroxyls than what is found in oxyhydroxide structure, or that there is a lower average volume distortion in each polyhedron-characterized by more variable bond lengths but less variable bond angles.

Comparing these theorized properties to the structure for ferrihydrite proposed by the Michel model (Fig. 3e-g); we find a pretty good agreement. Their model reports a presence of 10-20% structural Fe(III) in tetrahedral coordination, although subsequent Fe L-edge work has suggested that the amount of tetrahedral Fe(III) could be as high as 40% (Peak and Regier, 2012). Because our amorphous Fe ΔeV value is larger than the maghemite ΔeV value, an explanation based solely on the presence of tetrahedral Fe(III) would then argue for a lower percentage contribution of Fe(III) in tetrahedral coordination, in agreement with data from Michel et al., 2007. The Michel model, which is based on the structure of the mineral akdalaite ($Al_{10}O_{14}(OH)_2$), suggests that the ferrrihydrite chemical formula is $Fe_{10}O_{14}(OH)_2$. This presence of hydroxyl ligands can explain the low (<0.55) intensity ratio observed in our results, however the low proportion of hydroxyl ligands relative to oxygen ligands may also be (partially) causative for the lower ΔeV value (Fig. 1c). Distortion effects can cause third order variations to the ΔeV values; particularly, an increase in %volume distortion favours higher ΔeV values (Fig. 4a). However, the average percentage volume distortion for ferrihydrite (2.21%), predicted by the Michel model, is higher than for the goethite and akaganeite distortion values (Fig. 3a, c-g). This indicates that this distortion effect cannot be responsible for the observed low ΔeV value, thereby highlighting the importance of the other chemical factors (i.e. tetrahedral Fe and the presence of hydroxyls) for explaining our observed results.

4. CONCLUSIONS

The Fe L_3-edge splitting can be parameterized into ΔeV and intensity ratio values, both of which can be easily quantified and explained in terms of molecular level chemistry. The ΔeV value exists and is primarily controlled by crystal field splitting whereas the intensity ratio is explained by orbital selection rules, with orbital character and vacancies being the first order effect. For variations in both the ΔeV and intensity ratio parameters, ligand effects and polyhedral distortions represent second and third order influences respectively.

For the whole iron system, interpretations of the variations in the parameters are complicated by the sheer number of factors that exert an influence on the local coordination environment. These factors include the Fe valence state, coordination number, symmetry, ligand properties and structural concerns. This study focuses on the Fe oxide and oxyhydroxide system in which valence state, coordination number and ligand effects have largely been limited. The distribution of the spectral parameters of Fe oxides and –oxyhydroxides on a ΔeV versus intensity ratio plot is interpreted in terms of their respective mineral structures. Shifts in the ΔeV value (a value related to the energy positions of the valence orbitals) are attributed primarily to the first order impacts of valence state and coordination number (e.g. low ΔeV values are associated with magnetite and maghemite, characterised by the presence of tetrahedral Fe(III)). A secondary control is the presence of hydroxyl ligands, which are modelled to increase the splitting of the valence orbitals (Fig. 1c). Third order effects, particularly distortions to the local Fe polyhedra, are used to explain differences in the ΔeV values of the Fe oxyhydroxide polymorphs. High values are favoured when there is a high degree of angle variance, a smaller degree in the variability in bond lengths (quadratic elongation) and a high degree of volume distortion.

Similarly, the distribution of intensity ratio values on the two parameter plot can be explained by considering structural and chemical differences between Fe oxide and oxyhydroxide phases. The largest control on the intensity ratio in the Fe L_3-edge is the Fe valence state, and the intensity ratio can easily be used to differentiate between Fe(II) and Fe(III) phases (Fig. 2a). With the exception of the magnetite data point, the valence state of Fe in the ΔeV versus intensity ratio plot is limited to the Fe(III) system, and it is thus the secondary effect of ligand type that is most significant in separating the distribution of the oxide phases from the oxyhydroxide phases. Because intensity ratio is linked to orbital composition, and because it is difficult to estimate (or model) the effects of polyhedral distortion and linkages on orbital composition, we rely on the relationships plotted in figure 4a to determine the respective roles of these third order impacts. An absence of percentage volume distortion- as polyhedral shapes approach a perfect octahedron- favours higher intensity ratios, as does an increase in the total number of polyhedral linkages.

We thus present a plot that defines the different Fe oxide and oxyhydroxide minerals according to their unique spectral features and which is expected to have significant application to Fe speciation studies,

particularly in the realm of nano- and micron-scale sciences. This is especially true for environmental systems where chemically precise data is needed to understand the behaviour and fate of colloids in aerosol and aquatic systems. Indeed, the plot has already proven its utility, in that our experimental results for the amorphous Fe spectral parameters lend support to the structural model proposed by Michel et al. (2007). The applicability of the plot is highest for clean experimental systems, as trace impurities in natural samples can cause structural and chemical alterations that will be reflected in the spectral parameters (von der Heyden et al., in prep). Although still highly applicable to differentiating between Fe(II) and Fe(III) phases (Fig. 2a), the applicability of our plot to Fe(II) phase-specific identification may further be hampered by technique limitations. Electron Energy Loss Spectroscopy (EELS), Fluorescent Yield (FY) and Total Electron Yield (TEY) L-edge probes are all surface sensitive techniques and collected spectra will thus easily be contaminated by surface oxidation. Furthermore, despite the bulk sensitivity of the STXM probe, its reliance on X-ray transmission necessitates an extremely small sample thickness, resulting in a large surface area to volume ratio, and enhanced spectral signal from any surface oxidation.

ACKNOWLEDGEMENTS.

This research is supported by grants from NRF, South Africa (Blue Skies Program), Stellenbosch University VR(R) fund, NSF (chemical sciences), US-DOE (BES & SBR), and Princeton in Africa program. The authors would like to thank the support staff at the Advanced Light Source for helping with data collection and sample preparation and Prof. Len Barbour for his help with the crystallographic program XSeed.

REFERENCES

Atwood J. L. and Barbour L. J. (2003) Molecular graphics: from science to art. *Cryst. Growth Des.* **3,** 3.

Augustsson A., Zhuang G. V., Butorin S. M., Osorio-Guillen J. M., Dong C. L., Ahuja R., Chang C. L., Ross P. N., Nordgren J., and Guo J.-H. (2005) Electronic structure of phospho-olivines Li_xFePO_4 (x = 0, 1) from soft-x-ray-absorption and -emission spectroscopies. *J. Chem. Phys.* **123,** 184717_1-9.

Balic Zunic T. and Vickovic I. (1996) IVTON- program for the calculation of geometrical aspects of crystal structures and some crystal chemical applications. *J. Appl. Crystallogr.* **29,** 305-306.

Balic Zunic T. (2007) Use of three-dimensional parameters in the analysis of crystal structures under compression. In: Grzechnik A, editor. Pressure-induced phase transitions. Trivandrum: Transworld Research Network; pp. 157-184.

Benzerara K., Menguy N., Banerjee N. R., Tyliszczak T., Brown Jr G. E., and Guyot F. (2007) Alteration of submarine basaltic glass from the Ontong Java Plateau: A STXM and TEM study. *Earth Planet. Sci. Lett.* **260,** 187-200.

Blake R. L., Hessevick R. E., Zoltai T., and Finger, L. W. (1966) Refinement of the hematite structure. *Am. Mineral.* **51,** 123–129.

Bluhm H., Andersson K., Araki T., Benzerara K., Brown G. E., Dynes J. J., Ghosal S., Gilles M. K., Hansen H.-Ch., Hemminger J. C., Hitchcock A. P., Ketteler G., Kilcoyne A. L. D., Kneedler E., Lawrence J. R., Leppard G. G., Majzlam J., Mun B. S., Myneni S. C. B., Nilsson A., Ogasawara H., Ogletree H. F., Pecher K., Salmeron M., Shuh D.

K., Tonner B., Tyliszczak T., Warwick T., and Yoon T. H. (2006) Soft X-ray microscopy and spectroscopy at the molecular environmental science beamline at the Advanced Light Source. *J. Electron Spectrosc.* **150,** 86-104.

Burns R. G. (1970) Mineralogical applications of crystal field theory. Harland W. B., Agrell S. O., Davies D., Hughes H. F., editors. Cambridge University Press.

Calvert C. C., Brown A., and Brydson R. (2005) Determination of the local chemistry of iron in inorganic and organic materials. *J. Electron Spectrosc.* **143,** 173-187.

Cavé L., Al T., Loomer D., Cogswell S., and Weaver L. (2006) A STEM/EELS method for mapping iron valence ratios in oxide minerals. *Micron* **37,** 301-309.

Chan C. S., Fakra S. C., Edwards D. C., Emerson D., and Banfield J. F. (2009) Iron oxyhydroxide mineralization on microbial extracellular polysaccharides. *Geochim. Cosmochim. Ac.* **73,** 3807-3818.

Chen K.-F., Lo S.-C., Chang L., Egerton R., Kai J.-J., Lin J.-J., and Chen, F.-R. (2007) Valence state map of iron oxide thin film obtained from electron spectroscopy imaging series. *Micron.* **38,** 354-361.

Cornell R. M. and Schwertmann U. (2003) The iron oxides: Structure, properties, reactions, occurrences and uses. Weinheim, New York, Basel, Cambidge, Tokyo: VCH.

Cramer S. P., Chen J., George S. J., van Elp J., Moore J., Tensch O., Colaresi J., Yocum M., Mullins O. C., and Chen C. T. (1992) Soft -ray spectroscopy of metalloproteins using fluorescence detection. *Nucl. Instrum. Methods Phys. Res. Sect. A.* **319,** 285-289.

Cressey G., Henderson C. M. B., and van der Laan G. (1993) Use of L-edge x-ray absorption spectroscopy to characterize multiple valence states of 3d transition metals; a new probe for mineralogical and geochemical research. *Phys. Chem. Minerals.* **20,** 111-119.

Crocombette J. P., Pollack M., Jollet F., Thromat N., and Gautier-Soyer M. (1995) X-ray-absorption spectroscopy at the iron $L_{2,3}$ threshold in iron oxides. *Phys. Rev. B.* **52,** 3143-3150.

de Groot F. M. F., Grioni M., Fuggle J. C., Ghijsen J., Sawatzky G. A., and Peterson H. (1989) Oxygen 1s X-ray-absorption edges of transition-metal oxides. *Phys. Rev. B.-Cond. Matt.* **40,** 5715-5723.

de Groot, F. M. F., Fuggle J. C., Thole B. T., and Sawatzky G. A. (1990) 2p x-ray absorption of 3d transition metal compounds: An atomic multiplet description including the crystal field. *Phys. Rev. B.* **42,** 5459-5468.

de Groot F. M. F. (2005) 1s2p resonant inelastic X-ray scattering of iron oxides. *J. Phys. Chem. B.* **109,** 20751.

de Smit E., Creemer J. F., Zandbergen H. W., Weckhuysen B. M., and de Groot F. M. F. (2009) In-situ scanning transmission X-ray microscopy of catalytic materials under reaction conditions. *J. Phys. Conf. Ser.* **190,** 1-4.

Dynes J. J., Tyliszczak T., Araki T., Lawrence J. R., Swerhone G. D. W., Leppard G. G., and Hitchcock A. P. (2006) Speciation and quantitative mapping of metal species in microbial biofilms using scanning transmission X-ray microscopy. *Environ. Sci. Technol.* **40,** 1556-1565.

Fleet, M. E. (1986). The structure of magnetite: symmetry of cubic spinels. *J. Solid State Chem.* **62,** 75-82.

Gilbert B., Katz K. E., Denlinger J. D., Yin Y., Falcone R., and Waychunas G. A. (2010) Soft X-ray spectroscopy study of the electronic structure of oxidized and partially oxidized magnetite nanoparticles. *J Phys. Chem. C.* **114,** 21994-22001.

Grandjean F., Waddill G. D., Cummins T. R., Moore D. P., Long G. J., and Buschow K. H. J. (1999) A cerium M-edge X-ray absorption and an iron L-edge magnetic circular dichroism study of the $Ce_2Fe_{17-x}M_x$ solid solutions, where M is Al and Si. *Solid State Commun.* **109,** 779-784.

Gualtieri A. F. and Venturelli P. (1999) In situ study of the goethite-hematite phase transformation by real time synchrotron powder diffraction. *Am. Mineral.* **84,** 895-904.

Hitchcock A. P. (2008) aXis2000 is written in interactive data language (IDL) and is freely available online for non-commecial use. http://unicorn.mcmaster.ca/aXis2000.html.

Hochella Jr. M. F., Moore J. N., Putnis C. V., Putnis A., Kasama T., and Eberl D. D. (2005) Direct observation of heavy metal-mineral association from the Clark Fork River superfund complex: Implications for metal transport and bioavailability. *Geochim. Cosmochim. Ac.* **69,** 1651-1663.

Hocking R. K., George S. D., Raymond K. N., Hodgson K. O., Hedman B., and Solomon E. I. (2010) Fe L-edge x-ray absorption spectroscopy determination of differential orbital covalency of siderophore model compounds: Electronic structure contributions to high stability constants. *J. Am. Chem. Soc.* **132,** 4006-4015.

Jambor J. L. and Dutrizac J. E. (1998) The occurrence and constitution of natural and synthetic ferrihydrite, a widespread iron oxyhydroxide. *Chem. Rev.* **98,** 2549-2585.

Janney D. E., Cowley J. M., and Buseck P. R. (2001) Structure of synthetic 6-line ferrihydrite by electron nanodiffraction. *Am. Mineral.* **86,** 327-335.

Kendelewicz T., Liu P., Doyle C. S., and Brown Jr. G. E. (2000) Spectroscopic study of the reaction of aqueous Cr(VI) with Fe_3O_4 (111) surfaces. *Surf. Sci.* **469,** 144-163.

Krueger B. J., Grassian V. H., Cowin J. P., and Laskin A. (2004) Heterogeneous chemistry of individual mineral dust particles from different dust source regions: The importance of particle mineralogy. *Atmos. Environ.* **38,** 6253-6261.

Labatut C., Berjoan R., Armas B., Shamm S., Sevely J., Riog A., and Molins E. (1998) Studies of LPCVD Al–Fe–O deposits by XPS, EELS and Mössbauer spectroscopies. *Surf. Coat. Tech.* **105,** 31-37.

Lead J. R. and Wilkinson K. J. (2006) Aquatic colloids and nanoparticles: Current knowledge and future trends. *Environ. Chem.* **3,** 159-171.

Majestic B. J., Schauer J. J., and Shafer M. M. (2007) Application of synchrotron radiation for measurement of iron redox speciation in atmospherically processed aerosols. *Atmos. Chem. Phys.* **7,** 2475-2487.

Makovicky E. and Balic Zunic T. (1998) New measure of distortion for coordination polyhedra. *Acta Crystallogr. B* **54,** 766-773.

Manceau A. (2012) Comment on “Direct observation of tetrahedrally coordinated Fe(III) in ferrihydrite". *Environ. Sci. Technol.* **46,** 6882-6884.

Michel F. M., Ehm L., Antao S. M., Lee P. L., Chupas P. J., Liu G., Strongin D. R., Schoonen M. A. A., Phillips B. L., and Parise J. B. (2007) The structure of ferrihydrite, a nanocrystalline material. *Science* **316,** 1726-1729.

Miedema P. S. and de Groot F. M. F. (2013) Fe 2p X-ray absorption and electron energy loss spectroscopy. *J. Electron Spectrosc.* **187,** 32-48.

Mikhlin Y., Tomashevich Y., Tauson V., Vyalikh D., Molodtsov S., and Szargan R. (2005) A comparative X-ray absorption near-edge structure study of bornite, Cu_5FeS_4, and chalcopyrite, $CuFeS_2$. *J. Electron Spectrosc.* **142,** 83-88.

Miot J., Benzerara K., Morin G., Kappler A., Bernard S., Obst M., Férard C., Skouri-Panet, F., Guigner J.-M., Posth N., Galvez M., Brown Jr. G. E., and Guyot, F. (2009) Iron biomineralization by anaerobic neutrophilic iron-oxidizing bacteria. *Geochim. Cosmochim. Ac.* **73,** 696-711.

Miyajima N., Langenhorst F., Frost D. J., and Yagi T. (2004) Electron channelling spectroscopy of iron in majoritic garnet and silicate perovskite using a transmission electron microscope. *Phys. Earth Planet. In.***143-144,** 601-609.

Padmore H. A. and Warwick T. (1994) Soft X-ray monochromators for third-generation undulator sources. *J. Synchrotron Radiat.* **1,** 27-36.

Peak D. and Regier T. (2012) Direct observation of tetrahedrally coordinated Fe(III) in ferrihydrite. *Environ. Sci. Technol.* **46,** 3163-3168.

Post J. E. and Buchwald V. F. (1991) Crystal structure refinement of akaganeite. *Am. Mineral.* **76,** 272-277.

Regan T. J., Ohldag H., Stamm C., Nolting F., Lüning J., Stöhr J., and White R. L. (2001) Chemical effects at metal oxide interfaces studied by x-ray-absorption spectroscopy. *Phys. Rev. B* **64,** 1-11.

Ressler T. (1998) WinXAS: A program for X-ray absorption spectroscopy data analysis under MS-windows. *J. Synchrotron Radiat.* **5,** 118.

Robinson K., Gibbs G. V., and Ribbe P. H. (1971) A quadratic measure of distortion in coordination polyhedra. *Science* **172,** 567-570.

Schofield P. F., Henderson C. M. B., Cressey G., and van der Laan G. (1995) 2p X-ray absorption spectroscopy in the earth sciences. *J. Synchrotron Radiat.* **2,** 93-98.

Schwertmann U., Cornell R. M. (2000) Iron oxides in the laboratory: preparation and characterization. 2nd Edition, Wiley VCH, 67-143.

Sherman D. M. (1985a) The electronic structure of Fe^{3+} coordination sites in iron oxides; applications to spectra, bonding and magnetism. *Phys. Chem. Miner.* **12,** 161-175.

Sherman D. M. (1985b) SCF-Xα-SW MO study of Fe-O and Fe-OH chemical bonds; Applications to the Mössbauer Spectra and the magnetochemistry of hydroxyl-bearing Fe^{3+} oxides and silicates. *Phys. Chem. Miner.* **12,** 311-314.

Sherman D. M. and Waite T. D. (1985) Electronic spectra of Fe^{3+} oxides and oxide hydroxides in the near IR to near UV. *Am Mineral.* **70,** 1262-1269.

Sherman D. M. (2005) Electronic structures of iron(III) and manganese(IV) (hydr) oxide minerals: Thermodynamics of photochemical reductive dissolution in aquatic environments. *Geochim. Cosmochim. Ac.* **69,** 3249-3255.

Shirakawa J., Nakayama M., Wakihara M., and Uchimoto Y. (2007) Changes in electronic structure upon lithium insertion into $Fe_2(SO_4)_3$ and $Fe_2(MoO_4)_3$ investigated by X-ray absorption spectroscopy. *J. Chem. Phys. B.* **111,** 1424-1430.

Shmakov A. N., Kryukova G. N., Tsybulya S. V., Chuvilin A. L., and Solovyeva L. P. (1995) Vacancy ordering in-Fe_2O_3: Synchrotron x-ray powder diffraction and high-resolution electron microscopy studies. *J. Appl. Crystallogr.* **28,** 141-145.

Takahama S., Gilardoni S., and Russell L. M. (2008) Single-particle oxidation state and morphology of atmospheric iron aerosols. *J. Geophys. Res.* **113,** 1-16.

Todd E. C., Sherman D. M., and Purton J. A. (2003a) Surface oxidation of pyrite under ambient atmospheric and aqueous (pH=2-10) conditions: Electronic structure and mineralogy from X-ray absorption spectroscopy. *Geochim. Cosmochim. Ac.* **67,** 881-893.

Todd E. C., Sherman D. M., and Purton J. A. (2003b) Surface oxidation of chalcopyrite ($CuFeS_2$) under ambient atmospheric and aqueous (pH 2-10) conditions: Cu, Fe L- and O K-edge x-ray spectroscopy. *Geochim. Cosmochim. Ac.* **67,** 2137-2146.

Toner B. M., Fakra S. C., Manganini S. J., Santelli C. M., Marcus M. A., Moffett J. W., Rouxel O., German C. R., and Edwards K. J. (2009) Preservation of iron(II) by carbon-rich matrices in a hydrothermal plume. *Nat. Geosci.* **2,** 197-201.

Tossell J. A., Vaughan D. J., and Johnson K. H. (1974) The electronic structure of rutile, wustite and hematite from molecular orbital calculations. *Am. Mineral.* **59,** 319-334.

van Aken P. A., Liebscher B., and Styrsa V. J. (1998) Quantitative determination of iron oxidation states in minerals using Fe $L_{2,3}$-edge electron energy-loss near-edge structure spectroscopy. *Phys. Chem. Miner.* **25,** 323-327.

van Aken P. A. and Liebscher B. (2002) Quantification of ferrous/ferric ratios in minerals: New evaluation schemes of Fe $L_{2,3}$ electron energy-loss near-edge spectra. *Phys. Chem. Miner.* **28,** 188-200.

van der Laan G. and Kirkman I. W. (1992) The 2p absorption spectra of 3d transition metal compounds in tetrahedral and octahedral symmetry. *J. Phys-Condens. Mat.* **4,** 4189-4204.

Vaughan D. J., Tossell, J. A., and Johnson K. H. (1974) The bonding of ferrous iron to sulphur and oxygen in tetrahedral coordination: a comparative study using SCF Xα scattered wave molecular orbital calculations. *Geochim. Cosmochim. Ac.* **38,** 993-1005.

Von der Heyden B. P., Roychoudhury A. N., Mtshali T. N., Tyliszczak T., and Myneni S. C. B. (2012) Chemically and geographically distinct solid-phase iron pools in the Southern Ocean. *Science* **338,** 1199-1201.

Von der Heyden B. P., Roychoudhury A. N., Tyliszczak T., Myneni S. C. B. (in prep.) Composition and structure of Fe-rich aquatic particles, western margin of South Africa.

Wang H., Peng G., Miller L. M., Scheuring E. M., George S. J., Chance MR, and Cramer S. P. (1997) Iron L-edge X-ray absorption spectroscopy of myoglobin complexes and photolysis products. *J. Am. Chem. Soc.* **119,** 4921-4928.

Wiggington N. S., Haus K. L., and Hochella Jr. M. F. (2007) Aquatic environmental nanoparticles. *J. Environ Monitor.* **9,** 1306-1316.

Wycoff R. W. G. (1963) 2nd edition, Interscience Publishers, New York, Crystal Structures 1, 290-295.

CHAPTER 4

Chemically and geographic distinct solid-phase iron pools in the Southern Ocean

A presentation of the research paper

This paper has been published by the research journal *Science* in November 2012. I am the first author and Prof Alakendra Roychoudhury, Dr Thato Mtshali, Dr Tolek Tyliszczak and Prof Satish Myneni are the co-authors.

The speciation probe described in the previous chapter is applied to environmental samples collected from two surface water transects in the South Atlantic and Southern Oceans, and an additional depth profile in the Cape Basin (supplementary material). The Fe L-edge proves to be a useful probe for understanding marine particle speciation by using differences in spectral characteristics. Five major classes of Fe particles are identified and differentiated according to predominantly their valence state and mineralogy. The associations between Fe and aluminium are also investigated. The distribution and relative abundance of these chemical differences across the different frontal zones of the Southern Ocean is expected to have significant Implication for Fe particle influence on marine primary productivity, particularly via dissolution pathways. Both the published paper as well as the related supplementary material is incorporated into this thesis chapter.

I was responsible for sample collection of the depth profile, all of the data analyses, the initial write up of this manuscript and for generating most of the figures. The manuscript was improved via an iterative writing process in which Prof Alakendra Roychoudhury, Prof Satish Myneni and I contributed equally. Prof Roychoudhury contributed significantly to the final set of figures and played a supervisory role on aspects relating to oceanography. Data collection was conducted by both Prof Myneni and I, and Prof Myneni further played a supervisory role on the x-ray related aspects of the paper. Dr Tolek Tyliszczak contributed towards data collection in his capacity as the beamline scientist. Additional acknowledgement must be extended to Mr Matt Frith who helped out with data collection. Finally, Dr Thato Mtshali was responsible for sample collection during SANAE 49. Additional samples were collected by Mr Raimund Rentel (SANAE 50).

Chemically and Geographically Distinct Solid-phase Iron Pools in the Southern Ocean

B.P. von der Heyden[1,4], A.N. Roychoudhury[1,*], T.N. Mtshali[1,2], T. Tyliszczak[3] and S.C.B. Myneni[4]

1. Department of Earth Sciences, Stellenbosch University, Private Bag X1, Matieland, 7602, South Africa
2. CSIR, P.O. Box 320, Stellenbosch, 7600, South Africa
3. Advanced Light Source, Lawrence Berkeley National Laboratory, University of California, Berkeley, CA 94720, USA
4. Department of Geosciences, Princeton University, Princeton, NJ 08544, USA

Iron is a limiting nutrient in many parts of the oceans, including the unproductive regions of the Southern Ocean. Although the dominant fraction of the marine iron pool occurs in the form of solid-phase particles, its chemical speciation and mineralogy are challenging to characterize on a regional scale. Here we describe a diverse array of iron particles, ranging from 20 nm to 700 nm in diameter, in the waters of the Southern Ocean euphotic zone. Distinct variations in the oxidation state and composition of these iron particles exist between the coasts of South Africa and Antarctica, with different iron pools occurring in different frontal zones. These speciation variations can result in solubility differences, a limiting factor in the production of bioavailable dissolved iron.

Dissolved, or soluble, iron plays a central role in vital phytoplankton cellular processes including photosynthesis and the coupled uptake of CO_2 in oceans (*1,2*), and the concentration of soluble Fe is strongly linked to ocean primary productivity. The solubility of Fe, however, is low in oxygenated seawater; the majority of Fe in oceans exists in the form of nanoparticles (<0.2 µm), and biogenic and lithogenic colloids (>0.2 µm). This particulate bound Fe constitutes as much as 65% or more of the total dissolvable Fe fraction in the mixed layer of the Southern Ocean (*3,4*, supplementary material). Considering the magnitude of this particulate bound Fe pool, which is an important reserve source of Fe for photosynthetic organisms, the observation of Fe limitation in certain parts of the Southern Ocean is surprising.

The solubility and bioavailability of Fe associated with particles vary with Fe oxidation state, mineralogy, crystallinity, structural impurities (e.g. Al), and the structure and concentration of dissolved organic ligands (*5-7*). To improve our understanding of Fe limitation in the Southern Ocean, we examined the structure and chemistry of Fe particles from water samples collected on three different scientific cruises (SANAE 49, SANAE 50, GEOTRACES D357) (*8*). This strategy ensured samples across the fronts of the Southern Ocean, which distinguish water masses with different hydrographic characteristics. The distribution of Fe in particles as a function of particle size was analyzed by collecting high-resolution Fe-maps (resolution ~12

nm) at the Fe L_3-absorption edge (~710 eV) (Fig. 1). The oxidation state and coordination environment of Fe in particles were analyzed by collecting Fe L_3-edge X-ray absorption near edge structure (XANES) spectra. We also measured the association of Fe with Al, a solubility modifier and source indicator. The distribution and chemistry of Al was analyzed similarly using Al maps and XANES spectra at the Al K-edge (~ 1570 eV). All samples were analyzed using the X-ray spectromicroscopy facility at the Advanced Light Source (CA, USA), which allows collection of images and XANES spectra at 12 nm resolution under ambient conditions (*9*).

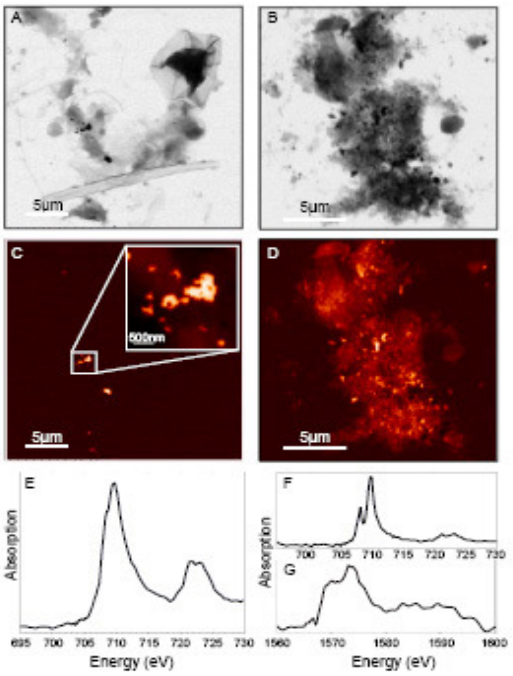

Fig. 1. a,b: *X-ray images (710 eV) of magnetite particles collected from regions between the Sub-tropical and Sub-Antarctic Fronts (a) and ferric (oxyhydr-) oxides (hot-spots) and Fe-rich matrix collected from the Orange River, South Africa (b).* ***c,d:*** *False colour Fe-maps produced by subtracting the back-ground absorption to identify Fe-containing particles in figures 1a and 1b respectively. Inset in Fig. 1c shows Fe nanoparticles are included in the particulate matter.* ***e,f:*** *Fe L-edge XANES spectra of the Fe-rich particles analyzed from Fig. 1c and d respectively.* ***g:*** *Al K-edge spectrum for fluvial particles displaying significant Al substitution, and exhibiting features similar to AlOOH (or a 1:1 clay-mineral).*

The Fe L_3-edge XANES spectra are sensitive to the oxidation state and the coordination environment of Fe (*10,11*). Specifically, the energy differences (ΔeV) between the two main transitions and their intensity ratios can be used to distinguish the Fe(II) phases from Fe(III) phases, and variations in the coordination environment for each oxidation state (Fig. 2). Based on their ΔeV and intensity ratio values in the L_3 edge, we categorize the Fe-rich phases into five distinct chemical classes: pure Fe(III) species (including oxyhydroxides; purity refers to valence state and not speciation), pure Fe(II) species, magnetite, and two mixed valences phases that show a more varied distribution on the spectral plot (Fig. 2). Although constituent mineral phases in Fe particles can be identified using the Fe L_3-edge spectra (Fig. S1), we have limited our classification to these five broad classes because mineral identification in natural samples is complicated by the presence of chemical impurities, surface coatings and poor crystallinity.

The Fe maps of particulate matter from the Southern Ocean are largely characterized by single isolated particles and where present, the surrounding organic and mineral matrix is conspicuously poor in Fe (Fig. 1a,c). The discrete particles are in the size range of 20-30 nm to 700 nm in diameter, with a mean size of ~200 nm. Larger particles, exceeding sizes of 500 nm, are much less common and are uniquely confined to sites near continental and island shelves. Although an apparent correlation between the size of particles and their Fe valence state and coordination environment was absent, the pure Fe(II) phases are generally larger and have spectral features indicative of greater

variability in their Fe coordination environment. The chemistry of mixed valence phases is not uniform and their spectra do not correlate to known Fe minerals (Fig. S1). This suggests the presence of mineral mixtures and structural heterogeneity possibly caused by the presence of Fe(II)- and Fe(III)-amorphous phases and by binding to inorganic and organic ligands. Contrasting the discrete nature and sparse distribution of these marine particles, fluvial Fe-rich particles in streams draining into the South Atlantic Ocean (Orange, Olifants and Berg Rivers) are much more abundant, larger (20 nm to 5 µm), and are commonly associated with Fe-rich inorganic and organic matrices (Fig. 1b,d).

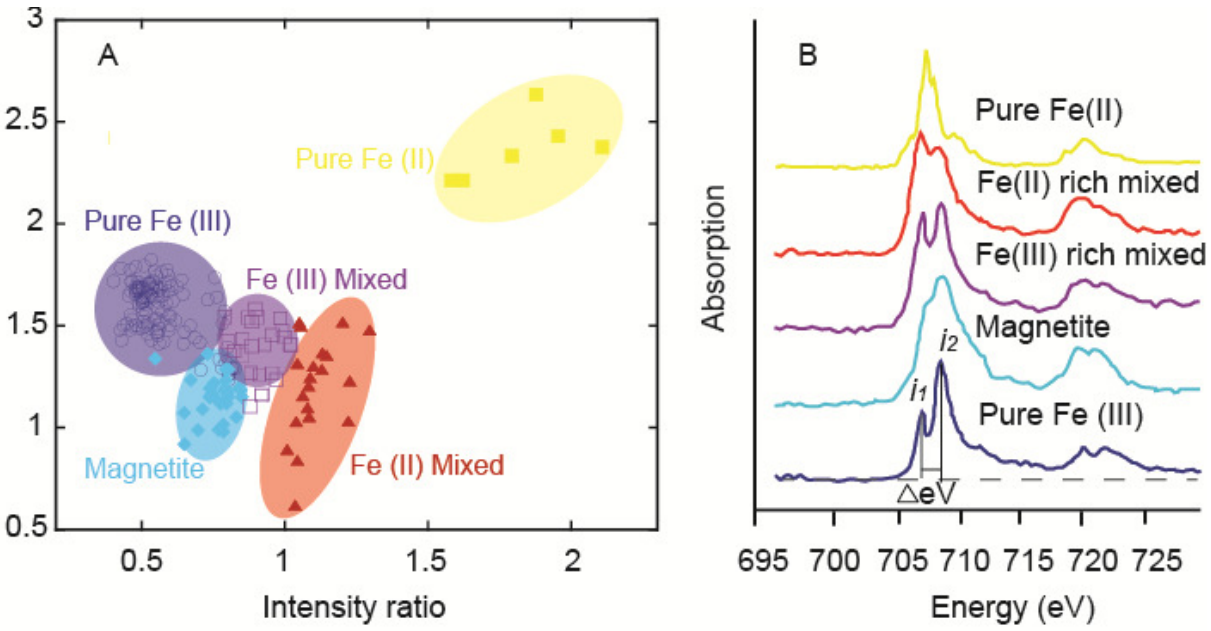

Fig. 2. a: *Iron particle speciation plotted and defined according to their spectral features. Pure Fe(III), pure Fe(II) and magnetite phases occupy discrete fields and the mixed valence species are distinguished by their variations in spectral intensity ratios.* ***b****: Generalized Fe L-edge XANES spectra of the five species identified in the South Atlantic and Southern Oceans with colors corresponding to fields on the plot. The ΔeV value is calculated as the energy difference between peak* i_1 *and* i_2 *and the intensity ratio value is given as absorption intensity* i_1/i_2.

Iron associated with solid phases displayed speciation variation along the two transects sampled between Cape Town, SANAE and South Georgia Island (Fig. 3). Samples from north of the Sub-Tropical Front, those most proximal to the African continent, show the largest degree of chemical heterogeneity consisting of predominantly Fe(III)-rich particles with significant Al association. The water mass between the Sub-Tropical- and Sub-Antarctic Fronts, which receives relatively high atmospheric dust inputs from Patagonia (*12*), is overwhelmingly dominated by magnetite. Between the Sub-Antarctic Front and the Southern Boundary where deep circumpolar waters up-well (*13,14*), Fe particles predominantly contain Fe(III) phases. The Fe(III) phases in these frontal zones display X-ray spectral features more characteristic of Fe(III)-oxyhydroxides than Fe(III)-oxides (Figs. 2, S1). In contrast, samples from south of the Southern Boundary, in the Weddell Sea gyre, are largely composed of particles rich in Fe(II). Such a high abundance of Fe(II)-rich particles and magnetite in the oxygen-rich photic zone is surprising, and additional X-ray spectroscopy measurements at the aluminum, silicon (~1840 eV) and carbon (~285 eV) edges show that these phases are

not ferrous aluminosilicates and that they exhibit strong association with organic carbon. The presence of thick organic coatings (or organic complexes) on the surfaces of Fe(II)- particles, photochemical reduction of Fe(III), structural impurities, and slower oxidation rate of Fe(II) at low temperatures may contribute to the stability of these Fe(II)-particles.

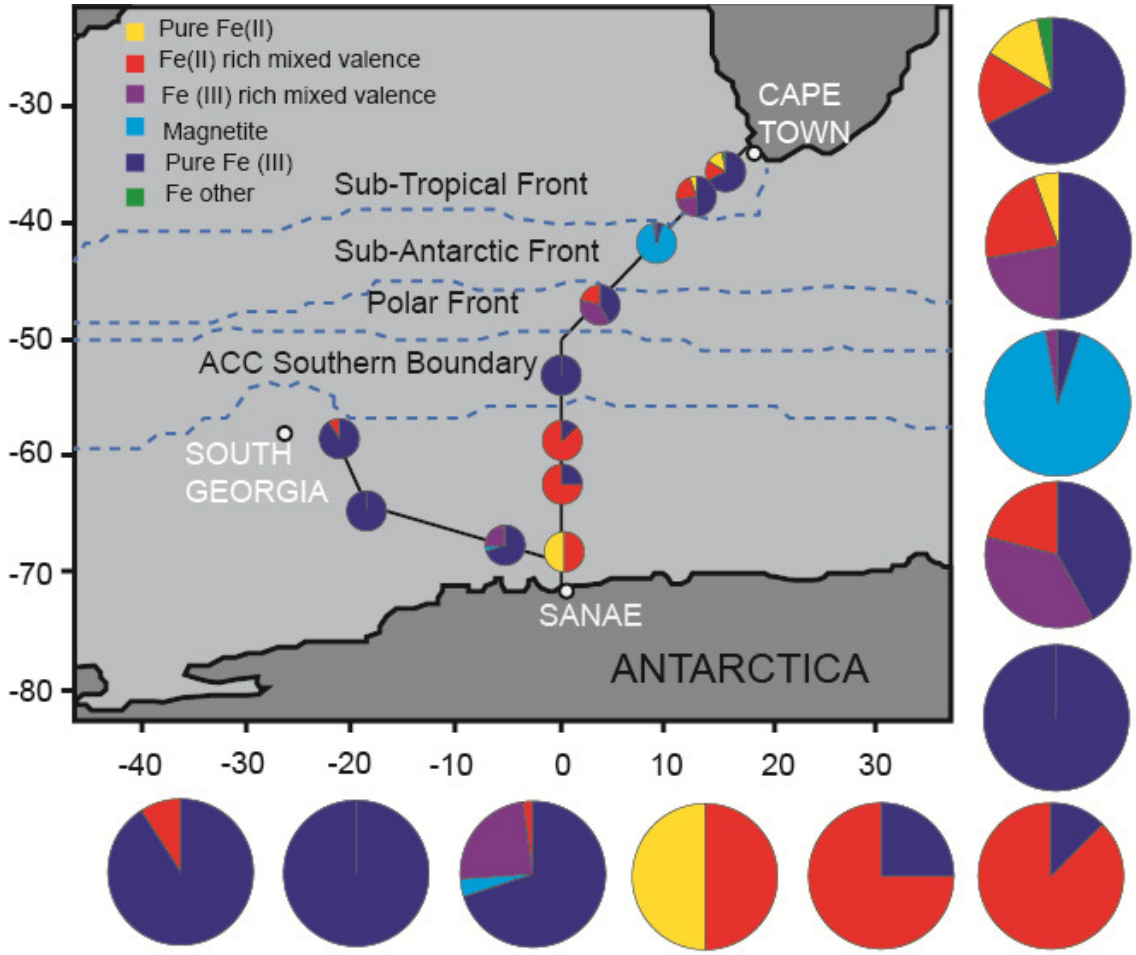

Fig. 3. *Surface water transects (SANAE 49 and SANAE 50) of the South Atlantic and Southern Oceans and Fe speciation along the cruise transects. Sampling was conducted at different locations on these transects so as to ensure complete spatial resolution between the pertinent oceanic fronts. The pie charts show the relative contribution of Fe species, as defined by their spectral features, in the solid-phase Fe pool at that site. The Antarctic Circumpolar Current (ACC) Southern Boundary is defined as the southern terminus of the Upper Circumpolar Deep Water (13).*

We also found Fe(III)-rich particles within the Southern Boundary front on the SANAE - South Georgia transect. The differences in Fe speciation between the two transects off of the Antarctic shelf may be caused by differences in Fe sources, with westward samples likely displaying island effects from the upstream South Sandwich Island chain. Although not extensively examined, variable speciation with water column depth was observed based on a single depth profile collected beyond the continental slope of Southern Africa, suggesting internal recycling and possible differences in biological processing and Fe sources at different depths (Fig. S2).

The association of Al [a well-known solubility modifier of Fe(III) minerals] with Fe in particles also showed variations along the two transects (Fig. 4). Aluminum substitution for Fe(III) in Fe-oxides is commonly encountered in weathered material in the pedosphere where Al/Fe ratios range between 0 and 0.47 for soil goethite (*15*) with amorphous phases often displaying higher values. We found that surface Fe particles, collected nearer to and down-stream of continental and island arc shelves, with the exception of the Antarctic shelf where Fe(II) phases predominate, typically exhibit relatively high Al/Fe ratios between the range of 0.01 and 0.27. Off of the African coast, the Al/Fe ratio increased with distance away from the fluvial source before dropping to lower values in the open ocean (Fig. 4). The Antarctic Shelf showed predominantly Fe(II)-rich phases, and their Al/Fe ratios were low or below detection because of limited substitution of Al for Fe(II). Where depth samples were analyzed, the Al/Fe ratios were much higher (~0.17) at depth relative to the corresponding surface values (~0.08), possibly a consequence of the solubility-depressing effect of Al-substitution on sinking Fe particles, preserving only the most recalcitrant Al-rich phases from mineralization.

Laboratory studies have indicated that the biological availability of Fe is strongly linked to its solubility, which is influenced by chemical speciation [Fe(II) is more soluble, as in south of the Southern Boundary], mineralogy (amorphous phases are more soluble), and Al substitution in Fe(III)-oxides (Al-rich Fe phases are less soluble, as in the Subtropical domain). Because all of these Fe forms exist in different abundances in different parts of the Southern Ocean, variation in the bioavailability of the Fe pool should be influenced by these factors. In addition, heterogeneity in the surface chemistry of the different Fe particles found in the water column is expected to impact the ability of microorganisms to scavenge Fe and other essential trace elements such as Cu and Zn, which are strongly associated with the Fe particle surfaces (*16*).

Sustained primary productivity requires the constant replenishment of the truly dissolved bioavailable Fe pool, which is continually being utilized by ambient phytoplankton species. One mechanism for this replenishment is by dissolution of the solid phase Fe pool. Given that Fe solubility for the relatively simple Fe oxide and oxyhydroxide system varies over 3 orders of magnitude (*7*), our findings on heterogeneity in Fe particle chemistry imply the solubility and expected dissolution rates of Fe particles vary regionally in the Southern Ocean. The causes for the observed heterogeneity in Fe speciation, and the implication of this heterogeneity on Fe bioavailability are uncertain. However, a comparison between the average summertime chlorophyll-*a* concentration and the abundance and distribution of labile Fe forms (for example Fe(II)) exhibit trends (supplementary material, Figs. S3-S5), which allude to the role of Fe-speciation on biology and vice versa.

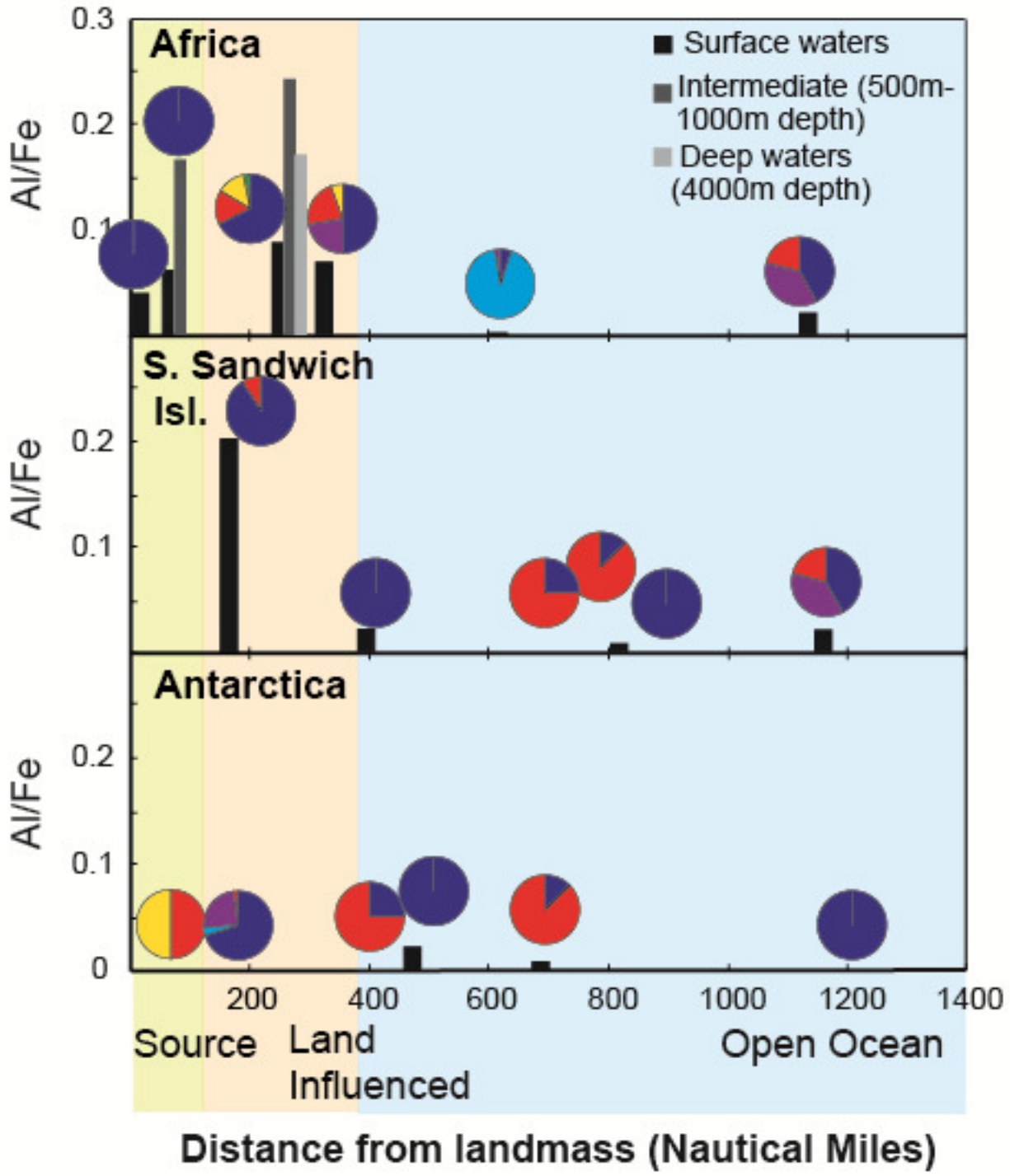

***Fig. 4**. Variations in the Al/Fe ratio of Fe-particles with increasing distance from land mass and with depth. Source regions include fluvial inputs from the African river systems described in the main text as well as marine sites located on the respective continental shelves. Land-influenced sites, which typically show higher Al/Fe ratios, are potentially influenced by continental and shelf sources. They are designated taking into account the vectors of ocean current movement and are all located within distances previously reported for continental Fe supply (17). Iron speciation pie charts are included to match the Al/Fe data to the sampling sites shown in Fig. 3.*

SUPPLEMENTARY MATERIALS*

2.1. Materials and Methods

2.1.1. Water Sample collection and filtration

Using trace metal clean techniques and GEOTRACES protocol, 25 L of seawater was collected from ten surface water sites in the South Atlantic and Southern Oceans and additionally ten liters were collected each from four depths (0-4000 m) down a vertical profile proximal to the African Margin. Samples were collected on three oceanographic cruises; SANAE 49 (Dec 2009-Feb 2010), SANAE 50 (Dec 2010- Feb 2011) and GEOTRACES D357 (Nov 2011) to complete two surface water transects between Cape Town, SANAE and the South Sandwich Island chain, in the Southern Ocean. Fluvial and near-shore marine waters from South Africa's western margin were sampled similarly, with ten liter samples collected from each the Berg, Olifants and Orange rivers and two coastal sites located at 32.6937ºS:16.4566ºE and 34.2955ºS:17.1120ºE. The particulates were separated from water samples using 0.2 µm PTFE membrane filters, and filtration was continued until the filter pores became blocked (up to ~12 L of water filtered from each site). This strategy ensured that even the smallest-sized particles, including nanosized-particles, were trapped for subsequent analysis. These samples were preserved frozen to inhibit any sample changes. To obtain high-resolution images, these filtered particles were rinsed prior to analysis with a few drops of de-ionized water to remove excess salt. Prior spectroscopic analyses showed that the sample state was not affected by this rinsing procedure (*18*).

2.1.2. X-ray Imaging and XANES Spectroscopy

Each rinsed sample was transferred from the filter paper into an acid-cleaned 15mL test tube and re-suspended in a small volume (<1 mL) of de-ionized water. Between 2 and 10 µL of this concentrate was pipetted, droplet-by-droplet, onto a silicon nitride (SiN_3) membrane window (500x500 or 750x750 m^2), covered and allowed to air-dry a few minutes prior to characterization. Dry sample windows were transferred to Scanning Transmission X-ray Microscope (STXM) at the Molecular Environmental Sciences beamline 11.0.2 (Advanced Light Source, CA, USA) for further analysis (*9*). The experimental design and end-station specifications: 17 nm zone plate, a 1200 l/mm grating and 25 µm exit slits, ensured spatial and spectral resolutions of 12nm and 0.2 eV respectively. The monochromator energy was calibrated using $1s \rightarrow 3p$ transition in Neon (set to 867.3 eV).

For imaging Fe particles, 10x10 μm^2 to 30x30 μm^2 images of random regions of the SiN_3 window were collected initially at coarse resolution (~ 0.1-0.5 µm). Fe-maps were prepared by collecting X-ray images below (703 eV) and at the Fe L_3 absorption edge (710 eV), and the absorption differences between these two images showed particles rich in Fe (Fig. 1c, d (main text)). Once Fe-particles were identified, image stacks were collected from

**Supplementary Material found online at: www.sciencemag.org/cgi/content/full/338/6111/1199/DC1*

695 to 730 eV with a 0.2 eV step size close to the absorption edge and 0.5 eV below and above the absorption edges. The sample exposure to X-ray beam at each energy increment was 1-2 msec, and to prevent sample exposure to the beam, the shutter was always used when data were not being collected. Although image stacks allowed collection of point XANES spectra for every pixel in Fe-particles, preliminary detailed analyses of several particles indicated that intra-particle chemical variations were too small to detect. Hence the analysis focused on particle-by-particle characterization. These image stacks were collected at much finer resolution with step sizes varying from 10 to 50 nm. Once the representative spectrum was obtained for a particle, the ΔeV and intensity ratio for spectral features in L_3 edge were determined after background correction. Aluminum XANES spectra were also collected from Fe-particles using image stacks with energy resolution of 0.2 eV at the Al K-edge (1560-1575 eV) and 0.5 eV above and below this edge.

Data integrity and reproducibility was ensured by preparing and running replicate samples; with up to four SiN_3 sample windows being analyzed per site. These replicates showed high reproducibility for the results reported. Since such a characterization used approximately 2 days of synchrotron beamtime for complete characterization of each sample, subsequent analysis focused on analyzing 1-2 sample windows per site.

2.2. Supplementary Text

2.2.1. Nomenclature and solid-phase Fe contribution to total Fe pool

Historical changes in the ultra-filtration techniques employed, and their associated size cut-offs, have led to much confusion in the nomenclature associated with marine particles. For the purposes of this article, we have referred to all of the discrete solid-phase bound Fe suspended in the water column as Fe particles or particulate Fe. This definition does not bear any reference to the size of the particle other than that, by virtue of the resolution of the microscopy technique used, the particles are all larger than 12 nm in diameter. The smallest particles analyzed are on the order of 20 nm in diameter and all particles smaller than the 0.2 µm pore-size cut-off are referred to as “nanoparticles” in the main text. We acknowledge that this is a misnomer (nanoparticles have one size dimension <0.1 µm) however it has been employed purely to draw special attention to these smallest sized particles, which may have properties and behaviour differing to their bulk counter-parts.

We report the concentration of the solid phase bound Fe as making up to >65% of the total Fe in the mixed layer of the Southern Ocean. This value is derived from careful analysis of data reported in Chever et al. (2010) where mixed layer depth and the iron concentration values are taken from their Table 1 and Table 2

respectively (*3*). To derive this >65% estimate, we consider the values reported by Chever et al. (2010) for the Southern Ocean total dissolvable Fe and the soluble Fe pools (*3*).

Total dissolvable iron (TDFe): is defined as the biogenic Fe and labile lithogenic particulate Fe, and iron adsorbed on lithogenic and biogenic particles (*19*). These samples were collected without any filtration procedure and analyzed only after acidification with 0.2% in volume Ultrapur® HCL (Merck) and five months storage. Thus, all Fe except the most refractory particulate Fe is expected to be released into its dissolved form for analysis.

Soluble Fe (sFe): is defined as the concentration of Fe in seawater that has been passed through an acid- (10% Suprapur® HCl (Merck)) and milli-Q rinsed 0.02 µm aluminium oxide ultra-filtration membrane (ANOTOP 25®). sFe samples were analyzed after acidification with 0.1% in volume Ultrapur® HCL (Merck) and two months storage and represent the truly dissolved Fe fraction as well as an un-quantified proportion of Fe nano-particles <20 nm.

Where sFe and TDFe are reported for the same sampling site and depth within the Southern Ocean mixed layer (*3*), we were able to calculate the percentage concentration of Fe bound to discrete particles >0.02 µm using the following equation:

% solid phase bound Fe = (TDFe - sFe)/TDFe x 100

From the analysis of a very limited dataset (n = 3), in which all reported values with standard deviation greater than 15% of Fe concentration were rejected, we found a maximum value of 62.2 ±11.1% contribution of particulate Fe to the total Fe pool of the mixed layer of the Southern Ocean. Below the mixed layer depth, the maximum value for the proportion of particle-bound Fe was 85.5 ±3.3% and, as a much more extensive dataset was reported (n = 63), we were able to derive an average of 69.6 ±0.4% contribution by this pool. Similar calculations from data from Nishioka et al., (2005) yield a value of 76.5% solid-phase bound Fe in the mixed layer of the Polar Frontal Zone of the Southern Ocean (*4*). Bergquist et al., (2007) estimate particulate Fe pool of 30% in the mixed layer in subtropical South Atlantic (*20*); however, their estimates are based on measurement of total iron in 0.4 µm-filtered water fractions and not unfiltered water as with the other two studies. In light of these calculations, we believe that our reported value of >65% is a conservative yet accurate upper estimate for the magnitude of this Southern Ocean particle-bound Fe pool.

2.2.2. Two parameter plot (ΔeV vs intensity ratio) for Fe standard phases

The spectral parameters, ΔeV and intensity ratio, used in this study are measured from the spectra collected as discussed in the materials and methods section. The ΔeV corresponds to the energy difference between the two main electronic transitions corresponding to the *1s* to t_{2g} and e_g orbitals, and the intensity ratio

corresponds to the ratio of intensities of low-energy to high energy transitions. These two spectral parameters are sensitive to the local Fe coordination environment (i.e. valence state, crystal field splitting and distortion) which varies between Fe phases of differing mineralogy and structure. Plotting the ΔeV and intensity ratio values for a range of standard Fe phases reported in the literature and from our own STXM experiments enabled differentiation between the Fe particle classes reported in the main text (Fig. S1).

All Fe(III) standards are clustered with ΔeV and intensity ratio values ranging between approximately 1.2 - 1.8eV and 0.4 - 0.9 respectively. The distribution of natural Fe(III) phases agree well with this range and natural particles plot more prevalently on the lower end of the intensity ratio range, indicating that Fe oxyhydroxides (e.g. goethite) are more common than Fe-oxides (e.g. hematite) in marine environments. Pure Fe(II) standards show much more varied distribution for ΔeV versus intensity ratio (Fig. S1), and the natural Fe(II) particles do not agree closely with these literature values. However, the proximity and spectral shapes of natural sample spectral features with these Fe(II) standards provide sufficient confidence in our designation of this field as being purely Fe(II) rich. Natural magnetite particles show scatter around standard magnetite (Fig. 2. (main text)). Because the spectral shapes of natural magnetite closely match that of the standard, much of this scatter is attributed to the effects of particle size, crystallinity, presence of trace impurities, mineral surface coatings, and the possibility that 'discrete particles' are in fact aggregates of minerals that are smaller than the microscope resolution (12 nm). Although the standards are limited, Fe(II)-rich and Fe(III)-rich mixed valence can encompass a range of amorphous particle chemistries and mechanical aggregates and we use a nominal intensity ratio cut-off of 1 to differentiate between the two classes. The pyrite standard spectrum plots within the range of our designated Fe(II)-rich mixed valence natural phases, however differences in reported pyrite standard spectra (*18,21*) and surface oxidation in natural samples prevent us from definitively identifying pyrite in ocean waters without additional sulphur XANES.

2.2.3. Fe speciation with depth

Although speciation with depth was not the focus of this investigation, Fe speciation, and its correlation with Al distribution in particles was also observed to vary with depth in the only profile examined in this investigation (Fig. S2). At this site; proximal to the African shelf yet beyond the lateral extent of the slope (36º 27.87'S, 13º 12.66'E; GEOTRACES 357), we found heterogeneous Fe speciation in the photic zone, pure Fe(III) phases, including Fe- (oxyhydr-) oxides with high Al/Fe values at 500m, highly heterogeneous Fe speciation at 2000m (no Al data), and again pure Fe(III)-species with significant Al co-occurrence in the deepest water sample at 4000m (Fig. 4 (main text)). This zigzag pattern for Fe-speciation and variations in Al and Fe associations reflect active internal cycling and possibly variable source of iron at mid-depths.

2.2.4. Fe particle speciation and productivity

Southern Ocean chlorophyll concentration is both spatially and temporally variable and is influenced by a range of bottom-up, top-down and regional-scale physical controls (*22*). To evaluate the relationship between our Fe particle speciation and chlorophyll concentration, we have plotted our data against both instantaneous (Fig. S3) and summer-time average chlorophyll-*a* concentration measurements (Fig. S4). Whereas only weak correlation is found with comparison to chlorophyll spot measurements, speciation data comparison to the averaged chlorophyll data show stronger trends, particularly along the Cape Town-SANAE transect where high proportions of Fe(II) are matched by higher chlorophyll-*a* values. The better match to averaged chlorophyll measurements is likely related to the prolonged residence time and slow dissolution kinetics of Fe particles in the surface ocean, resulting in them having a more sustained effect on stimulating phytoplankton growth. Because of the intimate link between particle chemistry, mineralogy and solubility, the extent of this influence on biology can be expected to vary with the observed variations in Fe particle speciation. More detailed work over a growth cycle is required, however, to better constrain the seasonal dynamics of the particulate Fe- biology relationship.

2.3. Supplementary Figures

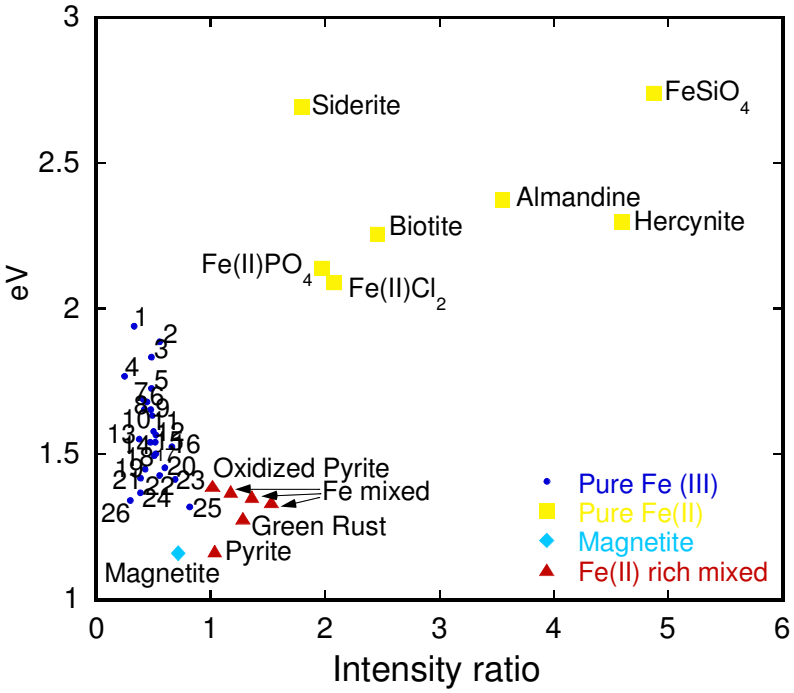

Fig. S1: *Intensity ratio versus ΔeV plot highlighting the positions of standard Fe phases as measured from our STXM experiments and additional phases collected from reported literature. All data and references for these standards are provided in Table S1. Numbered Fe(III) standards: 1- Andradite Garnet; 2- Methaemoglobin; 3- amorphous $FePO_4$; 4- Catalase; 5- oxygen-bridged complex: Fe(bpmp); 6- Fe(acetylacetonate)$_3$; 7- FeF_3; 8- $Fe_2(SO_4)_3$; 9- Lepidocrocite; 10- K_3(Fe(oxalate)$_3$); 11- $Fe_2(SO_4)_3$; 12- oxygen-bridged complex: Fe(salmp); 13- $Fe_2(MO_4)_3$; 14- Akaganeite; 15- Goethite; 16- Hematite; 17- $FeCl_3$-$6H_2O$; 18- Amorphous Fe; 19- Fe(propyl-hydroxamate)$_3$; 20- Tooeliete; 21- Fe$(NO_3)_3$; 22- Maghemite; 23- Schwertmannite; 24- K_3(Fe(catecholate)$_3$); 25- Bornite; 26- Rodolicoite. "Fe mixed" data-points refer to spectra collected from a working catalyst at different stages of chemical reaction (23).*

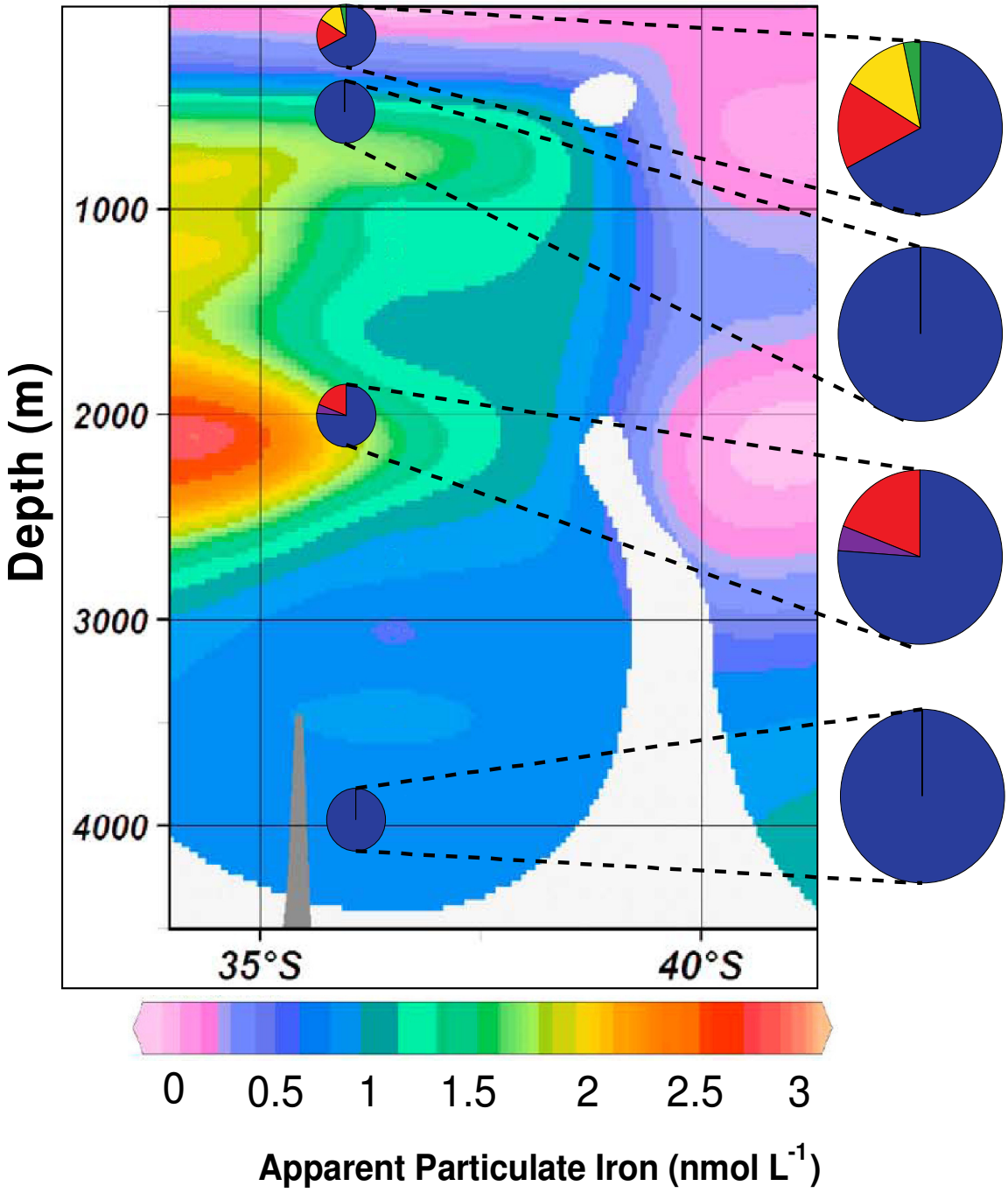

Fig. S2: *Speciation of iron with depth in the water column for a sample site located proximal to the African continent. Background color map gives the Fe apparent particulate concentration (3) and essentially represents all Fe trapped on a 0.2µm filter paper. The pie chart colour legend is the same as for Fig. 3 (main text).*

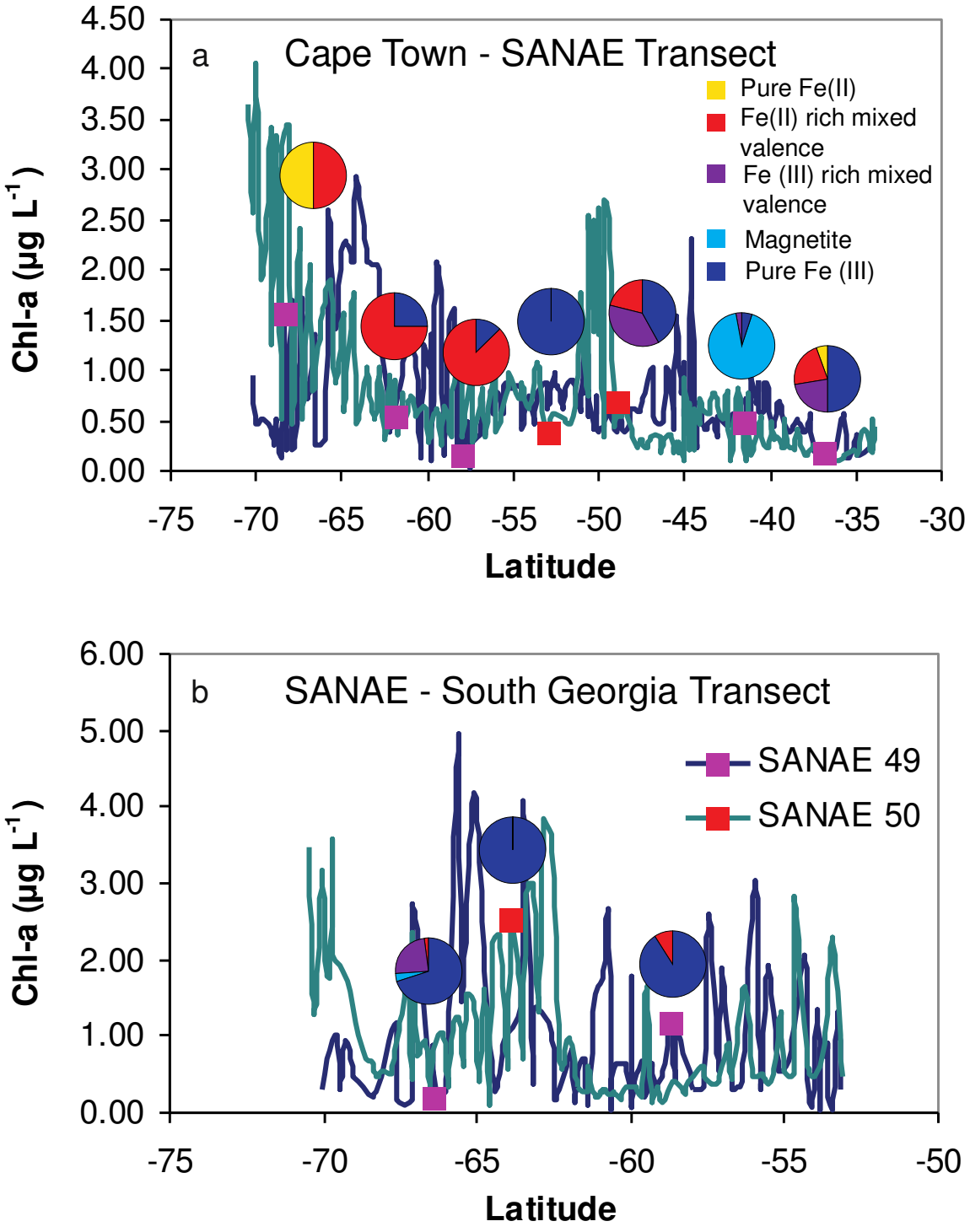

Fig. S3: *Fe colloid speciation (pie charts; colours represent the same as those in Fig 3, main text) compared to spot measurements for chlorophyll-a along the respective cruise tracks. There appears to be correlation between chl-a and proportion of Fe(II) in the Cape Town- SANAE transect (a) whereas there is no apparent correlation in the SANAE-South Georgia transect (b).*

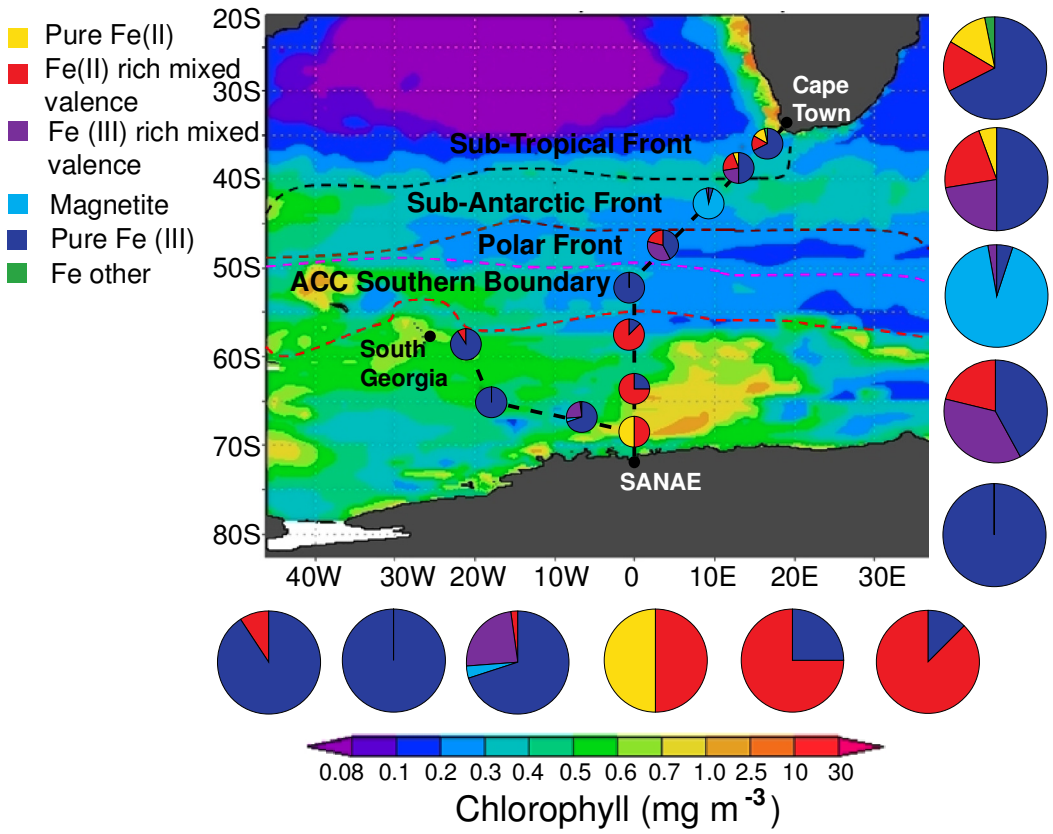

Fig. S4: *Fe particle speciation data plotted as pie charts against a background of average summertime chlorophyll-a concentrations (taken from SeaWiFS*

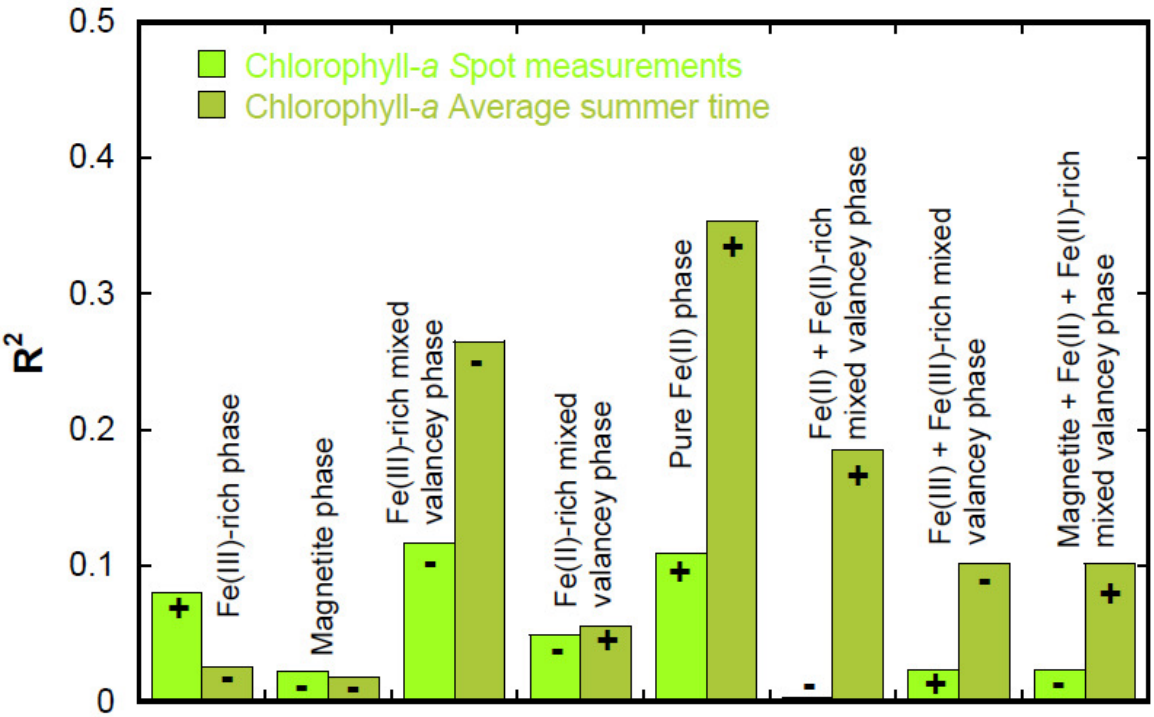

Fig. S5: *Goodness of fit obtained on correlation of iron particles with identified valency state and spot or average summer time chlorophyll-a concentrations. Respective signs on each bar depict a positive or a negative correlation.*

2.4. Table S1.

Literature compilation of intensity ratio and ΔeV values for a number of Fe-rich phases, along with their experimental apparatus and conditions. Discrepancies between the values reported by different authors are a caveat of the differences in experimental techniques and conditions.

Phase	Intensity Ratio	ΔeV	Method used*	Beamline	Experimental conditions	Ref.
			Fe(III) rich phases:			
Akaganeite	0.472	1.540	STXM	ALS 11.0.2	0.2eV resolution, room temperature, 1Atm P, zone plate, a 1200 l/mm grating and 25µm exit slits	(*24*)
Amorphous Fe	0.505	1.495				
Goethite	0.516	1.541				
Hematite	0.663	1.525				
Lepidocrocite	0.477	1.653				
Maghemite	0.554	1.427				
Hematite	0.5134	1.56	TEY	Bessy	0.2 eV resolution, room temp, 5mbar P	(*25*)
Rodolicoite	0.299	1.341				
Hematite	0.6004	1.376	TEY	LURE-Orsay SA 72	0.9eV resolution, 5x10E-11 P, TGM monochromator	(*26*)
Hematite	0.5752	1.4545	TEY	Stanford 10.1	Energy resolution of 200meV at 800meV	(*27*)
Hematite	0.4761	1.5766	TEY	Max-II I51	Aqueous solution	(*28*)
Hematite	0.4517	1.4701	STXM	ALS 11.0.2		(*9*)
Hematite	0.6984	1.41	STXM	ALS 11.0.2	1200l/m grating 30um slits 160meV resolution Calibrate hematite	(*29*)
Tooeliete	0.601	1.454				
Hematite	0.513	1.623	TEY	Bessy U49/2-PGM-1; UE56/2-PGM-1	0.2eV spectral resolution	(*30*)
Hematite	0.553	1.52	TEY	Bessy II VLS-PGM	0.3eV resolution Calibrated with F 1s transition in K_2TiF_6	(*31*)
FeF_3	0.408	1.689				
$Fe(acac)_3$	0.444	1.680				
Hematite	0.633	1.521	STXM	ALS 11.0.2	35nm zone plate, 40nm spatial resolution	(*23*)
Goethite	0.7761	1.511	STXM	ALS 11.0.2	40nm resolution, 0.1eV, ambient T; <1atm P, calibrated with ferrihydrite	(*32*)
Schwertmannite	0.689	1.413				
$FeCl_3$-$6H_2O$	0.522	1.502				

Ferrihydrite	0.4851	1.502				
Akaganeite	0.6288	1.413				
Goethite	0.602	1.483	STXM	ALS 11.0.2	Calibrated to $L_{3/2}$ peak	(*33*)
$FeCl_3$-$6H_2O$	0.699	1.49		5.3.2	accuracy~0.2eV	
Goethite	0.5957	1.652	TEY	BL-7 spectro microscopy facility	Anaerobic conditions	(*34*)
Maghemite	0.6839	1.536	FY	ALS 7.0	Energy resolution 0.3eV	(*35*)
Swertmannite Crystalline	0.576	1.386	X-PEEM	SPHINX, Hermon	-20kV and 10^{E-10} Torr vacuum	(*36*)
Swertmannite Poorly crystalline	0.532	1.478				
Akaganeite	0.54	1.467				
Ferrihydrite	0.5133	1.397				
Maghemite	0.659	1.194	TEY, Auger Yield	SSRL 10-1	Wiggler magnet beamline, spherical grating monochromator	(*37*)
Bornite	0.816	1.318	TEY	Bessy II	Room temp, 0.05eV step size, 10^{-9}Pa, resolution better than 0.1eV. x-ray spot 0.2mm, calibrated with Ne	(*38*)
Andradite Garnet	0.332	1.94	EELS	Phillips CM 12 Gatan PEELS 666	0.1eV/channel, 30s reading. Other parameters	(*39*)
$Fe_2(SO_4)_3$	0.420	1.654	TEY	BL-11A Photon Factory	Calibrated to Fe_2O_3, N_2 atmosphere	(*40*)
$Fe_2(MO_4)_3$	0.376	1.551				
$Fe_2(SO_4)_3$	0.502	1.578	IPFY	SGM, CLS	Powder sample, 0.1eV resolution, partial fluorescence to remove saturation effects	(*41*)
$Fe(NO_3)_3$	0.387	1.417				
$FePO_4$	0.449	1.591	TEY	ALS 7.0.1	Room temp, $5x10^{-9}$mbar, 0.75eV resolution, 0.3eV beam	(*42*)
$FePO_4$ (amorphous)	0.482	1.833	STXM	SLS PolluX, CLS 10ID-1	He 1atm P, energy resolving power > 3000, calibrated to hematite peak	(*43*)

Azidomet myoglobin	0.412	2.891	FY	Stanford 10.1	2x2mm spot size, 0.4eV resolution, 10^{-9} Torr, Fe_2O_3 calibration	(*44*)
Fe(salmp)	0.524	1.566	TEY	NSLS U4B	160meV resolution, 20um slits, 2º K, $2x10^{-9}$ mbar, calibrated to $K_4Fe(CN)_6$	(*45*)
Fe(bpmp)	0.484	1.726				
$K_3Fe(CN)_6$	0.273	3.29	FY	LBNL STJ spectrometer		(*46*)
$K3(Fe(ox)_3)$	0.49	1.632	TEY	Stanford 10.1 and 8.2	0.1eV stepsize, 20ºC, calibrated with Fe_2O_3, inert atmosphere	(*47*)
$Fe(Pha)_3$	0.428	1.448				
$K_3(Fe(cat)_3)$	0.386	1.367				
Methaemoglobin	0.554	1.886	FY	BESSY II U41-PGM	25ºC, pH 7, Ref: Aziz 2009	(*48*)
Catalase	0.249	1.768				
				Fe(II)(III) rich phases:		
Magnetite	0.718	1.160	STXM	ALS 11.0.2	0.2eV resolution, room temperature, 1Atm P, zone plate, a 1200 l/mm grating and 25µm exit slits	(*24*)
Magnetite	0.592	1.15	TEY	Stanford 10.1	Energy resolution of 200meV at 800meV	(*27*)
Catalyst 1	1.176	1.371	STXM	ALS 11.0.2	25% Fe^0; 25% Fe_2SiO_4; 50% Fe_3O_4	(*23*)
Catalyst 2	1.532	1.336			40% Fe^0; 50% Fe_2SiO_4; 10% Fe_3O_4	
Catalyst 3	1.361	1.353			33% Fe^0; 50% Fe_2SiO_4; 17% Fe_3O_4	
Magnetite	0.534	1.483	STXM	ALS 11.0.2, 5.3.2	Calibrated to $L_{3/2}$ peak accuracy~0.2eV	(*33*)
Green rust	1.284	1.279	TEY	BL-7 spectro microscopy facility	Anaerobic conditions	(*34*)
Magnetite	0.733	1.491	STXM	ALS 11.0.2, CLS 10ID-1	35nm res. Gas path length = 50um. 1bar H_2 atmos. 150ºC	(*49*)
Magnetite	0.507	1.453	TEY	LNLS SGM		(50)
Magnetite	0.470	1.371	STXM	-		(*51*)

Fe(II) rich phases:

Hercynite $FeAl_2O_4$	4.595	2.296	TEY	Bessy	0.2 eV, room temp, 5mbar P	(*25*)
$FeSiO_4$	4.507	2.414				
Hercynite	4.141	2.481	TEY	Bessy U49; UE56	0.2eV spectral resolution, probe depth 4nm	(*30*)
FeO	0.751	1.112	TEY	Bessy II VLS-PGM	0.3eV resolution	(*31*)
FeF_2	0.608	1.702			Calibrated with F 1s transition in K_2TiF_6	
FeS	0.805	1.716				
$FeCO_3$	3.249	2.616				
$Fe(II)Cl_2$	2.08	2.088	STXM	ALS 11.0.2 5.3.2	Calibrated to $L_{3/2}$ peak accuracy~0.2eV	(*33*)
$Fe(II)Cl_2$	2.929	2.076	TEY	BL-7 spectro microscopy facility	Anaerobic conditions	(*34*)
$Fe(II)PO_4$	1.976	2.139	STXM	SLS PolluX, CLS 10ID-1	He 1atm P, energy resolving power > 3000, calibrated to hematite peak	(*43*)
Deoxy Myoglobin	0.412	2.205	FY	Stanford 10.1	2x2mm spot size, 0.4eV resolution, 10^{-9} Torr, Fe_2O_3 calibration	(*44*)
$FeSiO_4$	4.876	2.74	STXM			(*51*)
FeO	0.661	1.653	NEXAFS	ALS 8.0.1	0.3eV, monochromator and spectra calibrated to Fe metal	(*52*)
Pyrite FeS_2	1.106	1.062				
Pyrite (FeS_2)	1.052	0.936	TEY	Duresbury Synchrotron, 5U.1	$<5x10^{-6}$, 25ºC, 50µm slits, SX700 type monochromator	(*53*)
Oxidized pyrite	1.017	1.392				
Pyrite (FeS_2)	1.037	1.167	STXM	ALS 11.0.2 and 5.3.2	Ambient temp, <1atm He, 40nm spatial resolution, 0.1eV spectral resolution, calibrated with ferrihydrite 2p transition	(*54*)
Biotite	2.458	2.256				
Siderite ($FeCO_3$)	1.801	2.692				
$FeTe_2$	0.745	0.966	TEY	SRS 5U1	SX 700 grating monochromator, 10^{-6}mbar P, room temp, 0.5eV resolution	(*21*)
$K_4[Fe(CN)_6]$	0.798	1.702	TEY	Photon factory	High vacuum, micro-	(*55*)

				BL-11A	channel plate detector		
Almandine Garnet	3.555	2.374	EELS	Phillips CM 12 with Gatan PEELS 666	0.1eV/channel, reading. Other parameters	30s	(*56*)

** There are several different technologies able to collect Fe L-edge data. These include; Scanning Transmission X-ray Microscopy (STXM), Total Electron Yield (TEY), Fluorescence Yield (FY), X-ray Photoelectron Emission Spectromicroscopy (X-PEEM), Inverse Partial Fluorescence Yield (IPFY), Electron Energy-Loss Spectroscopy (EELS)*

ACKNOWLEDGEMENTS

This research is supported by grants from NRF, South Africa (Blue Skies Program), Stellenbosch University VR(R) fund, NSF (chemical sciences), US-DOE (BES & SBR), and Princeton in Africa program. The authors would like to thank the support staff at the Advanced Light Source for helping with data collection and sample preparation. This work benefitted from discussions with F. Morel, D. Sigman, and four anonymous reviewers. Additional data are provided in Supporting Online Material.

FULL REFERENCES

1. P.W. Boyd, M.J. Ellwood, The biogeochemical cycle of iron in the ocean. *Nat. Geosci.* **3**, 675-682 (2010).

2. W.G. Sunda, in *The Biogeochemistry of Iron in Seawater,* D.R. Turner, K.A. Hunter, Eds. (Wiley, New York, 2001), chpt. 2, pp. 41-84.

3. F. Chever *et al.*, Physical speciation of iron in the Atlantic sector of the Southern Ocean along a transect from the Subtropical domain to the Weddell Sea gyre. *J. Geophys. Res.* **115**, C10059 (2010).

4. J. Nishioka *et al.*, Changes in the concentration of iron in different size fractions during an iron enrichment experiment in the open Southern Ocean. *Mar. Chem.* **95**, 51-63 (2005).

5. R.M. Cornell, U. Schwertmann, The iron oxides: structure, properties, reactions, occurrences and uses (VCH, Weinheim, Germany, 2003), pp. 703.

6. M. Oakes, R.J. Weber, B. Lai, A. Russell, E.D. Ingall, Characterization of iron speciation in urban and rural single particles using XANES spectroscopy and micro X-ray fluorescence measurements: investigating the relationship between speciation and fractional iron solubility. *Atmos. Chem. Phys.* **12**, 745-756 (2012).

7. S.M. Kraemer, Iron oxide dissolution and solubility in the presence of siderophores. *Aquat. Sci.* **66**, 3-18 (2004).

8. Materials and methods are available as supplementary materials on *Science* online.

9. H. Bluhm *et al.*, Soft X-ray microscopy and spectroscopy at the Molecular Environmental Science beamline at the Advanced Light Source. *J. Electron Spectrosc.* **150** (2-3), 86-104 (2006).

10. G. van der Laan, I.W. Kirkman, The 2p absorption spectra of 3d transition metal compounds in tetrahedral and octahedral symmetry. *J. Phys- Condens. Mat.* **4**, 4189-4204 (1992).

11. F.M.F. de Groot, XANES spectra of transition metal compounds. *J. Phys. Conf. Series* **190**, 012004 (2009).

12. N. Cassar *et al.*, The Southern Ocean biological response to aeolian iron deposition. *Science* **317**, 1067-1070 (2007).

13. R.T. Pollard, M.I. Lucas, J.F. Read, Physical controls on biogeochemical zonation in the Southern Ocean. *Deep-Sea Res Pt II* **49**, 3289-3305 (2002).

14. R.F. Anderson *et al.*, The wind-driven upwelling in the Southern Ocean and deglacial rise in atmospheric CO_2. *Science* **323**, 1443-1448 (2009).

15. R.W. Fitzpatrick, U. Schwertmann, Al-substituted goethite- an indicator of pedogenic and other weathering environments in South Africa. *Geoderma* **27** (4), 335-347 (1982).

16. L. Balistrieri, J.W. Murray, Metal-solid interactions in the marine environment: estimating apparent equilibrium binding constants. *Geochim. Cosmochim. Ac*. **47**, 1091-1098 (1983).

17. P.J. Lam *et al.*, Winter phytoplankton bloom in the subarctic Pacific supported by continental margin iron. *Global Biogeochem. Cy.* **20**, GB1006, doi:10.1029/2005GB002557 (2006).

18. B.M. Toner *et al.*, Preservation of iron(II) by carbon-rich matrices in a hydrothermal plume. *Nature Geosci.* **2**, 197-201 (2009).

19. H.J.W. de Baar *et al.*, Low dissolved Fe and the absence of diatom blooms in remote Pacific waters of the Southern Ocean. *Mar. Chem.* **66**, 1–34 (1999).

20. B.A. Bergquist, J. Wu, E.A. Boyle, Variability in oceanic dissolved iron is dominated by the colloidal fraction. *Geochim. Cosmochim. Ac*. **71**, 2960-2974 (2007).

21. J.M. Charnock, C.M.B. Henderson, J.F.W. Mosselmans, R.A.D. Pattrick, 3d transition metal L-edge X-ray absorption studies of the dichalcogenides of Fe, Co and Ni. *Phys. Chem. Minerals* **23**, 403-408 (1996).

22. S.J. Thomalla, N. Fauchereau, S. Swart, P.M.S. Monteiro, Regional scale characteristics of the seasonal cycle of chlorophyll in the Southern Ocean. *Biogeosciences* **8**, 2849-2866 (2011) http://dx.doi.org/10.5194/bg-8-2849-2011

23. E. de Smit *et al.*, Nanoscale imaging of a working catalyst by scanning transmission X-ray microscopy. *Nature* **456**, 222-6 (2008).

24. This study

25. F.M.F. de Groot *et al.*, 1s2p resonant inelastic X-ray scattering of iron oxides. *J. Phys. Chem. B.* **19**, 20751-20762 (2005).

26. J.P. Crocombette, M. Pollack, F. Jollet, N. Thromat, M. Gautier-Soyer, X-ray-absorption spectroscopy at the iron $L_{2,3}$ threshold in iron oxides. *Phys. Rev. B.* **52**, 3143-3150 (1995).

27. T.J. Regan *et al.*, Chemical effects at metal oxide interfaces studied by x-ray-absorption spectroscopy. *Phys. Rev. B.* **64**, 1-11 (2001).

28. E.C. Todd, D.M. Sherman, J.A. Purton, Surface oxidation of chalcopyrite ($CuFeS_2$) under ambient atmospheric and aqueous (pH 2-10) conditions: Cu, Fe L- and O K-edge X-ray spectroscopy. *Geochim. Cosmochim. Ac.* **67**, 2137-2146 (2003).

29. K. Benzerara *et al.*, Nanoscale study of as biomineralization in an acid mine drainage system. *Geochimic. Cosmochim. Ac*. **72**, 3949-3963 (2008).

30. W.M. Heijboer, D.C. Koningsberger, B.M. Weckhuysen, F.M.F. de Groot, New frontiers in X-ray spectroscopy in heterogeneous catalysis: Using Fe/ZSM-5 as test-system. *Catal. Today.* **110**, 228-238 (2005).

31. A.S. Vinogradov *et al.*, X-ray absorption evidence for the back donation in iron cyanide complexes. *Surf. Rev. Lett.* **9**, 359-364 (2002).

32. C.S. Chan, S.C. Fakra, D.C. Edwards, D. Emerson, J.F. Banfield, Iron oxyhydroxide mineralization on microbial extracellular polysaccharides. *Geochim. Cosmochim. Ac.***73**, 3807-3818 (2009).

33. J.J. Dynes *et al.*, Speciation and quantitative mapping of metal species in microbial biofilms using scanning transmission X-ray microscopy. *Environ. Sci. Technol.* **40**, 1556- 1565 (2006).

34. E.M. Kneedler, J. Rothe, K.W. Weissmahr, K. Pecher, B.P. Tonner, Identification of green rust in environmental compounds using XANES of Fe-$L_{II,III}$ edges. In: *Advanced Light Source Annual Compendium of Abstracts*, Lawrence Berkeley Publications (1997).

35. B. Gilbert *et al.*, Soft X-ray spectroscopy study of the electronic structure of oxidized and partially oxidized magnetite nanoparticles. *J. Phys. Chem. C.* **114**, 21994-22001 (2010).

36. C.S. Chan *et al.*, Microbial polysaccharides template assembly of nanocrystal fibers. *Science* **303**, 1656-1658 (2004).

37. T. Kendelewicz, P. Liu, C.S. Doyle, G.E. Brown Jr., Spectroscopic study of the reaction of aqueous Cr(VI) with Fe_3O_4 (III) surfaces. *Surf. Sci.* **469**, 144-163 (2000).

38. Y. Mikhlin *et al.*, A comparative X-ray absorption near-edge structure study of bornite, Cu_5FeS_4, and chalcopyrite, $CuFeS_2$. *J. Electron Spectrosc.* **142**, 83-88 (2005).

39. P.A. van Aken, B. Liebscher, Quantification of ferrous/ferric ratios in minerals: New evaluation schemes of Fe L_{23} electron energy-loss near-edge spectra. *Phys. Chem. Miner.* **29**, 188-200 (2002).

40. J. Shirakawa, M. Nakayama, M. Wakihara, Y. Uchimoto, Changes in electronic structure upon lithium insertion into $Fe_2(SO_4)_3$ and $Fe_2(MoO_4)3$ investigated by X-ray absorption spectroscopy. *J. Phys. Chem. B.* **111**, 1424-1430 (2007).

41. D. Peak, T. Regier, Direct observation of tetrahedrally coordinated Fe(III) in ferrihydrite. *Environ. Sci. Technol.***46**, 3163-3168 (2012).

42. A. Augustsson *et al.*, Electronic structure of phospho-olivines Li_xFePO_4 (x = 0,1) from soft-x-ray-absorption and emission spectroscopies. *J. Chem. Phys.* **123**, 184717 (2005).

43. J. Miot *et al.*, Iron biomineralization by anaerobic neutrophilic iron-oxidizing bacteria. *Geochimic. Cosmochim. Ac.* **73**, 696-711 (2009).

44. H. Wang *et al.*, Iron L-edge X-ray absorption spectroscopy of myoglobin complexes and photolysis products. *J. Am. Chem. Soc.* **119**, 4921-4928 (1997).

45. G. Peng *et al.*, L-edge x-ray absorption and x-ray magnetic circular dichroism of oxygen-bridged dinuclear iron complexes. *J. Am. Chem. Soc.* **117**, 2515-2519 (1995).

46. O.B. Drury, Development of high resolution x-ray spectrometers for the investigation of bioinorganic chemistry in metalloproteins. Thesis, University of California, Davis (2007).

47. R.K. Hocking *et al.*, Fe L-edge x-ray absorption spectroscopy determination of differential orbital covalency of siderophore model compounds: Electronic structure contributions to high stability constants. *J. Am. Chem. Soc.* **132**, 4006-4015 (2010).

48. N. Bergmann *et al.*, On the enzymatic activity of catalase: An iron L-edge X-ray absorption study of the active centre. *Phys. Chem. Chem. Phys.* **12**, 4827-4832 (2010).

49. E. de Smit, J.F. Creemer, H.W. Zandbergen, B.M. Weckhuysen, F.M.F. de Groot, In-situ scanning transmission X-ray microscopy of catalytic materials under reaction conditions. *J. Phys. Conf. Ser.* **190**, 1-4 (2009).

50. A.R.B. de Castro *et al.*, L-edge inner shell spectroscopy of nanostructured Fe_3O_4. *J. Magn. Magn. Mater.* **233**, 69-73 (2001).

51. F.M.F. de Groot, XANES spectra of transition metal compounds. *J. Phys. Conf. Ser.* **190**, 1-9 (2009).

52. K.C. Prince *et al.*, Core-level spectroscopic study of FeO and FeS_2. *Phys. Rev. B.* **71**, 085102 (2005).

53. E.C. Todd, D.M. Sherman, J.A. Purton, Surface oxidation of pyrite under ambient atmospheric and aqueous (pH=2-10) conditions: Electronic structure and mineralogy from X-ray absorption spectroscopy. *Geochem. Cosmochem. Ac.* **67**, 881-893 (2003).

54. B.M. Toner *et al.*, Preservation of iron(II) by carbon-rich matrices in a hydrothermal plume. *Nat. Geosci.* **2**, 197-201 (2009).

55. Y. Kitajima *et al.*, First observation of soft X-ray induced phase transition of $RbMn[Fe(CN)_6]$ studied by Fe L-edge X-ray absorption spectroscopy. *J. Phys. Conf. Ser.***148**, 1-3 (2009).

56. P.A. van Aken, B. Liebscher, V.J. Styrsa, Quantitative determination of iron oxidation states in minerals using Fe $L_{2,3}$-edge electron energy-loss near-edge structure spectroscopy. *Phys. Chem. Miner.* **25**, 323-327 (1998).

CHAPTER 5

A presentation of the submitted research paper

This manuscript has been prepared for submission to the research journal *Environmental Science & Technology*. I am the lead author and Ms Emily Hauser is second author. Additional co-authors include; Dr Gustavo Martinez, Dr Bhoopesh Mishra, Prof Alakendra Roychoudhury, Dr Andrew Bowie, Dr Tolek Tyliszczak and Prof Satish Myneni.

Ferrous iron (Fe(II)) is the thermodynamically unfavourable valence state of this important trace metal under oxygenated conditions. Yet Fe(II) has been positively identified in a range of lacustrine and marine waters although the redox potentials in these aquatic environments favour oxidized Fe(III). We apply our Fe L_3-edge XANES spectro-microscopic technique to the evaluation of particles collected from the south-western Pacific and Southern Oceans as well as from two fresh water environments (Pine Barrens, NJ, USA and La Plata Lake, Puerto Rico). The associations with organic carbon are investigated on a particle-by-particle resolution by collecting complementary C K-edge XANES spectra. These associations are discussed in terms of biological influences, Fe(II) stabilization and effective surface chemistry.

Iron L-edge and carbon K-edge XANES spectra were collected equally by Ms Emily Hauser and I, with additional help from Mr Matt Frith. I was responsible for the analyses and write up of the sections relating to Fe L-edge speciation and I further prepared five of the final figures. Ms Hauser performed the C K-edge analyses and was responsible for the write up of that section. Prof Satish Myneni prepared parts of the introduction and supervised the write up. The final integrated manuscript is the end-product of an iterative write-up process shared equally by Prof Myneni and I. Dr Andrew Bowie provided filtered marine samples and Dr Gustavo Martinez and Dr Bhoopesh Mishra respectively collected and performed Fe K-edge analyses on the La Plata Lake samples and were responsible for the write up related to the complementary Fe K-edge dataset. Dr Tolek Tyliszczak was the beamline scientist and helped out during data collection. Prof Alakendra Roychoudhury provided funding and gave input during the final write-up.

Ubiquitous presence of Fe(II) in aquatic colloids and its association with organic carbon

Bjorn P. Von der Heyden[1], Emily J. Hauser[2], Bhoopesh Mishra[3], Gustavo A. Martinez[4], Andrew R. Bowie[5], Tolek Tyliszczak[6], Alakendra N. Roychoudhury[1], Satich C.B. Myneni[2]

1. Department of Earth Sciences, Stellenbosch University, Private Bag X1, Matieland, 7602, South Africa
2. Department of Geosciences, Princeton University, Princeton, NJ 08544, USA
3. Illinois Institute of Technology, Chicago, IL 60616, USA
4. University of Peurto Rico, San Juan, Puerto Rico
5. Institute of Marine and Antarctic Studies, University of Tasmania, Tasmania, Australia
6. Advanced Light Source, Lawrence Berkeley National Laboratory, University of California, Berkeley, CA 94720, USA

ABSTRACT

Iron minerals are predominantly ferric in nature and are ubiquitous throughout the natural environment where they play an important role in contaminant and nutrient cycling and transport processes. The chemistry, structure and reasons for the persistence of small ferrous colloids, however, are still poorly understood. Here we use x-ray based Fe L-edge technology to address the speciation of such particles, ranging in diameter between 20 nm and 2 µm, collected from sampling sites in both marine and fresh water environments. We show that despite the vast degree of chemical heterogeneity observed in environmental Fe(II) colloids, they are always characterised by significant association with organic moieties, particularly those with alcohol and carboxamine functional groups. These finding have implication for how we understand the behaviour of Fe(II) colloids in oxygenated aquatic (bio-)geochemical systems.

1. INTRODUCTION

Iron minerals are common in soils and sediments, where they represent important sources of Fe for biological processes and act as strong sorbents for various contaminant and nutrient entities. In aquatic environments, these phases can persist as colloids in the micron to submicron size range, where their stability is governed by water composition and mineral surface chemistry. Colloidal Fe-phases can exert a strong control on the solubility and transport of contaminants in aquatic systems (Hochella et al., 2005) and the dissolution, and redox and photochemical transformations of these phases can eventually modify the fate of associated contaminants and nutrients. While the importance of colloidal Fe in various biogeochemical processes is well understood, the compositional and mineralogical properties of Fe-phases in the colloidal

fraction of natural waters have not been well studied. Here we present the chemical characteristics of selected freshwater and seawater Fe-colloids and their organic carbon associations as determined using x-ray spectroscopy and microscopy techniques.

Colloidal and dissolved Fe can exist in two different oxidation states in aquatic environments, Fe(II) and Fe(III). While Fe(III) is thermodynamically favourable and overwhelmingly more prevalent in oxygenated waters, Fe(II) has been measured in significant concentrations in a variety of fresh water and seawater regimes (Shaked et al., 2002; Boyé et al., 2006; Ussher et al., 2007; Shaked et al., 2008; Toner et al., 2009). While large suspended particles typically consist of detrital Fe(II) alumnosilicates, these observations of Fe(II) in the smaller dissolved and colloidal size classes are surprising. Photochemical reduction of Fe(III) (Barbeau, 2006; Shaked et al., 2008), reduced benthic porewaters (Ussher et al., 2007) and hydrothermal inputs (Bennett et al., 2008; Tagliabue et al., 2010) constitute potential sources of Fe(II) for incorporation into natural colloids; and organic and inorganic complexation reactions may play a role in their subsequent stabilization and persistence in the water column (Toner et al., 2009).

Better understanding of the structures of Fe colloids and the factors affecting Fe colloid stability can now be explored by utilizing synchrotron based x-ray spectromicroscopy methods to directly probe colloid chemical and mineralogical characteristics. Specifically, the zone-plate based scanning transmission x-ray microscopy (STXM) is an ideal tool for examining the chemical characteristics of Fe-colloids and their association with organic carbon, as this technique enables a 10-15 nm spatial resolution at the Fe L-absorption edge. In addition, the colloidal samples can also be examined directly in their native hydrated state without any special sample preparation. Several researchers have examined natural Fe-containing particles using x-ray mapping and speciation techniques at both the K-, and L-edges of Fe (Bluhm et al., 2006; Dynes et al., 2006; Chan et al., 2009; Miot et al., 2009; Schroth et al., 2009; Toner et al., 2009; Lam et al., 2012; von der Heyden et al., 2012). Iron K-edge techniques, which are associated with a lower spatial resolution (>100-150 nm), have been utilized to determine bulk or average Fe speciation in heterogeneous samples (Lam and Bishop, 2008; Schroth et al., 2009) and to determine particle specific speciation in larger micron-sized particles (Lam et al., 2012). In comparison, the Fe L-edge has a much higher spatial resolution (down to a few nanometers) and has successfully been applied to the speciation of hydrothermal vent and open ocean colloids (Toner et al., 2009; von der Heyden et al., 2012) and to sub-micron scale biomineralization investigations (Chan et al., 2009; Miot et al., 2009).

Spectromicroscopy of Colloidal Fe and Organic Carbon

In the last decade, x-ray spectroscopic and spectromicroscopic techniques have been widely used to evaluate the functional group composition of organic molecules in soils, sediments, biofilms, and aquatic humic substances. Although the x-ray spectroscopy of K-edge of C, N and other light elements or the L-edges (or higher edges) of heavy elements can be conducted using vacuum beamlines or STXM beamlines, researchers

preferred the latter technology because of sample flexibility and the preservation of hydration state (Bluhm et al., 2006). One of the added advantages to using STXM is that it allows for determining the organic carbon speciation and mapping their distribution in natural samples. Additionally, the associations between C and Fe can be explored by directly examining the specimens at the Fe-absorption edge (discussed below). Typically the C K-edge x-ray absorption near-edge structure (XANES) spectra exhibit several 1s to π^* or σ^* transitions at various energies, each corresponding to different functional group chemistries. At the Fe L-absorption edge (where 2s or 2p electrons are excited to partially occupied or vacant atomic or molecular orbitals), the absorption cross-section is much higher than that of the K-absorption edge (where 1s electrons are excited to vacant atomic or molecular orbitals). This high absorption cross-section results in high contrast images and high spatial resolution at the Fe L-edge relative to the Fe K-absorption edge; however, the high absorption cross-section also limits the examination of particles thicker than a few microns at the Fe L-edge (because of limited penetration of x-rays to such depths). Since the majority of aquatic colloids are in the size range between tens of nanometers to a few microns, Fe L-edge spectromicroscopy is well suited for studying Fe-colloids.

Historically, the Fe L-edge XANES spectra have had application in various valence state quantification studies (Cressey et al., 1993; van Aken and Liebscher, 2002; Calvert et al., 2005; Cavé et al., 2006). Because the Fe L-edge XANES spectra also contain local coordination information, more recent studies have expanded on spectral interpretations to incorporate both structural and chemical observations (Hocking et al., 2010; Peak and Regier, 2012; von der Heyden et al., 2012). In particular, our previous work has shown that chemical and mineralogical variability in natural Fe-rich particulates can be characterized using XANES L_3-edge splitting parameters (von der Heyden et al., 2012). The energy difference between the two L_3 peaks is measured as the ΔeV value and the quotient of their peak intensities is given as the intensity ratio value (Fig. 1). Because each individual Fe mineral has a unique Fe coordination environment, and thus XANES spectral shape, mineral phases can be characterized by a unique combination ΔeV and intensity ratio values. Examination of over 80 standard Fe spectra, collected from the literature and from phases synthesized in our laboratory, has shown that Fe phases with similar chemical properties occupy discreet fields on a ΔeV versus intensity ratio plot (Fig. 2a). Ferrous standard phases are characterized by both high ΔeV values (2.0-2.8) and high intensity ratio values (1.8-4.9). Ferrous-rich mixed valence standards have smaller ΔeV values than the purely ferrous standards (Fig. 2a) and occupy a region on the plot bounded by ΔeV values between 1.2 and 1.4; and intensity ratio values between 1 and 1.6. Both groups of minerals can be easily distinguished from phases with majority ferric contribution by an intensity ratio cut-off value of 1 (von der Heyden et al., 2012).

The goal of this study is to identify the common forms of Fe in the colloidal fractions of natural waters and the association of different Fe pools with natural organic moieties. To compare Fe speciation and its relationship with organic carbon, samples were collected from a variety of aquatic sources- including coastal and open ocean waters and fluvial and lacustrine settings. The lacustrine samples were collected from fresh water systems in New Jersey and Puerto Rico and the marine samples focused primarily on the Southern

Ocean and the western South Pacific Ocean basins, with additional samples from a near-coastal site on the continental slope off of South Africa's western margin. Although this study focused on the Fe L-edge, we also used both L- and K-edge XANES for Fe-rich samples from Puerto Rico.

2. MATERIALS AND METHODS

Sample collection

Southern Ocean marine surface water samples were collected using a towed fish and PFA Teflon tubing continuous sampling system (after de Jong et al., 1998). Samples were collected into 25L acid-cleaned carboys for subsequent filtration. In total, ten surface water samples (Fig. S1) were collected over two oceanographic cruises; SANAE 49 (Dec 2009-Feb 2010) and SANAE 50 (Dec 2010- Feb 2011). Using trace-metal clean CTD rosettes, additional 10L samples were collected from various depths (0-4000m) from a near-coastal site (34.296ºS: 17.112ºE) and an open ocean site (36.465°S: 13.211°E) in the South Atlantic Ocean (Fig. S1). Because of higher suspended particle loads associated with near-coastal and depth samples, smaller 10L sample volumes were sufficient at these sites, relative to the particle (and Fe) depleted Southern Ocean surface waters. Low pressure vacuum filtration of all collected water was done using 47 mm diameter Millipore™ 0.2 µm PTFE membrane filters and filtration proceeded until the filters were fully loaded, thereby ensuring that the entire particle size spectrum was trapped for subsequent STXM analysis.

Pacific Ocean samples were collected from three sampling sites (30°S: 175°E; 32.5°S: 180°E; 32.5°S: 175°E) located near to the Kermadec Ridge during GEOTRACES cruise GP13 during May, 2011 (Fig. S2). Samples were collected from four depths (30m, 100m, 300m, 1000m) at each site, by pumping between 180-420L of seawater through quartz microfiber filters using a set of McLane pumps.

Because marine waters are typically associated with sparingly low Fe concentrations and are thus especially sensitive to contamination, care was taken to follow GEOTRACES protocol and to observe trace-metal clean techniques during all collection of marine water samples. All loaded filters were stored in acid-cleaned petri dishes and retained in a frozen state during transport and storage prior to their STXM analysis.

Lacustrine samples were collected from two freshwater settings characterised by markedly different geology and climate. The 'Pine Barrens' samples were collected in HDPE bottles from the surface waters of Pakim Pond, Brendan T. Byrne State Park, NJ, USA (39.8801°N: 74.5316°W). These samples were filtered to remove large particulates, and the supernatant was stored frozen, and otherwise unaltered, until STXM analysis. Settling particulates were collected from La Plata reservoir, in the north central region of Puerto Rico (18.3336°N: 66.2381°W). Samples (in duplicates) were collected in 500mL amber polypropylene bottles tied to a nylon rope at different depths (e.g., 1m, 5m, 8m, 10m, 14m, 16m). The collection system

was anchored to a buoy positioned near the reservoir's dam for a two-week period. At the time of collection, the bottles were brought to the surface and capped while still under water. The bottle caps were secured on site using parafilm tape and stored frozen until further synchrotron analyzes.

X-ray spectromicroscopy studies

Fe L-edge and C K-edge

Prior to spectroscopic characterisation, the frozen filters from marine samples were rinsed with de-ionized water to remove excess salt, thereby ensuring that high-quality images could be obtained (Toner et al., 2009; von der Heyden et al., 2012). Rinsed filters were transferred to acid-cleaned 15 mL test tubes to which a small volume (<1 mL) of de-ionized water was added so that trapped particles could be re-suspended. Between 2-10 µL of this re-suspension was placed onto a silicon nitride (SiN_3) membrane window (500x500 or 750x750 μm^2) and covered and allowed to air dry for a few minutes. Lacustrine samples, containing a high abundance of particulates and free of significant salt, did not require these initial concentration and desalination steps. For these samples, between 2 and 10 µL of the defrosted supernatant was placed on a SiN_3 membrane window and allowed to dry for approximately 1-3 minutes under a laminar flow hood. Previous work has shown that this sample preparation procedure maintains the sample integrity and that analysing 1-2 windows, prepared in this manner, resulted in reproducible and representative data (Toner et al., 2009; von der Heyden et al., 2012).

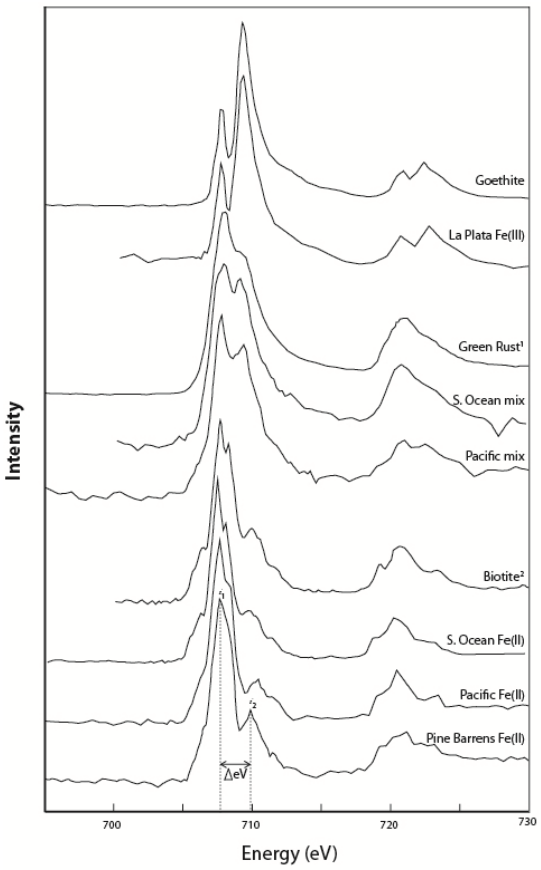

Figure 1: *Representative Fe L-edge XANES spectra collected from four different aquatic sampling sites and compared to relevant reference spectra ([1]Kneedler et al, 1997; [2]Toner et al, 2009). The characteristic L_3 peak splitting is parameterized according to its ΔeV value (difference in energy between the high energy and the low energy peaks) and its intensity ratio value (peak intensity quotient i_1/i_2).*

For STXM analysis, dry sample windows were placed in the STXM endstation (11.0.2, Advanced Light Source, CA, USA (Bluhm et al., 2006)) and investigated at their Fe L- and C K-edges. The imaging and spectroscopic studies were conducted using a 17 nm zone plate, a 1200 l/mm grating and 25 µm exit slits. Calibration of the monochromator was conducted using the Neon 1s→3p transition set to 863.7 eV. The sample chamber was purged with He gas during the data collection.

Iron rich particles were located on the SiN_3 sample window using coarse 10x10 μm^2 or 30x30 μm^2 image maps generated by subtracting an edge-region (709-710 eV) x-ray image from an image of the same area collected at an energy below the Fe L_3 absorption edge (700 eV). Once located, Fe-rich regions and Fe-rich particles were analyzed for their XANES (X-ray Absorption Near-Edge Structure) spectra using either linescans or image stacks (10-50 nm spatial resolution) over the Fe $L_{2,3}$ edge region. Energy increments of 0.5 eV were used above and below the edge (695-703 eV; 715-730 eV) and a step-size of 0.2 eV was used close to the Fe L_3 edge (703-715 eV). These sample scan parameters and protocols followed were selected to minimize sample alterations.

Once Fe-enriched particles and regions had been identified and analyzed, the x-ray energy was changed to the carbon K-edge and STXM C-mapping and XANES spectroscopy was conducted. Although analyses focused on particles in which Fe had already been located, subtraction maps generated using carbon edge- and pre-edge energy images were used to determine the prevalence of carbon on each SiN_3 window. XANES spectra were collected for both Fe-enriched and Fe-poor organic particulates by generating either line-scans or image stacks and using energy increments of 0.2 eV at the C K-edge edge (283-300 eV) and 0.5 eV above and below the edge (280-283 eV; 300-315 eV). During all x-ray analyses, beam damage effects were minimized by limiting the x-ray exposure dwell time to 1-2 msec and ensuring that the beam shutter was always used whenever data were not being collected.

Fe K-edge

Particulate-rich samples from Pueto Rico freshwater reservoir were also examined directly using Fe K-edge XANES spectroscopy at the X-18B beamline, National Synchrotron Light Source (Brookhaven National Laboratories, NY). The energy of the incident X-rays was scanned using a Si(111) reflection plane of a double-crystal monochromator. Since X18B is a bending magnet beamline, variation in the incident photon intensity for the scanned energy range was less than 15%. Higher harmonics were removed by detuning the second monochromator crystal by 30%. The ionization chamber used to measure the incident photons was filled with a mixture of 50% N_2 and 50% He, while the ion chambers used to measure the sample transmission were filled with a mixture of 60% N_2 and 40% Ar gas. An energy dispersive solid state (13-element) Canberra Ge detector was used for the fluorescence mode detection of the x-ray signal. Samples were loaded into a slotted Plexiglas holder and covered with Kapton film. Consecutive spectra were monitored for possible radiation-induced changes. A total of 5 to 7 consecutive scans were collected for each sample. All scans were calibrated using a simultaneously collected spectrum of a Fe foil (first inflection point in the spectrum at 7112 eV), and averaged before further spectral analysis. The XANES spectra were analyzed using the UWXAFS package. Processing of the raw data, including the alignment of spectra and background removal, were implemented by using ATHENA. The maximum frequency of the background was set to 1.0 Å for background subtraction.

3. RESULTS

The size ranges of Fe-rich particles varied significantly: Fe(II)-rich particles were present in the size range of 60 nm- 2.6 µm and were observed in all of the sampling sites considered in this study; whereas Fe(III)-particles occurred commonly as smaller sized colloids (down to 20 nm). The ubiquity of Fe(III) particles had been anticipated given the oxygenated nature of the aquatic systems studied; however, the presence of Fe(II) particles is surprising. Our interest thus lay primarily in understanding the chemical state of Fe, and factors that contribute to the stability of Fe(II) colloids, particularly in the smallest size fractions where high surface area to volume ratios typically result in a relatively larger reactive surface area and phase metastability (Waychunas et al., 2005).

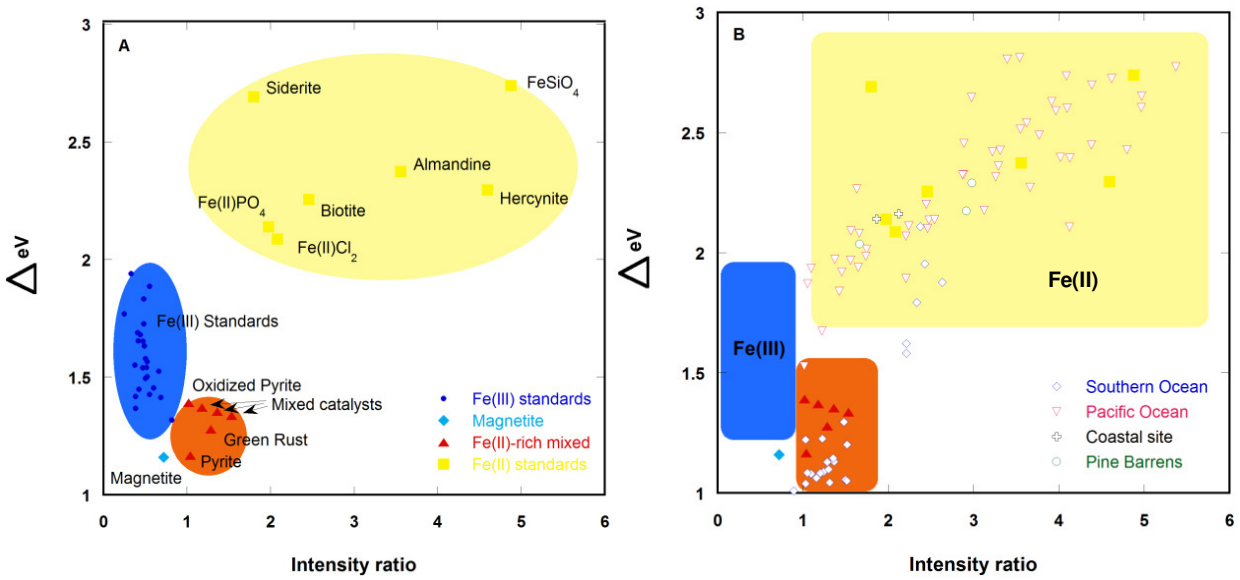

Figure 2a: *Intensity ratio versus ΔeV characterization plot for Fe-rich standard phases collected from the literature (adapted from von der Heyden et al., 2012). Iron phases with different valences can clearly be distinguished by their unique fields on the plot.* ***2b:*** *Distribution of natural Fe(II) and Fe(II)-rich mixed-valence phases collected from four different aquatic sampling sites, plotted on the intensity ratio versus ΔeV diagram.*

Near-coastal marine samples

Particles collected from surface waters and 1000 m depth at the South African continental slope were predominantly ferric and ranged in size between 30 nm and 4 µm. The prevalence of Fe(III) is not surprising given the proximity of fluvial sources (Berg, Olifants and Orange Rivers, western margin of South Africa) which are characterized by colloids and particulates containing only ferric phases (von der Heyden et al., in prep). The two larger Fe(II) particles (~1.1µm and ~2.6µm) identified in these samples may be indicative of a detrital nature, and the spectral ΔeV and intensity ratio coordinates for these two particles plot in close agreement to the spectral parameters of a reported $Fe(II)PO_4$ spectrum (Miot et al., 2009; Fig 2b). Seasonal upwelling events with associated hypoxic conditions in the nearby southern Benguela Upwelling System (Monteiro and van der Plas, 2006) may provide a plausible source of both reduced iron and the major nutrient phosphate. Confirmation of this characterization and the reasons for its persistence in the water

column will however require further investigation into seasonal variations associated with different Fe sources.

Southern Ocean samples

Iron-rich particles in the South Atlantic and Southern Oceans have previously been shown to classify into five distinctly different chemical categories according to their ΔeV and intensity ratio spectral parameters (von der Heyden et al., 2012). Despite the oxic nature of surface seawater, a remarkable 12.1% of particles analysed in this study were classed as either purely ferrous, or as Fe(II)-rich mixed valence phases (Figs. 1, 2b). The majority of these particles were mixed valence and their spectral characteristics did not match those of any standard mixed valence phases (Fig. 2b), likely because of the variabilities in the chemistry and extent of oxidation in natural colloids, which are also commonly structurally amorphous. Similarly, the ΔeV versus intensity ratio values of purely Fe(II) phases did not agree with any of the plotted points for literature reported standard phases. Again, variability in the chemistry of bonded inorganic and organic ligands, the presence of structural impurities and the extent of oxidation were invoked to explain this mismatch, however, differences in the standard sample preparation and data collection techniques may also have played a role. One likely explanation for the prevalence and persistence of Fe(II) enriched phases at these sites is that they are being stabilized by organic-rich surface coatings. This study thus undertook to explore these relationships further by examining the Fe(II)-C associations in particles collected from the South Pacific Ocean and from two terrestrial lacustrine settings.

Pacific Ocean samples

Over sixty particles were analyzed from various depths at the three sampling sites in the South Pacific Ocean. The majority of these particles (~80%) had Fe(II) as the dominant oxidation state with mostly pure Fe(II) and a few Fe(II)-rich mixed valence phases identified (Figs 1, 2b). At all three sites and at all sampling depths (30-1000 m), the reduced form of Fe was the dominant oxidation state in the particles analyzed. The only exception was found in a 1000 m depth sample collected at the sampling site farthest away from the Kermadec Ridge. Here, Fe(III) was found to be the dominant oxidation state of the Fe-rich particles analyzed, although a substantial proportion (40%) of the particles were still Fe(II) enriched. Given the proximal location of the sampling locations to sites of active tectonism (Mortimer et al., 1998; Fig. S2) it is likely that hydrothermal sources contribute a proportion of this flux of reduced Fe (Tagliabue et al., 2010; Bennett et al., 2008; Toner et al., 2009).

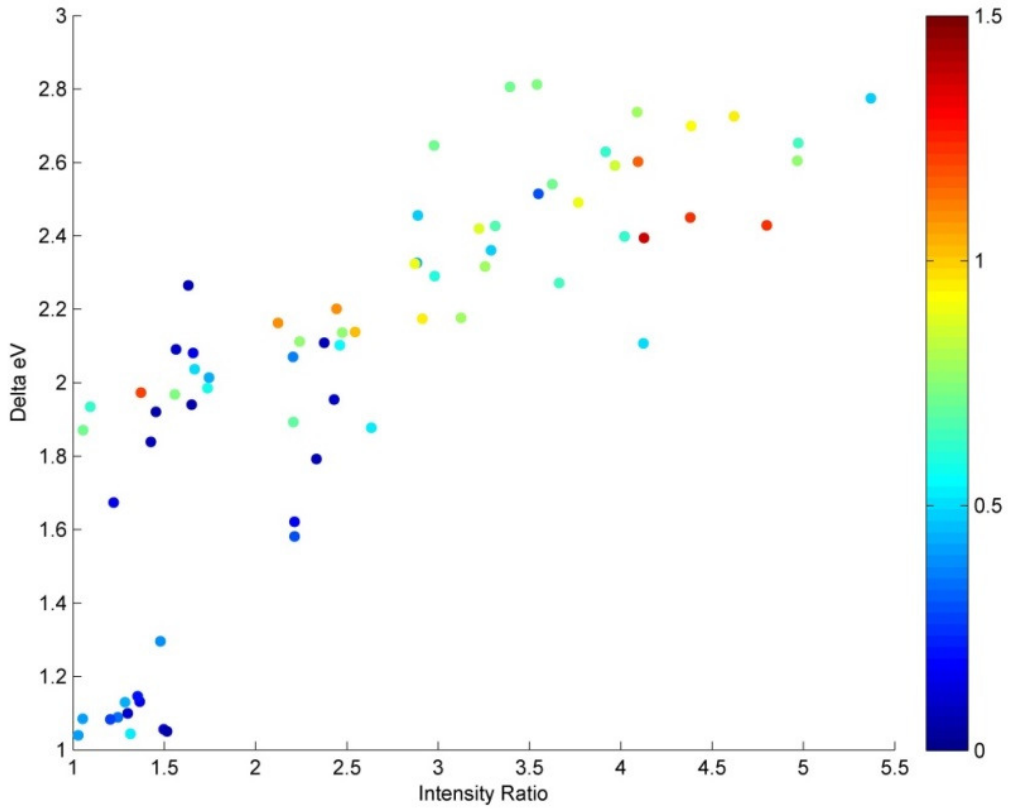

Figure 3: *Relationship between particle size (z-axis, units in µm) and the distribution of south-western Pacific Ocean samples on an intensity ratio versus ΔeV diagram. Mixed-valence Fe(II)-rich particles (bottom left corner) are typically smaller than pure ferrous phases and larger intensity ratio and ΔeV values are associated with larger sized particles.*

Although the sizes of Fe(II) rich particles ranged from as small as 60 nm up to 2.3 µm, the average particle size tended towards larger values (mean=0.70 µm, N=50). As particle size increased, there was a slight positive trend with both the measured intensity ratio and the ΔeV values (Fig. 3). The spectral parameters of Fe(II)-rich particles sampled from the Pacific Ocean showed the largest range in distribution (Fig. 2b; ΔeV: 1.5-2.8; intensity ratio: 1.0-5.4) and data points did not cluster around any of the standard mineral phases reported. The distribution of the data points in figure 2b did not appear to show any strong correlation with either the sample location or the depth from which samples were collected (Figs. S3, S4). The vast spread in the distribution on the plot can thus only be attributed to particle size effects (minor influence) and an expected high degree of chemical heterogeneity between individual particles.

Lacustrine samples

Of the two lacustrine settings investigated, only the Pine Barrens samples showed appreciable Fe(II) abundance when examined using the Fe L-edge XANES spectroscopy. Only three discrete Fe-rich particles, ranging in size between 500 nm and 1 µm, were investigated in detail at this site and all had spectra indicative of Fe(II) (Figs. 1, 2b). The spectral parameters for these Fe(II) particles did not precisely match

any of the examined standard mineral phases, however one of the particles had spectral features similar to that of Fe(II)PO_4 whereas the other with their Fe coordination environments most similar to that of Fe in biotite (Fig. 2b).

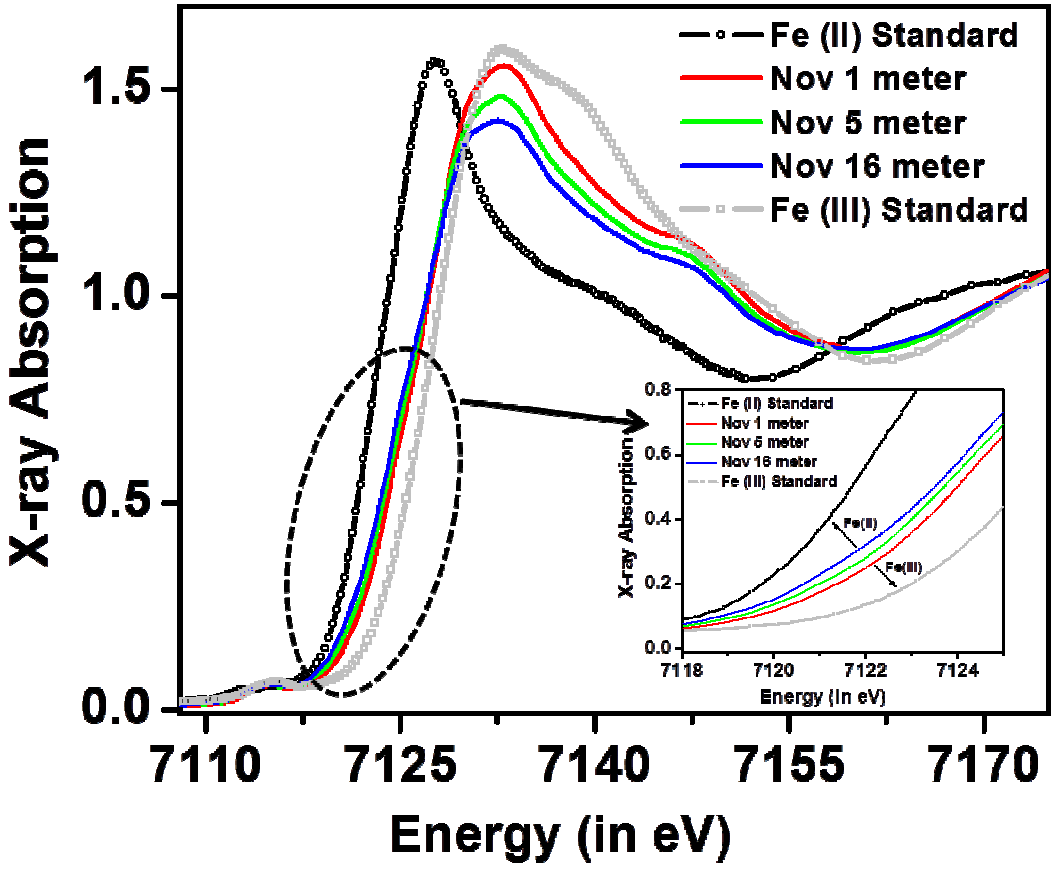

Figure 4: *Fe K edge XANES of Fe(II) and Fe(III) standards with 1, 5, and 16 meter water column sampled from La Plata lake in November 2008. Inset shows the blown-up portion of XANES adsorption edge for clarity.*

The L-edge spectromicroscopy of particulate samples collected from the top and bottom parts of the water column in the La Plata reservoir consisted only of Fe(III). Comparison of the spectral features of these natural ferric phases to those of standard Fe-oxide and –oxyhydroxides, showed that only ~21% of these particles have ΔeV and intensity ratio values characteristic of the crystalline standards. The majority (two thirds) of these had spectral features typically of the goethite (αFeOOH), which has previously been shown to be a dominant phase in lake settings (van der Zee et al., 2003). In contrast to the Fe L-edge, the bulk Fe-XANES spectra of particulates at the Fe K-absorption edge indicated the presence of a significant fraction of Fe(II) (Fig. 4). Linear combination fitting of these bulk Fe K-edge XANES spectra indicated that the Fe(II) species associated with the particulates increased from 16% in the top water column to 33% in the bottom water column (Figure 4; Table S1). Regardless of the highly oxidizing conditions in the surface water column, a detectable amount of Fe(II) and Fe(III) containing particles were observed at all depths.

It has also been shown that Fe(II) in aluminosilicates is resistant to oxidation to Fe(III) under oxic conditions. However, the STXM maps and NEXAFS spectroscopy at the C and Al K edges, and Fe L_3 edge showed that organic matter served as the backbone for the formation of loosely packed large (~20 µm) clusters of inorganic colloids in the top (1 meter) water column of La Plata lake. Complexation of Fe with organic ligands is, therefore, the likely reason for stabilization of Fe(II) in the oxic zone of the lake, consistent with observed fraction of Fe(II) in the top water column.

Speciation of colloidal organic carbon

Carbon K-edge XANES spectra were used to identify the dominant organic functional groups associated with Fe in marine and lacustrine particulates (Fig. 5). All C spectral features are classified into the following broad classes because of their common occurrence: unsaturated carbon, including both carbon double and triple bonds, is associated with C 1s→π* transitions at approximately 285 eV; 286.0-286.4 eV represent a prevalence of aryl- and vinyl-keto functional groups; between 286.5- 287.4 eV signify the presence of aliphatic carbon, heterocycles and aldehydes; between 287.5- 288.8 eV represent amide, ketone and carboxylate transitions; and at 289.5-290.5 eV, transitions indicate substantial presence of alcohol and carboxamide organic moieties and carbonate.

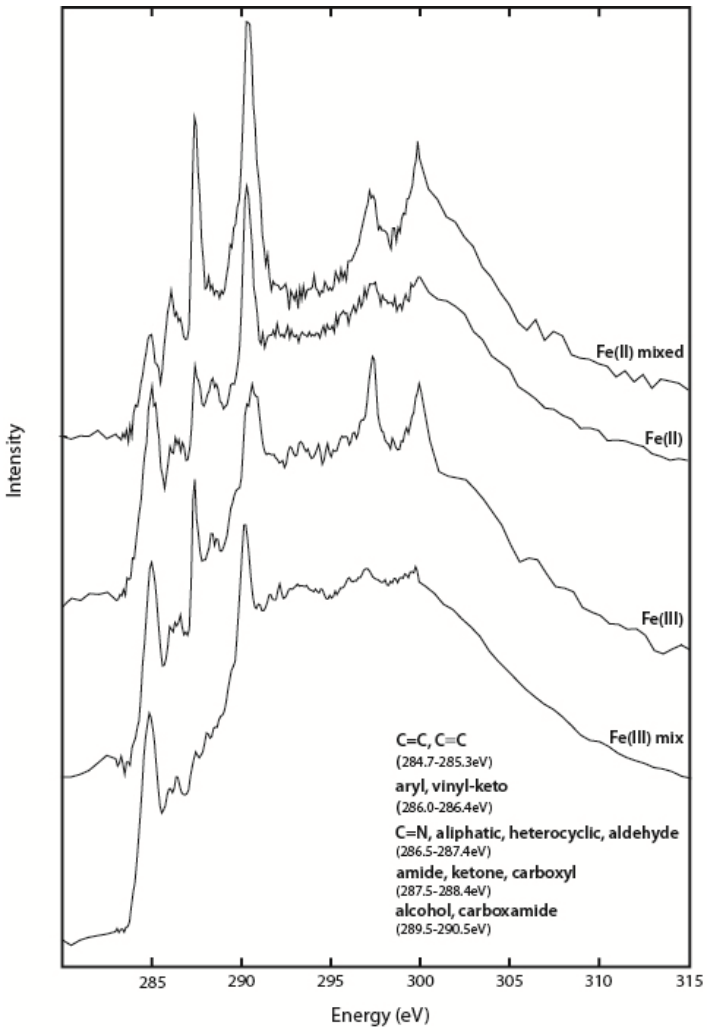

Figure 4: *Representative carbon K-edge XANES spectra associated with Fe particulates of differing chemical speciation. Major peaks, representing C 1s→π* electronic transitions, are used to identify the presence and ubiquity of various broad organic functional groups.*

Although this study focusses on the associations between organic carbon and Fe speciation and on reduced Fe persistence, analyses were also conducted on Fe-poor regions for comparative study. In total, forty-one Fe-enriched particles were analyzed for their corresponding C K-edge spectra, of which most (~80%) were sampled from the southwestern Pacific Ocean, with the remaining particles collected from freshwater (Pine Barrens and La Plata Lake). This dataset represents an extensive and significant time investment at the synchrotron beam-line, where time-requirements limit analyses to the complete characterization of only three to five particles daily. It should be noted that the STXM spectra and images give an average Fe or C signature of all material present in each pixel in an image (from regions as small as ~ 10 nm). Since there is much more C in many samples

than Fe and because of the sample volume, it is difficult to conclude a specific organic carbon group binding Fe (unless, Fe-complexation of a specific group exhibits distinct electronic transition). Hence the focus has been on the specific organic moieties associated with Fe(II) and Fe(III) phases. Figure 6 plots the frequency of organic function group association with particles of differing Fe chemistry and with particles without significant Fe presence. Bars represent averaged data for twenty-seven Fe(II) particles, three Fe(II) mixed valence particles, two Fe(III) mixed valence particles and two Fe(III) particles, all collected from the marine sampling sites. Similarly, lacustrine data is averaged from four Fe(III) particles and three Fe(II) particles. In each instance, the corresponding number of analyses was conducted on Fe-poor regions of the SiN_3 sample window to generate the data shown in Figure 6b.

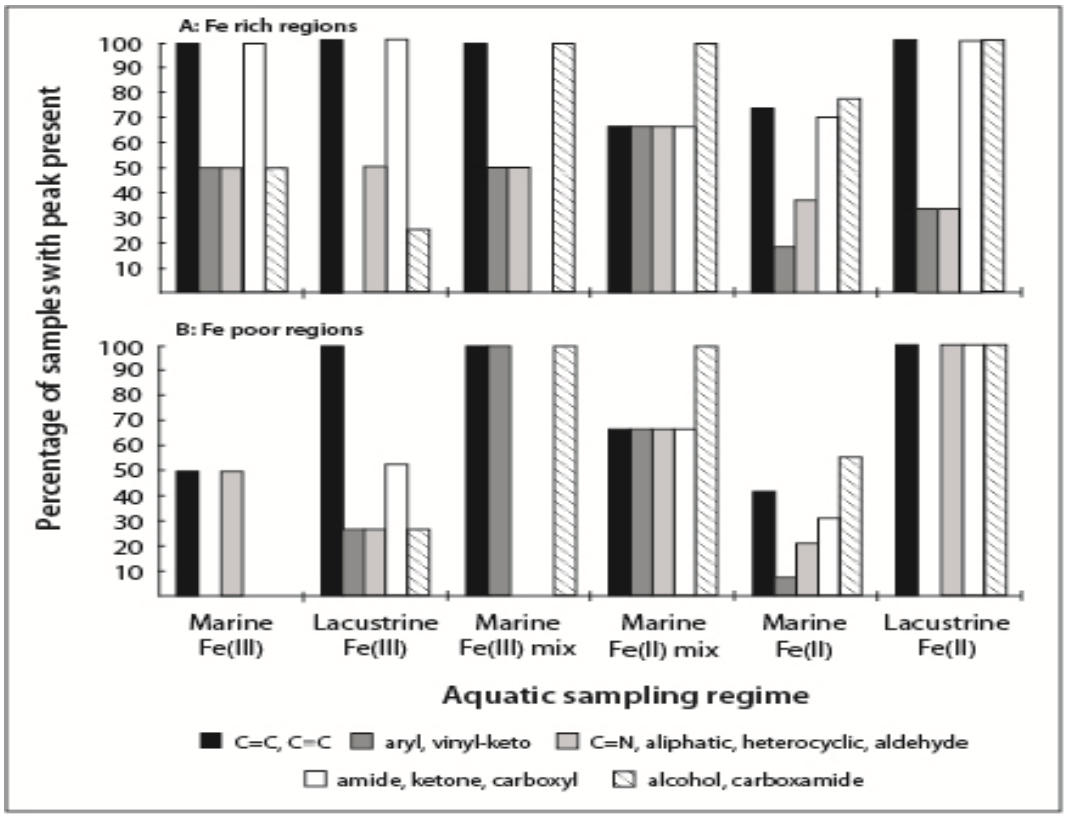

Figure 6a: *Frequency of each set of organic functional groups as found in association with Fe-rich particulates of varying chemistry and sampling location.* ***6b:*** *Corresponding analyses of organic functional group frequency for Fe-poor regions of each particle or sample window.*

Aside from the absence of aryl- and vinyl-keto functional groups associated with lacustrine Fe(III) particles, all organic functional groups considered have been positively identified to associate with Fe particulates, irrespective of Fe chemical speciation or aquatic sampling regime. The good agreement between organic moieties found in lacustrine environments and in marine environments is perhaps surprising, given the host of chemical and biological differences expected between the two sampling regimes. Marine and lacustrine Fe(II) particles show similar trends in their association with organic carbon functional groups, whereas lacustrine Fe(III) particulates, in addition to their absence of aryl- and vinyl-keto functional groups, are associated with less alcohol and carboxamine moieties than their marine counterparts. These alcohol and carboxamine moieties are also much more strongly associated with particulates containing Fe(II) (including

both mixed valence phases), relative to pure Fe(III) particulates. This could signify a higher affinity for binding of these organic moieties to Fe(II), but may also reflect the role that these functional groups play in stabilizing Fe in its reduced valence state. Comparisons of organic functional group frequency between Fe-rich and Fe-poor regions reveal that Fe-poor regions are typically characterized by less variety and lower frequencies in organic functional group chemistry; particularly for amide, ketone, carboxyl, C=N, aliphatic, heterocyclic and aldehyde groups.

4. ENVIRONMENTAL SIGNIFICANCE

Because of the rapid oxidation kinetics between Fe(II) and Fe(III) (Rose and Waite, 2002), substantial concentrations of Fe(II) are not expected in oxygenated water systems. Previous results have, however, reported significant concentrations of Fe(II) in the operationally-defined dissolved fraction in a variety of aquatic environments (Shaked et al., 2002; Boyé et al., 2006; Ussher et al., 2007; Shaked et al., 2008). In surface waters, persistent Fe(II) concentrations are often ascribed to rapid photochemical-induced redox-cycling steady state concentrations (e.g. Shaked et al., 2008), however, with our identification of stable Fe(II) colloidal phases, this steady state assumption, and our understanding of photochemical cycling kinetics, may require re-evaluation.

In marine systems, particularly in the open ocean, the concentration of bioavailable iron can limit the efficiency and magnitude of primary productivity (e.g. Boyd and Ellwood, 2010). For phytoplankton uptake mechanisms, Fe(II) is regarded as the preferred form of Fe for transport across cellular membranes (Shaked et al., 2005). Reduced iron is also much more soluble than Fe(III), and it is thus plausible that Fe(II) colloids represent a more bioavailable source of Fe than their colliodal Fe(III) counterparts; either by a prior dissolution pathway, or by direct utilization (Chen et al., 2003).

Colloidal Fe phases are well known for their binding affinity for various contaminant and nutrient functional groups. Fe(III) oxide and oxyhydroxides have been especially well studied in this regard (e.g. Waychunas et al., 2005), however, because of a prior lack in Fe(II) colloid speciation data, there is a general paucity in work relating to the role that Fe(II) colloids play in sorbing and transporting contaminants and nutrients. The difference in valence of surface Fe atoms can be expected to result in differing binding affinities and complexation geometries for anionic contaminants (e.g. AsO_3^{3-}; SeO_3^{2-}) and nutrients (e.g. PO_4^{3-}). Similarly, the observed colloid speciation differences and saturation of surface sites by organic functional groups will both equate to surface chemistry differences that can be expected to affect the binding of both cationic and anionic sorbents. Future work should focus on addressing these unknowns to elucidate and better predict the role that natural Fe colloids play biogeochemical systems.

ACKNOWLEDGEMENTS

This research is supported by grants from NRF, South Africa (Blue Skies Program), Stellenbosch University VR(R) fund, NSF (chemical sciences), US-DOE (BES & SBR), and Princeton in Africa program. The authors would like to thank the support staff at the Advanced Light Source for helping with data collection and sample preparation. Additional data are provided in Supporting Online Material.

SUPPLEMENTARY INFORMATION

Table S1: Fe speciation using linear combination fit of Fe K-edge XANES

Sample	% Fe(II)	% Fe(III)
Nov 1 meter	16	84
Nov 5 meters	26	74
Nov 16 meters	33	67

Figures:

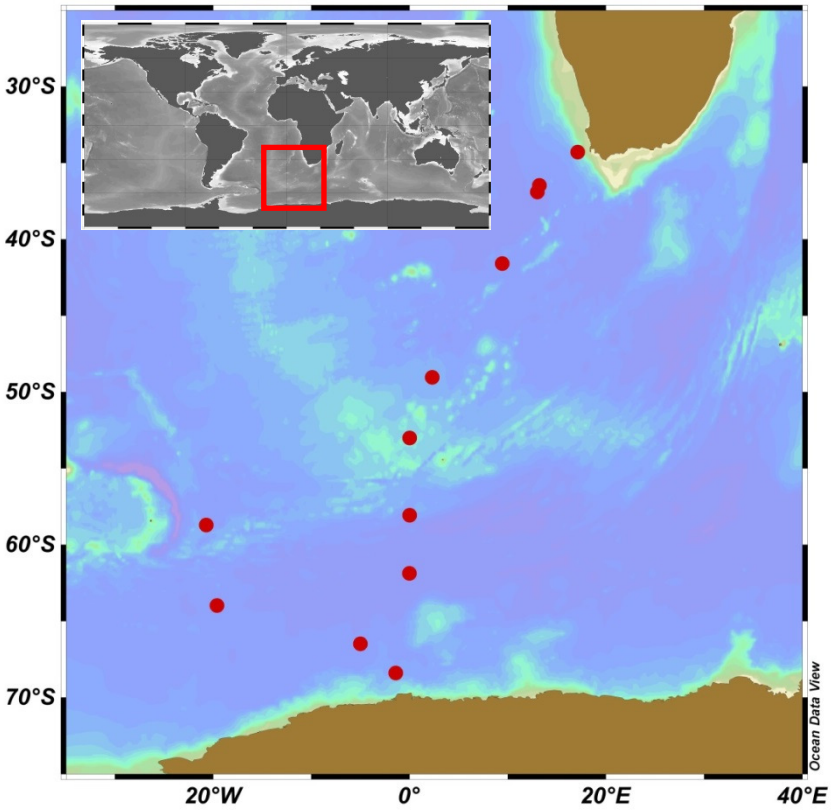

Figure S1: *Sample locations for surface and depth samples for the South Atlantic and Southern Oceans. From North to South: 34.30°S:17.12°E (continental slope sample); 36.46°S:13.21°E (GEOTRACES D357 (Nov 2011)); 36.91°S:12.99°E; 41.58°S:9.43°E; 49.03°S:2.31°E; 53.00°S:0.00°E; 58.05°S:0.00°W; 58.69°S:20.71°W; 61.86°S:0.02°W; 63.96°S:19.63°W; 66.48°S:5.02°W; 68.39°S:1.42°W.*

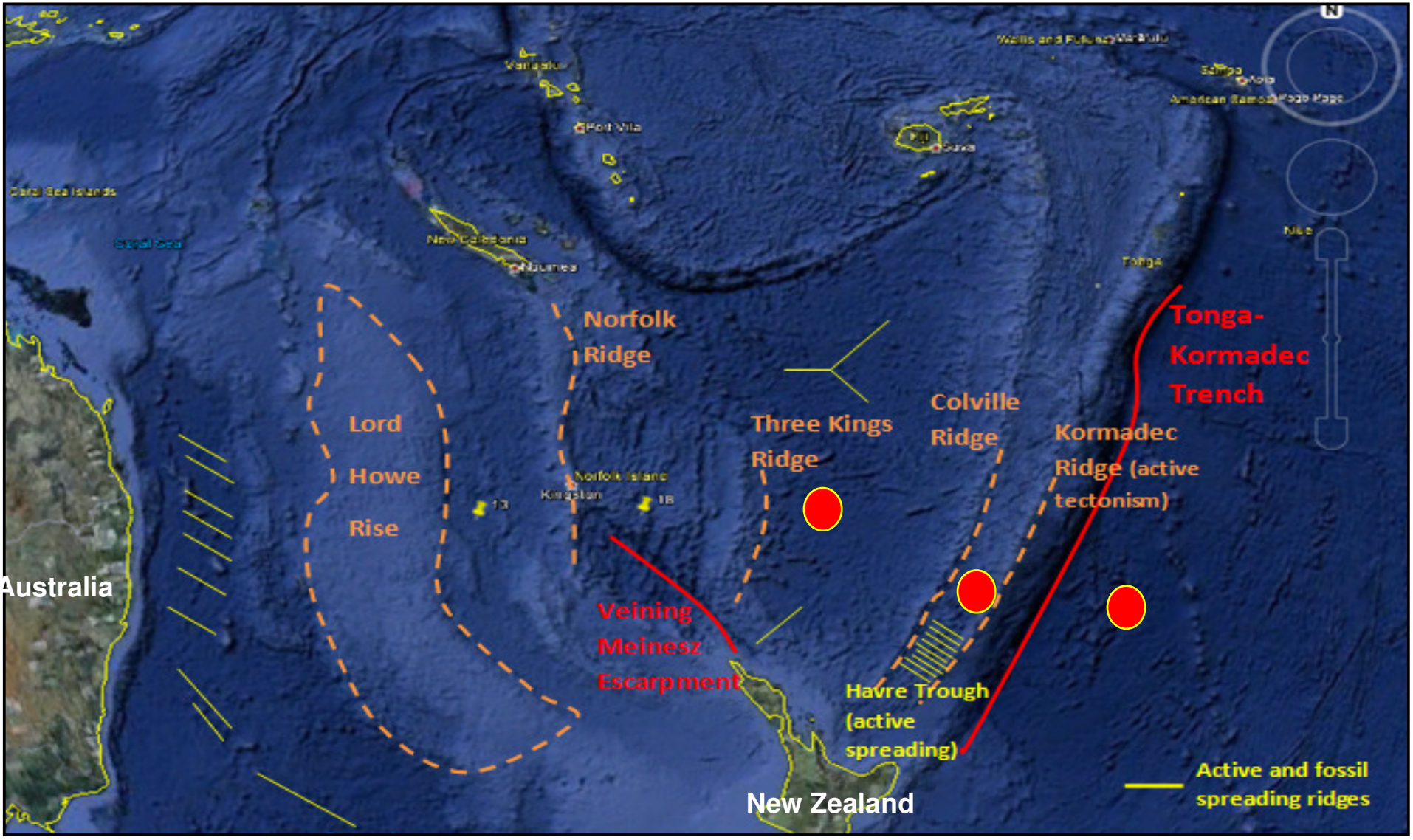

Figure S2: *Red circles indicate the location of the three southwestern Pacific Ocean sampling sites (30°S: 175°E; 32.5°S: 180°E; 32.5°S: 175°E) and their proximity to areas of active tectonism and spreading (after Mortimer et al., 1998). The background satellite image is from Google Earth.*

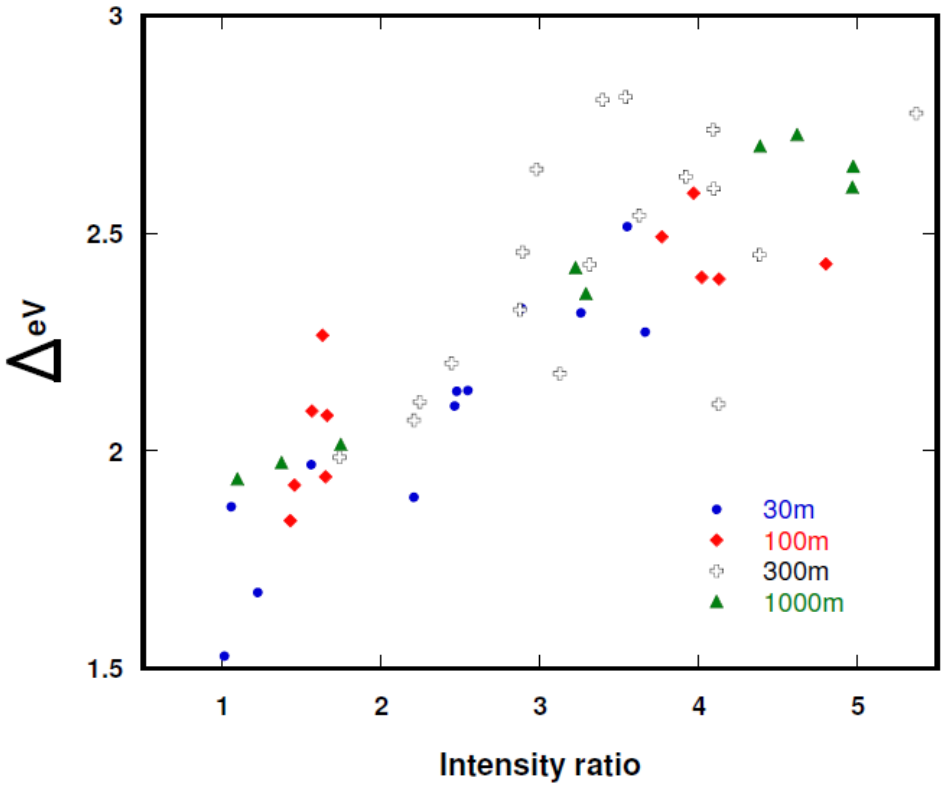

Figure S3: *Plot of ΔeV versus intensity ratio for south western Pacific Ocean Fe(II) colloids according to sampling depth. Depth does not appear to control the distribution of the points on this plot.*

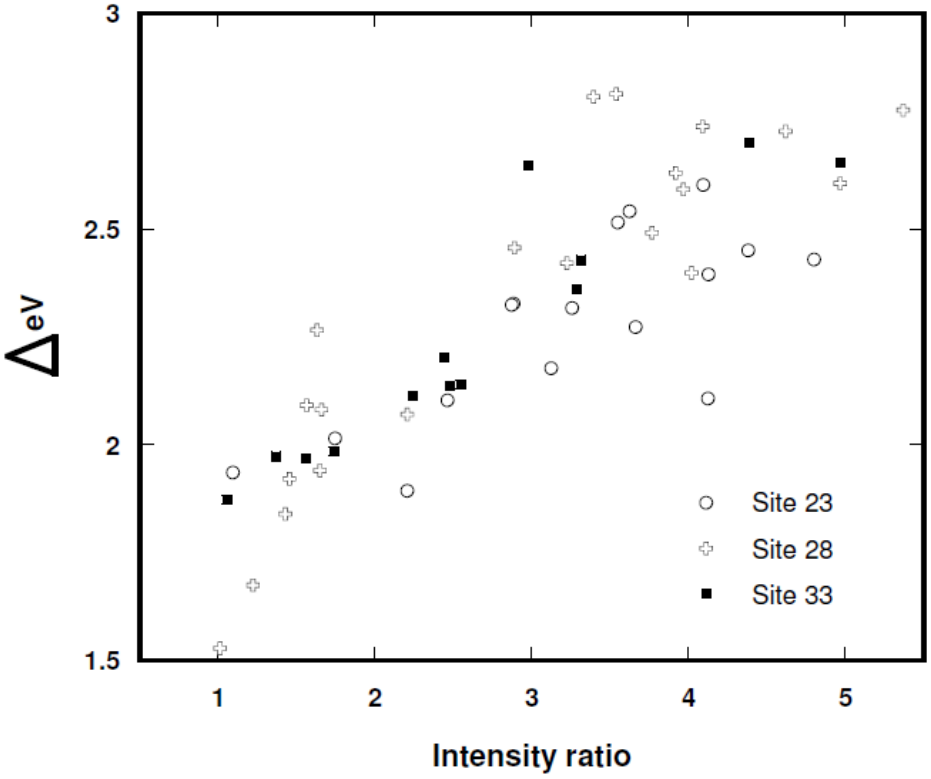

Figure S4: *Plot of ΔeV versus intensity ratio for south western Pacific Ocean Fe(II) colloids according to sampling site. The distribution of the points on the plot do not appear to be a function of sampling site.*

REFERENCES

Barbeau, K. Photochemistry of organic iron(III) complexing ligands in oceanic systems. *Photochem. Photobiol.* **2006,** *82,* 1505-1516.

Bennett, S. A.; Achterberg, E. P.; Connelly, D. P.; Statham, P. J.; Fones, G. R.; German, C. R. The distribution and stabilization of dissolved Fe in deep-sea hydrothermal plumes. *Earth Planet. Sc. Lett.* **2008,** *270,* 157-167.

Bluhm, H.; Andersson, K.; Araki, T.; Benzerara, K.; Brown, G. E.; Dynes, J. J.; Ghosal, S.; Gilles, M. K.; Hansen, H.-Ch.; Hemminger, J. C.; Hitchcock, A. P.; Ketteler, G.; Kilcoyne, A. L. D.; Kneedler, E.; Lawrence, J. R.; Leppard, G. G.; Majzlam, J.; Mun, B. S.; Myneni, S. C. B.; Nilsson, A.; Ogasawara, H.; Ogletree, H. F.; Pecher, K.; Salmeron, M.; Shuh, D. K.; Tonner, B.; Tyliszczak, T.; Warwick, T.; Yoon, T. H. Soft X-ray microscopy and spectroscopy at the molecular environmental science beamline at the Advanced Light Source. *J. Electron Spectrosc.* **2006,** *150,* 86-104.

Boyé, M.; Aldrich, A. P.; van den Berg, C. M. G.; de Jong, J. T. M.; Nirmaier, H.; Veldhuis, M.; Timmermans K. R.; de Baar, H. J. W. The chemical speciation of iron in the north-east Atlantic Ocean. *Deep Sea Res. I* **2006,** *53,* 667-683.

Boyd, P. W.; Ellwood, M. J. The biogeochemical cycle of iron in the ocean. *Nat. Geosci.* **2010,** *3,* 675-682.

Calvert, C. C.; Brown, A.; Brydson, R. Determination of the local chemistry of iron in inorganic and organic materials. *J. Electron Spectrosc.* **2005,** *143,* 173-187.

Cavé, L.; Al, T.; Loomer, D.; Cogswell, S.; Weaver, L. A STEM/EELS method for mapping iron valence ratios in oxide minerals. *Micron.* **2006,** *37,* 301-309.

Chan, C. S.; Fakra, S. C.; Edwards, D. C.; Emerson, D.; Banfield, J. F. Iron oxyhydroxide mineralization on microbial extracellular polysaccharides. *Geochim. Cosmochim. Acta.* **2009,** *73,* 3807-3818.

Chen, M.; Dei, R. C. H.; Wang, W.; Guo, L. Marine diatom uptake of iron bound with natural colloids of different origins. *Mar. Chem.* **2003,** *81,* 177-189.

De Jong, J. T. M.; Den Das, J.; Bathmann, U.; Stoll, M. H. C.; Kattner, G.; Nolting, R. F.; De Baar, H. J. W. Dissolved iron at subnanomolar levels in the Southern Ocean as determined by ship-board analysis. *Anal. Chim. Acta* **1998,** *377,* 113-124.

Dynes, J. J.; Tyliszczak, T.; Araki, T.; Lawrence, J. R.; Swerhone, G. D. W.; Leppard, G. G.; Hitchcock, A. P. Speciation and quantitative mapping of metal species in microbial biofilms using scanning transmission X-ray microscopy. *Environ. Sci. Technol.* **2006,** *40,* 1556-1565.

Hochella, M. F., Moore, J. N., Putnis, C. V., Putnis, A., Kasama, T., Eberl, D. D. Direct observation of heavy metal-mineral association from the Clark Fork River Superfund Complex: Implications for metal transport and bioavailability. *Geochim. Cosmochim. Acta* **2005,** *69,* 1651-1663.

Kneedler, E. M.; Rothe, J.; Weissmahr, K. W.; Pecher, K.; Tonner, B. P. Identification of green rust in environmental compounds using XANES of Fe-$L_{II,III}$ edges. In *Advanced Light Source Annual Compendium of Abstracts,* Lawrence Berkeley Publications **1997.**

Lam, P. J.; Bishop, J. K. B. The continental margin is a key source of iron to the HNLC North Pacific Ocean. *Geophys. Res. Lett.* **2008,** *35,* L07608.

Lam, P. J.; Ohnemus, D. C.; Marcus, M. A. The speciation of marine particulate iron adjacent to active and passive continental margins. *Geochim. Cosmochimic. Acta* **2012,** *80,* 108-124.

Miot, J.; Benzerara, K.; Morin, G.; Kappler, A.; Bernard, S.; Obst, M.; Férard, C.; Skouri-Panet, F.; Guigner, J.-M.; Posth, N.; Galvez, M.; Brown Jr. G. E.; Guyot, F. Iron biomineralization by anaerobic neutrophilic iron-oxidizing bacteria. *Geochim. Cosmochim. Acta* **2009,** *73,* 696-711.

Monteiro, P. M. S.; van der Plas, A. K. Low Oxygen Water (LOW) variability in the Benguela system: key processes and forcing scales relevant to forecasting. In: Shannon V, Hempel G, Malanotte-Rizzoli P, Moloney C, Woods J (eds) Benguela: predicting a large marine ecosystem. Large marine ecosystems **2006,** 14, Elsevier, Amsterdam, 91–109.

Mortimer, N.; Herzer, R. H.; Gans, P. B.; Parkinson, D. L.; Seward, D. Basement geology from the Three Kings Ridge to West Norfolk Ridge, southwest Pacific Ocean: evidence from petrology, geochemistry and isotopic dating of dredge samples. *Mar. Geol.* **1998,** *148,* 135-162.

Peak, D; Regier, T. Direct observation of tetrahedrally coordinated Fe(III) in ferrihydrite. *Environ. Sci. Technol.* **2012,** *46,* 3163-3168.

Rose, A. L.; Waite T. D. Kinetic model for Fe(II) oxidation in seawater in the absence and presence of natural organic matter. *Environ. Sci. Technol.* **2002,** *36,* 433–444.

Schroth, A. W.; Crusius, J.; Sholkovitz, E. R.; Bostick, B. C. Iron solubility driven by speciation in dust sources to the ocean. *Nat. Geosci.* **2009,** *2,* 337-340.

Shaked, Y.; Erel, Y.; Sukenik, A. Phytoplankton-mediated redox cycle of iron in the epilimnion of Lake Kinneret. *Environ. Sci. Technol.* **2002,** *36,* 460-467.

Shaked, Y.; Kustka, A. B.; Morel, F. M. M. A general kinetic model for iron acquisition by eukaryotic phytoplankton. *Limnol. Oceanogr.* **2005,** *50,* 872-882.

Shaked, Y. Iron redox dynamics in the surface waters of the Gulf of Aqaba, Red Sea. *Geochimic. Cosmochim. Acta* **2008,** *72,* 1540-1554.

Tagliabue, A.; Bopp, L.; Dutay, J.-C.; Bowie, A. R.; Chever, F.; Jean-Baptiste, P.; Bucciarelli, E.; Lannuzel, D.; Remenyi, T.; Sarthou, G.; Aumont, O.; Gehlen, M.; Jeandel, C. Hydrothermal contribution to the dissolved iron inventory. *Nat. Geosci.* **2010,** *3,* 252-256.

Toner, B. M.; Fakra, S. C.; Manganini, S. J.; Santelli, C. M.; Marcus, M. A.; Moffett, J. W.; Rouxel, O.; German, C. R.; Edwards, K. J. Preservation of iron(II) by carbon-rich matrices in a hydrothermal plume. *Nat. Geosci.* **2009,** *2,* 197-201.

Ussher, S. J.; Worsfold, P. J.; Achterberg, E. P.; Laës, A.; Blain, S.; Laan, P.; de Baar, H. J. W. Distribution and redox speciation of dissolved iron on the European continental margin. *Limnol. Oceangr.* **2007,** *42,* 2530-2539.

van Aken, P. A.; Liebscher, B. Quantification of ferrous/ferric ratios in minerals: New evaluation schemes of Fe $L_{2,3}$ electron energy-loss near-edge spectra. *Phys. Chem. Minerals* **2002,** *29,* 188-200.

Van der Zee, C.; Roberts, D. R.; Rancourt, D. G.; Slomp, C. P. Nanogoethite is the dominant reactive oxyhydroxide phase in lake and marine sediments. *Geology* **2003,** *31,* 993-996.

Von der Heyden, B. P.; Roychoudhury, A. N.; Mtshali, T. N; Tyliszczak, T.; Myneni, S. C. B. Chemically and geographically distinct solid-phase iron pools in the Southern Ocean. *Science* **2012,** *338,* 1199-1201.

Von der Heyden, B. P.; Roychoudhury, A. N.; Tyliszczak, T.; Myneni, S. C. B. Composition and structure of Fe-rich aquatic particles, western margin of South Africa. *In preparation.*

Waychunas, G. A.; Kim, C. S.; Banfield, J. F. Nanoparticulate iron oxide minerals in soils and sediments: unique properties and contaminant scavenging mechanisms. *J. Nanopart. Res.* **2005,** *7,* 409-433.

CHAPTER 6

Synopsis

Interest in marine iron chemistry has stemmed from its intimate link with biology, particularly in the high nutrient low chlorophyll regions of the world's oceans, where exceedingly low iron concentrations limit primary productivity (e.g. Boyd and Ellwood, 2011). Historical marine iron investigations, focussed primarily on size-fractionated Fe study, typically differentiate between different operationally-defined iron pools based on filtration and ultrafiltration size cut-offs. The colloidal iron pool (cFe), calculated empirically as the difference between dissolved and soluble Fe measurements, has thus far received the least scientific attention; despite having been shown to be highly dynamic and sometimes dominant (Wu et al., 2001; Bergquist et al., 2007). This thesis reviews the status of scientific knowledge pertaining to this important Fe pool (Chapter 2). Size-fractionated Fe study has, however, largely overlooked the contribution of particle (or colloid) mineralogy and speciation towards the greater Fe biogeochemical cycle. This thesis endeavours to address this vital oversight by developing a novel, particle-specific probe for understanding colloid speciation (Chapter 3). Application of this tool to marine Fe-rich particles has yielded interesting results pertaining to particle speciation differences (Chapter 4) and Fe(II) persistence (Chapter 5).

Major contributions

This thesis includes the first comprehensive compilation of over 750 global soluble iron and colloidal iron measurements (Appendix A), which is presented for further use by the scientific community. Our analyses are largely limited to cFe concentration values reported for the open ocean euphotic zone (258 measurements), with the aims of understanding the distribution and behaviour of this important pool of iron. Open ocean cFe values are thus found to be controlled primarily by total Fe supply terms and the presence and abundance of Fe complexing ligands, yet thermodynamic controls cannot be excluded. Mounting evidence (relationships between cFe concentration and depth and cFe concentration and season) suggests that biological processes exert a significant control on the cFe pool, warranting continued research in this direction.

The biogeochemical behaviour of suspended marine particles, however, is not controlled solely by concentration of the cFe pool and it is important to also consider the chemical and mineralogical speciation of these phases. Because of their small size and low concentration, such speciation measurements are difficult to probe using traditional techniques. This thesis documents the development of a novel x-ray spectromicroscopic technique that can be used to investigate Fe particle speciation in their pristine state. The split peaks of the Fe L_3-edge collected using XANES spectra are parameterized according to their peak splitting (ΔeV) and intensity ratio. When the spectral values of the model Fe oxide and oxyhydroxide system

are plotted on the ΔeV vs intensity ratio two-parameter plot, the position of each respective phase can be explained by invoking Fe valence and coordination, ligand effects and distortions to the local coordination polyhedron.

This two parameter plot is used to interpret XANES data from environmental Fe particles collected from the Southern Ocean and the southwestern Pacific Ocean. In the Southern Ocean five different classes of iron particles were identified from the chemical and mineralogical information contained in their L_3-edge spectral parameters. The distribution of these different particle classes showed maximal heterogeneity near to landmasses as well as a higher prevalence of Fe(II) in the high latitudes. Further investigation, incorporating Al K-edge x-ray data, showed trends between the association of Al and Fe in Southern Ocean particles and the proximity to potential particle source regions. Both the observed particle chemical differences, as well as the presence of Al-substitution, are expected to have significant influence on the solubility of marine Fe particles- thereby impacting on the production, via dissolution processes, of truly dissolved, bioavailable Fe. The two-parameter speciation tool was further used to show a ubiquitous presence of Fe(II) in lacustrine and marine systems. By incorporating carbon K-edge data, the relationship between Fe(II) and C was explored- indicating the importance of organic carbon in stabilizing Fe(II) and the importance of these associations for affecting our understanding of colloid surface chemistry.

Recommendations and future work

By exploring the speciation of marine iron particle chemistry, this thesis has contributed substantially to enhancing scientific understanding of the biogeochemistry of Fe in ocean waters. It has also, however, identified a number concerns and raised a number of questions that future research should aim to address.

1) Chapter 2 of this thesis was hampered by differences in filter pore-sizes used and by the differences in the ultra-filtration techniques employed (molecular size/weight/diffusion rate cut-offs (e.g. Wen et al., 2006)) across different literature studies. Cut-offs used to investigate Fe size fractionation should thus be standardized globally. This will benefit the analyses and conclusions that are drawn in future inter-comparison exercises. GEOTRACES protocol has standardized the pore-size cut-off for future dFe sample collection (0.2 µm; Cutter et al., 2010), and it is strongly recommended that a similar standardization be agreed upon for the sFe pool. Future inter-comparison studies will also benefit from inter-calibration exercises, especially if new filter types or methodologies are being used (e.g. De Jong et al., 2000; Fitzsimmons and Boyle, 2012).

2) The field of marine trace metal chemistry developed substantially since the original Fe hypothesis was postulated. This development has been associated with significant increases in the number of trace metal groups and particularly, the number of dFe datapoints reported (see Tagliabue et al., 2012). The number of reported sFe measurements has however lagged somewhat, and still stand at

around 750 measurements (Chapter 2). Our understanding of the behaviour, distribution and processes affecting the distribution of sFe and cFe pools will benefit greatly from future increased sampling resolution of the sFe pool. This however, should be done in addition to routine Fe speciation measurements (e.g. plotting of ΔeV vs intensity ratio of XANES spectra (Chapters 3-5)) to gain a more holistic understanding of the factors affecting cFe behaviour.

3) Thermodynamic modelling of the behaviour of different iron pools (Liu and Millero, 2002; Cullen et al., 2006) can be improved upon by combining the effects of inorganic considerations (e.g. salinity, temperature, pH) with data pertaining to ligand bonding affinity and stability. These mathematical equilibrium relationships can then be incorporated into Fe biogeochemical models to further our understanding of Fe dynamics in the marine environment (Tagliabue and Völker, 2011).

4) The two parameter plot discussed in Chapter 3 was developed by considering the Fe oxide and Fe oxyhydroxide system only. It was further supplemented with the addition of literature-derived data for a variety of other phases, including Fe(II) standards (Chapters 4, 5). However, the theoretical understanding of the two parameter plot can still be enhanced by future in depth study into the ligand effects on ΔeV and intensity ratio values for Fe systems that are more complex than the Fe-O-H system. Understanding of these two parameters can further be enhanced by considering atomic multiplet theory, crystal field theory and charge transfer theory (Miedema and de Groot, 2013).

5) Relative to historical size-fractionated measurements, the identification of five different chemical classes of Fe particles in the Southern Ocean (Chapter 3) is considered a break-through in scientific approach to marine Fe biogeochemistry. The variable distribution of these phases and their apparent relationship to ambient biology suggest that future work should focus more intensely the extent of the influence of these Fe phases on primary productivity across the different frontal zones of the Southern Ocean. Specifically, it was inferred that the observed differences in chemical speciation will affect the solubility and bioavailability of the analyzed phases. This hypothesis should be tested more fully by conducting focussed solubility and phytoplankton incubation experiments. Linked to this, there remains the outstanding question of whether these phases are accessed directly or whether there is the requirement of a necessary solubilisation step (Maldonado and Price, 2001; Morel et al., 2008).

6) Although associations with organic moieties are suggested to have a stabilizing effect on Fe(II) (Chapter 5), the exact chemistry of these persistent phases is still unclear. Addition experimentation (e.g. TEM analysis) will add to our understanding of which organic and inorganic ligands are responsible for maintaining the particles in their reduced state.

7) The anticipated drop in ocean pH levels with increasing anthropogenic release of CO_2 is expected to induce a host of adverse effects to the marine biogeochemical system (Cooley and Doney, 2009). Acidification effects are also expected to impact of Fe behaviour and the solubility of Fe oxyhydroxide phases is expected to increase by 30% (Millero et al., 2009). Because of the heterogeneity discovered in marine Fe particles (Chapter 4), the effects of ocean acidification on these particles may be more complex and will require further investigation. Furthermore, Fe-ligand relationships (Bruland and Lohan, 2004) and Fe bioavailability (Shi et al., 2010) variations with decreasing ocean pH should be a key focus area if we are to fully understand and predict the extent of human activity on the natural marine environment.

References

Bergquist, B.A., Wu, J., Boyle, E.A., 2007. Variability in oceanic dissolved iron is dominated by the colloidal fraction. Geochimica et Cosmochimica Acta 71, 2960-2974.

Boyd, P.W., Ellwood, M.J., 2010. The biogeochemical cycle of iron in the ocean. Nature Geoscience 3, 675-682.

Bruland, K.W., Lohan, M.C., 2004. The control of trace metals in seawater. In The Oceans and Marine Geochemistry, Treatise on Geochemistry Vol 6.

Cooley, S.R., Doney, S.C., 2009. Anticipating ocean acidification's economic consequences for commercial fisheries. Environmental Research Letters 4, 024007.

Cullen J.T., Bergquist B.A., Moffett J.W., 2006. Thermodynamic characterization of the partitioning of iron between soluble and colloidal species in the Atlantic Ocean. Marine Chemistry 98, 295-303.

Cutter, G., Andersson, P., Codispoti, L., Croot, P., Francois, R., Lohan, M., Obata, H., van der Loeff, M.R., 2010. Sampling and sample-handling protocol for GEOTRACES cruises. 39-51.

De Jong, J.T.M., Boye, M., Schoemann, V.F., Nolting, R.F., de Baar, H.J.W., 2000. Shipboard techniques based on flow injection analysis for measuring dissolved Fe, Mn and Al in seawater. Journal of Environmental Monitoring 2, 496-502.

Fitzsimmons, J.N., Boyle, E.A., 2012. Iron colloids: intercalibration and tropical north Atlantic distribution. Conference Abstract, http://www.sgmeet.com/osm2012/viewabstract2.asp?AbstractID=12351

Liu, X.W., Millero, F.J. 2002. The solubility of iron in seawater. Marine Chemistry 77, 43-54.

Maldonado, M.T., Price, N.M., 2001. Reduction and transport of organically bound iron by Thalassiosira oceanica (Bacillariophyceae). Journal of Phycology 37, 298-310.

Miedema, P.S., de Groot, F.M.F., 2013. Fe 2p X-ray absorption and electron energy loss spectroscopy. Journal of Electron Spectroscopy and Related Phenomena 187, 32-48.

Millero, F.J., Woosley, R., DiTrolio, B. Waters, J., 2009. Effect of ocean acidification on the speciation of metals in natural waters. Oceanography 22(4), 72.

Morel, F.M.M., Kustka, A.B., Shaked, Y., 2008. The role of unchelated Fe in the iron nutrition of phytoplankton. Limnology and Oceanography 53(1), 400–404.

Shi,D., Xu,Y., Hopkinson,B.M., Morel,F.M.M., 2010. Effect of ocean acidification on iron availability to marine phytoplankton. Science 327, 676-679.

Tagliabue, A., Völker, C., 2011. Towards accounting for dissolved iron speciation in global ocean models. Biogeosciences Discussions 8, 2775-2810.

Tagliabue, A., Mtshali, T., Aumont, O., Bowie, A.R., Klunder, M.B., Roychoudhury, A.N, Swart, S., 2012. A global compilation of dissolved iron measurments: focus on distributions and processes in the Southern Ocean. Biogeosciences 9, 2333-2349.

Wen, L.-S.; Jiann, K.-T.; Santschi, P. H., 2006. Physicochemical speciation of bioactive trace metals (Cd, Cu, Fe, Ni) in the oligotrophic South China Sea. Marine Chemistry 101, 104-129.

Wu, J., Boyle, E.A., Sunda, W., Wen, L., 2001. Soluble and colloidal iron in the oligotrophic North Atlantic and North Pacific. Science 293, 847-849.

APPENDIX A

This appendix contains a single table containing a complete global compilation of marine soluble iron (sFe: <0.02µm, or <200kDa, or <1000kDa) and dissolved iron (dFe: <0.2µm or <0.4µm) measurements. The data are presented alongside, where reported, total iron (or total dissolvable Fe) measurements, salinity and temperature data.

Pertinent subsets of this data were used for all analyses and related discussions referred to in Chapter 2 of this thesis. The cited references included in this table are all listed in the references section of Chapter 2. The only exceptions are the Fe, salinity and temperature datasets provided by the British Oceanographic Data Centre, for which Simon Ussher provided the Fe measurements from research cruise AMT16.

All data included in this dataset were compiled from literature tables, or by contacting the relevant corresponding authors directly. Many of the temperature and salinity data values were, however, derived manually by pixelating published figures. This was also necessary for the Wu *et al.* (2001) and Boyle *et al.* (2005) Fe datasets. The error induced through this process was deemed negligible, particularly if compared to the standard errors reported for sFe and dFe analytical concentration measurements.

Appendix A: Complete compilation of marine sFe measurements with derived cFe concentrations and other parameters.

Cruise/Station	Month	Year	Lat	Long	Depth	[sFe] (nM)	Size	[dFe] (nM)	Size	[cFe] (nM)	Total Fe (nM)	Salinity (psu)	Temp (°C)	Reference
Vertigo-K2	8	2005	47.00	160.00	0	0.3	0.01				3.1			Baeyens et al, 2011
SR3 Geotraces ST 1	3	2005	-60.40	140.70	0	0.68	0.01				2.5			Baeyens et al, 2011
SR3 Geotraces ST 3	4	2005	-49.90	143.80	0	0.165	0.01				2.4			Baeyens et al, 2011
SJ0101	1	2001	30.00	-45.30	0	0.37	0.02	0.48	0.4	0.11				Bergquist et al, 2006
SJ0101	1	2001	23.00	-45.00	0	0.4	0.02	0.79	0.4	0.39				Bergquist et al, 2006
SJ0101	1	2001	18.00	-45.00	0	0.51	0.02	0.63	0.4	0.12				Bergquist et al, 2006
SJ0101	1	2001	15.80	-45.00	0	0.42	0.02	0.65	0.4	0.23				Bergquist et al, 2006
SJ0101	1	2001	10.20	-45.00	0	0.22	0.02	0.54	0.4	0.32				Bergquist et al, 2006
En367	3	2002	10.50	-54.50	0	0.31	0.02	0.71	0.4	0.4				Bergquist et al, 2006
En367	3	2002	7.00	-49.50	0	0.36	0.02	0.5	0.4	0.14				Bergquist et al, 2006
En367	3	2002	6.20	-48.40	0	0.27	0.02	0.53	0.4	0.26				Bergquist et al, 2006
En367	3	2002	4.30	-45.60	0	0.21	0.02	0.5	0.4	0.29				Bergquist et al, 2006
En367	3	2002	3.34	-44.50	0	0.21	0.02	0.62	0.4	0.41				Bergquist et al, 2006
En367	3	2002	-0.50	-35.00	0	0.21	0.02	0.51	0.4	0.3				Bergquist et al, 2006
En367	3	2002	-11.70	-32.20	0	0.33	0.02	0.35	0.4	0.02				Bergquist et al, 2006
En367	3	2002	-11.70	-32.10	0	0.23	0.02	0.26	0.4	0.03				Bergquist et al, 2006
En367	3	2002	-14.90	-32.90	0	0.25	0.02	0.28	0.4	0.03				Bergquist et al, 2006
En367	3	2002	-23.50	-36.40	0	0.31	0.02	0.38	0.4	0.07				Bergquist et al, 2006
En367	3	2002	-24.10	-36.70	0	0.23	0.02	0.35	0.4	0.12				Bergquist et al, 2006
SJ0101, 30N profile	1	2001	30.00	-45.30	0.2	0.34	0.02	0.68	0.4	0.34		36.86		Bergquist et al, 2006
SJ0101, 30N profile	1	2001	30.00	-45.30	41	0.34	0.02	0.58	0.4	0.24		36.88		Bergquist et al, 2006
SJ0101, 30N profile	1	2001	30.00	-45.30	63	0.32	0.02	0.39	0.4	0.07		36.88		Bergquist et al, 2006
SJ0101, 30N profile	1	2001	30.00	-45.30	77	0.33	0.02	0.37	0.4	0.04		36.88		Bergquist et al, 2006
SJ0101, 30N profile	1	2001	30.00	-45.30	165	0.28	0.02	0.41	0.4	0.13		36.54		Bergquist et al, 2006
SJ0101, 30N profile	1	2001	30.00	-45.30	250	0.33	0.02	0.42	0.4	0.09		36.51		Bergquist et al, 2006

SJ0101, 30N profile	1	2001	30.00	-45.30	850	0.42	0.02	0.55	0.4	0.13	35.29	Bergquist et al, 2006
SJ0101, 30N profile	1	2001	30.00	-45.30	950	0.41	0.02	0.57	0.4	0.16	35.24	Bergquist et al, 2006
SJ0101, 30N profile	1	2001	30.00	-45.30	1050	0.35	0.02	0.51	0.4	0.16	35.20	Bergquist et al, 2006
SJ0101, 10N profile	1	2001	10.20	-45.00	0	0.22	0.02	0.54	0.4	0.32	36.26	Bergquist et al, 2006
SJ0101, 10N profile	1	2001	10.20	-45.00	30	0.35	0.02	0.68	0.4	0.33	36.24	Bergquist et al, 2006
SJ0101, 10N profile	1	2001	10.20	-45.00	165	0.33	0.02	0.98	0.4	0.65	35.27	Bergquist et al, 2006
SJ0101, 10N profile	1	2001	10.20	-45.00	200	0.41	0.02	1.19	0.4	0.78	35.09	Bergquist et al, 2006
SJ0101, 10N profile	1	2001	10.20	-45.00	250	0.46	0.02	1.05	0.4	0.59	34.98	Bergquist et al, 2006
SJ0101, 10N profile	1	2001	10.20	-45.00	375	0.41	0.02	1.19	0.4	0.78	34.89	Bergquist et al, 2006
SJ0101, 10N profile	1	2001	10.20	-45.00	525	0.45	0.02	1.11	0.4	0.66	34.77	Bergquist et al, 2006
SJ0101, 10N profile	1	2001	10.20	-45.00	725	0.31	0.02	1.06	0.4	0.75	34.73	Bergquist et al, 2006
SJ0101, 10N profile	1	2001	10.20	-45.00	850	0.4	0.02	1.16	0.4	0.76	34.66	Bergquist et al, 2006
SJ0101, 10N profile	1	2001	10.20	-45.00	1050	0.46	0.02	1.01	0.4	0.55	34.75	Bergquist et al, 2006
SJ0101, 10N profile	1	2001	10.20	-45.00	1250	0.42	0.02	0.98	0.4	0.56	34.89	Bergquist et al, 2006
SJ0101, 10N profile	1	2001	10.20	-45.00	1500	0.58	0.02	0.77	0.4	0.19	34.99	Bergquist et al, 2006
SJ0101, 10N profile	1	2001	10.20	-45.00	1750	0.45	0.02	0.7	0.4	0.25	34.98	Bergquist et al, 2006
SJ0101, 10N profile	1	2001	10.20	-45.00	3400	0.36	0.02	0.86	0.4	0.5	34.90	Bergquist et al, 2006
SJ0101, 10N profile	1	2001	10.20	-45.00	4200	0.42	0.02	0.63	0.4	0.21	34.87	Bergquist et al, 2006
KN162, 30N profile	7	2001	30.00	-45.00	4	0.43	0.02	0.54	0.4	0.11	37.07	Bergquist et al, 2006
KN162, 30N profile	7	2001	30.00	-45.00	6	0.29	0.02	0.56	0.4	0.27	37.06	Bergquist et al, 2006
KN162, 30N profile	7	2001	30.00	-45.00	8	0.33	0.02	0.47	0.4	0.14	37.06	Bergquist et al, 2006
KN162, 30N profile	7	2001	30.00	-45.00	11	0.34	0.02	0.44	0.4	0.1	37.05	Bergquist et al, 2006
KN162, 30N profile	7	2001	30.00	-45.00	19	0.23	0.02	0.45	0.4	0.22	36.94	Bergquist et al, 2006
KN162, 30N profile	7	2001	30.00	-45.00	30	0.41	0.02	0.42	0.4	0.01	36.99	Bergquist et al, 2006
KN162, 30N profile	7	2001	30.00	-45.00	39	0.39	0.02	0.42	0.4	0.03	36.97	Bergquist et al, 2006
KN162, 30N profile	7	2001	30.00	-45.00	79	0.32	0.02	0.36	0.4	0.04	36.70	Bergquist et al, 2006
KN162, 10N profile	7	2001	10.10	-45.50	0	0.41	0.02	0.6	0.4	0.19		Bergquist et al, 2006
KN162, 10N profile	7	2001	10.10	-45.50	2	0.37	0.02	0.71	0.4	0.34		Bergquist et al, 2006
KN162, 10N profile	7	2001	10.10	-45.50	5	0.4	0.02	0.59	0.4	0.19		Bergquist et al, 2006
KN162, 10N profile	7	2001	10.10	-45.50	10	0.4	0.02	0.48	0.4	0.08		Bergquist et al, 2006

KN162, 10N profile	7	2001	10.10	-45.50	13	0.34	0.02	0.45	0.4	0.11			Bergquist et al, 2006
KN162, 10N profile	7	2001	10.10	-45.50	19	0.36	0.02	0.62	0.4	0.26			Bergquist et al, 2006
KN162, 10N profile	7	2001	10.10	-45.50	22	0.42	0.02	0.56	0.4	0.14			Bergquist et al, 2006
KN162, 10N profile	7	2001	10.10	-45.50	25	0.44	0.02	0.53	0.4	0.09			Bergquist et al, 2006
KN162, 10N profile	7	2001	10.10	-45.50	28	0.45	0.02	0.55	0.4	0.1			Bergquist et al, 2006
KN162, 10N profile	7	2001	10.10	-45.50	148	0.4	0.02	0.54	0.4	0.14			Bergquist et al, 2006
EN367, 24.5S profile	3	2002	-24.50	-37.00	1	0.24	0.02	0.36	0.4	0.12	36.57		Bergquist et al, 2006
EN367, 24.5S profile	3	2002	-24.50	-37.00	18	0.3	0.02	0.39	0.4	0.09	36.57		Bergquist et al, 2006
EN367, 24.5S profile	3	2002	-24.50	-37.00	113	0.26	0.02	0.29	0.4	0.03	36.76		Bergquist et al, 2006
EN367, 24.5S profile	3	2002	-24.50	-37.00	394	0.26	0.02	0.26	0.4	0	35.21		Bergquist et al, 2006
EN367, 24.5S profile	3	2002	-24.50	-37.00	709	0.31	0.02	0.37	0.4	0.06	34.44		Bergquist et al, 2006
EN367, 24.5S profile	3	2002	-24.50	-37.00	841	0.31	0.02	0.39	0.4	0.08	34.33		Bergquist et al, 2006
EN367, 24.5S profile	3	2002	-24.50	-37.00	1181	0.35	0.02	0.38	0.4	0.03	34.56		Bergquist et al, 2006
EN367, 24.5S profile	3	2002	-24.50	-37.00	1366	0.32	0.02	0.45	0.4	0.13	34.78		Bergquist et al, 2006
EN367, 24.5S profile	3	2002	-24.50	-37.00	1649	0.38	0.02	0.43	0.4	0.05	34.95		Bergquist et al, 2006
EN367, 24.5S profile	3	2002	-24.50	-37.00	2198	0.33	0.02	0.46	0.4	0.13	34.98		Bergquist et al, 2006
EN367, 24.5S profile	3	2002	-24.50	-37.00	2494	0.3	0.02	0.49	0.4	0.19	34.94		Bergquist et al, 2006
EN367, 24.5S profile	3	2002	-24.50	-37.00	2676	0.4	0.02	0.5	0.4	0.1	34.93		Bergquist et al, 2006
EN367, 24.5S profile	3	2002	-24.50	-37.00	3051	0.35	0.02	0.48	0.4	0.13	34.91		Bergquist et al, 2006
EN367, 24.5S profile	3	2002	-24.50	-37.00	3308	0.27	0.02	0.49	0.4	0.22	34.90		Bergquist et al, 2006
EN367, 24.5S profile	3	2002	-24.50	-37.00	3806	0.29	0.02	0.43	0.4	0.14	34.79		Bergquist et al, 2006
EN367, 24.5S profile	3	2002	-24.50	-37.00	4029	0.35	0.02	0.41	0.4	0.06	34.72		Bergquist et al, 2006
EISENEX St.007	11	2000	-49.29	20.02	50	0.03	200kDa	0.05	0.2	0.02	33.81	3.49	Boye et al, 2010
EISENEX St.007	11	2000	-49.29	20.02	1000	0.18	200kDa	0.39	0.2	0.21	34.63	2.45	Boye et al, 2010
EISENEX St.009	11	2000	-47.82	20.79	20	0.05	200kDa	0.08	0.2	0.03	33.81	3.42	Boye et al, 2010
EISENEX St.009	11	2000	-47.82	20.79	40	0.03	200kDa	0.06	0.2	0.03	33.82	3.23	Boye et al, 2010
EISENEX St.009	11	2000	-47.82	20.79	60	0.03	200kDa	0.04	0.2	0.01	33.83	2.60	Boye et al, 2010
EISENEX St.009	11	2000	-47.82	20.79	80	0.04	200kDa	0.07	0.2	0.03	33.84	2.41	Boye et al, 2010
EISENEX St.009	11	2000	-47.82	20.79	200	0.08	200kDa	0.1	0.2	0.02	34.00	2.07	Boye et al, 2010
EISENEX St.009	11	2000	-47.82	20.79	250	0.08	200kDa	0.14	0.2	0.06	34.09	2.23	Boye et al, 2010

EISENEX St.009	11	2000	-47.82	20.79	300	0.13	200kDa	0.16	0.2	0.03		34.17	2.27	Boye et al, 2010
EISENEX St.009	11	2000	-47.82	20.79	400	0.17	200kDa	0.2	0.2	0.03		34.29	2.18	Boye et al, 2010
EISENEX St.048	11	2000	-48.59	20.72	20	0.03	200kDa	0.05	0.2	0.02		33.86	3.50	Boye et al, 2010
EISENEX St.048	11	2000	-48.59	20.72	40	0.03	200kDa	0.04	0.2	0.01		33.86	3.47	Boye et al, 2010
EISENEX St.048	11	2000	-48.59	20.72	60	0.04	200kDa	0.06	0.2	0.02		33.86	3.24	Boye et al, 2010
EISENEX St.048	11	2000	-48.59	20.72	80	0.08	200kDa	0.09	0.2	0.01		33.87	2.71	Boye et al, 2010
EISENEX St.048	11	2000	-48.59	20.72	100	0.08	200kDa					33.89	2.40	Boye et al, 2010
EISENEX St.091	11	2000	-48.17	21.09	50	0.07	200kDa	0.11	0.2	0.04		33.81	3.70	Boye et al, 2010
EISENEX St.091	11	2000	-48.17	21.09	200	0.05	200kDa	0.07	0.2	0.02		33.94	1.88	Boye et al, 2010
EISENEX St.091	11	2000	-48.17	21.09	300	0.11	200kDa	0.18	0.2	0.07		34.18	2.42	Boye et al, 2010
EISENEX St.091	11	2000	-48.17	21.09	400	0.12	200kDa	0.18	0.2	0.06		34.28	2.42	Boye et al, 2010
EISENEX St.091	11	2000	-48.17	21.09	500	0.15	200kDa	0.26	0.2	0.11		34.38	2.42	Boye et al, 2010
EISENEX St.091	11	2000	-48.17	21.09	600	0.19	200kDa	0.35	0.2	0.16				Boye et al, 2010
EISENEX St.091	11	2000	-48.17	21.09	800	0.15	200kDa	0.34	0.2	0.19				Boye et al, 2010
EISENEX St.091	11	2000	-48.17	21.09	1000	0.21	200kDa	0.41	0.2	0.2				Boye et al, 2010
Bonus-Goodhope S1	3	2008	-36.50	13.10	30	0.525	0.02	0.72	0.2	0.195	0.767	35.55	18.53	Chever et al, 2010
Bonus-Goodhope S1	3	2008	-36.50	13.10	40	0.425	0.02				0.817	35.50	17.87	Chever et al, 2010
Bonus-Goodhope S1	3	2008	-36.50	13.10	300	0.563	0.02				2.248	34.88	10.85	Chever et al, 2010
Bonus-Goodhope S1	3	2008	-36.50	13.10	700	0.646	0.02				2.727	34.40	5.82	Chever et al, 2010
Bonus-Goodhope S1	3	2008	-36.50	13.10	1200	0.628	0.02	0.943	0.2	0.315	2.38	34.55	3.27	Chever et al, 2010
Bonus-Goodhope S1	3	2008	-36.50	13.10	1600	0.366	0.02	0.724	0.2	0.358	1.619	34.69	2.73	Chever et al, 2010
Bonus-Goodhope S1	3	2008	-36.50	13.10	3050	0.368	0.02	0.911	0.2	0.543	1.536	34.84	1.92	Chever et al, 2010
Bonus-Goodhope S1	3	2008	-36.50	13.10	3800	0.448	0.02	1.154	0.2	0.706	1.838	34.77	1.05	Chever et al, 2010
Bonus-Goodhope L2	3	2008	-41.18	9.92	45	0.431	0.02	0.59	0.2	0.159	1.261	34.67	13.16	Chever et al, 2010
Bonus-Goodhope L2	3	2008	-41.18	9.92	800	0.266	0.02	1.098	0.2	0.832	1.265	34.27	3.66	Chever et al, 2010
Bonus-Goodhope S2	3	2008	-42.47	8.93	120	0.162	0.02	0.164	0.2	0.002	0.314	34.53	9.51	Chever et al, 2010
Bonus-Goodhope S2	3	2008	-42.47	8.93	461	0.200	0.02				0.604	34.23	5.10	Chever et al, 2010
Bonus-Goodhope S2	3	2008	-42.47	8.93	1029	0.319	0.02	0.431	0.2	0.112	0.736	34.35	2.88	Chever et al, 2010
Bonus-Goodhope S2	3	2008	-42.47	8.93	1250	0.364	0.02	0.46	0.2	0.096	0.823	34.48	2.70	Chever et al, 2010
Bonus-Goodhope S2	3	2008	-42.47	8.93	1441	0.415	0.02	0.641	0.2	0.226	0.834	34.58	2.64	Chever et al, 2010

Bonus-Goodhope S2	3	2008	-42.47	8.93	2156	0.369	0.02	1.028	0.2	0.659	1.069	34.79	2.34	Chever et al, 2010
Bonus-Goodhope S2	3	2008	-42.47	8.93	2548	0.378	0.02	0.785	0.2	0.407	1.24	34.82	2.13	Chever et al, 2010
Bonus-Goodhope S2	3	2008	-42.47	8.93	2891	0.33	0.02	1.459	0.2	1.129	1.828	34.83	1.95	Chever et al, 2010
Bonus-Goodhope S2	3	2008	-42.47	8.93	3626	0.339	0.02	0.716	0.2	0.377	1.687	34.77	1.20	Chever et al, 2010
Bonus-Goodhope L3	3	2008	-44.88	6.88	30	0.215	0.02				0.265	33.94	9.33	Chever et al, 2010
Bonus-Goodhope L3	3	2008	-44.88	6.88	150	0.097	0.02	0.121	0.2	0.024	0.268	34.32	7.02	Chever et al, 2010
Bonus-Goodhope L3	3	2008	-44.88	6.88	400	0.327	0.02	0.337	0.2	0.01	0.651	34.17	4.56	Chever et al, 2010
Bonus-Goodhope L3	3	2008	-44.88	6.88	1400	0.335	0.02	0.621	0.2	0.286	1.283	34.54	2.70	Chever et al, 2010
Bonus-Goodhope L3	3	2008	-44.88	6.88	2100	0.339	0.02	0.6	0.2	0.261	1.852	34.76	2.46	Chever et al, 2010
Bonus-Goodhope L4	3	2008	-46.02	5.87	60	0.103	0.02				0.276	33.74	7.71	Chever et al, 2010
Bonus-Goodhope L4	3	2008	-46.02	5.87	270	0.119	0.02	0.28	0.2	0.161	0.582	34.12	4.47	Chever et al, 2010
Bonus-Goodhope L4	3	2008	-46.02	5.87	480	0.145	0.02	0.381	0.2	0.236	0.637	34.15	3.45	Chever et al, 2010
Bonus-Goodhope L4	3	2008	-46.02	5.87	800	0.239	0.02	0.331	0.2	0.092	0.806	34.33	2.79	Chever et al, 2010
Bonus-Goodhope L4	3	2008	-46.02	5.87	1600	0.15	0.02	0.699	0.2	0.549	1.034	34.69	2.55	Chever et al, 2010
Bonus-Goodhope L4	3	2008	-46.02	5.87	2050	0.236	0.02	0.782	0.2	0.546	1.09	34.78	2.37	Chever et al, 2010
Bonus-Goodhope S3	3	2008	-47.55	4.37	20	0.144	0.02	0.161	0.2	0.017	0.318	33.73	6.51	Chever et al, 2010
Bonus-Goodhope S3	3	2008	-47.55	4.37	40	0.186	0.02				0.261	33.73	6.51	Chever et al, 2010
Bonus-Goodhope S3	3	2008	-47.55	4.37	200	0.14	0.02	0.141	0.2	0.001	0.629	33.97	3.75	Chever et al, 2010
Bonus-Goodhope S3	3	2008	-47.55	4.37	800	0.283	0.02	0.557	0.2	0.274	0.735	34.38	2.67	Chever et al, 2010
Bonus-Goodhope S3	3	2008	-47.55	4.37	1070	0.268	0.02	0.656	0.2	0.388	0.843	34.51	2.55	Chever et al, 2010
Bonus-Goodhope S3	3	2008	-47.55	4.37	1500	0.284	0.02	0.6	0.2	0.316	0.882	34.66	2.40	Chever et al, 2010
Bonus-Goodhope S3	3	2008	-47.55	4.37	3000	0.02	0.02	0.591	0.2	0.571	0.077	34.74	1.26	Chever et al, 2010
Bonus-Goodhope S3	3	2008	-47.55	4.37	3500	0.3	0.02	0.825	0.2	0.525	1.345	34.72	0.93	Chever et al, 2010
Bonus-Goodhope S3	3	2008	-47.55	4.37	3980	0.34	0.02	0.761	0.2	0.421	1.946	34.71	0.63	Chever et al, 2010
Bonus-Goodhope L5	3	2008	-49.03	2.84	1000	0.425	0.02	0.504	0.2	0.079	0.812	34.53	2.52	Chever et al, 2010
Bonus-Goodhope L5	3	2008	-49.03	2.84	2200	0.517	0.02	0.722	0.2	0.205	1.323	34.78	2.01	Chever et al, 2010
Bonus-Goodhope L6	3	2008	-50.38	1.33	300	0.304	0.02	0.421	0.2	0.117	0.598	34.29	2.22	Chever et al, 2010
Bonus-Goodhope L6	3	2008	-50.38	1.33	850	0.38	0.02	0.449	0.2	0.069	0.775	34.64	2.28	Chever et al, 2010
Bonus-Goodhope L6	3	2008	-50.38	1.33	2100	0.566	0.02	1.123	0.2	0.557	1.26	34.75	1.50	Chever et al, 2010
Bonus-Goodhope S4	3	2008	-51.85	0.00	30	0.128	0.02	0.182	0.2	0.054	0.338	33.71	2.58	Chever et al, 2010

Bonus-Goodhope S4	3	2008	-51.85	0.00	500	0.334	0.02	0.447	0.2	0.113	0.708	34.63	1.92	Chever et al, 2010
Bonus-Goodhope S4	3	2008	-51.85	0.00	900	0.287	0.02				0.546	34.71	1.74	Chever et al, 2010
Bonus-Goodhope S4	3	2008	-51.85	0.00	1950	0.29	0.02				0.799	34.70	0.78	Chever et al, 2010
Bonus-Goodhope S4	3	2008	-51.85	0.00	2300	0.335	0.02				1.51	34.69	0.57	Chever et al, 2010
Bonus-Goodhope S4	3	2008	-51.85	0.00	2500	0.339	0.02	0.787	0.2	0.448	1.24	34.69	0.45	Chever et al, 2010
Bonus-Goodhope L7	3	2008	-55.23	0.03	1500	0.282	0.02	0.482	0.2	0.2	1.044	34.69	0.69	Chever et al, 2010
Bonus-Goodhope L7	3	2008	-55.23	0.03	2100	0.326	0.02	0.39	0.2	0.064	1.171	34.68	0.33	Chever et al, 2010
Bonus-Goodhope S5	3	2008	-57.55	-0.03	120	0.245	0.02	0.313	0.2	0.068	0.894	34.16	0.27	Chever et al, 2010
Bonus-Goodhope S5	3	2008	-57.55	-0.03	450	0.326	0.02	0.517	0.2	0.191	0.758	34.67	0.57	Chever et al, 2010
Bonus-Goodhope S5	3	2008	-57.55	-0.03	750	0.268	0.02	0.713	0.2	0.445	0.933	34.68	0.51	Chever et al, 2010
Bonus-Goodhope S5	3	2008	-57.55	-0.03	1250	0.214	0.02	0.417	0.2	0.203	1.03	34.68	0.27	Chever et al, 2010
Bonus-Goodhope S5	3	2008	-57.55	-0.03	3050	0.237	0.02	0.418	0.2	0.181	0.909	34.66	-0.30	Chever et al, 2010
Bonus-Goodhope S5	3	2008	-57.55	-0.03	3840	0.212	0.02	0.511	0.2	0.299	1.121	34.65	-0.45	Chever et al, 2010
EN367- St 3	4	2002	3.50	-44.50	5	0.23	0.02	0.66	0.4	0.43				Cullen et al, 2006
EN367- St 3	4	2002	3.50	-44.50	5256	0.26	0.02	0.42	0.4	0.16				Cullen et al, 2006
EN367- St 6	4	2002	-19.00	-34.00	4200	0.22	0.02	0.43	0.4	0.21				Cullen et al, 2006
OCE382- St H			36.08	-65.00	15	0.04	0.02	0.43	0.4	0.39				Cullen et al, 2006
OCE382- St H			36.08	-65.00	3000	0.28	0.02	0.41	0.4	0.13				Cullen et al, 2006
Geotraces IC2	5	2009	30.00	-140.00	1000	0.65	0.02	0.85	0.4	0.2				Fitzsimmons and Boyle, 2012
HOT 231	4	2011	22.75	-158.00	1000	0.7	0.02	1.08	0.2	0.38				Fitzsimmons and Boyle, 2012
Coastal C1a					0	2.4	0.025	6.63	0.45	4.23				Kuma et al, 1998
Coastal C1b					0	4.13	0.025	10.8	0.45	6.67				Kuma et al, 1998
Coastal C1c					0	1.57	0.025	3.54	0.45	1.97				Kuma et al, 1998
Coastal C2					0	2.66	0.025	7.28	0.45	4.62				Kuma et al, 1998
Coastal C3					0	1.72	0.025	5.27	0.45	3.55				Kuma et al, 1998
Estuarine E1					0	1.19	0.025	17.6	0.45	16.41				Kuma et al, 1998
Estuarine E2					0	2.01	0.025	20.8	0.45	18.79				Kuma et al, 1998
Oceanic			53.00	-150.00	200	0.32	0.025	0.37	0.45	0.05				Kuma et al, 1998
Oceanic			53.00	-150.00	500	0.28	0.025	0.31	0.45	0.03				Kuma et al, 1998

Oceanic			53.00	-150.00	800	0.34	0.025	0.39	0.45	0.05				Kuma et al, 1998
Funka Bay F			42.27	140.60	2	2.05	0.025	14.1	0.45	12.05		31.50	15.30	Kuma et al, 1998
Funka Bay F			42.27	140.60	5	1.53	0.025	15.1	0.45	13.57		31.50	13.20	Kuma et al, 1998
Funka Bay F			42.27	140.60	10	1.27	0.025	9.04	0.45	7.77		31.82	11.60	Kuma et al, 1998
Funka Bay F			42.27	140.60	20	2.31	0.025	3.43	0.45	1.12		32.26	9.00	Kuma et al, 1998
Funka Bay F			42.27	140.60	50	1.8	0.025	2.19	0.45	0.39		33.01	4.60	Kuma et al, 1998
Funka Bay F			42.27	140.60	80	1.73	0.025	2.86	0.45	1.13		33.43	3.10	Kuma et al, 1998
Funka Bay, Site 30	2	1995	42.27	140.60	2	0.75	0.025	2.53	0.22	1.78	6.43	33.68	5.13	Kuma et al, 2000
Funka Bay, Site 30	2	1995	42.27	140.60	5	0.34	0.025	0.9	0.22	0.56	4.6	33.69	5.05	Kuma et al, 2000
Funka Bay, Site 30	2	1995	42.27	140.60	10	3.03	0.025	3.11	0.22	0.08	6.41	33.71	4.99	Kuma et al, 2000
Funka Bay, Site 30	2	1995	42.27	140.60	20	3.19	0.025	3.95	0.22	0.76	11.15	33.79	5.12	Kuma et al, 2000
Funka Bay, Site 30	2	1995	42.27	140.60	50	6.25	0.025	6.85	0.22	0.6	39.65	34.02	5.75	Kuma et al, 2000
Funka Bay, Site 30	2	1995	42.27	140.60	80	6.89	0.025	8.22	0.22	1.33	201.12	34.02	5.65	Kuma et al, 2000
Funka Bay, Site 30	2	1995	42.27	140.60	2	12.89	0.025	13.7	0.22	0.81	28.5	33.11	3.56	Kuma et al, 2000
Funka Bay, Site 30	2	1995	42.27	140.60	5	10.67	0.025	12.62	0.22	1.95	19.32	33.08	3.55	Kuma et al, 2000
Funka Bay, Site 30	2	1995	42.27	140.60	10	11.3	0.025	12.36	0.22	1.06	19.06	33.09	3.57	Kuma et al, 2000
Funka Bay, Site 30	2	1995	42.27	140.60	20	6.87	0.025	9.47	0.22	2.6	14.77	33.19	3.89	Kuma et al, 2000
Funka Bay, Site 30	2	1995	42.27	140.60	50	8.35	0.025	15.93	0.22	7.58	29.33	33.48	4.36	Kuma et al, 2000
Funka Bay, Site 30	2	1995	42.27	140.60	80	5	0.025	8.58	0.22	3.58	52.88	33.90	5.53	Kuma et al, 2000
Funka Bay, Site 30	3	1995	42.27	140.60	2	10.11	0.025	12.4	0.22	2.29	32.2	32.63	1.99	Kuma et al, 2000
Funka Bay, Site 30	3	1995	42.27	140.60	5	7.34	0.025	10.72	0.22	3.38	17.42	32.63	1.99	Kuma et al, 2000
Funka Bay, Site 30	3	1995	42.27	140.60	10	6	0.025	7.12	0.22	1.12	16.22	32.64	2.01	Kuma et al, 2000
Funka Bay, Site 30	3	1995	42.27	140.60	20	3.71	0.025	6.08	0.22	2.37	7.78	33.15	3.62	Kuma et al, 2000
Funka Bay, Site 30	3	1995	42.27	140.60	50	4.54	0.025	6.18	0.22	1.64	42.08	33.68	5.23	Kuma et al, 2000
Funka Bay, Site 30	3	1995	42.27	140.60	80	2.89	0.025	4.01	0.22	1.12	53.91	33.91	5.74	Kuma et al, 2000
Funka Bay, Site 30	3	1995	42.27	140.60	2	0.8	0.025	1.21	0.22	0.41	3.61	32.53	2.24	Kuma et al, 2000
Funka Bay, Site 30	3	1995	42.27	140.60	5	2.6	0.025	2.72	0.22	0.12	6.32	32.50	1.84	Kuma et al, 2000
Funka Bay, Site 30	3	1995	42.27	140.60	10	5.54	0.025	5.89	0.22	0.35	8.99	32.75	2.00	Kuma et al, 2000
Funka Bay, Site 30	3	1995	42.27	140.60	20	6.17	0.025	6.54	0.22	0.37	8.84	33.02	3.35	Kuma et al, 2000
Funka Bay, Site 30	3	1995	42.27	140.60	50	11.9	0.025	12.99	0.22	1.09	22.89	33.27	4.11	Kuma et al, 2000

Funka Bay, Site 30	3	1995	42.27	140.60	80	4.95	0.025	5.23	0.22	0.28	79.13	33.89	5.67	Kuma et al, 2000
Funka Bay, Site 30	3	1995	42.27	140.60	2	1.25	0.025	1.36	0.22	0.11	4.16	32.36	3.01	Kuma et al, 2000
Funka Bay, Site 30	3	1995	42.27	140.60	5	2.22	0.025	3.22	0.22	1	5.72	32.36	2.90	Kuma et al, 2000
Funka Bay, Site 30	3	1995	42.27	140.60	10	0.8	0.025	1.32	0.22	0.52	2.42	32.63	2.74	Kuma et al, 2000
Funka Bay, Site 30	3	1995	42.27	140.60	20	3.22	0.025	3.87	0.22	0.65	4.77	32.71	2.78	Kuma et al, 2000
Funka Bay, Site 30	3	1995	42.27	140.60	50	6	0.025	8.23	0.22	2.23	14.73	33.23	4.17	Kuma et al, 2000
Funka Bay, Site 30	3	1995	42.27	140.60	80	5.27	0.025	13.84	0.22	8.57	85.54	33.77	5.44	Kuma et al, 2000
Funka Bay, Site 30	4	1995	42.27	140.60	2	1.73	0.025	1.98	0.22	0.25	3.78	32.30	3.90	Kuma et al, 2000
Funka Bay, Site 30	4	1995	42.27	140.60	5	1.99	0.025	4.01	0.22	2.02	5.31	32.29	3.90	Kuma et al, 2000
Funka Bay, Site 30	4	1995	42.27	140.60	10	2.07	0.025	3.1	0.22	1.03	4.8	32.29	3.91	Kuma et al, 2000
Funka Bay, Site 30	4	1995	42.27	140.60	20	3.99	0.025	8.85	0.22	4.86	10.35	32.29	3.84	Kuma et al, 2000
Funka Bay, Site 30	4	1995	42.27	140.60	50	12.35	0.025	17.98	0.22	5.63	22.88	33.11	3.59	Kuma et al, 2000
Funka Bay, Site 30	4	1995	42.27	140.60	80	12.76	0.025	17.88	0.22	5.12	74.38	33.61	4.88	Kuma et al, 2000
North Pacific			26.83	139.83	10	0.234	200kDa	0.32	0.2	0.07995	0.41			Nishioka and Takeda, 2000
GEOTRACES 64PE267 St. 14	4	2007	39.73	-14.17	26	0.029	1000kDa	0.13	0.2	0.101	0.953	36.15	14.45	Thuroczy et al, 2010
GEOTRACES 64PE267 St. 14	4	2007	39.73	-14.17	102	0.019	1000kDa	0.2	0.2	0.181	0.906	36.09	13.80	Thuroczy et al, 2010
GEOTRACES 64PE267 St. 14	4	2007	39.73	-14.17	202	0.047	1000kDa	0.46	0.2	0.413	2.767	35.98	12.12	Thuroczy et al, 2010
GEOTRACES 64PE267 St. 14	4	2007	39.73	-14.17	501	0.088	1000kDa	0.69	0.2	0.602	2.153	35.82	9.76	Thuroczy et al, 2010
GEOTRACES 64PE267 St. 14	4	2007	39.73	-14.17	800	0.077	1000kDa	0.67	0.2	0.593	3.788	35.83	14.43	Thuroczy et al, 2010
GEOTRACES 64PE267 St. 14	4	2007	39.73	-14.17	999	0.129	1000kDa	0.57	0.2	0.441	4.097	35.78	15.22	Thuroczy et al, 2010
GEOTRACES 64PE267 St. 14	4	2007	39.73	-14.17	1998	0.22	1000kDa	0.58	0.2	0.36	2.264	35.14	2.91	Thuroczy et al, 2010
GEOTRACES 64PE267 St. 14	4	2007	39.73	-14.17	3497	0.164	1000kDa	0.67	0.2	0.506	1.747	35.01	1.51	Thuroczy et al, 2010
GEOTRACES 64PE267 St. 14	4	2007	39.73	-14.17	3998	0.143	1000kDa	0.7	0.2	0.557	1.999	34.99	1.32	Thuroczy et al, 2010
ARK XXII/2 St. 239	9	2007	80.99	33.98	5	0.354	1000kDa	0.408	0.2	0.054	3.01	31.66	-1.04	Thuroczy et al, 2011
ARK XXII/2 St. 239	9	2007	80.99	33.98	25	0.241	1000kDa	0.308	0.2	0.067	3.61	33.97	-0.84	Thuroczy et al, 2011
ARK XXII/2 St. 239	9	2007	80.99	33.98	75	0.469	1000kDa	1.051	0.2	0.582	8.47	34.47	-0.17	Thuroczy et al, 2011
ARK XXII/2 St. 239	9	2007	80.99	33.98	125	0.391	1000kDa	0.502	0.2	0.111	54.79	34.61	0.55	Thuroczy et al, 2011
ARK XXII/2 St. 239	9	2007	80.99	33.98	175	0.441	1000kDa	0.486	0.2	0.045	63.08	34.71	0.84	Thuroczy et al, 2011
ARK XXII/2 St. 255	9	2007	82.50	33.95	19	0.23	1000kDa	0.308	0.2	0.078	0.75	34.21	-1.74	Thuroczy et al, 2011
ARK XXII/2 St. 255	9	2007	82.50	33.95	37	0.19	1000kDa	0.43	0.2	0.24	1.16	34.26	-1.78	Thuroczy et al, 2011

ARK XXII/2 St. 255	9	2007	82.50	33.95	98	0.44	1000kDa	0.526	0.2	0.086	6.28	34.58	1.95	Thuroczy et al, 2011
ARK XXII/2 St. 255	9	2007	82.50	33.95	200	0.49	1000kDa	0.556	0.2	0.066	6.54	34.97	2.70	Thuroczy et al, 2011
ARK XXII/2 St. 255	9	2007	82.50	33.95	754	0.493	1000kDa	0.587	0.2	0.094	17.35	34.95	0.63	Thuroczy et al, 2011
ARK XXII/2 St. 255	9	2007	82.50	33.95	1198	0.53	1000kDa	0.882	0.2	0.352	12.72	34.91	-0.43	Thuroczy et al, 2011
ARK XXII/2 St. 255	9	2007	82.50	33.95	1796	0.757	1000kDa	0.855	0.2	0.098	7.78	34.92	-0.70	Thuroczy et al, 2011
ARK XXII/2 St. 255	9	2007	82.50	33.95	2096	0.6	1000kDa	1.3	0.2	0.7	10.41	34.92	-0.75	Thuroczy et al, 2011
ARK XXII/2 St. 255	9	2007	82.50	33.95	2944	0.64	1000kDa	0.86	0.2	0.22	15.49	34.94	-0.76	Thuroczy et al, 2011
ARK XXII/2 St. 260	9	2007	84.49	36.12	50	0.138	1000kDa	0.274	0.2	0.136	0.69	34.18	-1.81	Thuroczy et al, 2011
ARK XXII/2 St. 260	9	2007	84.49	36.12	100	0.275	1000kDa	0.277	0.2	0.002	0.95	34.22	-1.82	Thuroczy et al, 2011
ARK XXII/2 St. 260	9	2007	84.49	36.12	300	0.346	1000kDa	0.512	0.2	0.166	2.42	34.92	1.99	Thuroczy et al, 2011
ARK XXII/2 St. 260	9	2007	84.49	36.12	698	0.433	1000kDa	0.514	0.2	0.081	2.91	34.92	0.54	Thuroczy et al, 2011
ARK XXII/2 St. 260	9	2007	84.49	36.12	1497	0.418	1000kDa	0.578	0.2	0.16	3.68	34.92	-0.62	Thuroczy et al, 2011
ARK XXII/2 St. 260	9	2007	84.49	36.12	2494	0.648	1000kDa	0.946	0.2	0.298	5.26	34.92	-0.79	Thuroczy et al, 2011
ARK XXII/2 St. 260	9	2007	84.49	36.12	2991	0.561	1000kDa	0.667	0.2	0.106	4.83	34.94	-0.78	Thuroczy et al, 2011
ARK XXII/2 St. 260	9	2007	84.49	36.12	3926	0.55	1000kDa	0.64	0.2	0.09	4.52	34.94	-0.68	Thuroczy et al, 2011
ARK XXII/2 St. 279	9	2007	81.21	81.21	11	0.537	1000kDa	0.887	0.2	0.35	6.12	32.85	-1.41	Thuroczy et al, 2011
ARK XXII/2 St. 279	9	2007	81.21	81.21	25	0.444	1000kDa	1.102	0.2	0.658	5.04	34.11	-1.60	Thuroczy et al, 2011
ARK XXII/2 St. 279	9	2007	81.21	81.21	51	0.572	1000kDa	1.326	0.2	0.754	11.87	34.43	-1.78	Thuroczy et al, 2011
ARK XXII/2 St. 279	9	2007	81.21	81.21	101	0.63	1000kDa	0.733	0.2	0.103	8.48	34.78	1.30	Thuroczy et al, 2011
ARK XXII/2 St. 279	9	2007	81.21	81.21	201	0.539	1000kDa	0.631	0.2	0.092	10.01	34.85	-0.32	Thuroczy et al, 2011
ARK XXII/2 St. 279	9	2007	81.21	81.21	300	0.79	1000kDa	0.802	0.2	0.012	11	34.86	-0.72	Thuroczy et al, 2011
ARK XXII/2 St. 309	9	2007	87.03	104.95	50	0.927	1000kDa	1.444	0.2	0.517	2.44	33.21	-1.75	Thuroczy et al, 2011
ARK XXII/2 St. 309	9	2007	87.03	104.95	101	0.272	1000kDa	0.448	0.2	0.176	2.39	34.21	-1.34	Thuroczy et al, 2011
ARK XXII/2 St. 309	9	2007	87.03	104.95	201	0.239	1000kDa	0.407	0.2	0.168	1.95	34.76	0.99	Thuroczy et al, 2011
ARK XXII/2 St. 309	9	2007	87.03	104.95	501	0.316	1000kDa	0.403	0.2	0.087	1.8	34.88	0.62	Thuroczy et al, 2011
ARK XXII/2 St. 309	9	2007	87.03	104.95	1001	0.23	1000kDa	0.294	0.2	0.064	3.5	34.88	-0.29	Thuroczy et al, 2011
ARK XXII/2 St. 309	9	2007	87.03	104.95	2001	0.287	1000kDa	0.336	0.2	0.049	2.83	34.92	-0.70	Thuroczy et al, 2011
ARK XXII/2 St. 309	9	2007	87.03	104.95	2750	0.406	1000kDa	0.559	0.2	0.153	3.52	34.93	-0.77	Thuroczy et al, 2011
ARK XXII/2 St. 309	9	2007	87.03	104.95	3499	0.283	1000kDa	0.325	0.2	0.042	4.25	34.94	-0.73	Thuroczy et al, 2011
ARK XXII/2 St. 309	9	2007	87.03	104.95	4251	0.172	1000kDa	0.223	0.2	0.051	2.66	34.94	-0.66	Thuroczy et al, 2011

ARK XXII/2 St. 352	9	2007	86.64	177.56	100	0.442	1000kDa	0.651	0.2	0.209	1.58	34.04	-1.51	Thuroczy et al, 2011
ARK XXII/2 St. 352	9	2007	86.64	177.56	200	0.31	1000kDa	0.444	0.2	0.134	1.1	34.65	0.36	Thuroczy et al, 2011
ARK XXII/2 St. 352	9	2007	86.64	177.56	751	0.345	1000kDa	0.451	0.2	0.106	1.89	34.87	0.06	Thuroczy et al, 2011
ARK XXII/2 St. 352	9	2007	86.64	177.56	1500	0.248	1000kDa	0.33	0.2	0.082	1.51	34.93	-0.37	Thuroczy et al, 2011
ARK XXII/2 St. 352	9	2007	86.64	177.56	2251	0.172	1000kDa	0.241	0.2	0.069	1.53	34.95	-0.40	Thuroczy et al, 2011
ARK XXII/2 St. 352	9	2007	86.64	177.56	3001	0.101	1000kDa	0.167	0.2	0.066	1.72	34.94	-0.36	Thuroczy et al, 2011
ARK XXII/2 St. 352	9	2007	86.64	177.56	3900	0.204	1000kDa	0.219	0.2	0.015	1.52	34.94	-0.28	Thuroczy et al, 2011
ARK XXII/2 St. 407	9	2007	76.18	122.13	10	0.698	1000kDa	0.819	0.2	0.121		29.78	-0.11	Thuroczy et al, 2011
ARK XXII/2 St. 407	9	2007	76.18	122.13	30	0.563	1000kDa	0.715	0.2	0.152		33.35	-1.48	Thuroczy et al, 2011
ARK XXII/2 St. 407	9	2007	76.18	122.13	56	1.004	1000kDa	1.112	0.2	0.108		33.78	-1.63	Thuroczy et al, 2011
ANT XXIV/3 St. 101	2	2008	-42.34	9.08	48	0.102	1000kDa	0.18	0.2	0.078		34.39	11.10	Thuroczy thesis
ANT XXIV/3 St. 101	2	2008	-42.34	9.08	76	0.073	1000kDa	0.105	0.2	0.032		34.65	10.46	Thuroczy thesis
ANT XXIV/3 St. 101	2	2008	-42.34	9.08	199	0.253	1000kDa	0.27	0.2	0.017		34.28	7.52	Thuroczy thesis
ANT XXIV/3 St. 101	2	2008	-42.34	9.08	502	0.307	1000kDa	0.377	0.2	0.07		34.34	5.47	Thuroczy thesis
ANT XXIV/3 St. 101	2	2008	-42.34	9.08	1001	0.23	1000kDa	0.587	0.2	0.357		34.38	3.16	Thuroczy thesis
ANT XXIV/3 St. 101	2	2008	-42.34	9.08	1502	0.24	1000kDa	0.54	0.2	0.3		34.62	2.69	Thuroczy thesis
ANT XXIV/3 St. 101	2	2008	-42.34	9.08	2501	0.359	1000kDa	0.63	0.2	0.271		34.82	2.22	Thuroczy thesis
ANT XXIV/3 St. 101	2	2008	-42.34	9.08	3505	0.25	1000kDa	0.63	0.2	0.38		34.79	1.41	Thuroczy thesis
ANT XXIV/3 St. 101	2	2008	-42.34	9.08	4353	0.205	1000kDa	0.572	0.2	0.367		34.74	0.68	Thuroczy thesis
ANT XXIV/3 St. 103	2	2008	-46.00	4.51	45	0.172	1000kDa	0.187	0.2	0.015		33.75	7.83	Thuroczy thesis
ANT XXIV/3 St. 103	2	2008	-46.00	4.51	73	0.193	1000kDa	0.28	0.2	0.087		33.83	5.70	Thuroczy thesis
ANT XXIV/3 St. 103	2	2008	-46.00	4.51	203	0.211	1000kDa	0.318	0.2	0.107	1.292	34.09	4.38	Thuroczy thesis
ANT XXIV/3 St. 103	2	2008	-46.00	4.51	404	0.339	1000kDa	0.522	0.2	0.183		34.15	3.62	Thuroczy thesis
ANT XXIV/3 St. 103	2	2008	-46.00	4.51	499	0.447	1000kDa				1.425	34.18	3.23	Thuroczy thesis
ANT XXIV/3 St. 103	2	2008	-46.00	4.51	751	0.362	1000kDa	0.551	0.2	0.189		34.31	2.81	Thuroczy thesis
ANT XXIV/3 St. 103	2	2008	-46.00	4.51	1253	0.389	1000kDa	0.532	0.2	0.143		34.61	2.47	Thuroczy thesis
ANT XXIV/3 St. 103	2	2008	-46.00	4.51	2001	0.447	1000kDa	0.582	0.2	0.135		34.78	2.21	Thuroczy thesis
ANT XXIV/3 St. 103	2	2008	-46.00	4.51	3099	0.405	1000kDa	0.56	0.2	0.155		34.74	1.15	Thuroczy thesis
ANT XXIV/3 St. 107	2	2008	-50.27	1.05	49	0.078	1000kDa	0.096	0.2	0.018	0.574	33.76	3.19	Thuroczy thesis
ANT XXIV/3 St. 107	2	2008	-50.27	1.05	75	0.263	1000kDa	0.54	0.2	0.277		33.76	3.19	Thuroczy thesis

ANT XXIV/3 St. 107	2	2008	-50.27	1.05	199	0.137	1000kDa	0.199	0.2	0.062	0.352	34.09	1.45	Thuroczy thesis
ANT XXIV/3 St. 107	2	2008	-50.27	1.05	301	0.214	1000kDa	0.246	0.2	0.032		34.41	2.09	Thuroczy thesis
ANT XXIV/3 St. 107	2	2008	-50.27	1.05	499	0.332	1000kDa	0.52	0.2	0.188		34.53	2.17	Thuroczy thesis
ANT XXIV/3 St. 107	2	2008	-50.27	1.05	749	0.259	1000kDa	0.37	0.2	0.111	0.714	34.64	2.13	Thuroczy thesis
ANT XXIV/3 St. 107	2	2008	-50.27	1.05	1250	0.356	1000kDa	0.56	0.2	0.204	0.858	34.74	1.91	Thuroczy thesis
ANT XXIV/3 St. 107	2	2008	-50.27	1.05	1749	0.376	1000kDa	0.507	0.2	0.131	1.659	34.75	1.49	Thuroczy thesis
ANT XXIV/3 St. 107	2	2008	-50.27	1.05	3500	0.454	1000kDa	0.508	0.2	0.054	8.315	34.69	0.34	Thuroczy thesis
ANT XXIV/3 St. 128	2	2008	-58.00	0.00	87	0.096	1000kDa	0.162	0.2	0.066	0.873	34.09	0.07	Thuroczy thesis
ANT XXIV/3 St. 128	2	2008	-58.00	0.00	311	0.378	1000kDa	0.49	0.2	0.112	1.217	34.66	0.59	Thuroczy thesis
ANT XXIV/3 St. 128	2	2008	-58.00	0.00	498	0.629	1000kDa	0.759	0.2	0.13	2.223	34.68	0.56	Thuroczy thesis
ANT XXIV/3 St. 128	2	2008	-58.00	0.00	1001	0.163	1000kDa	0.345	0.2	0.182	1.031	34.68	0.30	Thuroczy thesis
ANT XXIV/3 St. 128	2	2008	-58.00	0.00	1744	0.263	1000kDa	0.439	0.2	0.176	1.256	34.67	-0.05	Thuroczy thesis
ANT XXIV/3 St. 128	2	2008	-58.00	0.00	2498	0.478	1000kDa	0.682	0.2	0.204	1.664	34.66	-0.34	Thuroczy thesis
ANT XXIV/3 St. 128	2	2008	-58.00	0.00	3497	0.319	1000kDa	0.64	0.2	0.321	2.893	34.66	-0.55	Thuroczy thesis
ANT XXIV/3 St. 128	2	2008	-58.00	0.00	4466	0.345	1000kDa	0.481	0.2	0.136	4.499	34.65	-0.68	Thuroczy thesis
ANT XXIV/3 St. 131	2	2008	-59.00	0.00	50	0.097	1000kDa	0.1	0.2	0.003		34.01	0.14	Thuroczy thesis
ANT XXIV/3 St. 131	2	2008	-59.00	0.00	748	0.192	1000kDa	0.235	0.2	0.043		34.68	0.23	Thuroczy thesis
ANT XXIV/3 St. 131	2	2008	-59.00	0.00	1250	0.321	1000kDa	0.473	0.2	0.152		34.67	-0.03	Thuroczy thesis
ANT XXIV/3 St. 131	2	2008	-59.00	0.00	1750	0.224	1000kDa	0.348	0.2	0.124	1.152	34.67	-0.22	Thuroczy thesis
ANT XXIV/3 St. 131	2	2008	-59.00	0.00	3495	0.099	1000kDa	0.362	0.2	0.263	1.896	34.66	-0.38	Thuroczy thesis
ANT XXIV/3 St. 131	2	2008	-59.00	0.00	4245	0.37	1000kDa	0.453	0.2	0.083	3.561	34.65	-0.73	Thuroczy thesis
ANT XXIV/3 St. 131	2	2008	-59.00	0.00	4514	0.234	1000kDa	0.307	0.2	0.073	4.862			Thuroczy thesis
ANT XXIV/3 St. 163	2	2008	-67.00	0.00	44	0.043	1000kDa	0.045	0.2	0.002	0.611	34.64	0.68	Thuroczy thesis
ANT XXIV/3 St. 163	2	2008	-67.00	0.00	210	0.107	1000kDa	0.18	0.2	0.073	0.607	34.69	0.99	Thuroczy thesis
ANT XXIV/3 St. 163	2	2008	-67.00	0.00	300	0.118	1000kDa	0.192	0.2	0.074	0.93	34.70	0.92	Thuroczy thesis
ANT XXIV/3 St. 163	2	2008	-67.00	0.00	1001	0.141	1000kDa	0.235	0.2	0.094		34.69	0.40	Thuroczy thesis
ANT XXIV/3 St. 163	2	2008	-67.00	0.00	1501	0.199	1000kDa	0.27	0.2	0.071		34.68	0.14	Thuroczy thesis
ANT XXIV/3 St. 163	2	2008	-67.00	0.00	2501	0.174	1000kDa	0.418	0.2	0.244		34.66	-0.23	Thuroczy thesis
ANT XXIV/3 St. 163	2	2008	-67.00	0.00	4499	0.217	1000kDa	0.581	0.2	0.364	2.766	34.65	-0.58	Thuroczy thesis
ANT XXIV/3 St. 178	2	2008	-69.40	0.00	137	0.075	1000kDa	0.081	0.2	0.006				Thuroczy thesis

ANT XXIV/3 St. 178	2	2008	-69.40	0.00	451	0.017	1000kDa	0.171	0.2	0.154			Thuroczy thesis
ANT XXIV/3 St. 193	2	2008	-66.59	-27.12	101	0.069	1000kDa	0.094	0.2	0.025	0.279	34.47	-1.77	Thuroczy thesis
ANT XXIV/3 St. 193	2	2008	-66.59	-27.12	402	0.132	1000kDa	0.192	0.2	0.06	2.778	34.68	0.48	Thuroczy thesis
ANT XXIV/3 St. 193	2	2008	-66.59	-27.12	3997	0.492	1000kDa	0.534	0.2	0.042		34.65	-0.64	Thuroczy thesis
ANT XXIV/3 St. 193	2	2008	-66.59	-27.12	4799	0.382	1000kDa	0.592	0.2	0.21		34.65	-0.82	Thuroczy thesis
ANT XXIV/3 St. 210	2	2008	-64.01	-48.37	99	0.057	1000kDa	0.06	0.2	0.003	0.319	34.50	-1.44	Thuroczy thesis
ANT XXIV/3 St. 210	2	2008	-64.01	-48.37	249	0.14	1000kDa	0.16	0.2	0.02		34.67	0.34	Thuroczy thesis
ANT XXIV/3 St. 210	2	2008	-64.01	-48.37	351	0.085	1000kDa	0.15	0.2	0.065	0.342	34.67	0.38	Thuroczy thesis
ANT XXIV/3 St. 210	2	2008	-64.01	-48.37	750	0.132	1000kDa	0.24	0.2	0.108		34.69	0.41	Thuroczy thesis
ANT XXIV/3 St. 210	2	2008	-64.01	-48.37	1000	0.133	1000kDa	0.46	0.2	0.327		34.68	0.27	Thuroczy thesis
ANT XXIV/3 St. 210	2	2008	-64.01	-48.37	1501	0.154	1000kDa	0.46	0.2	0.306		34.67	0.03	Thuroczy thesis
ANT XXIV/3 St. 210	2	2008	-64.01	-48.37	2000	0.175	1000kDa	0.31	0.2	0.135		34.67	-0.16	Thuroczy thesis
ANT XXIV/3 St. 210	2	2008	-64.01	-48.37	3500	0.188	1000kDa	0.32	0.2	0.132	1.454	34.66	-0.49	Thuroczy thesis
ANT XXIV/3 St. 210	2	2008	-64.01	-48.37	3946	0.209	1000kDa	0.36	0.2	0.151	8.327	34.65	-0.60	Thuroczy thesis
ANT XXIV/3 St. 244	2	2008	-57.77	-62.16	73	0.024	1000kDa	0.172	0.2	0.148		33.93	5.47	Thuroczy thesis
ANT XXIV/3 St. 244	2	2008	-57.77	-62.16	147	0.025	1000kDa	0.128	0.2	0.103	0.858	34.02	3.80	Thuroczy thesis
ANT XXIV/3 St. 244	2	2008	-57.77	-62.16	748	0.103	1000kDa	0.276	0.2	0.173	0.45	34.39	2.78	Thuroczy thesis
ANT XXIV/3 St. 244	2	2008	-57.77	-62.16	1250	0.195	1000kDa	0.381	0.2	0.186		34.62	2.26	Thuroczy thesis
ANT XXIV/3 St. 244	2	2008	-57.77	-62.16	1749	0.26	1000kDa	0.405	0.2	0.145	3.577	34.70	1.92	Thuroczy thesis
ANT XXIV/3 St. 244	2	2008	-57.77	-62.16	2497	0.173	1000kDa	0.361	0.2	0.188		34.73	1.32	Thuroczy thesis
ANT XXIV/3 St. 244	2	2008	-57.77	-62.16	3501	0.195	1000kDa	0.441	0.2	0.246	4.222	34.71	0.68	Thuroczy thesis
ANT XXIV/3 St. 244	2	2008	-57.77	-62.16	4002	0.164	1000kDa	0.362	0.2	0.198		34.70	0.56	Thuroczy thesis
IRONAGES III Cast 8	10	2002	31.71	-20.00	2	0.28	0.02	0.45	0.2	0.17				Ussher et al, 2010
IRONAGES III Cast 8	10	2002	31.71	-20.00	25	0.39	0.02	0.58	0.2	0.19				Ussher et al, 2010
IRONAGES III Cast 10	10	2002	31.71	-22.00	25	0.14	0.02	0.31	0.2	0.17		37.34	21.79	Ussher et al, 2010
IRONAGES III Cast 10	10	2002	31.71	-22.00	50	0.17	0.02	0.31	0.2	0.14		36.85	19.81	Ussher et al, 2010
IRONAGES III Cast 10	10	2002	31.71	-22.00	70	0.15	0.02	0.37	0.2	0.22		36.51	18.58	Ussher et al, 2010
IRONAGES III Cast 10	10	2002	31.71	-22.00	100	0.26	0.02	0.33	0.2	0.07		36.34	18.02	Ussher et al, 2010
IRONAGES III Cast 10	10	2002	31.71	-22.00	125	0.21	0.02	0.4	0.2	0.19		36.28	17.45	Ussher et al, 2010
IRONAGES III Cast 10	10	2002	31.71	-22.00	150	0.22	0.02	0.47	0.2	0.25		36.23	17.17	Ussher et al, 2010

IRONAGES III Cast 10	10	2002	31.71	-22.00	600	0.27	0.02	0.44	0.2	0.17	35.54	10.98	Ussher et al, 2010
IRONAGES III Cast 10	10	2002	31.71	-22.00	1300	0.32	0.02	0.54	0.2	0.22	35.49	7.01	Ussher et al, 2010
IRONAGES III Cast 11	10	2002	31.71	-24.00	25	0.15	0.02	0.3	0.2	0.15	37.33	21.89	Ussher et al, 2010
IRONAGES III Cast 11	10	2002	31.71	-24.00	50	0.15	0.02	0.18	0.2	0.03	36.99	20.00	Ussher et al, 2010
IRONAGES III Cast 11	10	2002	31.71	-24.00	70	0.19	0.02	0.27	0.2	0.08	36.76	19.81	Ussher et al, 2010
IRONAGES III Cast 11	10	2002	31.71	-24.00	80	0.13	0.02	0.58	0.2	0.45	36.69	19.91	Ussher et al, 2010
IRONAGES III Cast 11	10	2002	31.71	-24.00	100	0.18	0.02	0.4	0.2	0.22	36.57	19.53	Ussher et al, 2010
IRONAGES III Cast 11	10	2002	31.71	-24.00	150	0.16	0.02	0.37	0.2	0.21	36.37	18.21	Ussher et al, 2010
IRONAGES III Cast 13	10	2002	29.62	-23.98	25	0.14	0.02	0.44	0.2	0.3	37.39	23.58	Ussher et al, 2010
IRONAGES III Cast 13	10	2002	29.62	-23.98	50	0.14	0.02	0.38	0.2	0.24	37.34	23.21	Ussher et al, 2010
IRONAGES III Cast 13	10	2002	29.62	-23.98	70	0.1	0.02	0.42	0.2	0.32	36.93	21.60	Ussher et al, 2010
IRONAGES III Cast 13	10	2002	29.62	-23.98	100	0.16	0.02	0.39	0.2	0.23	36.71	20.85	Ussher et al, 2010
IRONAGES III Cast 13	10	2002	29.62	-23.98	125	0.13	0.02	0.33	0.2	0.2	36.61	20.19	Ussher et al, 2010
IRONAGES III Cast 13	10	2002	29.62	-23.98	150	0.2	0.02	0.42	0.2	0.22	36.57	19.81	Ussher et al, 2010
IRONAGES III Cast 15	10	2002	26.78	-24.00	2	0.11	0.02	0.3	0.2	0.19			Ussher et al, 2010
IRONAGES III Cast 15	10	2002	26.78	-24.00	25	0.16	0.02	0.82	0.2	0.66			Ussher et al, 2010
IRONAGES III Cast 15	10	2002	26.78	-24.00	50	0.14	0.02	0.39	0.2	0.25			Ussher et al, 2010
IRONAGES III Cast 15	10	2002	26.78	-24.00	150	0.41	0.02	0.49	0.2	0.08			Ussher et al, 2010
IRONAGES III Cast 16	10	2002	25.00	-24.00	150	0.47	0.02	0.88	0.2	0.41			Ussher et al, 2010
IRONAGES III Cast 18	10	2002	25.00	-21.37	25	0.24	0.02	0.62	0.2	0.38	37.45	22.07	Ussher et al, 2010
IRONAGES III Cast 18	10	2002	25.00	-21.37	50	0.16	0.02	0.54	0.2	0.38	37.45	22.07	Ussher et al, 2010
IRONAGES III Cast 18	10	2002	25.00	-21.37	70	0.19	0.02	0.64	0.2	0.45	37.16	21.69	Ussher et al, 2010
IRONAGES III Cast 18	10	2002	25.00	-21.37	100	0.19	0.02	0.27	0.2	0.08	36.74	20.41	Ussher et al, 2010
IRONAGES III Cast 18	10	2002	25.00	-21.37	125	0.2	0.02	0.35	0.2	0.15	36.58	19.46	Ussher et al, 2010
IRONAGES III Cast 18	10	2002	25.00	-21.37	150	0.31	0.02	0.49	0.2	0.18	36.49	18.82	Ussher et al, 2010
IRONAGES III Cast 20	10	2002	25.00	-18.86	2	0.18	0.02	0.63	0.2	0.45			Ussher et al, 2010
IRONAGES III Cast 20	10	2002	25.00	-18.86	25	0.17	0.02	0.46	0.2	0.29	37.29	19.44	Ussher et al, 2010
IRONAGES III Cast 20	10	2002	25.00	-18.86	50	0.27	0.02	0.46	0.2	0.19	36.91	18.19	Ussher et al, 2010
IRONAGES III Cast 20	10	2002	25.00	-18.86	70	0.49	0.02	0.54	0.2	0.05	36.69	17.88	Ussher et al, 2010
IRONAGES III Cast 20	10	2002	25.00	-18.86	100	0.35	0.02	0.73	0.2	0.38	36.58	17.88	Ussher et al, 2010

IRONAGES III Cast 20	10	2002	25.00	-18.86	125	0.17	0.02	0.56	0.2	0.39		36.57	19.25	Ussher et al, 2010
IRONAGES III Cast 20	10	2002	25.00	-18.86	150	0.29	0.02	0.78	0.2	0.49		36.48	18.69	Ussher et al, 2010
IRONAGES III Cast 22	10	2002	26.70	-19.99	2	0.44	0.02	0.72	0.2	0.28				Ussher et al, 2010
IRONAGES III Cast 22	10	2002	26.70	-19.99	25	0.28	0.02	0.83	0.2	0.55				Ussher et al, 2010
IRONAGES III Cast 22	10	2002	26.70	-19.99	50	0.48	0.02	0.51	0.2	0.03				Ussher et al, 2010
IRONAGES III Cast 22	10	2002	26.70	-19.99	70	0.2	0.02	0.59	0.2	0.39				Ussher et al, 2010
IRONAGES III Cast 22	10	2002	26.70	-19.99	100	0.32	0.02	0.53	0.2	0.21				Ussher et al, 2010
IRONAGES III Cast 22	10	2002	26.70	-19.99	150	0.33	0.02	0.53	0.2	0.2				Ussher et al, 2010
IRONAGES III Cast 23	10	2002	29.25	-20.03	25	0.23	0.02	0.31	0.2	0.08		37.30	21.35	Ussher et al, 2010
IRONAGES III Cast 23	10	2002	29.25	-20.03	50	0.32	0.02	0.33	0.2	0.01		37.27	21.10	Ussher et al, 2010
IRONAGES III Cast 23	10	2002	29.25	-20.03	70	0.35	0.02	0.61	0.2	0.26		36.80	19.65	Ussher et al, 2010
IRONAGES III Cast 23	10	2002	29.25	-20.03	100	0.19	0.02	0.25	0.2	0.06		36.54	19.28	Ussher et al, 2010
IRONAGES III Cast 23	10	2002	29.25	-20.03	125	0.44	0.02	0.45	0.2	0.01		36.42	18.52	Ussher et al, 2010
IRONAGES III Cast 23	10	2002	29.25	-20.03	150	0.2	0.02	0.45	0.2	0.25		36.32	17.83	Ussher et al, 2010
SEATS '02	3	2002	18.00	116.00	25	0.15	1kDa	0.24	0.4	0.09		33.87	25.16	Wen et al, 2006
SEATS '02	3	2002	18.00	116.00	60	0.25	1kDa	0.34	0.4	0.09		34.40	21.89	Wen et al, 2006
SEATS '02	3	2002	18.00	116.00	100	0.31	1kDa	0.41	0.4	0.1		34.57	19.68	Wen et al, 2006
SEATS '02	3	2002	18.00	116.00	200	0.23	1kDa	0.45	0.4	0.22		34.54	13.68	Wen et al, 2006
SEATS '02	3	2002	18.00	116.00	500	0.47	1kDa	0.56	0.4	0.09		34.43	8.63	Wen et al, 2006
SEATS '02	3	2002	18.00	116.00	1000	0.52	1kDa	0.62	0.4	0.1		34.53	4.53	Wen et al, 2006
SEATS '02	3	2002	18.00	116.00	2000	0.54	1kDa	0.66	0.4	0.12		34.61	2.53	Wen et al, 2006
SEATS '04	3	2004	18.00	116.00	10	0.1	1kDa	0.18	0.4	0.08		34.27	23.79	Wen et al, 2006
SEATS '04	3	2004	18.00	116.00	70	0.2	1kDa	0.36	0.4	0.16		34.38	22.21	Wen et al, 2006
SEATS '04	3	2004	18.00	116.00	100	0.29	1kDa	0.44	0.4	0.15		34.57	20.63	Wen et al, 2006
SEATS '04	3	2004	18.00	116.00	200	0.37	1kDa	0.46	0.4	0.09		34.58	14.84	Wen et al, 2006
SEATS '04	3	2004	18.00	116.00	500	0.41	1kDa	0.54	0.4	0.13		34.43	8.63	Wen et al, 2006
SEATS '04	3	2004	18.00	116.00	1000	0.51	1kDa	0.64	0.4	0.13		34.53	4.53	Wen et al, 2006
SEATS '04	3	2004	18.00	116.00	2000	0.54	1kDa	0.7	0.4	0.16		34.61	2.53	Wen et al, 2006
SEATS '04	3	2004	18.00	116.00	3000	0.57	1kDa	0.74	0.4	0.17		34.63	2.42	Wen et al, 2006
9715 OSP	9	1997	50.00	-145.00	0	0.06	200kDa	0.12	0.2	0.06	0.15	32.53	14.93	Nishioka et al, 2001

9715 OSP	9	1997	50.00	-145.00	10	0.06	200kDa	0.07	0.2	0.01	0.19		Nishioka et al, 2001
9715 OSP	9	1997	50.00	-145.00	25	0.05	200kDa	0.21	0.2	0.16	0.25	32.53	14.90 Nishioka et al, 2001
9715 OSP	9	1997	50.00	-145.00	50	0.04	200kDa	0.07	0.2	0.03	0.08	32.68	6.78 Nishioka et al, 2001
9715 OSP	9	1997	50.00	-145.00	75	0.03	200kDa	0.06	0.2	0.03	0.06	32.72	5.55 Nishioka et al, 2001
9715 OSP	9	1997	50.00	-145.00	100	0.04	200kDa	0.09	0.2	0.05	0.1	32.79	5.12 Nishioka et al, 2001
9715 OSP	9	1997	50.00	-145.00	200	0.13	200kDa	0.17	0.2	0.04	0.28	33.81	4.40 Nishioka et al, 2001
9715 OSP	9	1997	50.00	-145.00	300	0.17	200kDa	0.34	0.2	0.17	0.36	33.92	4.12 Nishioka et al, 2001
9715 OSP	9	1997	50.00	-145.00	400	0.24	200kDa	0.42	0.2	0.18	0.5	34.03	3.98 Nishioka et al, 2001
9715 OSP	9	1997	50.00	-145.00	600	0.34	200kDa	0.56	0.2	0.22	0.64	34.20	3.54 Nishioka et al, 2001
9815 OSP	6	1998	50.00	-145.00	10	0.05	200kDa	0.08	0.2	0.03	0.12	32.68	9.01 Nishioka et al, 2001
9815 OSP	6	1998	50.00	-145.00	25	0.06	200kDa	0.07	0.2	0.01	0.1	32.69	7.62 Nishioka et al, 2001
9815 OSP	6	1998	50.00	-145.00	40	0.07	200kDa	0.11	0.2	0.04	0.16		Nishioka et al, 2001
9815 OSP	6	1998	50.00	-145.00	75	0.08	200kDa	0.09	0.2	0.01	0.1	32.71	5.69 Nishioka et al, 2001
9815 OSP	6	1998	50.00	-145.00	100	0.06	200kDa	0.08	0.2	0.02	0.11	32.94	5.41 Nishioka et al, 2001
9815 OSP	6	1998	50.00	-145.00	200	0.28	200kDa	0.36	0.2	0.08	0.48	33.79	4.12 Nishioka et al, 2001
9815 OSP	6	1998	50.00	-145.00	300	0.35	200kDa	0.41	0.2	0.06	0.54	33.95	3.97 Nishioka et al, 2001
9815 OSP	6	1998	50.00	-145.00	400	0.38	200kDa	0.44	0.2	0.06	0.56	34.05	3.87 Nishioka et al, 2001
9815 OSP	6	1998	50.00	-145.00	600	0.42	200kDa	0.5	0.2	0.08	0.61	34.21	3.55 Nishioka et al, 2001
9829 OSP	9	1998	50.00	-145.00	25	0.07	200kDa	0.09	0.45	0.02	0.09	32.63	12.09 Nishioka et al, 2001
9829 OSP	9	1998	50.00	-145.00	40	0.06	200kDa	0.07	0.45	0.01	0.08	32.64	12.09 Nishioka et al, 2001
9829 OSP	9	1998	50.00	-145.00	75	0.09	200kDa	0.11	0.2	0.02	0.14	32.74	6.35 Nishioka et al, 2001
9829 OSP	9	1998	50.00	-145.00	100	0.13	200kDa	0.16	0.2	0.03	0.19	33.00	5.66 Nishioka et al, 2001
9829 OSP	9	1998	50.00	-145.00	200	0.18	200kDa	0.34	0.2	0.16	0.37	33.81	4.41 Nishioka et al, 2001
9829 OSP	9	1998	50.00	-145.00	300	0.26	200kDa	0.43	0.2	0.17	0.48	33.93	4.23 Nishioka et al, 2001
9829 OSP	9	1998	50.00	-145.00	400	0.33	200kDa	0.53	0.2	0.2	0.54	34.04	4.11 Nishioka et al, 2001
9829 OSP	9	1998	50.00	-145.00	600	0.35	200kDa	0.54	0.2	0.19	0.62		Nishioka et al, 2001
9829 OSP	9	1998	50.00	-145.00	800	0.44	200kDa	0.58	0.2	0.14	0.69		Nishioka et al, 2001
9901 OSP	2	1999	50.00	-145.00	10	0.21	200kDa	0.23	0.45	0.02	0.31		Nishioka et al, 2001
9901 OSP	2	1999	50.00	-145.00	40	0.2	200kDa	0.25	0.45	0.05	0.37		Nishioka et al, 2001
9901 OSP	2	1999	50.00	-145.00	75	0.23	200kDa	0.23	0.45	0	0.32	32.86	5.30 Nishioka et al, 2001

9901 OSP	2	1999	50.00	-145.00	100	0.2	200kDa	0.22	0.45	0.02	0.31	32.87	5.33	Nishioka et al, 2001
9901 OSP	2	1999	50.00	-145.00	200	0.37	200kDa	0.64	0.45	0.27	0.64	33.79	4.29	Nishioka et al, 2001
9901 OSP	2	1999	50.00	-145.00	300	0.56	200kDa	0.73	0.45	0.17	0.87	33.91	4.06	Nishioka et al, 2001
9901 OSP	2	1999	50.00	-145.00	400	0.54	200kDa	0.72	0.45	0.18	0.86	34.03	4.06	Nishioka et al, 2001
9901 OSP	2	1999	50.00	-145.00	600	0.57	200kDa	0.92	0.45	0.35	0.95	34.20	3.68	Nishioka et al, 2001
9901 OSP	2	1999	50.00	-145.00	800	0.47	200kDa	0.85	0.45	0.38	1.13	34.30	3.23	Nishioka et al, 2001
9901 OSP	2	1999	50.00	-145.00	1000	0.55	200kDa	1.08	0.45	0.53	1.29	34.38	2.90	Nishioka et al, 2001
9829 P4	8	1998	48.65	-126.67	0	0.15	200kDa	0.16	0.2	0.01	0.22			Nishioka et al, 2001
9829 P4	8	1998	48.65	-126.67	10	0.13	200kDa	0.21	0.2	0.08	0.29			Nishioka et al, 2001
9829 P4	8	1998	48.65	-126.67	40	0.14	200kDa	0.14	0.2	0.00	0.22			Nishioka et al, 2001
9829 P4	8	1998	48.65	-126.67	75	0.19	200kDa	0.40	0.2	0.21	0.42			Nishioka et al, 2001
9829 P4	8	1998	48.65	-126.67	100	0.19	200kDa	0.29	0.2	0.10	0.63			Nishioka et al, 2001
9829 P4	8	1998	48.65	-126.67	200	0.48	200kDa	0.70	0.2	0.21	1.95			Nishioka et al, 2001
9829 P4	8	1998	48.65	-126.67	300	0.97	200kDa	2.33	0.2	1.36	4.85			Nishioka et al, 2001
9829 P4	8	1998	48.65	-126.67	400	0.58	200kDa	1.05	0.2	0.47	2.44			Nishioka et al, 2001
9829 P4	8	1998	48.65	-126.67	600	1.41	200kDa	5.95	0.2	4.54	7.55			Nishioka et al, 2001
9829 P4	8	1998	48.65	-126.67	800	1.67	200kDa	2.25	0.2	0.58	5.58			Nishioka et al, 2001
9829 P4	8	1998	48.65	-126.67	1000	1.08	200kDa	1.25	0.2	0.16	2.66			Nishioka et al, 2001
9829 P16	8	1998	49.28	-134.67	25	0.08	200kDa	0.08	0.2	0.00	0.09			Nishioka et al, 2001
9829 P16	8	1998	49.28	-134.67	40	0.07	200kDa	0.07	0.2	0.00	0.11			Nishioka et al, 2001
9829 P16	8	1998	49.28	-134.67	100	0.13	200kDa	0.24	0.2	0.11	1.40			Nishioka et al, 2001
9829 P16	8	1998	49.28	-134.67	200	0.28	200kDa	0.57	0.2	0.28	1.44			Nishioka et al, 2001
9829 P16	8	1998	49.28	-134.67	400	0.60	200kDa	0.65	0.2	0.05	1.16			Nishioka et al, 2001
9829 P16	8	1998	49.28	-134.67	600	0.44	200kDa	0.74	0.2	0.31	1.12			Nishioka et al, 2001
9829 P15	9	1998	47.47	-133.42	10	0.11	200kDa	0.12	0.2	0.01	0.16			Nishioka et al, 2001
9829 P15	9	1998	47.47	-133.42	25	0.11	200kDa	0.11	0.2	0.00	0.13			Nishioka et al, 2001
9829 P15	9	1998	47.47	-133.42	40	0.12	200kDa	0.13	0.2	0.01	0.18			Nishioka et al, 2001
9829 P15	9	1998	47.47	-133.42	600	0.71	200kDa	0.98	0.2	0.27	1.21			Nishioka et al, 2001
9901 P4	2	1999	48.65	-126.67	10	0.55	200kDa	1.03	0.2	0.49	6.29			Nishioka et al, 2001
9901 P4	2	1999	48.65	-126.67	25	0.68	200kDa	0.94	0.2	0.26	7.07			Nishioka et al, 2001

9901 P4	2	1999	48.65	-126.67	40	0.44	200kDa	0.70	0.2	0.26	4.97	Nishioka et al, 2001
9901 P4	2	1999	48.65	-126.67	75	0.54	200kDa	0.84	0.2	0.30	6.76	Nishioka et al, 2001
9901 P4	2	1999	48.65	-126.67	100	0.79	200kDa	1.03	0.2	0.24	8.73	Nishioka et al, 2001
9901 P4	2	1999	48.65	-126.67	200	1.41	200kDa	1.70	0.2	0.29	8.54	Nishioka et al, 2001
9901 P4	2	1999	48.65	-126.67	300	0.69	200kDa	0.89	0.2	0.21	2.77	Nishioka et al, 2001
9901 P4	2	1999	48.65	-126.67	400	1.49	200kDa	2.40	0.2	0.91	6.80	Nishioka et al, 2001
9901 P4	2	1999	48.65	-126.67	600	2.28	200kDa	2.33	0.2	0.05	6.55	Nishioka et al, 2001
9901 P4	2	1999	48.65	-126.67	800	1.72	200kDa	1.95	0.2	0.22	5.38	Nishioka et al, 2001
9901 TR15	2	1999	50.02	-130.98	10	0.51	200kDa	1.25	0.2	0.74	5.22	Nishioka et al, 2001
9901 TR15	2	1999	50.02	-130.98	25	0.45	200kDa	1.25	0.2	0.79	5.05	Nishioka et al, 2001
9901 TR15	2	1999	50.02	-130.98	40	0.35	200kDa	0.79	0.2	0.44	3.14	Nishioka et al, 2001
9901 TR15	2	1999	50.02	-130.98	75	0.64	200kDa	1.36	0.2	0.73	5.87	Nishioka et al, 2001
9901 TR15	2	1999	50.02	-130.98	100	0.55	200kDa	1.11	0.2	0.56	5.38	Nishioka et al, 2001
9901 TR15	2	1999	50.02	-130.98	200	0.99	200kDa	1.90	0.2	0.91	6.95	Nishioka et al, 2001
9901 TR15	2	1999	50.02	-130.98	300	0.90	200kDa	1.49	0.2	0.59	5.03	Nishioka et al, 2001
9901 TR15	2	1999	50.02	-130.98	400	1.35	200kDa	2.15	0.2	0.80	5.13	Nishioka et al, 2001
9901 TR15	2	1999	50.02	-130.98	600	1.76	200kDa	3.13	0.2	1.37	6.46	Nishioka et al, 2001
9901 TR15	2	1999	50.02	-130.98	800	1.23	200kDa	2.17	0.2	0.94	4.74	Nishioka et al, 2001
9901 TR15	2	1999	50.02	-130.98	1000	1.28	200kDa	2.22	0.2	0.94	5.97	Nishioka et al, 2001
Station 22	5	2000	49.00	157.50	10	0.1	200kDa	0.11	0.2	0.01	0.70	Nishioka et al, 2003
Station 22	5	2000	49.00	157.50	20	0.06	200kDa	0.08	0.2	0.02	0.83	Nishioka et al, 2003
Station 22	5	2000	49.00	157.50	40	0.02	200kDa	0.05	0.2	0.03	0.36	Nishioka et al, 2003
Station 22	5	2000	49.00	157.50	80	0	200kDa	0.08	0.2	0.08	0.36	Nishioka et al, 2003
Station 22	5	2000	49.00	157.50	100	0.01	200kDa	0.14	0.2	0.13	0.55	Nishioka et al, 2003
Station 22	5	2000	49.00	157.50	125	0.05	200kDa	0.29	0.2	0.24	0.91	Nishioka et al, 2003
Station 22	5	2000	49.00	157.50	150	0.3	200kDa	0.79	0.2	0.49	1.49	Nishioka et al, 2003
Station 22	5	2000	49.00	157.50	200	0.44	200kDa	0.95	0.2	0.51	1.39	Nishioka et al, 2003
Station 22	5	2000	49.00	157.50	300	0.53	200kDa	0.98	0.2	0.45	1.65	Nishioka et al, 2003
Station 22	5	2000	49.00	157.50	400	0.74	200kDa	1.37	0.2	0.63	2.13	Nishioka et al, 2003
Station 22	5	2000	49.00	157.50	600	0.78	200kDa	1.5	0.2	0.72	2.25	Nishioka et al, 2003

Station 22	5	2000	49.00	157.50	800	0.9	200kDa	1.66	0.2	0.76	2.29		Nishioka et al, 2003
Station Knot	5	2000	44.00	155.00	10	0.15	200kDa	0.15	0.2	0	0.37		Nishioka et al, 2003
Station Knot	5	2000	44.00	155.00	20	0.08	200kDa	0.11	0.2	0.03	0.32		Nishioka et al, 2003
Station Knot	5	2000	44.00	155.00	40	0.09	200kDa	0.16	0.2	0.07	0.43		Nishioka et al, 2003
Station Knot	5	2000	44.00	155.00	80	0.12	200kDa	0.23	0.2	0.11	0.67		Nishioka et al, 2003
Station Knot	5	2000	44.00	155.00	100	0.14	200kDa	0.35	0.2	0.21	0.82		Nishioka et al, 2003
Station Knot	5	2000	44.00	155.00	120	0.15	200kDa	0.41	0.2	0.26	1.01		Nishioka et al, 2003
Station Knot	5	2000	44.00	155.00	140	0.22	200kDa	0.84	0.2	0.62	1.84		Nishioka et al, 2003
Station Knot	5	2000	44.00	155.00	200	0.39	200kDa	1.06	0.2	0.67	2.05		Nishioka et al, 2003
Station Knot	5	2000	44.00	155.00	300	0.51	200kDa	1.20	0.2	0.69	1.95		Nishioka et al, 2003
Station Knot	5	2000	44.00	155.00	400	0.47	200kDa	1.24	0.2	0.77	1.95		Nishioka et al, 2003
Station Knot	5	2000	44.00	155.00	600	0.55	200kDa	1.41	0.2	0.86	1.80		Nishioka et al, 2003
Station Knot	5	2000	44.00	155.00	4000	0.31	200kDa	0.68	0.2	0.37	1.10		Nishioka et al, 2003
Station P26	9	1998	50.00	-144.50	40	0.06	200kDa	0.07	0.2	0.01	0.08		Nishioka et al, 2003
Station P26	9	1998	50.00	-144.50	75	0.09	200kDa	0.11	0.2	0.02	0.14		Nishioka et al, 2003
Station P26	9	1998	50.00	-144.50	100	0.13	200kDa	0.16	0.2	0.03	0.19		Nishioka et al, 2003
Station P26	9	1998	50.00	-144.50	200	0.18	200kDa	0.34	0.2	0.15	0.37		Nishioka et al, 2003
Station P26	9	1998	50.00	-144.50	300	0.26	200kDa	0.43	0.2	0.17	0.48		Nishioka et al, 2003
Station P26	9	1998	50.00	-144.50	400	0.33	200kDa	0.53	0.2	0.20	0.54		Nishioka et al, 2003
Station P26	9	1998	50.00	-144.50	600	0.35	200kDa	0.54	0.2	0.19	0.62		Nishioka et al, 2003
Station P26	9	1998	50.00	-144.50	800	0.44	200kDa	0.58	0.2	0.14	0.69		Nishioka et al, 2003
Sabin Point	7	1994	41.77	-71.38	0	11.4245	8kDa	97.9	0.2	86.476	1056.7	24.92	Wells et al, 2000
Conimicut Point	7	1994	41.74	-71.37	0	7.7828	8kDa	35.2	0.2	27.417	705.2	27.89	Wells et al, 2000
Rumstick Point	7	1994	41.70	-71.31	0	7.094	8kDa	34	0.2	26.906	273	28.64	Wells et al, 2000
General Rocks	7	1994	41.53	-71.40	0	1.2692	8kDa	17.6	0.2	16.331	913.6	30.34	Wells et al, 2000
T1-1 1335	8	2003	55.05	-178.11	0	0.210	0.03	0.211	0.2	0.001	0.608	32.99	11.06 Hurst et al, 2010
T1-2 1555	8	2003	55.32	-175.48	0	0.021	0.03	0.108	0.2	0.087	0.752	32.83	11.49 Hurst et al, 2010
T1-3 1404	8	2003	55.57	-173.81	0	0.055	0.03	0.104	0.2	0.048	16.770	32.41	11.16 Hurst et al, 2010
T1-3 1643	8	2003	55.56	-173.94	0	0.006	0.03	0.283	0.2	0.277	15.470	32.50	10.93 Hurst et al, 2010
T1-3 1804	8	2003	55.58	-173.69	0	0.058	0.03	0.231	0.2	0.174	14.257	32.45	10.94 Hurst et al, 2010

T1-3 2054	8	2003	55.67	-173.18	0	0.024	0.03	0.069	0.2	0.045	19.762	32.45	11.03	Hurst et al, 2010
T1-3 2201	8	2003	55.58	-173.16	0	0.152	0.03	0.342	0.2	0.190	8.346	32.50	10.84	Hurst et al, 2010
T1-4 1551	8	2003	56.40	-171.51	0	0.061	0.03	0.071	0.2	0.010	1.489	32.48	10.43	Hurst et al, 2010
T1-4 1632	8	2003	56.44	-171.42	0	0.032	0.03	0.051	0.2	0.020	1.134	32.40	10.49	Hurst et al, 2010
T1-4 1755	8	2003	56.54	-171.24	0	0.063	0.03	0.183	0.2	0.120	2.080	32.34	10.58	Hurst et al, 2010
T1-4 2130	8	2003	56.75	-170.80	0	0.149	0.03	0.199	0.2	0.050	2.957	31.76	10.85	Hurst et al, 2010
T1-5 0848	8	2003	56.83	-170.71	0	0.172	0.03	0.269	0.2	0.097	3.362	31.69	10.89	Hurst et al, 2010
T1-51039	8	2003	57.00	-170.54	0	0.922	0.03	2.981	0.2	2.059	44.216	31.82	9.48	Hurst et al, 2010
T1-5 1554	8	2003	57.17	-169.94	0	2.821	0.03	5.337	0.2	2.517	66.924	31.82	9.74	Hurst et al, 2010
T1-5 2046	8	2003	57.32	-169.38	0	0.704	0.03	0.959	0.2	0.255	10.837	31.89	11.23	Hurst et al, 2010
T1-6 0812	8	2003	57.35	-169.32	0	0.571	0.03	0.743	0.2	0.172	15.249	31.92	11.10	Hurst et al, 2010
T1-6 1202	8	2003	57.53	-169.00	0	0.288	0.03	0.442	0.2	0.155	15.137	31.99	10.96	Hurst et al, 2010
T1-6 1401	8	2003	57.64	-168.83	0	0.352	0.03	0.551	0.2	0.199		32.00	10.94	Hurst et al, 2010
T1-7 1518	8	2003	57.92	-168.39	0	0.625	0.03	0.984	0.2	0.359	15.065	31.99	10.83	Hurst et al, 2010
T1-7 2011	8	2003	58.47	-167.60	0	1.096	0.03	1.746	0.2	0.650	16.107	31.58	10.82	Hurst et al, 2010
T1-8 0829	8	2003	58.68	-167.29	0	1.297	0.03	1.482	0.2	0.185	32.180	31.51	9.80	Hurst et al, 2010
T1-8 1222	8	2003	59.05	-166.73	0	1.965	0.03	2.044	0.2	0.079	79.886	31.23	10.41	Hurst et al, 2010
T1-8 1628	8	2003	59.57	-165.95	0	1.446	0.03	2.558	0.2	1.111	259.520	30.81	12.01	Hurst et al, 2010
T2-1 1423	8	2003	58.43	-159.90	0	0.930	0.03	4.126	0.2	3.196	303.366	29.51	12.29	Hurst et al, 2010
T2-1 1544	8	2003	58.29	-159.99	0	1.580	0.03	4.476	0.2	2.896	289.249	29.93	12.19	Hurst et al, 2010
T2-1 1919	8	2003	58.01	-160.72	0	1.821	0.03	3.767	0.2	1.946	77.405	30.92	10.83	Hurst et al, 2010
T2-2 1122	8	2003	57.59	-161.87	0	1.607	0.03	2.528	0.2	0.921	31.059	30.94	11.42	Hurst et al, 2010
T2-2 1329	8	2003	57.46	-162.19	0	0.992	0.03	1.652	0.2	0.661	23.991	31.09	11.63	Hurst et al, 2010
T2-2 1947	8	2003	57.01	-163.36	0	0.883	0.03	1.017	0.2	0.134	12.145	31.52	12.24	Hurst et al, 2010
T2-3 0950	8	2003	56.74	-164.07	0	0.429	0.03	0.725	0.2	0.295	5.401	31.60	12.21	Hurst et al, 2010
T2-4 1030	8	2003	56.45	-164.81	0	0.795	0.03	0.848	0.2	0.053	11.617	31.61	11.55	Hurst et al, 2010
T2-4 1230	8	2003	56.30	-165.24	0	0.353	0.03	0.423	0.2	0.070	7.962	31.59	11.44	Hurst et al, 2010
T2-4 1702	8	2003	56.02	-165.82	0	0.430	0.03	0.677	0.2	0.247	6.225	31.60	11.50	Hurst et al, 2010
T2-4 2104	8	2003	55.77	-166.43	0	0.409	0.03	0.724	0.2	0.315	12.885	31.79	11.00	Hurst et al, 2010
T2-5 0834	8	2003	55.74	-166.50	0	0.113	0.03	0.455	0.2	0.343	6.185	31.70	10.88	Hurst et al, 2010

T2-6 1230	8	2003	55.36	-167.56	0	0.253	0.03	0.363	0.2	0.110	8.628	31.89	10.81	Hurst et al, 2010
T2-6 1459	8	2003	55.29	-167.75	0	0.105	0.03	0.429	0.2	0.324	4.887	32.16	10.47	Hurst et al, 2010
T2-6 2111	8	2003	55.11	-168.43	0	0.070	0.03	0.198	0.2	0.128	4.002	32.26	10.54	Hurst et al, 2010
T2-7 1019	8	2003	55.02	-168.86	0	0.219	0.03	0.269	0.2	0.051	2.248	32.26	10.50	Hurst et al, 2010
T2-7 1609	8	2003	54.72	-170.18	0	0.134	0.03	0.188	0.2	0.054	2.840	32.41	10.26	Hurst et al, 2010
T3-1 0820	8	2003	55.10	-164.86	0	0.736	0.03	0.956	0.2	0.220		31.94	8.92	Hurst et al, 2010
T3-1 1237	8	2003	54.89	-165.38	0	0.390	0.03	0.410	0.2	0.019	0.410	32.15	10.16	Hurst et al, 2010
T3-1 1622	9	2003	54.62	-166.00	0	0.273	0.03	0.396	0.2	0.124	0.396	32.29	10.03	Hurst et al, 2010
T3-1 2044	9	2003	54.38	-166.62	0	0.147	0.03	0.212	0.2	0.066		32.38	10.27	Hurst et al, 2010
T3-2 0912	9	2003	54.25	-166.92	0	0.048	0.03	0.106	0.2	0.058	0.106	32.41	10.33	Hurst et al, 2010
T3-2 1228	9	2003	54.09	-167.39	0	0.093	0.03	0.180	0.2	0.087	0.180	32.45	9.75	Hurst et al, 2010
T3-2 2142	9	2003	53.78	-168.46	0	0.201	0.03	0.361	0.2	0.160	0.361	32.69	7.28	Hurst et al, 2010
T3-3 1041	9	2003	53.08	-169.87	0	0.172	0.03	0.419	0.2	0.247	0.419	33.00	6.46	Hurst et al, 2010
T3-3 1307	9	2003	52.92	-169.70	0	0.271	0.03	0.631	0.2	0.360	0.631	32.79	6.22	Hurst et al, 2010
T3-3 1613	9	2003	52.52	-169.57	0	0.025	0.03	0.146	0.2	0.121	0.146	32.13	11.78	Hurst et al, 2010
Station 4	8	2003	55.05	-178.23	0	1.821	0.03	3.767	0.2	1.946	77.405			Hurst et al, 2010
Station 4D	8	2003	55.05	-178.23	35	4.926	0.03	12.235	0.2	7.309	177.364			Hurst et al, 2010
Station 5	8	2003	55.21	-176.05	0	0.992	0.03	1.652	0.2	0.661	23.991			Hurst et al, 2010
Station 5D	8	2003	55.21	-176.05	35	1.594	0.03	3.053	0.2	1.458	83.940			Hurst et al, 2010
Station 6	8	2003	55.51	-174.15	0	0.883	0.030	1.017	0.2	0.134	12.145			Hurst et al, 2010
Station 6D	8	2003	55.51	-174.15	40	1.068	0.03	2.723	0.2	1.655	52.816			Hurst et al, 2010
Station 7	8	2003	56.20	-171.99	0	0.429	0.03	0.725	0.2	0.295	5.401			Hurst et al, 2010
Station 7D	8	2003	56.20	-171.99	45	1.930	0.03	4.252	0.2	2.322	83.276			Hurst et al, 2010
Station 8	8	2003	56.26	-171.85	0	0.795	0.03	0.848	0.2	0.053	11.617			Hurst et al, 2010
Station 8D	8	2003	56.26	-171.85	45	1.659	0.03	4.742	0.2	3.083	189.511			Hurst et al, 2010
Station 9	8	2003	56.34	-171.63	0	0.430	0.03	0.677	0.2	0.247	6.225			Hurst et al, 2010
Station 9D	8	2003	56.34	-171.63	50	1.560	0.03	4.292	0.2	2.732	205.837			Hurst et al, 2010
Station 10	8	2003	57.00	-170.50	0	0.409	0.03	0.724	0.2	0.315	12.885			Hurst et al, 2010
Station 11	8	2003	57.36	-169.43	0	0.244	0.03	0.262	0.2	0.018	4.167			Hurst et al, 2010
Station 11D	8	2003	57.36	-169.43	120	3.194	0.03	8.941	0.2	5.746	321.227			Hurst et al, 2010

Station 12	8	2003	57.67	-168.79	0	0.253	0.03	0.363	0.2	0.110	8.628		Hurst et al, 2010
Station 12D	8	2003	57.67	-168.79	140	2.937	0.03	6.625	0.2	3.688	39.342		Hurst et al, 2010
Station 13	8	2003	57.76	-168.63	0	0.070	0.03	0.198	0.2	0.128	4.002		Hurst et al, 2010
Station 13D	8	2003	57.76	-168.63	45	0.162	0.03	0.276	0.2	0.114	7.349		Hurst et al, 2010
Station 15	8	2003	59.60	-166.00	0	0.093	0.03	0.180	0.2	0.087	5.155		Hurst et al, 2010
Station 15D	8	2003	59.60	-166.00	50	0.248	0.03	0.389	0.2	0.141	11.633		Hurst et al, 2010
Station 3 depth	8	2003	57.70	-168.71	15	0.271	0.03	0.794	0.2	0.522	11.291		Hurst and Bruland, 2007
Station 3 depth	8	2003	57.70	-168.71	20	0.629	0.03	0.864	0.2	0.236	5.891		Hurst and Bruland, 2007
Station 3 depth	8	2003	57.70	-168.71	40	1.475	0.03	4.348	0.2	2.873	108.465		Hurst and Bruland, 2007
Station 3 depth	8	2003	57.70	-168.71	50	1.800	0.03	4.263	0.2	2.463	130.371		Hurst and Bruland, 2007
Station 3 depth	8	2003	57.70	-168.71	60	1.682	0.03	2.069	0.2	0.387	117.730		Hurst and Bruland, 2007
R/V Point Sur 1	6	2004	37.84	-122.75	0	3.510	200kDa	5.290	0.4	1.780	431.490	33.69	10.55 Hurst and Bruland, 2008
R/V Point Sur 2	6	2004	37.82	-122.71	0	3.200	200kDa	4.560	0.4	1.360	561.360	33.45	11.63 Hurst and Bruland, 2008
R/V Point Sur 3	6	2004	37.80	-122.66	0	4.930	200kDa	8.180	0.4	3.250	1365.180	32.74	13.32 Hurst and Bruland, 2008
R/V Point Sur 4	6	2004	37.79	-122.65	0	4.540	200kDa	7.750	0.4	3.210	2302.750	32.72	13.32 Hurst and Bruland, 2008
R/V Point Sur 5	6	2004	37.76	-122.64	0	3.970	200kDa	6.230	0.4	2.260	1346.330	32.72	13.38 Hurst and Bruland, 2008
R/V Point Sur 6	6	2004	37.73	-122.61	0	4.060	200kDa	7.120	0.4	3.060	1387.320	32.67	13.53 Hurst and Bruland, 2008
R/V Point Sur 7	6	2004	37.63	-122.59	0	1.610	200kDa	6.200	0.4	4.590	489.900	33.05	13.98 Hurst and Bruland, 2008
R/V Point Sur 8	6	2004	37.63	-122.66	0	1.760	200kDa	4.170	0.4	2.410	281.370	33.41	14.08 Hurst and Bruland, 2008
R/V Point Sur 9	6	2004	37.70	-122.71	0	1.520	200kDa	3.140	0.4	1.620	166.240	33.50	13.26 Hurst and Bruland, 2008
R/V Point Sur 10	6	2004	37.75	-122.74	0	1.020	200kDa	3.590	0.4	2.570	242.690	33.55	12.62 Hurst and Bruland, 2008
AMT 16- Fe01	5	2005	-28.74	-5.75	5	0.165	0.02	0.558	0.2	0.393	0.940	36.12	20.42 Ussher BODC dataset
AMT 16- Fe05	5	2005	-27.16	-13.83	5	0.311	0.02	0.433	0.2	0.123		36.72	22.46 Ussher BODC dataset
AMT 16- Fe07	5	2005	-26.28	-18.46	5	0.328	0.02	0.366	0.2	0.037	0.530	36.76	22.83 Ussher BODC dataset
AMT 16- Fe12	6	2005	-22.45	-25.00	5	0.235	0.02	0.302	0.2	0.067	0.240	37.32	25.23 Ussher BODC dataset
AMT 16- Fe14	6	2005	-15.41	-25.00	5	0.213	0.02	0.247	0.2	0.034	0.220	37.42	25.72 Ussher BODC dataset
AMT 16- Fe20	6	2005	2.06	-25.98	5	0.285	0.02	0.813	0.2	0.528	1.740	35.25	28.45 Ussher BODC dataset
AMT 16- Fe42	6	2005	13.19	-31.34	5	0.307	0.02	0.580	0.2	0.273	1.750	36.42	26.31 Ussher BODC dataset
AMT 16- Fe43	6	2005	16.32	-32.89	5	0.307	0.02	0.620	0.2	0.313	2.900	37.09	25.54 Ussher BODC dataset
AMT 16- Fe51	6	2005	26.84	-38.29	5	0.715	0.02	1.022	0.2	0.306	0.720	37.17	24.13 Ussher BODC dataset

AMT 16- Fe55	6	2005	29.40	-39.79	5	1.006	0.02	1.068	0.2	0.062	0.650	37.08	24.05	Ussher BODC dataset
AMT 16- Fe71	6	2005	33.92	-46.07	5	0.379	0.02	0.437	0.2	0.058	0.800	36.62	21.96	Ussher BODC dataset
AMT 16- Fe73	6	2005	35.10	-41.84	5	0.314	0.02	0.558	0.2	0.244	0.530	36.74	21.87	Ussher BODC dataset
AMT 16- Fe75	6	2005	36.46	-36.92	5	0.371	0.02	0.501	0.2	0.130		36.45	20.66	Ussher BODC dataset
AMT 16- Fe79a	6	2005	39.26	-28.82	5	0.312	0.02	0.566	0.2	0.254	0.660	36.11	18.74	Ussher BODC dataset
AMT 16- Fe83	6	2005	44.37	-22.00	5	0.458	0.02	0.472	0.2	0.014	0.490	35.90	17.31	Ussher BODC dataset
AMT 16- Fe86	6	2005	46.37	-18.84	5	0.387	0.02	0.530	0.2	0.144	0.440	35.78	17.04	Ussher BODC dataset
GAK13	5	2004	58.10	-147.79	0	0.13	0.025	0.25	0.4	0.12		32.02		Wu et al, 2009
GAK11	7	2004	58.39	-148.08	0	0.16	0.025	0.25	0.4	0.09		32.17		Wu et al, 2009
GAK7	7	2004	58.97	-148.62	0	0.08	0.025	0.14	0.4	0.06		31.94		Wu et al, 2009
GAK5	5	2004	59.26	-148.90	0	0.33	0.025	2.16	0.4	1.83		32.06		Wu et al, 2009
GAK5	7	2004	59.26	-148.90	0	0.57	0.025	1.18	0.4	0.61		31.62		Wu et al, 2009
GAK3	7	2004	59.55	-149.20	0	1.17	0.025	1.66	0.4	0.49		31.08		Wu et al, 2009
GAK1	5	2004	59.84	-149.47	0	0.76	0.025	4.38	0.4	3.62		30.90		Wu et al, 2009
GAK1	7	2004	59.84	-149.47	0	2.01	0.025	8.45	0.4	6.44		30.40		Wu et al, 2009
GAK11	7	2004	58.39	-148.08	20	0.16	0.025	0.25	0.4	0.09				Wu et al, 2009
GAK11	7	2004	58.39	-148.08	100	0.31	0.025	0.56	0.4	0.25				Wu et al, 2009
GAK11	7	2004	58.39	-148.08	200	0.48	0.025	0.7	0.4	0.22				Wu et al, 2009
GAK11	7	2004	58.39	-148.08	400	0.71	0.025	1.06	0.4	0.35				Wu et al, 2009
GAK11	7	2004	58.39	-148.08	600	0.71	0.025	0.89	0.4	0.18				Wu et al, 2009
GAK11	7	2004	58.39	-148.08	800	0.77	0.025	0.91	0.4	0.14				Wu et al, 2009
GAK11	7	2004	58.39	-148.08	1000	0.77	0.025	0.87	0.4	0.1				Wu et al, 2009
GAK11	7	2004	58.39	-148.08	1300	0.92	0.025	1.09	0.4	0.17				Wu et al, 2009
GAK13	7	2004	58.10	-147.79	2	0.17	0.025	0.28	0.4	0.11				Wu et al, 2009
GAK13	7	2004	58.10	-147.79	75	0.34	0.025	0.34	0.4	0				Wu et al, 2009
GAK13	7	2004	58.10	-147.79	1800	0.71	0.025	1.19	0.4	0.48				Wu et al, 2009
Endeavour 328	9	1999	22.00	-36.00	145	0.08	0.02	0.46	0.4	0.38				Wu et al, 2001
Endeavour 328	9	1999	22.00	-36.00	200	0.10	0.02	0.56	0.4	0.46				Wu et al, 2001
Endeavour 328	9	1999	22.00	-36.00	300	0.18	0.02	0.51	0.4	0.33				Wu et al, 2001
Endeavour 328	9	1999	22.00	-36.00	600	0.28	0.02	0.68	0.4	0.40				Wu et al, 2001

Endeavour 328	9	1999	22.00	-36.00	700	0.29	0.02	0.69	0.4	0.40		Wu et al, 2001
Endeavour 328	9	1999	22.00	-36.00	800	0.28	0.02	0.73	0.4	0.45		Wu et al, 2001
Endeavour 328	9	1999	22.00	-36.00	4000	0.25	0.02	0.63	0.4	0.38		Wu et al, 2001
Endeavour 328	9	1999	22.00	-36.00	4750	0.23	0.02	0.58	0.4	0.35		Wu et al, 2001
Endeavour 328	9	1999	22.00	-36.00	5500	0.26	0.02	0.63	0.4	0.37		Wu et al, 2001
Oceanus 326	7	1998	34.00	-57.00	0	0.12	0.02	0.59	0.4	0.47	36.32	Wu et al, 2001
Oceanus 326	7	1998	34.00	-57.00	500	0.26	0.02	0.28	0.4	0.02	36.29	Wu et al, 2001
Oceanus 326	7	1998	34.00	-57.00	650	0.22	0.02	0.64	0.4	0.42	36.04	Wu et al, 2001
Oceanus 326	7	1998	34.00	-57.00	950	0.39	0.02	0.64	0.4	0.25	35.17	Wu et al, 2001
Oceanus 326	7	1998	34.00	-57.00	1100	0.29	0.02	0.59	0.4	0.30	35.13	Wu et al, 2001
Oceanus 326	7	1998	34.00	-57.00	1750	0.32	0.02	0.68	0.4	0.36	35.04	Wu et al, 2001
Oceanus 326	7	1998	34.00	-57.00	3000	0.31	0.02	0.74	0.4	0.43	34.95	Wu et al, 2001
Oceanus 326	7	1998	34.00	-57.00	3500	0.29	0.02	0.54	0.4	0.25	34.94	Wu et al, 2001
Wecoma MP2	4	2001	23.00	-158.00	0	0.08	0.02	0.71	0.4	0.63		Wu et al, 2001
Wecoma MP2	4	2001	23.00	-158.00	20	0.14	0.02	0.54	0.4	0.40		Wu et al, 2001
Wecoma MP2	4	2001	23.00	-158.00	65	0.07	0.02	0.36	0.4	0.29		Wu et al, 2001
Wecoma MP2	4	2001	23.00	-158.00	350	0.06	0.02	0.20	0.4	0.14		Wu et al, 2001
Wecoma MP2	4	2001	23.00	-158.00	750	0.17	0.02	0.34	0.4	0.17		Wu et al, 2001
Wecoma MP2	4	2001	23.00	-158.00	1000	0.38	0.02	0.63	0.4	0.25		Wu et al, 2001
Wecoma MP2	4	2001	23.00	-158.00	1100	0.40	0.02	0.62	0.4	0.22		Wu et al, 2001
Wecoma MP2	4	2001	23.00	-158.00	1500	0.31	0.02	0.55	0.4	0.24		Wu et al, 2001
Wecoma MP2	4	2001	23.00	-158.00	3000	0.29	0.02	0.49	0.4	0.20		Wu et al, 2001
Wecoma MP2	4	2001	23.00	-158.00	3500	0.20	0.02	0.32	0.4	0.12		Wu et al, 2001
Wecoma MP2	4	2001	23.00	-158.00	4000	0.19	0.02	0.31	0.4	0.12		Wu et al, 2001
MP5	7	2002	25.44	-173.41	0	0.28	0.02	0.30	0.4	0.02		Boyle et al, 2005
MP5	7	2002	24.03	-168.53	0	0.30	0.02	0.40	0.4	0.10		Boyle et al, 2005
MP5	7	2002	23.05	-164.93	0	0.25	0.02	0.38	0.4	0.13		Boyle et al, 2005
MP5	7	2002	22.73	-163.81	0	0.31	0.02	0.37	0.4	0.06		Boyle et al, 2005
MP5	7	2002	22.74	-161.49	0	0.22	0.02	0.41	0.4	0.19		Boyle et al, 2005
MP5	7	2002	22.56	-160.33	0	0.31	0.02	0.44	0.4	0.13		Boyle et al, 2005

MP5	7	2002	22.73	-157.95	0	0.21	0.02	0.47	0.4	0.26			Boyle et al, 2005
HOT Transect	11	1998	21.63	-158.00	0	0.16	0.02	1.10	0.4	0.94	1.37		Boyle et al, 2005
HOT Transect	11	1998	21.74	-158.00	0	0.34	0.02	0.59	0.4	0.25	0.94		Boyle et al, 2005
HOT Transect	11	1998	21.78	-158.00	0	0.34	0.02	0.62	0.4	0.28	0.98		Boyle et al, 2005
HOT Transect	11	1998	21.88	-158.00	0	0.37	0.02	0.45	0.4	0.08	1.09		Boyle et al, 2005
HOT Transect	11	1998	21.95	-158.00	0	0.36	0.02	0.60	0.4	0.24	0.86		Boyle et al, 2005
HOT Transect	11	1998	22.05	-158.00	0	0.13	0.02	0.55	0.4	0.42	0.84		Boyle et al, 2005
HOT Transect	11	1998	22.14	-158.00	0	0.25	0.02	0.59	0.4	0.34	1.13		Boyle et al, 2005
HOT Transect	11	1998	22.23	-158.00	0	0.33	0.02	0.42	0.4	0.09	0.76		Boyle et al, 2005
R/V Hakuho-maru ER-6	12	2009	14.00	69.00	25	0.22	1000kDa	0.23	0.2	0.01		36.66	28.70 Nishioka et al, 2013
R/V Hakuho-maru ER-6	12	2009	14.00	69.00	100	0.91	1000kDa	0.98	0.2	0.07		36.03	22.30 Nishioka et al, 2013
R/V Hakuho-maru ER-6	12	2009	14.00	69.00	150	0.91	1000kDa	1.54	0.2	0.63		35.75	18.40 Nishioka et al, 2013
R/V Hakuho-maru ER-6	12	2009	14.00	69.00	200	0.67	1000kDa	1.48	0.2	0.81		35.72	15.80 Nishioka et al, 2013
R/V Hakuho-maru ER-6	12	2009	14.00	69.00	401	0.64	1000kDa	1.23	0.2	0.59		35.48	12.30 Nishioka et al, 2013
R/V Hakuho-maru ER-6	12	2009	14.00	69.00	603	0.62	1000kDa	1.16	0.2	0.54		35.51	11.20 Nishioka et al, 2013
R/V Hakuho-maru ER-6	12	2009	14.00	69.00	801	0.54	1000kDa	1.23	0.2	0.69		35.39	9.60 Nishioka et al, 2013
R/V Hakuho-maru ER-6	12	2009	14.00	69.00	1000	0.73	1000kDa	1.27	0.2	0.54		35.21	7.90 Nishioka et al, 2013
R/V Hakuho-maru ER-6	12	2009	14.00	69.00	1252	0.75	1000kDa	1.52	0.2	0.77		35.09	6.50 Nishioka et al, 2013
R/V Hakuho-maru ER-6	12	2009	14.00	69.00	1503	0.7	1000kDa	1.19	0.2	0.49		34.98	5.10 Nishioka et al, 2013
R/V Hakuho-maru ER-6	12	2009	14.00	69.00	2003	0.51	1000kDa	1.04	0.2	0.53		34.83	3.10 Nishioka et al, 2013
R/V Hakuho-maru ER-6	12	2009	14.00	69.00	2501	0.53	1000kDa	0.99	0.2	0.46		34.77	2.20 Nishioka et al, 2013
R/V Hakuho-maru ER-6	12	2009	14.00	69.00	3000	0.5	1000kDa	0.87	0.2	0.37		34.75	1.80 Nishioka et al, 2013
R/V Hakuho-maru ER-6	12	2009	14.00	69.00	3500	0.5	1000kDa	0.85	0.2	0.35		34.74	1.70 Nishioka et al, 2013
R/V Hakuho-maru ER-6	12	2009	14.00	69.00	4000	0.5	1000kDa	0.83	0.2	0.33		34.74	1.70 Nishioka et al, 2013
R/V Hakuho-maru ER-6	12	2009	14.00	69.00	4140	0.49	1000kDa	0.87	0.2	0.38		34.74	1.70 Nishioka et al, 2013
R/V Hakuho-maru ER-7	12	2009	10.00	68.75	25	0.08	1000kDa	0.09	0.2	0.01		36.55	29.10 Nishioka et al, 2013
R/V Hakuho-maru ER-8	12	2009	4.02	69.00	10	0.09	1000kDa	0.09	0.2	0		35.47	28.90 Nishioka et al, 2013
R/V Hakuho-maru ER-8	12	2009	4.02	69.00	200	0.4	1000kDa	0.83	0.2	0.43		35.17	13.20 Nishioka et al, 2013
R/V Hakuho-maru ER-8	12	2009	4.02	69.00	400	0.57	1000kDa	0.95	0.2	0.38		35.07	10.80 Nishioka et al, 2013
R/V Hakuho-maru ER-8	12	2009	4.02	69.00	800	0.68	1000kDa	1.1	0.2	0.42		35.09	8.60 Nishioka et al, 2013

R/V Hakuho-maru ER-8	12	2009	4.02	69.00	1000	0.6	1000kDa	1.15	0.2	0.55	35.02	7.10	Nishioka et al, 2013
R/V Hakuho-maru ER-8	12	2009	4.02	69.00	1500	0.49	1000kDa	0.98	0.2	0.49	34.87	4.60	Nishioka et al, 2013
R/V Hakuho-maru ER-8	12	2009	4.02	69.00	2001	0.6	1000kDa	1.19	0.2	0.59	34.79	2.80	Nishioka et al, 2013
R/V Hakuho-maru ER-8	12	2009	4.02	69.00	3000	0.81	1000kDa	1.32	0.2	0.51	34.74	1.80	Nishioka et al, 2013
R/V Hakuho-maru ER-8	12	2009	4.02	69.00	4073	0.52	1000kDa	1.01	0.2	0.49	34.74	1.70	Nishioka et al, 2013
R/V Hakuho-maru ER-10	12	2009	-20.00	72.55	25	0.02	1000kDa	0.03	0.2	0.01	35.19	25.00	Nishioka et al, 2013
R/V Hakuho-maru ER-10	12	2009	-20.00	72.55	51	0.04	1000kDa	0.07	0.2	0.03	35.23	23.10	Nishioka et al, 2013
R/V Hakuho-maru ER-10	12	2009	-20.00	72.55	150	0.07	1000kDa	0.07	0.2	0	35.67	20.70	Nishioka et al, 2013
R/V Hakuho-maru ER-10	12	2009	-20.00	72.55	200	0.07	1000kDa	0.07	0.2	0	35.77	19.50	Nishioka et al, 2013
R/V Hakuho-maru ER-10	12	2009	-20.00	72.55	801	0.33	1000kDa	0.33	0.2	0	34.47	6.30	Nishioka et al, 2013
R/V Hakuho-maru ER-10	12	2009	-20.00	72.55	1000	0.41	1000kDa	0.41	0.2	0	34.53	4.70	Nishioka et al, 2013
R/V Hakuho-maru ER-10	12	2009	-20.00	72.55	1250	0.37	1000kDa	0.48	0.2	0.11	34.66	4.30	Nishioka et al, 2013
R/V Hakuho-maru ER-10	12	2009	-20.00	72.55	1500	0.4	1000kDa	0.53	0.2	0.13	34.71	3.80	Nishioka et al, 2013
R/V Hakuho-maru ER-10	12	2009	-20.00	72.55	2000	0.66	1000kDa	1.07	0.2	0.41	34.72	2.60	Nishioka et al, 2013
R/V Hakuho-maru ER-10	12	2009	-20.00	72.55	2499	1.59	1000kDa	2.06	0.2	0.47	34.72	1.90	Nishioka et al, 2013
R/V Hakuho-maru ER-10	12	2009	-20.00	72.55	3001	0.82	1000kDa	1.54	0.2	0.72	34.72	1.60	Nishioka et al, 2013
R/V Hakuho-maru ER-10	12	2009	-20.00	72.55	3502	0.58	1000kDa	0.92	0.2	0.34	34.72	1.40	Nishioka et al, 2013
R/V Hakuho-maru ER-10	12	2009	-20.00	72.55	4002	0.54	1000kDa	0.71	0.2	0.17	34.72	1.40	Nishioka et al, 2013
R/V Hakuho-maru ER-10	12	2009	-20.00	72.55	4376	0.5	1000kDa	0.65	0.2	0.15	34.72	1.50	Nishioka et al, 2013
R/V Hakuho-maru ER-12	12	2009	-37.75	57.62	9	0.04	1000kDa	0.05	0.2	0.01	35.57	17.80	Nishioka et al, 2013
R/V Hakuho-maru ER-12	12	2009	-37.75	57.62	25	0.03	1000kDa	0.05	0.2	0.02	35.56	17.20	Nishioka et al, 2013
R/V Hakuho-maru ER-12	12	2009	-37.75	57.62	50	0.05	1000kDa	0.05	0.2	0	35.55	16.60	Nishioka et al, 2013
R/V Hakuho-maru ER-12	12	2009	-37.75	57.62	100	0.04	1000kDa	0.04	0.2	0	35.54	16.30	Nishioka et al, 2013
R/V Hakuho-maru ER-12	12	2009	-37.75	57.62	199	0.05	1000kDa	0.08	0.2	0.03	35.50	15.40	Nishioka et al, 2013
R/V Hakuho-maru ER-12	12	2009	-37.75	57.62	600	0.16	1000kDa	0.2	0.2	0.04	35.11	12.20	Nishioka et al, 2013
R/V Hakuho-maru ER-12	12	2009	-37.75	57.62	800	0.32	1000kDa	0.44	0.2	0.12	34.79	9.90	Nishioka et al, 2013
R/V Hakuho-maru ER-12	12	2009	-37.75	57.62	999	0.26	1000kDa	0.53	0.2	0.27	34.56	7.70	Nishioka et al, 2013
R/V Hakuho-maru ER-12	12	2009	-37.75	57.62	1251	0.52	1000kDa	0.59	0.2	0.07	34.38	4.70	Nishioka et al, 2013
R/V Hakuho-maru ER-12	12	2009	-37.75	57.62	1501	0.46	1000kDa	0.58	0.2	0.12	34.43	3.50	Nishioka et al, 2013
R/V Hakuho-maru ER-12	12	2009	-37.75	57.62	2000	0.44	1000kDa	0.67	0.2	0.23	34.65	2.70	Nishioka et al, 2013

R/V Hakuho-maru ER-12	12	2009	-37.75	57.62	2498	0.54	1000kDa	0.71	0.2	0.17	34.75	2.40	Nishioka et al, 2013
R/V Hakuho-maru ER-12	12	2009	-37.75	57.62	3000	0.46	1000kDa	0.73	0.2	0.27	34.76	2.00	Nishioka et al, 2013
R/V Hakuho-maru ER-12	12	2009	-37.75	57.62	3499	0.49	1000kDa	0.63	0.2	0.14	34.73	1.40	Nishioka et al, 2013
R/V Hakuho-maru ER-12	12	2009	-37.75	57.62	4000	0.48	1000kDa	0.55	0.2	0.07	34.69	0.60	Nishioka et al, 2013
R/V Hakuho-maru ER-12	12	2009	-37.75	57.62	4500	0.37	1000kDa	0.56	0.2	0.19	34.68	0.50	Nishioka et al, 2013
R/V Hakuho-maru ER-12	12	2009	-37.75	57.62	5000	0.3	1000kDa	0.56	0.2	0.26	34.68	0.50	Nishioka et al, 2013
R/V Hakuho-maru ER-12	12	2009	-37.75	57.62	5473	0.4	1000kDa	0.58	0.2	0.18	34.68	0.50	Nishioka et al, 2013
R/V Hakuho-maru ER-14	12	2009	-62.00	40.08	25	0.02	1000kDa	0.02	0.2	0	33.83	-1.40	Nishioka et al, 2013
R/V Hakuho-maru ER-14	12	2009	-62.00	40.08	50	0.02	1000kDa	0.02	0.2	0	34.02	-1.70	Nishioka et al, 2013
R/V Hakuho-maru ER-14	12	2009	-62.00	40.08	99	0.02	1000kDa	0.02	0.2	0	34.18	-1.10	Nishioka et al, 2013
R/V Hakuho-maru ER-14	12	2009	-62.00	40.08	149	0.08	1000kDa	0.13	0.2	0.05	34.51	1.20	Nishioka et al, 2013
R/V Hakuho-maru ER-14	12	2009	-62.00	40.08	179	0.16	1000kDa	0.22	0.2	0.06	34.57	1.40	Nishioka et al, 2013
R/V Hakuho-maru ER-14	12	2009	-62.00	40.08	201	0.11	1000kDa	0.23	0.2	0.12	34.60	1.50	Nishioka et al, 2013
R/V Hakuho-maru ER-14	12	2009	-62.00	40.08	399	0.18	1000kDa	0.29	0.2	0.11	34.69	1.50	Nishioka et al, 2013
R/V Hakuho-maru ER-14	12	2009	-62.00	40.08	599	0.22	1000kDa	0.33	0.2	0.11	34.71	1.30	Nishioka et al, 2013
R/V Hakuho-maru ER-14	12	2009	-62.00	40.08	799	0.26	1000kDa	0.38	0.2	0.12	34.72	1.10	Nishioka et al, 2013
R/V Hakuho-maru ER-14	12	2009	-62.00	40.08	1000	0.24	1000kDa	0.4	0.2	0.16	34.71	1.00	Nishioka et al, 2013
R/V Hakuho-maru ER-14	12	2009	-62.00	40.08	1249	0.28	1000kDa	0.4	0.2	0.12	34.70	0.80	Nishioka et al, 2013
R/V Hakuho-maru ER-14	12	2009	-62.00	40.08	1501	0.29	1000kDa	0.44	0.2	0.15	34.70	0.60	Nishioka et al, 2013
R/V Hakuho-maru ER-14	12	2009	-62.00	40.08	1999	0.3	1000kDa	0.47	0.2	0.17	34.68	0.40	Nishioka et al, 2013
R/V Hakuho-maru ER-14	12	2009	-62.00	40.08	2499	0.42	1000kDa	0.52	0.2	0.1	34.67	0.20	Nishioka et al, 2013
R/V Hakuho-maru ER-14	12	2009	-62.00	40.08	2999	0.37	1000kDa	0.54	0.2	0.17	34.67	0.00	Nishioka et al, 2013
R/V Hakuho-maru ER-14	12	2009	-62.00	40.08	3501	0.38	1000kDa	0.53	0.2	0.15	34.66	-0.10	Nishioka et al, 2013
R/V Hakuho-maru ER-14	12	2009	-62.00	40.08	4001	0.36	1000kDa	0.51	0.2	0.15	34.66	-0.20	Nishioka et al, 2013
R/V Hakuho-maru ER-14	12	2009	-62.00	40.08	4499	0.37	1000kDa	0.54	0.2	0.17	34.65	-0.20	Nishioka et al, 2013
R/V Hakuho-maru ER-14	12	2009	-62.00	40.08	5000	0.37	1000kDa	0.53	0.2	0.16	34.65	-0.20	Nishioka et al, 2013
R/V Hakuho-maru ER-14	12	2009	-62.00	40.08	5272	0.34	1000kDa	0.52	0.2	0.18	34.65	-0.20	Nishioka et al, 2013